EXECUTIVE SUMMARY REPORT

AMPERE
Autonomous Moon Power and Environmental Research Element

Project	SPACE MISSION DESIGN/SMD
Doc. Ref.	D1/SMD25/ESR/AMPERE/02
Doc. Type	Report
Issue	2
Revision	0
Date of issue	29/06/2025
Prepared by	AMPERE Team
Checked by	Niro Antonio
Approved by	Di Sarno Pietro
Distribution	Confidential

1 Document control data

1.1 Document change log and record

Change Log			
Reason for change	Issue	Revision	Date
Draft version 0	0	0	06/04/2025
Draft Version 1	1	0	13/05/2025
Final	2	0	29/06/2025

Change records Issue 0 Revision 0	
Reason for change	Paragraph(s)
Emission	7, 8
KoM AI #1	7, 8

Change records Issue 1 Revision 0	
Reason for change	Paragraph(s)
Emission	9, 10, 11
MDR AI #1	9, 10, 11

Change records Issue 2 Revision 0	
Reason for change	Paragraph(s)
Emission	9, 10, 11, 12, 13, 14

1.2 Applicable and reference documents

Applicable Documents (A.D.s):	[A.D. 1] Statement of Work, DII/SMD25/SoW/A/1.0, Issue 1, Revision 0, March 2025. [A.D. 2] COSPAR Panel on Planetary Protection, "Editorial to the New Restructured and Edited COSPAR Policy on Planetary Protection", Space Research Today, Vol. 220, 10–26. https://cosparhq.cnes.fr/assets/uploads/2024/07/PP-Policy_SRT_220-July 2024.pdf. [A.D. 3] United Nations General Assembly. "Resolution 2222 (XXI). Treaty on Principles Governing the Activities of States in the Exploration and Use of Outer Space, including the Moon and Other Celestial Bodies", December 1966. [A.D. 4] ECSS "Space project management: project planning and implementation", ECSS-M ST-10C. [A.D. 5] ECSS "Space project management: Risk management", ECSS-M-ST-80C. [A.D. 6] ECSS "Space project management: Cost and Schedule Management", ECSS-M-ST 60C. [A.D. 7] ECSS "Space Engineering: Space system engineering general requirements", ECSS E-ST-10C. [A.D. 8] ECSS "Space Engineering: Technical requirements specification", ECSS-E-ST-10 06C. [A.D. 9] Clarification No. 1 to Sow, DII/SMD25/CI/1.0 [A.D. 10] J. R. Wertz, D.F. Everett, J.J. Puschell, "Space Mission Engineering: The New SMAD", Space Technology Series, Space Technology Library Vol. 28, Springer, 2011. [A.D. 11] W. Ley, K. Wittmann, W. Hallmann, "Handbook of Space Technology", John Wiley & Sons, 2009. [A.D. 12] Ariane-6 User's Manual, Arianespace, Issue 2, Revision 0, February 2021. [A.D. 13] European Space Agency (ESA), "Argonaut Architecture and Terminology", ESA-E3P EL3-SP-004, Issue 1, Revision 0, November 2022 [A.D. 14] European Space Agency (ESA), "Argonaut Mission 1 Primary Payload - Artemis utility rover design description", ESA-E3P-EL3-DD-003, Issue 1, Revision 0 [A.D. 15] NASA Space Systems Engineering Handbook, NASA/SP-2007-6105 Rev1. [A.D. 16] European Space Agency (ESA), "European Large Logistic Lander (EL3) STEP model". Accessed: April 2025. [Online] Available at: https://esamultimedia.esa.int/docs/HRE/EL3_by_EAC_11mei21.stp

Reference Documents (R.D.s):	[R.D. 1] Renga A., “Space Mission Design: Lecture 4”, course slides. Università degli Studi di Napoli Federico II, 2025. [R.D. 2] Renga A., “Space Mission Design: Lecture 5”, course slides. Università degli Studi di Napoli Federico II, 2025. [R.D. 3] European Space Agency (ESA), “Station for the Moon”, CDF Study Report: CDF-218(A), August 2021. [R.D. 4] European Space Agency (ESA), “ISRU Pilot Plant”, CDF Study Report: CDF-182(A), June 2018. [R.D. 5] European Space Agency (ESA), “Terrae Novae 2030+ Strategy Roadmap”, June 2022. [R.D. 6] European Space Agency (ESA), “Lunar Surface Exobiology Exposure Payload: Preliminary Science Requirements”, ESA-HRE-RS-RS-0009_1.0, Issue 0, Revision 0, March 2021. [R.D. 7] Mostek, J.Q., Grile, T.M., Bettinger, R.A. et al., “Atlas of Lunar Historical Sites and Proposed Bases and Infrastructure”, Aerotecnica Missili & Spazio, 2024. Available: https://doi.org/10.1007/s42496-024-00239-z [R.D. 8] European Space Agency (ESA), “Polar Explorer”, CDF Study Report: CDF-212(A), April 2021 [R.D. 9] MARCINKOWSKI, Adam, et al. Lunar surface power architecture concepts. In: 2023 IEEE Aerospace Conference. IEEE, 2023. p. 1-19. [R.D. 10] ZUNIGA, Allison, et al. Building an economical and sustainable lunar infrastructure to enable human missions. In: International Astronautical Congress. 2019. [R.D. 11] European Space Agency (ESA), “Polar Explorer Model Payload Definition Document (MPDD)”, ESA-E3P-EL3-RS-007, Issue 2, Revision 2, June 2021. [R.D. 12] European Space Agency (ESA), “Lunar Exploration Objectives and Requirements Definition”, LL-ESA-ORD-413, Issue 1, Revision 0, February 2010. [R.D. 13] Basilevsky, A.T., Krasilnikov, S.S., Ivanoc, M.A., Malenkov, M.I., Michael, G.G., Liu, T., Head, J.W., Scott, D.R., Lark, L.: Potential lunar base on mons malapert: topographic, geologic and trafficability considerations. Sol. Syst. Res. (2019). [R.D. 14] Sharpe, B. L., Schrunk, D. G.: An operationally ideal location for the first permanent base on the moon. In: Seventh International Conference and Exposition on Engineering, Construction, Operations, and Business in Space (2000). [R.D. 15] Smith, H.J., Gurshtein, A.A., Mendell, W.: International manned lunar base: beginning the 21st century in space. Sci. Glob. Secur. (1991). [R.D. 16] P.D., Hood, L.I.: Geological and Geophysical Field Investigations from a Lunar Base at Mare Smythii. In: The Second Conference on Lunar Bases and Space Activities of the 21st Century (1988). [R.D. 17] Benaroya, H., Bernold, L., Chua, K.M.: Engineering, design and construction of lunar bases. J. Aerosp. Eng. (2022). [R.D. 18] European Space Agency (ESA), “Argonaut Mission 1 Secondary Payloads - Scientific instrument use cases”, ESA-E3P-EL3-DD-004, Issue 1, Revision 0, September 2023. [R.D. 19] European Space Agency (ESA), “Argonaut Mission 1 Secondary Payloads - Technology Demonstrator use cases”, ESA-E3P-EL3-DD-002, Issue 1, Revision 0, September 2023. [R.D. 20] European Space Agency (ESA), “Notional technology demonstration PDD for El3 Polar Explorer”, ESA-E3P-EL3-TN-002, Issue 1, Revision 2, February 2021. [R.D. 21] Trautner, R., et al. "PROSPECT: A comprehensive sample acquisition and analysis package for lunar science and exploration." Frontiers in Space Technologies 5 (2024): 1331828. [R.D. 22] Freeman, Ronald H. "Lunar Surface Operations: On the Science Investigations of Blue Ghost-1 Payloads." Journal of Space Operations & Communicator (ISSN 2410-0005) 21.2 (2025). [R.D. 23] Duvet, Ludovic, et al. "European Access to the Lunar Surface: EL3." 72nd International Astronautical Congress (IAC). 2021.

[R.D. 24] Argonaut LDE – European Access to the Moon, IAC 2024 Conference.
[R.D. 25] European Space Agency (ESA), “Argonaut Missions Environmental Specification”, ESA-TECEPS-SP-020864, Issue 4, Revision 2, February 2023.
[R.D. 26] European Space Agency (ESA), “Moonlight LCNS ESA Service Requirements Document”, ESA-TIA-T-RS-0001-ESRD, Issue 1, Revision 0, January 2023.
[R.D. 27] European Space Agency (ESA), “Moonlight LCNS ESA Service Concept of Operations”, ESA-TIA-T-TN-0006, Issue 1, Revision 0, January 2023.
[R.D. 28] B. Dellandrea, D. Rovelli, M. Mascarello, C. Nardini, A. Brocchetto, “HALO Lunar Communication System: the European module that connects the Gateway Space Station to the Moon”, 9th ESA International Workshop on Tracking, Telemetry and Command Systems for Space Applications, 2022.
[R.D. 29] European Space Agency (ESA), “LCNS Phase A/B1 Mission Assumptions and Technical Requirements (MATER)”, ESA-TIA-T-RS-0023, Issue 1, Revision 0, November 2020.
[R.D. 30] European Space Agency (ESA), “Lunar Radio Navigation specific aspects”, ESA-TEC-TN-020717, Issue 1, Revision 0, November 2020.
[R.D. 31] European Space Agency (ESA), “Astrophysical Lunar Observatory”, CDF Presentation, July 2021.
[R.D. 32] European Space Agency (ESA), “Argonaut Coordinate Frame Definition”, ESA-E3P-EL3-TN-001, Issue 2, Revision 0, February 2023.
[R.D. 33] Marco Grammatico, Lorenzo Casalino, “Fuel-Optimal Lander Trajectory for Lunar Soft-Precision Landing”, Polito, 2021.
[R.D. 34] ZUNIGA, Allison F., et al. Building an Economical and Sustainable Lunar Infrastructure to Enable Lunar Industrialization. In: AIAA SPACE and Astronautics Forum and Exposition. 2017. p. 5148.
[R.D. 35] ARGONAUT ARTEMIS MISSION CANDIDATES CONOPS, Esa.
[R.D. 36] European Large Logistic Lander (EL3) Generic Mission and System Requirements Document.
[R.D. 37] Apollo Lunar Descent Guidance, Nasa, 1974.
[R.D. 38] WILLIAMS, J.-P., et al. Seasonal polar temperatures on the Moon. Journal of Geophysical Research: Planets, 2019, 124.10: 2505-2521.
[R.D. 39] Vaniman, David, et al. "The lunar environment." Lunar Sourcebook 1 (1991): 27-60.
[R.D. 40] ESA, Explore 2040, “The European exploration strategy”, 2024.
[R.D. 41] “NASA, Power and energy for lunar surface”, 2022.
[R.D. 42] China National Space Administration, International Lunar Research Station: Guide for Partnership, June 2021.
[R.D. 43] “Moon Valley 2040 - Expanding Opportunities for Lunar Exploration”, Masayuki Urata, pdf presentation, 2024
[R.D. 44] “Türkiye plans over 60 Moon missions in next decade, boosts homegrown tech for lunar research”, 2025.
[R.D. 45] “National Space Strategy 2030”, The United Arab Emirates' Government portal, 2023.
[R.D. 46] “Republic of Korea Joins List of Nations to Sign Artemis Accords”, May 2021.
[R.D. 47] D. Saha et al., "Space Microgrids for Future Manned Lunar Bases: A Review," in IEEE Open Access Journal of Power and Energy, vol. 8, pp. 570-583, 2021, doi: 10.1109/OAJPE.2021.3116674.
[R.D. 48] “Can China beat the US in the 2nd Space race to the Moon?”, April 2025.
[R.D. 49] Totoya Drives Lunar Exploration with manned pressurized rover, 2019
[R.D. 50] China selects international payload for Chang’e-8 lunar south pole mission, April 2025.
[R.D. 51] Fincannon, J. (2024). “Lunar Power Supply, Power Needs, and Environmental Considerations.” In: Eckart, P., Aldrin, A. (eds) Handbook of Lunar Base Design and Development. Springer, Cham. Available: https://doi.org/10.1007/978-3-030-05323-9_39-1

[R.D. 52] Moon Valley 2040 – Expanding Opportunities for Lunar Exploration, Masayaki Urata, 2024
[R.D. 53] Flexible Levitation on a Track (FLOAT), NASA.
[R.D. 54] Astrobotic Technology, Inc. (2024). Astrobotic CubeRover™ Product User Guide V2.2. Pittsburgh, PA. [Online]. Available : https://www.astrobotic.com/wp-content/uploads/2024/01/Astrobotic_CubeRover-PUG_V2-2.pdf.
[R.D. 55] Li, C., Zuo, W., Wen, W., Overview of the Chang'e-4 Mission: Opening the Frontier of Scientific Exploration of the Lunar Far Side, Research in Astronomy and Astrophysics, 2020.
[R.D. 56] NASA, InSight: Mission to Mars, NASA Technical Reports Server, 2021.
[R.D. 57] Varadis RADFET Module RM-VT01-A datasheet, 2024
[R.D. 58] R. Williams, "Varadis radiation detection sensors to land on moon," *Varadis*, Oct. 10, 2023.
[R.D. 59] L. Desorgher et al., "ESA Next Generation Radiation Monitor," Proceedings of the European Conference on Radiation and Its Effects on Components and Systems, RADECS, pp. 1–5, Sep. 2013, doi: 10.1109/radecs.2013.6937362
[R.D. 60] "Next Generation Radiation Monitor (NGRM) – ESA Space Environment." Available: https://space-env.esa.int/r-and-d/instrumentation/next-generation-radiation-monitor-ngrm/
[R.D. 61] Bartington Mag566 datasheet
[R.D. 62] Bartington Instruments Ltd, "Lunar Vertex Mission", 2023, Available: https://www.bartington.com/lunar-vertex/
[R.D. 63] Honeywell HRTS Series Thin Film Platinum RTDs Datasheet, March 2015
[R.D. 64] G. Cucullu, "Robust Platinum Resistor thermometer (PRT) sensors and reliable bonding for space missions," 43rd International Conference on Environmental Systems, Jul. 2013, doi: 10.2514/6.2013-3316.
[R.D. 65] C. Carr et al., "RPC: The Rosetta Plasma Consortium," Space Science Reviews, vol. 128, no. 1–4, pp. 629–647, Feb. 2007, doi: 10.1007/s11214-006-9136-4
[R.D. 66] . L. Burch et al., "RPC-IES: the ion and electron sensor of the Rosetta Plasma Consortium," Space Science Reviews, vol. 128, no. 1–4, pp. 697–712, Dec. 2006, doi: 10.1007/s11214-006-9002-4
[R.D. 67] "RAMBHA-LP on-board Chandrayaan-3 measures near-surface plasma content." Available: https://www.isro.gov.in/Ch3_Rambha-LP_near-surface_Plasma.html
[R.D. 68] G. Manju *et al.*, "Lunar Near Surface Plasma Environment from Chandrayaan-2 Lander Platform: RAMBHA-LP payload," *Current Science*, vol. 118, no. 3, p. 383, Feb. 2020, doi: 10.18520/cs/v118/i3/383-391.
[R.D. 69] M. S. Alam, J. Paul, N. K. Upadhyay, S. J. Nalluveettil, G. Sateesh, and J. A, "Development of deployment mechanism for RAMBHA-LP Payload onboard Chandrayaan-3 Lander," *SAE Technical Papers on CD-ROM/SAE Technical Paper Series*, Jun. 2024, doi: 10.4271/2024-26-0455.
[R.D. 70] U.-H. Wong, Y. Wu, H.-C. Wong, Y. Liang, and Z. Tang, "Modeling the Reflectance of the Lunar Regolith by a New Method Combining Monte Carlo Ray Tracing and Hapke's Model with Application to Chang'E-1 IIM Data," *The Scientific World JOURNAL*, vol. 2014, pp. 1–14, Jan. 2014, doi: 10.1155/2014/457138
[R.D. 71] J. R. Gaier, S. Ellis, and N. Hanks, "Thermal optical properties of lunar dust simulants and their constituents," NASA Technical Reports Server (NTRS), Dec. 01, 2011
[R.D. 72] H. Lin *et al.*, "Photometric properties of lunar regolith revealed by the Yutu-2 rover," *Astronomy and Astrophysics*, vol. 638, p. A35, May 2020, doi: 10.1051/0004-6361/202037859.
[R.D. 73] J. A. Rodriguez-Manfredi et al., "The Mars Environmental Dynamics Analyzer, MEDA. A suite of environmental sensors for the Mars 2020 mission," Space Science Reviews, vol. 217, no. 3, Apr. 2021, doi: 10.1007/s11214-021-00816-9.

[R.D. 74] H. Lin *et al.*, "In situ photometric experiment of lunar regolith with Visible and Near-Infrared Imaging spectrometer on board the Yutu-2 Lunar Rover," *Journal of Geophysical Research Planets*, vol. 125, no. 2, Feb. 2020, doi: 10.1029/2019je006076
[R.D. 75] K.-H. Glassmeier, "Interaction of the solar wind with comets: a Rosetta perspective," Philosophical Transactions of the Royal Society a Mathematical Physical and Engineering Sciences, vol. 375, no. 2097, p. 20160256, May 2017, doi: 10.1098/rsta.2016.0256
[R.D. 76] NASA. (2017). *CubeSat 101: Basic concepts and processes for first-time CubeSat developers* (NASA CubeSat Launch Initiative. National Aeronautics and Space Administration.
[R.D. 77] Space Applications Services, "LUVMI – A Mobile Platform for Lunar Exploration & Experiments" Product Sheet, Mar. 2022. Available: https://www.spaceapplications.com/wp-content/uploads/2022/03/2-product-sheet-luvmi-updated.pdf
[R.D. 78] Secretariat, ECSS. "SpaceWire–Links, nodes, routers and networks." *ECSSE-ST-50–12C, Noordwijk* (2008).
[R.D. 79] "Who uses SpaceWire? - STAR-Dundee," STAR-Dundee, Jul. 22, 2024. Available: https://www.star-dundee.com/spacewire/getting-started/who-uses-spacewire/
[R.D. 80] ESA–European Space Components Coordination Committee (ESCC) (June 2008). ESCC Detail Specification No. 3902/003 – Cable, "SpaceWire", round quad using symmetric cables, flexible, –200 °C to +180 °C (Issue 2)
[R.D. 81] ESA – European Space Components Coordination Committee (ESCC). (January 2012). ESCC Detail Specification No. 3401/029 – Connectors, Electrical, Rectangular, Microminiature (MDM) (Issue 6)
[R.D. 82] D. M. Miles et al., "A miniature, low-power scientific fluxgate magnetometer: A stepping-stone to cube-satellite constellation missions," Journal of Geophysical Research Space Physics, vol. 121, no. 12, Dec. 2016, doi: 10.1002/2016ja023147.
[R.D. 83] Expected Productivity-Based Risk Analysis in Conceptual Design: With Application to the Terrestrial Planet Finder Interferometer Mission, Julie A. Wertz, S.B. Aeronautics & Astronautics Massachusetts Institute of Technology, 2000
[R.D. 84] Expected productivity-based risk analysis in conceptual design; Wertz , Miller; Acta Astronautica 59 (2006) 420–429, 2006
[R.D. 85] Satellite and satellite subsystems reliability: Statistical data analysis and modeling, Jean-Francois Castet, Joseph H. Saleh, School of Aerospace Engineering, Georgia Institute of Technology, 270 Ferst Drive, Atlanta, GA 30332-0150, USA, 2009
[R.D. 86] NASA Instrument Cost Model (NICM), Version 10c, 982-000 Rev 10, March 2023.
[R.D. 87] Euro Area Core Inflation Rate, Trading Economics, Available: https://tradingeconomics.com/euro-area/core-inflation-rate
[R.D. 88] Banca d'italia, Cambi di riferimento al 2 gennaio 2024, Available: https://www.bancaditalia.it/compiti/operazioni-cambi/cambio/cambi_rif_20040102/
[R.D. 89] ECSS "Space Engineering: Testing", ECSS-E-10-03A
[R.D. 90] ECSS "Space Engineering: Verification guidelines", ECSS-E-HB-10-02A
[R.D. 91] ECSS "Space Engineering: Technology Readiness Level (TRL) guidelines", ECSS-E-HB-11A
[R.D. 92] Barker, Michael K., et al. "A new view of the lunar south pole from the Lunar Orbiter Laser Altimeter (LOLA)." The Planetary Science Journal 4.9 (2023): 183.
[R.D. 93] Hayne, Paul O., et al. "Global regolith thermophysical properties of the Moon from the Diviner Lunar Radiometer Experiment." Journal of Geophysical Research: Planets 122.12 (2017): 2371-2400.
[R.D. 94] P. Gläser, J. Oberst, G.A. Neumann, E. Mazarico, E.J. Speyerer, M.S. Robinson, Illumination conditions at the lunar poles: Implications for future exploration, Planetary and Space Science,Volume 162,2018, Pages 170-178, ISSN 0032-0633.
[R.D. 95] Sachana Sathyan, Megha Bhatt, Monalisa Chowdhury, Philipp Gläser, Dibyendu Misra, Neeraj Srivastava, Shyama Narendranath, K.S. Sajinkumar, Anil Bhardwaj, Potential

landing sites characterization on lunar south pole: De-Gerlache to Shackleton ridge region, Icarus, Volume 412, 2024, 115988, ISSN 0019-1035.
[R.D. 96] P. Gläser, F. Scholten, D. De Rosa, R. Marco Figuera, J. Oberst, E. Mazarico, G.A. Neumann, M.S. Robinson, Illumination conditions at the lunar south pole using high resolution Digital Terrain Models from LOLA, Icarus, Volume 243, 2014, Pages 78-90, ISSN 0019-1035.
[R.D. 97] Moon to Mars Architecture Definition Documents, 2024.
[R.D. 98] Global Exploration Roadmap, August 2024.
[R.D. 99] Apollo Landing Sites with Moon Phases, NASA website, 2019
[R.D. 100] Why Artemis will focus on the lunar south polar region, 2022.
[R.D. 101] Characterizing the Visual Experience of Astronauts at the Lunar South Pole, December 2024.
[R.D. 102] NASA Provides Update on Artemis III Moon Landing Regions - NASA, October 2024.
[R.D. 103] NASA Identifies Candidate Regions for Landing Next Americans on Moon - NASA, August 2022.
[R.D. 104] Liu, H.; Wang, Y.; Wen, S.; Zhang, S.; Zhu, K.; Liu, J. Comprehensive Evaluation of the Lunar South Pole Landing Sites Using Self-Organizing Maps for Scientific and Engineering Purposes. *Remote Sens.* 2025, *17*, 1579.
[R.D. 105] Moon Trek, NASA website
[R.D. 106] Apollo Lunar Roving Vehicle. Available: https://nssdc.gsfc.nasa.gov/planetary/lunar/apollo_lrv.html.
[R.D. 107] Margin philosophy for science assessment studies, ESA, 2012
[R.D. 108] Hiranmay Srinivasan, Historical U.S. Inflaction Rate by Year: 1929 to 2025, Investopedia, Feb. 2025 [Online]. Available: https://www.investopedia.com/inflation-rate-by-year-7253832
[R.D. 109] Application of Risk Management to University CubeSat Missions.
[R.D. 110] Probabilistic Risk Assessment Procedures Guide for NASA Managers and Practitioners.
[R.D. 111] Andrew Holmes-Siedle, Leonard Adams, RADFET: A review of the use of metal-oxide-silicon devices as integrating dosimeters, International Journal of Radiation Applications and Instrumentation. Part C. Radiation Physics and Chemistry, Volume 28, Issue 2, 1986, Pages 235-244, ISSN 1359-0197.
[R.D. 112] Cohen, Barbara A. and Barber, et al., The Peregrine Ion Trap Mass Spectrometer (PITMS): Results from a CLPS-delivered Mass Spectrometer, The Planetary Science Journal.
[R.D. 113] Rodriguez, M., Paschalidis, N., Jones, S., Sittler, E., Chornay, D., Uribe, P., & Cameron, T. (2016). Miniaturized Ion and Neutral Mass Spectrometer for CubeSat Atmospheric Measurements (GSFC-E-DAA-TN34416). NASA Goddard Space Flight Center.
[R.D. 114] K. Durga Prasad, Chandan Kumar et al., Characterisation of Front-End Electronics of ChaSTE experiment onboard Chandayaan-3 lander, 2024.
[R.D. 115] SATNow. Available: https://www.satnow.com/community/why-are-solar-panels-used-in-satellites-spacecrafts.
[R.D. 116] «Apollo Lunar surface journal,». Available: https://www.nasa.gov/history/alsj/HamishALSEP.html
[R.D. 117] «NASA Space Science Data Coordinated Archive - Chang'e 5» [Online]. Available: https://nssdc.gsfc.nasa.gov/nmc/spacecraft/display.action?id=2020-087A
[R.D. 118] Grassi M., "Space systems" course slides. Università degli Studi di Napoli Federico II, 2023-2024.
[R.D. 119] Chamberlain, Matthew K., et al. "On-orbit flight testing of the Roll-Out Solar Array." *Acta Astronautica* 179 (2021): 407-414.
[R.D. 120] SPACEMART, Available https://www.spacemart.com/reports/ATK_Awarded_20_Million_UltraFlex_Solar_Array_Contract_from_Orbital_999.html
[R.D. 121] Radioisotope Power Systems - NASA RPS Missions,» [Online],

Available: https://science.nasa.gov/planetary-science/programs/radioisotope-power-systems/missions/#active.
[R.D. 122] Gunter Space PageChang'e 3, 4 (CE 3, 4) / Yutu 1, 2, [Online]. Available: https://space.skyrocket.de/doc_sdat/change-3.htm
[R.D. 123] NASA, Multi-Mission Radioisotope Thermoelectric Generator.
[R.D. 124] NASA, Fuel cell technology for energy storage.
[R.D. 125] «NASA POWER SUMMARY,» [Online]. Available: https://www.nasa.gov/smallsat-institute/sst-soa/power-subsystems/#3.7.2
[R.D. 126] WIRELESS CHARGING FOR LUNAR ROBOTS, Available: https://www.techbriefs.com/component/content/article/39148-wireless-charging-for-lunar-robots
[R.D. 127] Landis, Geoffrey A. "Laser power beaming for lunar polar exploration." *AIAA Propulsion and Energy 2020 Forum*. 2020
[R.D. 128] Eckard, James, and Joshua Schapiro. "FY23 Ultra Fast Proximity Charger (UFPC) TP Annual Review Presentation." *Space Technology Mission Directorate (STMD) Game Changing Development (GCD) Annual Program Review*. 2023.
[R.D. 129] Freid, Sheldon, et al. *Lunar wireless power transfer feasibility study*. No. DOE/NV/25946-488. National Security Technologies, LLC (NSTec), Mercury, NV (United States), 2008.
[R.D. 130] Amato, Michael, et al. "LESSH Lunar Experiment Support System and Handling Battery Charger Module." *Lunar Surface Innovation Consortium*. 2024.
[R.D. 131] Schuler, Jason M., et al. "Quick Attach Docking Interface for Lunar Electric Rover." *Earth and Space 2010: Engineering, Science, Construction, and Operations in Challenging Environments*. 2010. 1382-1393.
[R.D. 132] EaglePicher Technologies. *12 Ah Space Cell LP32975 Datasheet.* EaglePicher Technologies, 2023
[R.D. 133] 28-300-Battery Module, 28V Lithium-ion Battery, Datasheet, 135 Aerospace
[R.D. 134] Product Data Sheet Li-ion Rechargeable Battery ABSL 8s16p 28V 56Ah, EnerSys
[R.D. 135] Preger, Yuliya, et al. "Degradation of commercial lithium-ion cells as a function of chemistry and cycling conditions." *Journal of The Electrochemical Society* 167.12 (2020): 120532.
[R.D. 136] Qasem, Naef AA, and Gubran AQ Abdulrahman. "A recent comprehensive review of fuel cells: history, types, and applications." *International Journal of Energy Research* 2024.1 (2024): 7271748.
[R.D. 137] Jakupca, Ian. "Fuel Cell Technologies for Energy Storage." *ASCEND*. 2024.
[R.D. 138] Burke, Kenneth. "Fuel cells for space science applications." *1st International Energy Conversion Engineering Conference (IECEC)*. 2003
[R.D. 139] Jakupca, Ian. "NASA Activities in Fuel Cell and HydrogenTechnologies." *Lunar Space Innovation Consortium (LSIC) Monthly Power Meeting*. 2022
[R.D. 140] Mungiguerra S., “Space Propulsion” course slides, Università degli Studi di Napoli Federico II, 2024.
[R.D. 141] Hartwig, Jason W. "A detailed historical review of propellant management devices for low gravity propellant acquisition." *52nd AIAA/SAE/ASEE Joint Propulsion Conference*. 2016.
[R.D. 142] SOLAR ARRAYS ROLL OUT SOLAR ARRAY (ROSA), Redwire Datasheet, 2021
[R.D. 143] Wright Jr, Kenneth H., et al. "ROSA and Solar Cell Module Combined Environments Test Plan." 16th Spacecraft Charging and Technology Conference. 2022.
[R.D. 144] 32% Quadruple Junction GaAs Solar Cell Type: QJ Solar Cell 4G32C – Advanced, Azur Space datasheet, 2019
[R.D. 145] “GHPS Generic High Power System” Datasheet, Airbus
[R.D. 146] Starbuck-Nano-Plus PCDU, AAC CLYDE SPACE, 2021
[R.D. 147] Space Technology Mission Directorate. “GCD Annual Program Review — Project Presentation” Space Technology Mission Directorate Game Changing Development Program, presented by James Eckard and moderated by Chad Gray, NASA, 7 Sept. 2023

[R.D. 148] Painter, Tim. *Ultra Fast Proximity Charging for Critical Space Application*. Space Technology Mission Directorate Game Changing Development Program, 10–12 Sept. 2024.
[R.D. 149] PEABODY, Hume. Thermal Design for Spaceflight Fall 2022. 2023.
[R.D. 150] FINCKENOR, M. M.; DOOLING, D. *Multilayer insulation material guidelines*. 1999. Multilayer Insulation Material Guidelines - NASA Technical Reports Server (NTRS)
[R.D. 151] Smay, J., Hughes, J., Spangler, R., Tarau, C., & Alvarez-Hernandez, A. R. (n.d.). *Volatiles Investigating Polar Exploration Rover (VIPER) thermal management system (TMS) design, development, and testing*. Advanced Cooling Technologies. NASA Johnson Space Center.
[R.D. 152] TAILIN, Li, et al. Comprehensive modeling and characterization of Chang'E-4 radioisotope thermoelectric generator for lunar mission. *Applied Energy*, 2023, 336: 120865. Comprehensive modeling and characterization of Chang'E-4 radioisotope thermoelectric generator for lunar mission - ScienceDirect
[R.D. 153] Garg, Prateek & Almehisni, Reem. (2021). Publications Thermal management system design and analysis of rashid rover - Emirates Lunar Mission. (PDF) Publications Thermal management system design and analysis of rashid rover - Emirates Lunar Mission
[R.D. 154] ATHANASOPOULOS, N.; FARMASONIS, J.; SIAKAVELLAS, N. J. Preliminary design and comparative study of thermal control in a nanosatellite through smart variable emissivity surfaces. *Proceedings of the Institution of Mechanical Engineers, Part G: Journal of Aerospace Engineering*, 2019, 233.9: 3336-3350. Preliminary design and comparative study of thermal control in a nanosatellite through smart variable emissivity surfaces - N Athanasopoulos, J Farmasonis, NJ Siakavellas, 2019
[R.D. 155] DEMIRYONT, Hulya; MOOREHEAD, David. Electrochromic emissivity modulator for spacecraft thermal management. *Solar Energy Materials and Solar Cells*, 2009, 93.12: 2075-2078. Electrochromic emissivity modulator for spacecraft thermal management - ScienceDirect
[R.D. 156] LAK, Amin; ASEFI, Maziar. A new deployable pantographic lunar habitat. *Acta Astronautica*, 2022, 192: 351-367. A new deployable pantographic lunar habitat - ScienceDirect
[R.D. 157] COWAN, Darnell T. Actively Controlled Louver for Human Spacecraft Radiator Ultraviolet (UV), Dust, and Freeze Protection. In: *52nd International Conference on Environmental Systems (ICES)*. 2023. Actively Controlled Louver for Human Spacecraft Radiator Ultraviolet (UV), Dust, and Freeze Protection - NASA Technical Reports Server (NTRS)
[R.D. 158] IVANOV, Dmitri; FERNANDES, Domingos. Lunar dust tolerant thermal louver development for a light-weight rover system. Lunar dust tolerant thermal louver development for a light-weight rover system
[R.D. 159] SCHUNK, R. Gregory; BABIAK, Stephanie D.; EVANS, Brian W. Thermal Control System Architecture and Technology Challenges for a Lunar Surface Habitat. In: *2022 IEEE Aerospace Conference (AERO)*. IEEE, 2022. p. 1-8. IEEE Xplore Full-Text PDF:
[R.D. 160] YOST, Bruce; WESTON, Sasha. *State-of-the-art small spacecraft technology*. 2024. State of the Art Small Spacecraft Technology
[R.D. 161] DIACONU, Bogdan Marian; CRUCERU, Mihai; ANGHELESCU, Lucica. Phase change materials in space systems. Fundamental applications, materials and special requirements–A review. *Acta Astronautica*, 2024, 216: 163-213. Phase change materials in space systems. Fundamental applications, materials and special requirements – A review - ScienceDirect
[R.D. 162] LILLIBRIDGE, Sean; STEPHAN, Ryan. *Phase change material heat exchanger life test*. SAE Technical Paper, 2009. Phase Change Material Heat Exchanger Life Test
[R.D. 163] CHOI, Michael K. Using paraffin PCM for thermal management of BOLAS planetary CubeSats with ion thrusters. In: *AIAA Propulsion and Energy 2019 Forum*. 2019. p. 4300. Using Paraffin PCM for Thermal Management of BOLAS Planetary CubeSats with Ion Thrusters | AIAA Propulsion and Energy Forum
[R.D. 164] MAYDANIK, Y. F.; VERSHININ, S. V.; CHERNYSHEVA, M. A. The results of comparative analysis and tests of ammonia loop heat pipes with cylindrical and flat

evaporators. *Applied Thermal Engineering*, 2018, 144: 479-487. The results of comparative analysis and tests of ammonia loop heat pipes with cylindrical and flat evaporators - ScienceDirect

[R.D. 165] JASVANTH, V. S., et al. Design and testing of an ammonia loop heat pipe. Applied Thermal Engineering, 2017, 111: 1655-1663. Design and testing of an ammonia loop heat pipe - ScienceDirect

[R.D. 166] PATEL, Vivek K. An efficient optimization and comparative analysis of ammonia and methanol heat pipe for satellite application. *Energy conversion and Management*, 2018, 165: 382-395. An efficient optimization and comparative analysis of ammonia and methanol heat pipe for satellite application - ScienceDirect

[R.D. 167] XIANWEN, Ning, et al. Design and implementation of the integrated thermal control system for Chang'E− 5 lunar module. *Acta Astronautica*, 2022, 200: 188-195. Design and implementation of the integrated thermal control system for Chang'E−5 lunar module - ScienceDirect

[R.D. 168] MISSION, Europa Clipper. TFAWS Passive Thermal Paper Session. 2018. Thermal Analysis of Propulsion Components for the Europa Clipper Mission Heather Bradshaw, NASA GSFC

[R.D. 169] DE GROH, Kim K., et al. Solar Effects on Tensile and Optical Properties of Hubble Space Telescope Silver-Teflon Insulation. *MRS Online Proceedings Library (OPL)*, 2006, 929: 0929-II05-08.

[R.D. 170] ZOPPAS INDUSTRIES**.** Space stock polyimide flexible heating element [online]. Satsearch, [s.d]. Available: https://satsearch.co/products/zoppas-industries-space-stock-polyimide-flexible-heating-element

[R.D. 171] MOD-TRONIC INSTRUMENTS LIMITED. *Polyimide Thermofoil Heaters* [online]. Brampton, ON: Mod-Tronic Instruments Limited, [s.d.]. Available: https://mod-tronic.com/files/products/polyimide-thermofoil-heaters.pdf

[R.D. 172] COLLINS AEROSPACE. *Model 0118MF High Reliability Surface Temperature Sensor Data Sheet* [online]. Collins Aerospace, [s.d.]. Available: https://www.collinsaerospace.com/-/media/CA/product-assets/marketing/s/space/model-0118mf-high-reliability-surface-temperature-sensor-data-sheet.pdf?rev=2e384d150d0940f6afb128cf9299f7d3

[R.D. 173] LANG, FengPei, et al. Review on variable emissivity materials and devices based on smart chromism. *International Journal of Thermophysics*, 2018, 39: 1-20. Review on Variable Emissivity Materials and Devices Based on Smart Chromism | International Journal of Thermophysics

[R.D. 174] DUDON, Jean-Paul, et al. Development of variable emissivity coatings for thermal radiator. In: *ICES 2021-50th International Conference on Environmental Systems*. 2021. Development of variable emissivity coatings for thermal radiator - Archive ouverte HAL

[R.D. 175] BUHLER, C. R., et al. Current state of the electrodynamic dust shield for mitigation. In: *The Impact of Lunar Dust on Human Exploration Workshop*. 2020.

[R.D. 176] TISDALE, Malcom, et al. Design of a modular and orientable electrodynamic shield for lunar dust mitigation. In: *AIAA SCITECH 2022 Forum*. 2022. p. 2623.

[R.D. 177] NASA**.** *NASA's Dust Shield Successfully Repels Lunar Regolith on Moon* [online]. NASA, 2024. Available: https://www.nasa.gov/image-article/nasas-dust-shield-successfully-repels-lunar-regolith-on-moon/

[R.D. 178] Malla, Ramesh B., and Kevin M. Brown. "Determination of temperature variation on lunar surface and subsurface for habitat analysis and design." *Acta Astronautica* 107 (2015): 196-207.

[R.D. 179] DeHart R., "Prediction of Lunar Reconnaissance Orbiter Reaction Wheel Assembly Angular Momentum Using Regression Analysis", SciTech, Grapevine, Texas, 2017.

[R.D. 180] KARPENKO, Mark, et al. Fast Attitude Maneuvers for NASA's Lunar Reconnaissance Orbiter: Practical Flight Application of Attitude Guidance Using Birkhoff Pseudospectral Theory and Hamiltonian Programming. IEEE Control Systems Magazine, 2024, 44.2: 26-54.

[R.D. 181] Calhoun, J. R. (1970). Gravity gradient stabilization system for Applications Technology Satellites – volume 1: System software and analysis.
[R.D. 182] R. S. Park; W. M. Folkner; J. G. Williams; D. H. Boggs (2021). "The JPL Planetary and Lunar Ephemerides DE440 and DE441". Astronomical Journal. 161 (105).
[R.D. 183] Grassi M., Spacecraft dynamics and control, course slides. Università degli Studi di Napoli Federico II, 2025
[R.D. 184] HU, Junshan, et al. Fretting behaviors of interface between CFRP and coated titanium alloy in composite interference-fit joints under service condition. Materials & design, 2017, 134: 91-102.
[R.D. 185] Ridolfi, P., Allouis, E., Boyes, B., Hamilton, W., Michelin, J., Norridge, P., & Wayman, A. (2023). A miniaturised fetch rover concept for Mars sample return. Acta Astronautica, 206, 168-176.
[R.D. 186] Azkarate, M., Gerdes, L., Joudrier, L., & Pérez-del-Pulgar, C. J. (2020, May). A gnc architecture for planetary rovers with autonomous navigation. In 2020 IEEE International Conference on Robotics and Automation (ICRA) (pp. 3003-3009). IEEE.
[R.D. 187] Safran Electronics & Defense, STIM377H High Performance Tactical Grade IMU – Datasheet, Dec. 2022. [Online]. Available: https://safran-navigation-timing.com/wp-content/uploads/2022/12/STIM377H-Datasheet.pdf
[R.D. 188] Honeywell Aerospace, HMR3000 Digital Compass Solution – Datasheet. [Online].
[R.D. 189] Redwire Space, Coarse Sun Sensor (Cosine Type). [Online].
[R.D. 190] NewSpace Systems, Sun Sensor Datasheet, Apr. 2025. Available: https://www.newspacesystems.com/wp-content/uploads/2025/04/Sun-Sensor-Datasheet-2025-Apri.pdf
[R.D. 191] J.-P. Bibring et al., "CIVA," Space Science Reviews, vol. 128, pp. 397–412, 2007
[R.D. 192] Microcameras & Space Exploration SA, Rosetta Project – Imaging Equipment. [Online]. Available: https://microcameras.space/project/rosetta/
[R.D. 193] Broadcom, HSMW-A100 High Brightness White LED – Datasheet, Aug. 2021. [Online]. Available: https://www.mouser.it/datasheet/2/678/Broadcom_09082021_HSMW_A100_V40J1-2577804.pdf
[R.D. 194] Edgett, K. S., Yingst, R. A., Ravine, M. A., Caplinger, M. A., Maki, J. N., Ghaemi, F. T., ... & Goetz, W. (2012). Curiosity's Mars hand lens imager (MAHLI) investigation. Space science reviews, 170, 259-317.
[R.D. 195] A. Akemoto and F. Zhu, "Cooperative Lunar Surface Exploration using Transfer Learning with Multi-Agent Visual Teach and Repeat", 2023 IEEE Aerospace Conference, Big Sky, MT, USA, 2023
[R.D. 196] Bickel, V. T., & Kring, D. A. (2019). Lunar south pole boulders and boulder tracks: implications for crew and rover traverses. NASA Exploration Science Forum, 2019.
[R.D. 197] Scammell Rupert, Mars Exploration Rover Technical Data, July 16, 2004. Available: https://web.archive.org/web/20040716083742/http://hobbiton.thisside.net/rovermanual/
[R.D. 198] Modenini, A., Ripani, B. A Tutorial on the Tracking, Telemetry, and Command (TT&C) for Space Missions. TechRxiv – IEEE. 2022
[R.D. 199] Moonlight, pioneering communication and navigation for lunar exploration, Telespazio.
[R.D. 200] Ventura , J. ESA lunar navigation plans: Lunar Pathfinder & Moonlight, ICGNSS, 2016
[R.D. 201] Grenier, A., Giordano, P., et al., Positioning and velocity performance levels for a lunar lander using a dedicated lunar communication and navigation system. Institute of Navigation, 2022
[R.D. 202] Bhamidipati, S., Mina, T. et al., Satellite constellation design for a lunar navigation and communication system. Institute of Navigation, 2023
[R.D. 203] Ely, T., Stable constellations of frozen elliptical inclined lunar orbits. The Journal of the Astronautical Sciences, Vol. 53, No.3, 2005

[R.D. 204] Datasheet Next generation OBC. Available: https://www.satcatalog.com/component/next-generation-on-board-computer/
[R.D. 205] Datasheet NanoMind Z700, GomSpace, 2019. Available: https://ocw.mit.edu/courses/16-851-satellite-engineering-fall-2003/011313179d2d95d542e8cf5dde706e82_ps4_cs_solution.pdf
[R.D. 206] Satellite engineering memorandum – 16.851. Available: https://ocw.mit.edu/courses/16-851-satellite-engineering-fall-2003/011313179d2d95d542e8cf5dde706e82_ps4_cs_solution.pdf
[R.D. 207] LunaNet interoperability specification document. Vers.4, 2022
[R.D. 208] Datasheet C/TT-520 spacecraft S-band transponder. Available: https://www.l3harris.com/all-capabilities/ctt-520-spacecraft-s-band-transponder
[R.D. 209] Lunar Pathfinder Service guide, SSTL Lunar. 2023.
[R.D. 210] Hwu, S., et al. Lunar surface propagation modeling and effects on communications. 26th International Communications Satellite Systems Conference. AIAA 2008 – 5495. 2008
[R.D. 211] Datasheet NanoCom AX100, GomSpace, 2019. Available: https://gomspace.com/UserFiles/Subsystems/datasheet/gs-ds-nanocom-ax100.pdf
[R.D. 212] Piasecki, M., Downey, J., et al. Development and demonstration of a wideband RF user terminal for roaming between Ka-band relay satellite networks. 38th International Communications Satellite Systems Conference, 2021
[R.D. 213] Simons, R. N., Downey, J.A. et al. Ka-band GaN-on-SiC MMIC balanced high power amplifier for NASA's lunar missions, International Symposium on Antennas and Propagation and USNC-URSI Radio Science Meeting, 2023
[R.D. 214] Datasheet Anywaves compact S band TT&C antenna.
[R.D. 215] Datasheet PW2022-111: S-Band Dual CP Wideband Omni Antenna.
[R.D. 216] Datasheet Endurosat S-band transceiver. Available: https://www.endurosat.com/products/s-band-transceiver/
[R.D. 217] Datasheet WiRan S-band diplexer. Available: https://www.wiran.pl/en/s-band-diplexer
[R.D. 218] Qianchao,S., Guilian, C., et al. A design of UHF omnidirectional Antenna for deep space exploration. 4th China International SAR Symposium. 2023
[R.D. 219] Datasheet NanoCom ANT430. GomSpace. 2020
[R.D. 220] Datasheet AAC Clyde Space GNSS-700
[R.D. 221] Datasheet Endurosat GNSS patch antenna. Available: https://www.endurosat.com/products/gnss-patch-antenna/
[R.D. 222] Sirbu,G. et al. Evaluation of different satellite navigation methods for the Moon in the future exploration age. Acta Astronautica 208, 205-218. 2023
[R.D. 223] Melman, F. T. et al. LCNS Positioning of a Lunar Surface Rover Using a DEM-Based Altitude Constraint. Remote Sensing, 14, 3942. 2022
[R.D. 224] European Space Agency (ESA), “Lunar Radio Navigation specific aspects”, ESA-TEC-TN-020717, Issue 1, Revision 0, November 2020
[R.D. 225] Evans, D., Fischer, B. POCKET+, General presentation. ESA. 2017. Available: https://opssat.esa.int/pocket-plus/POCKET+_general_presentation_V2.pdf
[R.D. 226] Portell J. et al. FAPEC, a versatile and efficient data compressor for space missions. International Journal of Remote Sensing, 39(7):1-21, 2017
[R.D. 227] Barile, C., Casavola, C., Pappalettere, C., & Tursi, F. (2019). Mechanical characterization of carbon fiber reinforced plastics specimens for aerospace applications. Polymer Composites, 40(2), 716–722. https://doi.org/10.1002/pc.24765
[R.D. 228] Buchanan, D. R. (2007). Introduction to the Finite Element Analysis Using ANSYS Mechanical APDL. SDC Publications. ISBN: 9781585034016.[R.D. 3] Blinzler, B. J., Whitacre, W. W., & Wereszczak, A. A. (2016). Experimental Investigations of Carbon Fiber Reinforced Polymer Composites and Their Constituents to Determine Their Elastic Material Properties. NASA Glenn Research Center. NASA Technical Report NASA/TM–2016–219199.

[R.D. 229] National Air and Space Museum. (n.d.). Wheel, Lunar Rover. Smithsonian National Air and Space Museum. Available: https://airandspace.si.edu/collection-objects/wheel-lunar-rover/nasm_A19750830000
[R.D. 230] Lunar Roving Vehicle Operations Handbook. (1971, April 19). Prepared by The Boeing Company LRV Systems Engineering, Huntsville, Alabama.
[R.D. 231] Ensign-Bickford Aerospace & Defense Company, “TiNi™ Ejector Release Mechanisms: Family Technical Specifications,” Datasheet V3.4, September 2023. [Online]. Available: https://res.cloudinary.com/dbwyk3yk1/images/v1738540022/TiNi-EjctrReleaseMech-SllSht-SEPT-2023/TiNi-EjctrReleaseMech-SllSht-SEPT-2023.pdf
[R.D. 232] A. [Anthony], “How Vehicle Mass Impacts Brake System Design,” Engineering Cheat Sheet, Apr. 25, 2025. [Online]. Available: https://engineeringcheatsheet.com/how-vehicle-mass-impacts-brake-system-design/
[R.D. 233] Space Voyaging, "Cruising on the Moon: The Apollo Lunar Roving Vehicle," Space Voyaging, Nov. 22, 2022. [Online]. Available: https://www.spacevoyaging.com/insights/2022/11/22/cruising-on-the-moon-the-apollo-lunar-roving-vehicle/
[R.D. 234] 3M. (2018). 3M™ Safety-Walk™ Slip-Resistant Materials: Technical Data Sheet (BA-18-26617). 3M Commercial Solutions Division
[R.D. 235] SRO. (2023). Rover ramp deployment system for Chandrayaan-3: Concept, design, development and operations. Indian Space Research Organisation
[R.D. 236] Moog Inc. (2022). Model 965 Rotary Servo Actuator: Technical Datasheet [PDF]. Moog Inc
[R.D. 237] WITTENSTEIN SE & Co. KG. (2023). Planetary Gear Box NP015S-MF1-10-1C1-1S: 1:10 reduction ratio [Datasheet]. Unibotech
[R.D. 238] CubeMars. (n.d.). AK80-8 actuator – High-performance robotic servo motor., Available: https://www.cubemars.com/goods-1151-AK80-8.html
[R.D. 239] WITTENSTEIN Inc. (2025). Planetary gearbox NP005S-MF1-4-0A1-1S: 1:4 reduction ratio [Datasheet]. WITTENSTEIN.
[R.D. 240] Beyond Gravity Schweiz AG. (2025, January). SEPTA36: Solar Array Drive Mechanism – Datasheet (Feb. 2025 version). Beyond Gravity Schweiz AG. Available: lahttps://beyondgravity.com
[R.D. 241] DuPont. (2017). Kevlar® Technical Guide. DuPont™ Kevlar®. Available: https://www.dupont.com/content/dam/dupont/ amer/us/en/personal-protection/public/documents/en/Kevlar_Technical_Guide.pdf
[R.D. 242] Stewart, A. C., & Hair, J. H. (2002, May). Intricacies of using Kevlar cord and thermal knives in a deployable release system: Issues and solutions (NASA/CP--2002-211506). Proceedings of the 36th Aerospace Mechanisms Symposium, NASA Glenn Research Center. Available: https://ntrs.nasa.gov/citations/20020087651
[R.D. 243] Moog Inc., “Type 33 Antenna Pointing Mechanism,” Moog Space and Defense Group, 2024. [Online]. Available: https://www.moog.com/products/space-mechanisms/antenna-pointing-mechanisms/type-33.html
[R.D. 244] Ensign-Bickford Aerospace & Defense Company, “TiNi™ Ejector Release Mechanisms: Family Technical Specifications,” Datasheet V3.4, September 2023. [Online]. Available: https://res.cloudinary.com/dbwyk3yk1/images/v1738540022/TiNi-EjctrReleaseMech-SllSht-SEPT-2023/TiNi-EjctrReleaseMech-SllSht-SEPT-2023.pdf
[R.D. 245] Jet Propulsion Laboratory, “Cooperative Autonomous Distributed Robotic Exploration (CADRE),” NASA, 2024. [Online]. Available: https://www.jpl.nasa.gov/missions/cadre/.
[R.D. 246] M. Saboia, F. Rossi, V. Nguyen, G. Lim, D. Aguilar and J.-P. de la Croix, “CADRE MoonDB: Distributed Database for Multi-Robot Information-Sharing and Map-Merging for Lunar Exploration,” in Proc. of the 23rd Int. Conf. on Autonomous Agents and Multiagent Systems (AAMAS 2024), Auckland, New Zealand, May 6–10, 2024.
[R.D. 247] Astrobotic Technology, *Peregrine Lunar Lander Payload User’s Guide*, Pittsburgh, PA, Oct. 2018.

[R.D. 248] D. Patrascu, “Europe Names the Builder of Its First-Ever Moon Lander,” autoevolution, 3 Feb. 2025.
[R.D. 249] Sun, Zezhou. *Technologies for Deep Space Exploration*. Springer, 2021.
[R.D. 250] *ALSEP Flight System Familiarization Manual*, Rev. B, Manned Spacecraft Center, Houston, Texas, 1969. [Online]. Available: https://www.lpi.usra.edu/lunar/ALSEP/pdf/FSFM_RevB.pdf
[R.D. 251] Ottimizzazione indiretta del consumo di propellente per un lander lunare con dinamica rotazionale, L.Casalino, A.Santoro, Polito, 2022
[R.D. 252] Fuel-optimal and Energy-optimal guidance schemes for lunar soft landing at a desired location N. Remesh , R.V. Ramanan, V.R. Lalithambika, June 2020
[R.D. 253] European Space Agency (ESA), “Argonaut Coordinate Frame Definition”, ESAE3P-EL3-TN-001, Issue 2, Revision 0, February 2023
[R.D. 254] Zhang, Shuo, et al. "Self-calibration of the stereo vision system of the Chang’e-3 lunar rover based on the bundle block adjustment." *ISPRS Journal of Photogrammetry and Remote Sensing* 128 (2017): 287-297.
[R.D. 255] SHETTY, Akash A., et al. Rover ramp deployment system for Chandrayaan-3: Concept, design, development and operations. *Acta Astronautica*, 2025, 229: 1-12.
[R.D. 256] Ross, Wong, et al. “VIPER Visible Imaging System”, 53rd Lunar and Planetary Science Conference, 2022.
[R.D. 257] Elphic, Shirley, et al. “The Volatiles Investigating Polar Exploration Rover (VIPER) Mission – Measurements and Constraints”, 52nd Lunar and Planetary Science Conference, 2021.
[R.D. 258] J. J. Biesiadecki and M. W. Maimone, "The Mars Exploration Rover surface mobility flight software driving ambition," *2006 IEEE Aerospace Conference*, Big Sky, MT, USA, 2006, pp. 15 pp.-, doi: 10.1109/AERO.2006.1655723.
[R.D. 259] Eisenman, Allan Read, et al. "Mars exploration rover engineering cameras." *Sensors, Systems, and Next-Generation Satellites V*. Vol. 4540. SPIE, 2001.
[R.D. 260] Farkasvölgyi, A., Csurgai-Horváth, L., & Bohácek, P. (2023). The evolution of lunar communication – From the beginning to the present. International Journal of Satellite Communications and Networking, 42:200–216.
[R.D. 261] Cosby, M., Tai, W. et al. (2022). The Future Lunar Communications Architecture. *Report of the Interagency Operations Advisory Group Lunar Communications Architecture Working Group*.
[R.D. 262] Flanegan, M., Gal-Edd, J. et al. (2008). NASA’s Lunar Communication and Navigation Architecture. *SpaceOps 2008 Conference*, AIAA 2008-3589.
[R.D. 263] Recommendation SFCG 32-2R5 (2023), Communication and positioning, navigation, and timing frequency allocations and sharing in the Lunar region, Space Frequency Coordination Group.
[R.D. 264] Serria, E., Gadhafi, R. et al. (2023), A Review of Lunar Communications and Antennas: Assessing Performance in the Context of Propagation and Radiation. Sensors, 23, 9832.
[R.D. 265] Bryant, S. (2009). Lunar Pole Illumination and Communications Maps Computed from Goldstone Solar System Radar Elevation Data. IPN Progress Report, 42-176 .
[R.D. 266] Sutoh, M., Hoshino, T., & Wakabayashi, S. (2017). Rover deployment system for lunar landing mission. *Acta Astronautica, 138*, 454–461.
[R.D. 267] Canadian Space Agency. (2009). *Canadarm2 and Dextre: The Mobile Servicing System on the ISS*. Available: https://www.asc-csa.gc.ca/eng/iss/canadarm2/
[R.D. 268] NASA. (2020). *Mars 2020 Perseverance Rover: Robotic Arm Overview*. Jet Propulsion Laboratory, California Institute of Technology. Available: https://mars.nasa.gov/mars2020/spacecraft/rover/robotic-arm/
[R.D. 269] T. C. Jones, “Lightweight Surface Manipulation System (LSMS) Technology Transfer Overview,” presented at the Fifth Technology Transfer Industry Day Addressing On-orbit Spacecraft Servicing, Assembly, and Manufacturing (OSAM), online, Sep. 22–23, 2020, NASA Tech. Rep. 20205006993.

[R.D. 270] J. T. Dorsey, “Lightweight Surface Manipulation System (LSMS): A Versatile Lifting Device for Planetary Surface Payload Handling, Excavation and Surface Construction,” Presentation, 1st Annual NASA Excavation and Construction Technology Program Review, Virtual/Applied Physics Lab, Maryland, Aug. 31–Sep. 1, 2021, NASA Tech. Rep. 20210020847.
[R.D. 271] T. C. Jones, “Lightweight Surface Manipulation System (LSMS) Technology Overview for Blue Origin,” Presentation to Blue Origin, Virtual, Aug. 21, 2020, NASA Tech. Rep. 20205006977.
[R.D. 272] PiriSafe, “DAVIT – Anchorage system for confined spaces,” datasheet, May 2024. [Online]. Available: https://pirisafe.com/wp-content/uploads/2024/05/DAVIT-Datasheet.pdf
[R.D. 273] Blue Origin - Blue Moon Overview (PDF): Available: https://www.blueorigin.com/blue-moon
[R.D. 274] Williams, J-P., et al. "The global surface temperatures of the Moon as measured by the Diviner Lunar Radiometer Experiment." Icarus 283 (2017): 300-325.
[R.D. 275] Schwadron, Nathan A., et al. "Lunar radiation environment and space weathering from the Cosmic Ray Telescope for the Effects of Radiation (CRaTER)." Journal of Geophysical Research: Planets 117.E12 (2012).
[R.D. 276] Xia, Qing, et al. "Distribution of charged lunar dust in the south polar region of the moon." Chinese Physics B 31.4 (2022): 045201.
[R.D. 277] Pokorný, Petr, et al. "Meteoroid bombardment of lunar poles." The Astrophysical Journal 894.2 (2020): 114.
[R.D. 278] Lee, Seungil, et al. "Stability and form-finding of shelters subjected to moonquakes of the lunar south polar region." Acta Astronautica (2025).
[R.D. 279] Bernhardt, H., M. S. Robinson, and A. K. Boyd. "Geomorphic map and science target identification on the Shackleton-de Gerlache ridge." Icarus 379 (2022): 114963.
[R.D. 280] Zhang, Shenyi, et al. "First measurements of the radiation dose on the lunar surface." *Science Advances* 6.39 (2020)
[R.D. 281] Christiansen, Eric L. *Meteoroid/debris shielding*. No. S-898. Houston: National Aeronautics and Space Administration, Lyndon B. Johnson Space Center, 2003
[R.D. 282] Wang, Ya-Chun, et al. "Electrodynamic dust shield efficiency characterization under UV in vacuum for lunar application." *Advances in Space Research* 74.11 (2024):
[R.D. 283] Walton, Otis R. "Adhesion of lunar dust." (2007).
[R.D. 284] Gaier, James R. *The effects of lunar dust on EVA systems during the Apollo missions*. No. NASA/TM-2005-213610/REV1. 2007
[R.D. 285] Patel, S., et al. "A comprehensive review on dust removal using electrodynamic shield: Mechanism, influencing factors, performance, and progress." *Renewable and Sustainable Energy Reviews* n183 ,2023
[R.D. 286] S. Ulamec, Patrick Michel, Matthias Grott, Ute Böttger. A rover for the JAXA MMX Mission to Phobos
[R.D. 287] NASA - Intrepid Planetary Mission Concept Study Report available: https://science.nasa.gov/wp-content/uploads/2023/11/lunar-intrepid.pdf
[R.D. 288] TENACIOUS Lunar Micro Rover, available: https://ispace-inc.com/news-en/?p=5593
[R.D. 289] Peter Berkelman, Mei Chen, Design of a Day/Night Lunar Rover 1995.

2 Table of Contents

3 Figures

4 Tables

Page intentionally left blank.

5 Abbreviations and acronyms

3GPP	3rd Generation Partnership Project
A.D.	Applicable Document
ADCS	Attitude Determination & Control Subsystem
AGL	Above Ground Level
AIR	Argonaut Integration Review
ALSEP	Apollo Lunar Surface Experiments Package
AMPERE	Autonomous Moon Power and Environmental Research Element
AOP	Argument Of Periapsis
APDL	Ansys Parametric Design Language
APR	Array Power Regulator
ATP	Authorization To Proceed
AWG	American Wire Gauge
BB	Braking Burn
BCM	Battery Charging Module
BDCR	Battery Discharge Charge Regulator
BER	Bit Error Rate
BMT	Breadboard Module Test
BoL	Beginning of Life
BRF	Body Reference Frame
BVP	Boundary Value Problem
C	Charging
CAD	Computed Aided Design
CADRE	Cooperative Autonomous Distributed Robotic Exploration
CBI	Complexity-Based cost Index
CDF	Concurrent Design Facility
CDR	Critical Design Review
CER	Cost Estimating Relationship
CFRP	Carbon Fiber Reinforced Polymer
CIVA	Comet Infrared and Visible Analyzer
CHS	Cratered Highlands Surface
CoG	Centre of Gravity
CoM	Centre of Mass
COM	Commissioning
COMSAT	Communication Satellite
ConOps	Concept of Operations
COSPAR	Committee on Space Research
COTS	Commercial Off-The-Shelf
CPE	Cargo Platform Element
CPU	Central Processing Unit
CRaTER	Cosmic Ray Telescope
CSS	Coarse Sun Sensor
D&L	Descent & Landing
DC	Day Charging
DC	Direct Current
DEM	Digital Elevation Model
DH	Data Handling
DM	Day Motion
DM	Development Model
DSN	Deep Space Network
DSRP	Deep Space Radiation Probe
DTE	Direct-to-Earth
DTM	Digital Terrain Model
DUS	Day Users Supply

EA	Evolutionary Algorithm
ECC	Eccentricity
ECCR	Eagle Critical Components Review
ECSM	European Charging Station for the Moon
ED	Eagle Deployment
EDD	Eagle Design Done
EDS	Electrodynamic Dust Shield
EDRS-C	European Data Relay System – Satellite C
EFM	Electrical and Functional Model
EGSD	Energy Generation, Storage & Distribution
ELFO	Elliptical Lunar Frozen Orbit
ELY	Electrolyser
EM	Engineering Model
EMC	Electromagnetic Compatibility
EMCR	Extended Mission Close-out Review
EoL	End-of-Life
EOL&D	End-of-Life & Disposal
EoM	End-of-Mission
E-PFM	Eagle PFM Test
EPRA	Expected Productivity Risk Analysis
EPS	Electrical Power Subsystem
EQM	Engineering Qualification Model
EQR	Eagle Qualification Review
ERM	Ejector Release Mechanism
ERSA	European Radiation Sensor Array
ESA	European Space Agency
ESR	Executive Summary Report
EVA	Extra Vehicular Activities
FAPEC	Fully Adaptive Prediction Error Coder
FC	Fuel Cell
FE	Finite Element
FEA	Finite Element Analysis
FFF	Form, Fit and Function
FLOAT	Flexible Levitation On A Track
FM	Flight Model
FOV	Field Of View
FRR	Flight Readiness Review
FSS	Fine Sun Sensor
GA	Genetic Algorithm
GCR	Galactic Cosmic Rays
GDOP	Geometric Dilution of Precision
GG	Gravity Gradient
GIADA	Grain Impact Analyzer and Dust Accumulator
GNC	Guidance, Navigation and Control
GNSS	Global Navigation Satellite System
GS	Ground Segment
HDA	Hazard Detection and Avoidance
HGA	High Gain Antenna
HP	Heat Pipe
HRTS	High-Resolution Temperature Sensor
HTO	Hohmann Transfer Orbit
I	Impact
IES	Ion and Electron Spectrometer
ICD	Interface Control Document

ILRS	International Lunar Research Station
IMU	Inertial Measurement Unit
INC	Inclination
INMS	Ion and Neutral Mass Spectrometer
IR	Infrared
iROSA	ISS Roll Out Solar Array
ISECG	International Space Exploration Coordination Group
ISRU	In Situ Resource Utilization
ISS	International Space Station
JAXA	Japan Aerospace Exploration Agency
JUICE	Jupiter Icy Moons Explorer
KSAT	Kongsberg Satellite Services
KoM	Kick-off Meeting
LCL	Latching Current Limiter
LCNS	Lunar Communication and Navigation Services
L	Likelihood
LDE	Lunar Descent Element
LED	Light Emitting Diode
LESSH	Lunar Experiment Support System and Handling
LGA	Low Gain Antenna
LGA	Low Gate
LHP	Loop Heat Pipe
LL	Lunar Landing
LLO	Low Lunar Orbit
LNCA	Lithiated Nickel Cobalt Aluminum
LO	Lunar Orbit
LOI	Lunar Orbit Insertion
LOLA	Lunar Orbiter Laser Altimeter
LoS	Line-of-Sight
LP	Langmuir Probe
LPM	Lunar Power Module
LPS	Lunar Payload System
LRO	Lunar Reconnaissance Orbiter
LRR	Launch Readiness Review
LRV	Lunar Roving Vehicle
LS	Landing Site
LS	Lunar Surface
LSM	Lunar Sensors Module
LSMS	Lightweight Surface Manipulation System
LSM-M	Lunar Sensor Module-Mobile
LSM-S	Lunar Sensor Module-Stationary
MAHLI	Mars Hand Land Imager
MC	Mission Constraint
MCI’	Moon-Centred Inertial primed
MCMF	Moon Centered Moon Fixed
MCR	Mission Close-out Review
MDR	Mission Definition Review
MEDA	Mars Environmental Dynamics Analyzer
MEMS	Micro Electronic Mechanical System
MERs	Mars Exploration Rovers
MFF	Moon Fixed Frame
MIDAS	Micro-Imaging Dust Analysis System
MISSE	Materials International Space Station Experiment
MLHP	Mechanical Loop Heat Pipe

MLI	Multi-Layer Insulation
MFF	Moon Fixed Frame
MOC	Mission Operation Center
MoM	Minute of Meeting
MPPT	Maximum Power Point Tracker
MPS	Main Power System
MSA	Membrane Solar Array
N/A	Not Applicable
NAVSAT	Navigation Satellite
NASA	National Aeronautics and Space Administration
NC	Night Charging
NDA	Non-Disclosure Agreement
NGRM	New Generation Radiation Monitor
NICM	NASA Instrument Cost Model
NIR	Near Infrared
NLP	Nonlinear Programming
NM	Night Motion
NO	Night Operations
NOMDOP	Nominal Day Operations
NOMNOP	Nominal Night Operations
NRS	Night Rover Supply
OBC	On-Board Computer
OBDH	On-Board Data Handling
OC	Onboard Charger
ORF	Orbiting Reference Frame
OCXO	Oven-Controlled Crystal Oscillator
PCDU	Power Control and Distribution Unit
PCM	Phase Changing Material
PD	Primary Deployment
PD	PDS Deployment
PDD	Powered Descent and Diverts
PDR	Preliminary Design Review
PDS	Payload Delivery System
PET	PDS EM Test
PEM	Proton Exchange Membrae
PF	Packaging Factor
PFM	Protoflight Model
PGA	Peak Ground Acceleration
PIE	Polar Ice Explorer
PITMS	Peregrine Ion-Trap Mass Spectrometer
PLB	Periselene Lowering Burn
PLI	Post Landing Initialization
PMD	Propellant Management Device
PMO	Primary Mission Objective
PNT	Position Navigation and Timing
PQR	PDS Qualification Review
PRR	Preliminary Requirements Review
PRT	Platinum Resistance Thermometer
PSR	Permanently Shadowed Region
PSHA	Probabilistic Seismic Hazard Analysis
PSR	Permanently Shadowed Region
PU	Pitch-Up
QAR	Qualification Review
QC	QuickCost

QJ	Quadruple Junction
RF	Radio Frequency
RAAN	Right Ascension of Ascending Node
RADFET	Radiation Sensing Field Effect Transistor
RADOM	Radiation Dose Monitoring
RAMBHA-LP	Radio Anatomy of Moon Bound Hypersensitive ionosphere and Atmosphere – Langmuir Probe
RC	Root Cause
R.D.	Reference Document
RDS	Rover Delivery System
RF	Radio Frequency
RFC	Regenerative Fuel Cell
RFCR	Regenerative Fuel Cell Regulator
RFCS	Regenerative Fuel Cell System
ROSA	Roll-Out Solar Array
RPC	Rosetta Plasma Consortium
RTD	Resistance Temperature Detector
RTG	Radio-Isotope Thermoelectric Generator
SA	Solar Array
SADE	Solar Array Drive Electronics
SADM	Solar Array Drive Mechanism
SCR	Solar Cosmic Rays
SD	Scott Deployment
SD	Secondary Deployment
SDD	Scott Design Done
SEE	Standard Error of Estimate
SMA	Semi-Major Axis
SMD	Space Mission Design
SME	Space Mission Engineering
SMLI	Smart-Multi-Layer Insulation
SMO	Secondary Mission Objective
SoC	State of Charge
SoW	Statement of Work
SPE	Solar Particle Event
S-PFM	Scott PFM Test
SPR	Shackleton Perched Rim
SQP	System Qualification Plan Approval
SQR	Scott Qualification Review
SRDS	Solar Radiation and Dust Sensor
SREM	Standard Radiation Environment Monitor
SRP	Solar Radiation Pressure
SRR	System Requirements Review
SSA	Steady State Analysis
SSPA	Solid State Power Amplifier
STM	Structural and Thermal Model
STR&MEC	Structures & Mechanisms
TA	True Anomaly
TBC	To Be Confirmed
TC	Telecommand
TCS	Thermal Control Subsystem
TDD	Time Division Duplexing
TIE	Technical Implementation Effort
TM	Telemetry
TOA	Time Of Arrival

TR	Power Transmitter
TRL	Technology Readiness Level
TRR	Test Readiness Review
TT&C	Telemetry, Tracking & Command
TV	Television
UFPC	Ultra Fast Proximity Charger
UHF	Ultra High Frequency
UTC	Universal Time Coordinated
UV	Ultraviolet
VDA	Vacuum-Deposited Aluminium
VDL	Vertical Descent and Landing
VGA	Vertical Gate
VIPER	Volatiles Investigating Polar Exploration Rover
WBS	Work Breakdown Structure
WCC	Worst Case Cold
WCH	Worst Case Hot
WP	Work Package
WPD	Work Package Description
WSL	Work Study Logic
YoY	Year over Year

6 Abstract

The Autonomous Moon Power and Environmental Research Element (AMPERE) mission represents a pioneering initiative within European Space Agency's (ESA) Argonaut program to establish sustainable energy infrastructure on the lunar surface, capitalizing on the Lunar Descent Element (LDE) capabilities to address the growing energy demands of future lunar operations and scientific activities. The purpose of this document is to outline the primary requirements and preliminary design for the Lunar Payload System (LPS), designed for deployment via the ESA Argonaut lander platform. The mission objectives centre on the development and deployment of an autonomous demonstrative power station, capable of generating and storing energy, as well as recharging external lunar users through a robust and modular architecture. The LPS comprises three integrated modules: the Payload Delivery System (PDS) module, the Eagle module, which houses the effective power station and the Scott module, serving as the representative external user interface and validation system for the overall architecture. This preliminary design phase establishes critical operational parameters including power generation capacity, energy storage requirements, thermal management systems and communication protocols necessary for autonomous operation in the lunar environment. The modular approach ensures system scalability and adaptability to evolving mission requirements while maintaining reliability in the harsh lunar conditions, characterized by extreme temperature variations, vacuum exposure and extended periods of solar eclipse. The Scott module implementation provides a concrete validation framework for the energy distribution architecture, demonstrating the system's capability to support diverse external payloads and user requirements within the 800 kg mass constraint and 2.0 x 2.0 x 1.8 m^3 volume limitations of the LPS. Eventually, AMPERE mission also aims to comply with Committee on Space Research's (COSPAR) Planetary Protection Policy by implementing, at the end-of-life, material reuse and recycling strategies, ensuring alignment with sustainability objectives and long-term environmental responsibility. This PRR establishes preliminary requirements aligned with ESA's post-2035 lunar exploration strategy, contributing to the long-term vision of autonomous lunar energy infrastructure and sustainable surface operations that support scientific endeavours and future permanent lunar settlements.

7 Introduction

7.1 General

This document represents the final deliverable (D1) of the study conducted by the AMPERE team within the framework of the Space Mission Design (SMD) 2025 course at University of Naples Federico II. To ensure a structured and comprehensive presentation of the methodological approach and technical analyses, the document is organized into sections and subsections, following a logical order.

7.2 Scope

The present document provides a comprehensive overview of the study conducted to define the concept of AMPERE Mission, developed to address to the tasks outlined in the Statement of Work (SoW) [A.D. 1]. The activities pertain to the domains of Project Management, Space Systems Engineering and Design & Engineering.
Section 8 presents an overview of the project organization, including the Work Breakdown Structure (WBS), Work Package Descriptions (WPDs), Gantt chart, the team description, organizational chart, the Work Study Logic (WSL), as well as an assessment of risks, reliability, and costs analyses.
Section 9 responds to Task 1 (*Scientific Needs, Constraints, and Mission Requirements*), providing the identification of researchers and scientific community needs, the definition of the mission objectives, the assessment of the scientific requirements and constraints and the allocation of the mission requirements.
Section 10 addresses Task 2 (*System Architecture and Overall Feasibility*) by proposing different mission architectures, which include the definition of the landing site, the lunar surface segment, and the Concept of Operations (ConOps), evaluating their feasibility, and selecting the most suitable one by means of a trade-off analysis. System model philosophy and related hardware matrix, the master schedule, and the assessment of the requirements at system and segment level, up to subsystem level where necessary are produced as well.
In Section 11, Task 3 (*Space Segment and Lunar Payload Design*) is discussed, focusing on the preliminary design and sizing of the LPS and its subsystems, the required technologies, and their Technology Readiness Level (TRL). Mission and systems modes are detailed, and budgets are determined.
Finally, Section 12 is dedicated to Task 4 (*End-of-Mission Planning and Impact Assessment*), analysing disposal strategies and assessing their feasibility, benefits and compliance with applicable regulations [A.D. 2], [A.D. 3].

7.3 Purpose

The document is intended to support the feasibility assessment and preliminary design of a European lunar mission within the ESA's Argonaut's programme. AMPERE mission will utilize the Argonaut's LDE during the descent and landing from the Low Lunar Orbit (LLO), deploying a demonstrative power station, called Lunar Power Module (LPM), at the South Pole of the Moon from the Cargo Platform Element (CPE), also part of Argonaut. If successful, the LPM could serve future exploration missions and establish a foundation for extended lunar operations. Moreover, the payload will include environmental sensors, Lunar Sensors Module (LSM), to monitor the illumination and characterize the radiative and thermal environment, both to ensure the operational viability of the LPM and to assess the potential habitability of the area. The AMPERE mission aligns with ESA's objectives for sustainable and scalable lunar exploration beyond 2035, optimizing european resources in the pursuit of long-term lunar infrastructure.

8 Project organization and management

The following subsections provide an overview of the team organization and project work schedule, including the WBS, WPDs, Gantt chart, organizational chart, and WSL.

8.1 WBS and Work Logic

Figure 8.1 displays AMPERE's WBS. This is structured following three vertical nodes that are *Management*, *Space Systems Engineering* and *Design & Engineering*, which contain 12 Work Packages (WPs) that will cover specific aspects of the mission. Each WP has a responsible that refers to the corresponding chief for clear communication.

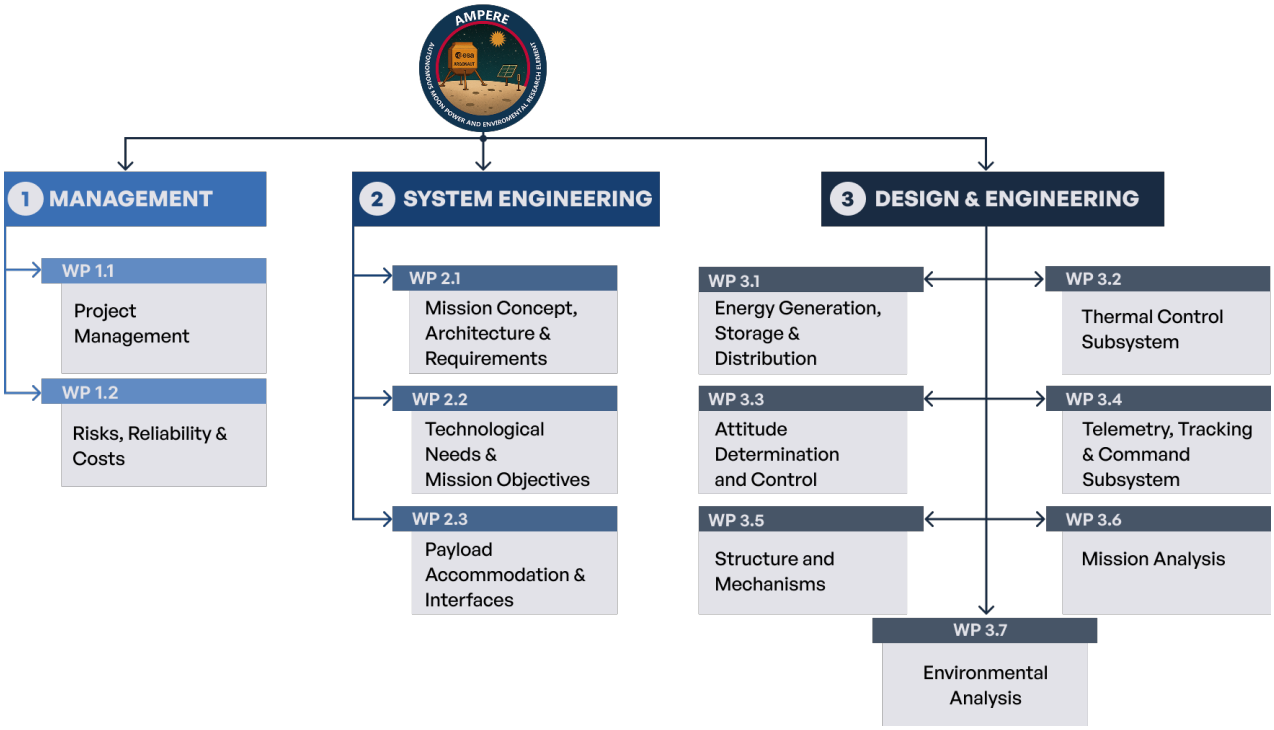

Figure 8.1: WBS

Figure 8.2 shows instead the project WSL, that guides the project work from an Initial Mission Concept Exploration phase up to the final Design Phase. All the WPs are connected to each other to ensure a robust feedback loop. This will allow the team to easily perform trade-offs.
The Platform Design area (right quadrant) delineates the technical subsystems critical to the LPM's functionality with the Energy Generation, Storage & Distribution (EGSD) at its core.
Simultaneously, the Detailed Development block describes the design process in a broader sense, also considering mission analysis, environmental analysis, how the payload is allocated to the CPE and the structures.

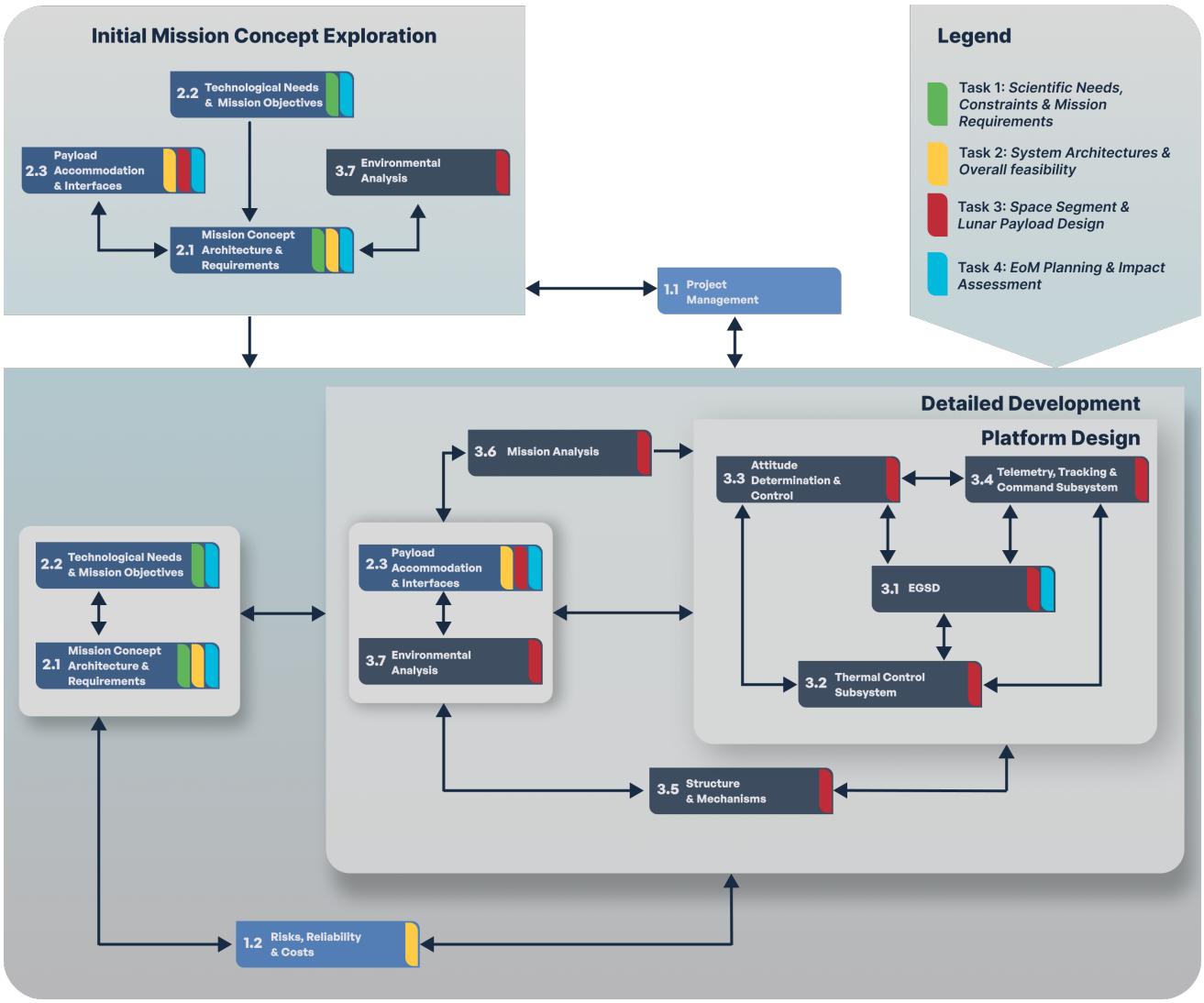

Figure 8.2: WSL

8.2 WPD

This Section provides a description of the already cited WPs that will be covered in the AMPERE mission.

8.2.1 Management

This Section reports the WPDs for the Management area which are detailed in Table 8.1 and Table 8.2. The objective of this area is to organize the teamwork and project timeline, assuring that every task is completed in due time. Also, risks and costs analyses of the mission are performed. This node is under the responsibility of the chief Niro Antonio.

WORK PACKAGE DESCRIPTION		
Project: AMPERE		
Work Package Title: Project Management	Work Package ID: WP 1.1	Responsible: NIRO Antonio
Start Event: Kick-off Meeting (KoM)	End Event: Preliminary Requirements Review (PRR)	
Start Date: T0	End Date: T0 + 83 days	
OBJECTIVES - Ensuring the successful accomplishment of the space mission objectives within the defined timeframe and budget constraints - Delivering the necessary documentation for the Mission Definition Review (MDR) and PRR within the prefixed deadlines - Coordination of all the activities carried out by the team - Coordination and allocation of team members, based on project needs - Scheduling and documentation of meetings in a proper and efficient way		
INPUTS - *SoW* [A.D. 1] - *ECSS-M ST-10C* [A.D. 4] - *Open literature* - *Feedbacks and inputs from all other WPs* - *Customer needs*		
TASKS DESCRIPTION TASK 1.1.1 – Timeline management - Development and adherence to a detailed project schedule to ensure timely completion of key milestones and deliverables TASK 1.1.2 – Project management - Monitoring and supervision of project activities, ensuring coordination between all the team members TASK 1.1.3 – Document and reports - Maintenance of comprehensive documentation of project activities, decisions and outcomes - Definition and preparation of the expected deliverables including Executive Summary Report (ESR), intermediate, final and candidate individual presentations, and design to be presented to the Customer - Drafting of the Minutes of Meetings (MoMs) TASK 1.1.4 – Human resources allocation - Optimization of the allocation of human resources to optimize the project and mitigate any resource constraint		
EXCLUDED TASKS - Drafting of documents and deliverables assigned to other WPs		
OUTPUTS and DELIVERABLES - *Definition of project Gantt, WBS, WSL, organizational chart, WPDs* - *ESR* - *Intermediate and final presentations* - *MoMs* - *Management of the project* - *Management of the internal meetings* - *Configuration and organization definition* - *Contribution to Section 8 of the ESR*		

Table 8.1: Project Management WPD

WORK PACKAGE DESCRIPTION		
Project: AMPERE		
Work Package Title: Risks, Reliability & Costs	Work Package ID: WP 1.2	Responsible: PALOMBA Gabriele
Start Event: KoM	End Event: Not Applicable (N/A)	
Start Date: T0	End Date: T0 + 75 days	
OBJECTIVES - Identification and mitigation of mission-related risks - Estimation and maximization of system and subsystems' reliability - Assessment and minimization of the costs, ensuring budgetary considerations are accounted for throughout the planning process		
INPUTS - *SoW* [A.D. 1] - *Open literature* - *R.D.s from* [R.D. 1] *to* [R.D. 4] - *ECSS-M-ST-80C* [A.D. 5] - *ECSS-M-ST 60C* [A.D. 6] - *Lessons learned databases* - *Inputs from all the other WPs*		
TASKS DESCRIPTION TASK 1.2.1 – Risk analysis - Identification of implementation and mission risks - Identification of risks that may arise during the mission design phases - Quantitative assessments of risks for different mission concept proposals - Evaluation of risks for the selected mission concept and design - Monitoring and mitigation of risks via suitable models and tools, including but not limited to fever charts TASK 1.2.2 – Reliability analysis - Identification of standards, models and tools suited for reliability evaluation - Preliminary reliability assessment, at system and subsystem level, of the proposed mission concepts - Refinement of the system's reliability estimate for the selected mission concept and architecture - Modification or refinement of the conducted reliability evaluation following the evolution of the mission design TASK 1.2.3 – Costs evaluation - Definition of models that will be used for costs evaluation - Estimation of costs for the different architectures - Comparison of the proposed concepts based on different cost estimates - Support to the design phases via cost analysis-based suggestions - Refinement of the costs estimate of the mission concept and architecture		
EXCLUDED TASKS - None		
OUTPUTS and DELIVERABLES - *Risk management plan* - *Fever chart* - *Reliability estimate* - *Costs estimates* - *Contribution to Task 2* - *Contribution to Section 10 of the ESR*		

Table 8.2: Risks, Reliability & Costs WPD

8.2.2 Space Systems Engineering

This Section reports the WPDs for the Space Systems Engineering area which are detailed in Table 8.3, Table 8.4 and Table 8.5. This node is under the responsibility of the chief Biscardi Valeria.

WORK PACKAGE DESCRIPTION		
Project: AMPERE		
Work Package Title: Mission Concept, Architecture and Requirements	Work Package ID: WP 2.1	Responsible: GAGLIARDI Antonio
Start Event: KoM	End Event: N/A	
Start Date: T0	End Date: T0 + 78 days	
OBJECTIVES - Development of alternative system architectures and mission concepts - Definition of the final mission concept related to the chosen architecture - Definition of requirements to ensure mission feasibility		
INPUTS - *SoW* [A.D. 1] - *Open literature* - *R.D.s from* [R.D. 3] *to* [R.D. 10] - *ECSS E-ST-10C* [A.D. 7] - *ECSS-E-ST-10 06C* [A.D. 8] - *Inputs from WPs 1.2, 2.2, 2.3, 3.1, 3.2, 3.3, 3.4, 3.5, 3.6, 3.7*		
TASKS DESCRIPTION TASK 2.1.1 – Mission concept and architecture exploration - Analysis of mission objectives and constraints - Definition of preliminary mission requirements, considering environmental conditions and technological constraints - Development and assessment of alternative architectures, ensuring compatibility with lunar environment TASK 2.1.2 – Trade-off analysis and concept selection - Identification of key system drivers and critical requirements - Trade-off analysis between different architectures - Selection of the optimal mission concept that best aligns with the mission objectives, guaranteeing the integration with ESA Argonaut lander TASK 2.1.3 – Requirements and ConOps Definition - Allocation of the mission-level, segment-level, system-level and subsystem-level requirements for CPE and LPS - Allocation of subsystem-level requirements for CPE and LPS - Identification of the ConOps and operational modes, including deployment, nominal operation, maintenance, potential expansion scenarios - Definition of the master schedule		
EXCLUDED TASKS - Definition of the model philosophy and hardware matrix		
OUTPUTS and DELIVERABLES - *Mission concepts proposal* - *Platform architectures proposal* - *Trade-off analysis of architectures* - *Final mission concept selection* - *Final requirements list* - *Operational modes* - *Master schedule* - *Contribution to Tasks 1, 2, 4 of the SoW* - *Contribution to Sections 9, 10 and 12 of the ESR*		

Table 8.3: Mission Concept, Architecture and Requirements WPD

WORK PACKAGE DESCRIPTION		
Project: AMPERE		
Work Package Title: Technological Needs & Mission Objectives	Work Package ID: WP 2.2	Responsible: MANZO Annarita
Start Event: KoM	End Event: N/A	
Start Date: T0	End Date: T0 + 75 days	
OBJECTIVES - Definition of possible and final landing site - Identification of technological needs and potential users - Definition of mission objectives and constraints		
INPUTS - *SoW* [A.D. 1] - *Open literature* - *R.D.s* [R.D. 3], [R.D. 4]*, from* [R.D. 6] *to* [R.D. 10]*, from* [R.D. 12] *to* [R.D. 17] - *Inputs from WPs 2.1, 3.7*		
TASKS DESCRIPTION TASK 2.2.1 – Definition of mission objectives - Definition of primary mission objectives - Definition of any potential secondary mission objective TASK 2.2.2 – Technological needs - Individuation of the potential users' power needs for future lunar human activities - Identification of the needs to validate and enhance the lunar environment knowledge TASK 2.2.3 – Definition of landing site - Preliminary assessment of lunar topography, leading to the selection of South Pole as the most suitable area for mission feasibility - Research of any potential landing site, in relation to Task 2.2.2 analysis - Definition of the final landing site based on environmental assessment TASK 2.2.4 – End-of-Mission (EoM) planning and impact assessment - Analysis of the impact of the mission on future lunar activities, as reported in the SoW TASK 2.2.5 – Constraints - Definition of mission constraints		
EXCLUDED TASKS - Environmental analysis of the landing site		
OUTPUTS and DELIVERABLES - *Definition of mission objectives* - *Definition of technological needs* - *Definition of the landing site* - *Definition of constraints* - *Guidance to the definition of the LPS architecture* - *Contribution to Tasks 1 and 4 of the SoW* - *Contribution to Sections 9 and 12 of the ESR*		

Table 8.4: Technological needs & mission objectives WPD

<table>
<tr><th colspan="3">WORK PACKAGE DESCRIPTION</th></tr>
<tr><td colspan="3">Project: AMPERE</td></tr>
<tr><td>Work Package Title: Payload Accommodation & Interfaces</td><td>Work Package ID: WP 2.3</td><td>Responsible: PETRONE Andrea</td></tr>
<tr><td>Start Event: KoM</td><td colspan="2">End Event: N/A</td></tr>
<tr><td>Start Date: T0</td><td colspan="2">End Date: T0 + 75 days</td></tr>
<tr><td colspan="3">OBJECTIVES
- Preliminary selection and performance assessment of the LSM
- Analysis of the LPS interface with the LDE as input to design activities
- Ensuring proper accommodation and functioning of the LPS on the CPE
- Definition of the LPS operations scheme
- Model philosophy and hardware matrix definition</td></tr>
<tr><td colspan="3">INPUTS
- SoW [A.D. 1]
- Open literature
- A.D.s from [A.D. 9] to [A.D. 14]
- R.D.s [R.D. 3], [R.D. 4], [R.D. 8], [R.D. 11], [R.D. 12], [R.D. 18], [R.D. 19], [R.D. 21], [R.D. 22]
- Inputs from WPs 2.1, 2.2, 3.1, 3.2, 3.3, 3.4, 3.5, 3.7</td></tr>
<tr><td colspan="3">TASKS DESCRIPTION
TASK 2.3.1 – Preliminary literature exploration
- Analysis of documentation from previous missions with similar payloads and discrimination between possible candidates
TASK 2.3.2 – Secondary payload (LSM) selection
- Definition of the ideal set of secondary payloads, according to technological needs, through a trade-off analysis
- Selection of hardware and software solutions available on the market, based on volume and power constraints
- TRL definition of the selected secondary payload components
TASK 2.3.3 – LPS accommodation and interfaces management
- Ensuring compliance with the defined functional and mechanical interface between LPS and LDE
- Providing for the spatial arrangement and configuration of the LPS on the CPE, as input to WP 3.5
- Compliance with volume, mass and positioning constraints, exploiting inputs from design WPs to ensure balance between platform elements
- Identification of the operations to be carried out by the LPS components
TASK 2.3.4 – Model philosophy and hardware matrix definition
- Selection of the type of model philosophy for each component based on costs, quality and risks considerations, including the depth of verification and test spectrum
- Collection of data from other WPs to compile the hardware matrix</td></tr>
<tr><td colspan="3">EXCLUDED TASKS
- Structural analysis of LPS</td></tr>
<tr><td colspan="3">OUTPUTS and DELIVERABLES
- Detailed list of LPS components
- Components allocation and location requirements overview
- Definition of LPS accommodation on the CPE
- Validation of LPS interface with the LDE
- Mass and volume constraints check
- TRL assessment of the LSM
- Model philosophy for each component
- Hardware matrix
- Contribution to Tasks 2, 3 and 4 of the SoW
- Contribution to Sections 10, 11 and 12 of the ESR</td></tr>
</table>

Table 8.5: Payload Accommodation & Interfaces WPD

8.2.3 Design and Engineering

This Section reports the WPDs for the Design and Engineering area which are detailed from Table 8.6 to Table 8.12 . This node is under the responsibility of the design chief Guerriero Antonio.

WORK PACKAGE DESCRIPTION		
Project: AMPERE		
Work Package Title: Energy Generation, Storage & Distribution	Work Package ID: WP 3.1	Responsible: VELLECCO Francesca
Start Event: N/A	End Event: N/A	
Start Date: T0 + 14 days	End Date: T0 + 75 days	
OBJECTIVES - Preliminary design of multiple possible Electrical Power Subsystem (EPS) and LPM solutions - Design and implementation of efficient power management systems to ensure continuous operations under all conditions including nighttime periods		
INPUTS - *SoW* [A.D. 1] - *Open literature* - *R.D.s* [R.D. 3],[R.D. 4], [R.D. 7], [R.D. 8] - Inputs from WPs 2.1, 2.2, 2.3, 3.2, 3.3, 3.4, 3.5, 3.6, 3.7		
TASKS DESCRIPTION TASK 3.1.1 – Power needs analysis - Evaluation of power needs of the LPS's subsystems during each mission phase - Evaluation of power needs of the LPM and of the LSM during each mission phase - Review of LDE power distribution capabilities until deployment TASK 3.1.2 - Preliminary architectures evaluation - Review of available design solutions selected in past missions and mission studies - Analysis of different LPM architectures to satisfy both subsystems and user needs - Analysis of EPS solutions with a focus on Power Control and Distribution Unit (PCDU) - Selection and sizing of LPM and EPS components considering subsystems and user needs TASK 3.1.3 – Final design - Final selection of the LPM components based on previous analysis - Final selection of EPS hardware components - TRL definition		
EXCLUDED TASKS - Selection of the landing site		
OUTPUTS and DELIVERABLES - *EPS solution* - *LPM architecture* - *EPS and LPM TRL assessment* - *Power budget* - *Mass budget of the EPS and of the LPM* - *Contribution to Tasks 3 and 4 of the SoW* - *Contribution to Sections 11 and 12 of the ESR*		

Table 8.6: Energy Generation, Storage & Distribution WPD

WORK PACKAGE DESCRIPTION		
Project: AMPERE		
Work Package Title: Thermal Control Subsystem (TCS)	Work Package ID: WP 3.2	Responsible: PANICO Gaetano
Start Event: N/A	End Event: N/A	
Start Date: T0 + 18 days	End Date: T0 + 75 days	
OBJECTIVES - Preliminary analysis of operative temperature ranges and margins - Evaluation of thermal equilibrium analysis - Design of the thermal control subsystem		
INPUTS - *SoW* [A.D. 1] - *Open literature* - *R.D.s* [R.D. 3], [R.D. 25] - *Inputs from WPs 2.1, 2.2, 2.3, 3.1, 3.3, 3.4, 3.5, 3.6, 3.7*		
TASKS DESCRIPTION TASK 3.2.1 – Thermal assessment of LDE - Review of available TCS solutions selected in past missions and mission studies - Definition of thermal inputs during LLO phase, descent and landing - Verification of a thermal equilibrium analysis, at least Worst Case Hot (WCH) and Worst Case Cold (WCC), considering LDE's TCS - Definition of any complementary thermal devices to the LDE's TCS, if deemed necessary TASK 3.2.2 – Thermal analysis and design for LPS - Definition of thermal inputs for LPS - Conduction of a thermal equilibrium analysis (at least WCH and WCC) for LPS - Selection and definition of any potential thermal control devices for LPS TASK 3.2.3 – TCS design - Preliminary estimation of TCS mass, volume and power - TRL definition		
EXCLUDED TASKS - None		
OUTPUTS and DELIVERABLES - *Verification of LDE's TCS* - *Evaluation of operating temperatures for LPS* - *TCS mass, size and power budgets* - *TCS TRL assessment* - *Contribution to Task 3 of the SoW* - *Contribution to Section 11 of the ESR*		

Table 8.7: Thermal Control Subsystem WPD

WORK PACKAGE DESCRIPTION		
Project: AMPERE		
Work Package Title: Attitude Determination & Control Subsystem (ADCS)	Work Package ID: WP 3.3	Responsible: FIENGO Imma Francesca
Start Event: N/A	End Event: N/A	
Start Date: T0 + 18 days	End Date: T0 + 75 days	
OBJECTIVES - Investigation of the LPS ADCS for the deployment and the operational phase		
INPUTS - *SoW* [A.D. 1] - *Open literature* - *A.D.* [A.D. 9] - *R.D.* [R.D. 3] - *Inputs from WPs 2.1, 2.2, 2.3, 3.1, 3.2, 3.4, 3.5, 3.6, 3.7*		
TASKS DESCRIPTION TASK 3.3.1 – Initial analysis - Review of available ADCS solutions selected in past missions and mission studies - Investigation of mission phases relevant for ADCS - Identification of control modes based on mission phases - Definition of attitude constraints and pointing requirements for each control mode - Evaluation of expected internal and external disturbance torques affecting the attitude in each phase TASK 3.3.2 – Post-landing attitude determination and control for the LPS and hardware selection - Identification of potential critical points during the LPS deployment - Identification of attitude stability or damping mechanisms during and after the LPS deployment, if deemed necessary - Definition of initial attitude acquisition strategies post-deployment - Sizing and selection of attitude sensors and actuators compatible with the defined needs during the LPS operations, if deemed necessary TASK 3.3.3 – ADCS design - Refinement of the baseline design of the ADCS - Estimation of ADCS components mass, size and power demand - TRL definition		
EXCLUDED TASKS - Design and development of the LDE's ADCS		
OUTPUTS and DELIVERABLES - *Post-deployment attitude acquisition and control strategy for the LPS* - *ADCS mass, size and power demand* - *ADCS TRL assessment* - *Contribution to Task 3 of the SoW* - *Contribution to Section 11 of the ESR*		

Table 8.8: Attitude Determination & Control Subsystem WPD

WORK PACKAGE DESCRIPTION		
Project: AMPERE		
Work Package Title: Telemetry, Tracking & Command (TT&C) Subsystem	Work Package ID: WP 3.4	Responsible: CIRILLO Andrea
Start Event: N/A	End Event: N/A	
Start Date: T0 + 18 days	End Date: T0 + 75 days	
OBJECTIVES - Ensuring robust, continuous, and reliable communication links between the mission elements and the Ground Segment (GS) - Definition of the preliminary design of the TT&C subsystem - Guarantee of proper data management and transmission		
INPUTS - *SoW* [A.D. 1] - *Open literature* - *R.D.s* [R.D. 3], *from* [R.D. 26] *to* [R.D. 30] - *Inputs from 2.1, 2.2, 2.3, 3.1, 3.2, 3.3, 3.5, 3.6, 3.7*		
TASKS DESCRIPTION TASK 3.4.1 – GS Analysis - Evaluation of the current performances and capabilities of Moonlight telecommunication services and eventually deep space telecommunication networks - Evaluation and comparison of different possible communication architectures exploited from literature - Analysis and assessment of LDE communication capabilities in support of the operations during LLO, descent and landing phases - Selection of adequate GS for mission operation - Coverage analysis to ensure reliable communications TASK 3.4.2 – LPS On-Board Computer (OBC) selection and Data Handling (DH) considerations - Selection of the OBC, considering mission operational, processing, and communication needs - Estimation of data volumes - Considerations on memory requirements, DH protocols and data management strategies - TRL definition TASK 3.4.3 – LPS TT&C subsystem design - Selection of hardware and architecture to communicate during operational phase - Definition of the configuration of the TT&C Subsystem - Link budget and link margin calculations and performance assessment - Estimation of power consumption and TT&C mass budget - TRL definition		
EXCLUDED TASKS - None		
OUTPUTS and DELIVERABLES - *TT&C and On-Board Data Handling (OBDH) mass and power budgets* - *Link budget and link margins* - *Data volumes and data rate* - *TT&C preliminary design* - *OBC selection* - *GS selection* - *TT&C and OBC TRL assessment* - *Contribution to Task 3 of the SoW* - *Contribution to Section 11 of the ESR*		

Table 8.9: Telemetry, Tracking & Command Subsystem WPD

WORK PACKAGE DESCRIPTION		
Project: AMPERE		
Work Package Title: Structure & Mechanisms (STR&MEC)	Work Package ID: WP 3.5	Responsible: GARCÍA PALOMARES Enrique
Start Event: N/A	End Event: N/A	
Start Date: T0 + 18 days	End Date: T0 + 75 days	
OBJECTIVES - Design of the structure and mechanisms to ensure the LPS integration on the CPE, its deployments and its proper functioning during all the operational phases - Preliminary estimation of the required inertia matrices, masses, volumes, and centres of gravity positions - Realization of a preliminary 3D model of the entire platform		
INPUTS - *SoW* [A.D. 1] - *Open literature* - *R.D.s* [R.D. 3], [R.D. 32] - *Ariane 6 constraints* [A.D. 12] - *Argonaut constraints* [A.D. 9] - *Inputs from WPs 2.1, 2.2, 2.3, 3.1, 3.2, 3.3, 3.4, 3.6, 3.7*		
TASKS DESCRIPTION TASK 3.5.1 - Preliminary structural analysis - Investigation of the previous and current solutions in similar missions - Verification of the compliance to the interface requirements of the selected launcher - Preliminary analysis of the loads operating on the structure in each mission phase TASK 3.5.2 - Mechanisms preliminary analysis - Preliminary design of the mechanisms required to integrate the LPS on the CPE and to deploy the LPS, exploiting inputs from WP 2.3 about interfaces - Preliminary design and definition of the required mechanisms for the LPS - Preliminary estimation of the power and mass budgets of the mechanisms TASK 3.5.3 - Platform overview model - Realization of a preliminary model of each LPS component - Realization of a preliminary 3D model of the entire platform, considering both the configuration of LPS on the CPE and the LPS itself, once deployed - Preliminary estimation of Centres of Gravity (CoG) and inertia matrices - TRL definition		
EXCLUDED TASKS - None		
OUTPUTS and DELIVERABLES - *Loads overview* - *Structure and mechanisms design* - *Structure mass budget* - *Mechanisms mass and power demand* - *Structure and mechanisms TRL assessment* - *CoG and inertia estimation* - *Contribution to Task 3 of the SoW* - *Contribution to Section 11 of the ESR*		

Table 8.10: Structure & Mechanisms WPD

WORK PACKAGE DESCRIPTION		
Project: AMPERE		
Work Package Title: Mission Analysis	Work Package ID: WP 3.6	Responsible: GIANNITTI Matteo
Start Event: N/A	End Event: N/A	
Start Date: T0 + 18 days	End Date: T0 + 75 days	
OBJECTIVES - Achievement of a soft landing on the lunar surface from LLO, while complying with the propulsion capabilities of the LDE and respecting acceleration constraints		
INPUTS - *SoW* [A.D. 1] - *Open literature* - *A.D.* [A.D. 9] - *R.D.s* [R.D. 3], [R.D. 8]*, from* [R.D. 30] *to* [R.D. 37] - *Inputs from WPs 2.1, 2.2, 2.3, 3.3, 3.7*		
TASKS DESCRIPTION TASK 3.6.1 – Landing strategy and trajectory design - Review of available solutions selected in past missions and mission studies - Analysis of possible trajectories to land at the site identified by WP 2.2 - Trajectory optimization - Thrust profile analysis - Acceleration analysis - Delta-V analysis TASK 3.6.2 - Trajectory compliance with LDE's capabilities assessment - Verification of the capability of the LDE to provide the required thrust and delta-V - Identification of potential critical points where thrust, or delta-V requirements exceed the LDE's capabilities - Proposal of adjustments to the trajectory and thrust profile to ensure compliance with LDE's capabilities TASK 3.6.3 - Acceleration profile compliance assessment - Verification of the acceleration profile remaining within the allowable limits for the mission - Identification of potential critical points where accelerations might exceed the constraints - Proposal of adjustments to the trajectory and thrust profile to ensure compliance		
EXCLUDED TASKS - Landing site definition - Design and development of the LDE's propulsion system		
OUTPUTS and DELIVERABLES - *Descent and landing optimal trajectory* - *Delta-V budget* - *Thrust profile and acceleration plots* - *Demonstration of the compliance of the trajectory with LDE capabilities* - *Demonstration of the compliance of the acceleration profile with mission constraints* - *Contribution to Task 3 of the SoW* - *Contribution to Section 11 of the ESR*		

Table 8.11: Mission Analysis WPD

WORK PACKAGE DESCRIPTION		
Project: AMPERE		
Work Package Title: Environmental Analysis	Work Package ID: WP 3.7	Responsible: RUSSO Francesco Antonio Aldo
Start Event: N/A	End Event: N/A	
Start Date: T0 + 14 days	End Date: T0 + 75 days	
OBJECTIVES - Analysis of environmental conditions for all the possible landing sites provided by system area - Environmental characterization of the final landing site - Definition of LPS, CPE factors which can affect mission success - Guarantee of a strong information flow between all the subsystems in terms of environment		
INPUTS - *SoW* [A.D. 1] - *Open literature* - *R.D.s* [R.D. 3], [R.D. 7], [R.D. 8], [R.D. 11], [R.D. 25], [R.D. 38], [R.D. 39] - *Inputs and feedbacks from WPs 2.1, 2.2, 2.3, 3.1, 3.2, 3.3, 3.4, 3.5, 3.6*		
TASKS DESCRIPTION TASK 3.7.1 - External environment analysis - Environmental analysis of possible landing sites provided by WP 2.2, to enhance criticalities of each proposal as a support for the final choice - Characterization of the crucial environmental factors of the final landing site, provided by WP 2.2, including dust and regolith effects - Ensuring that WP 3.6 properly accounts for the effects of the external environment during critical phases - Evaluation of environmental impact for future human activities TASK 3.7.2 - Effects of environment on the LPS - Check of the environmental effects on the LPS during the operative phase, with a focus on illumination conditions, radiations and thermal profile - Support for the TCS in determining appropriate sizing based on environmental conditions - Global checking with all the other subsystems		
EXCLUDED TASKS - Final landing site selection		
OUTPUTS and DELIVERABLES - *Environmental analysis of possible landing sites* - *Environmental analysis of final landing site* - *Validation of the LPS with respect to the environment* - *Contribution to the evaluation of the mission lifetime* - *Contribution to Task 3 of the SoW* - *Contribution to Section 11 of ESR*		

Table 8.12: Environmental Analysis WPD

8.3 Gantt

This Section presents the AMPERE project Gantt Chart in Figure 8.3, illustrating the scheduled timeline for all the WPs and key milestones. The project is organized into Management, Space Systems Engineering, and Design & Engineering categories. Management activities run the full project duration (April-June 2025) to ensure continuous oversight. System Engineering begins with the KoM, establishing the mission concept and requirements that guide all technical work. Design & Engineering activities commence in the last week of April, with all subsystem WPs running in parallel and concluding last week of June. Two critical milestones anchor the project: the MDR and the PRR. This structured timeline ensures proper development of technical requirements, coordinated subsystem design, and timely preparation for formal reviews.

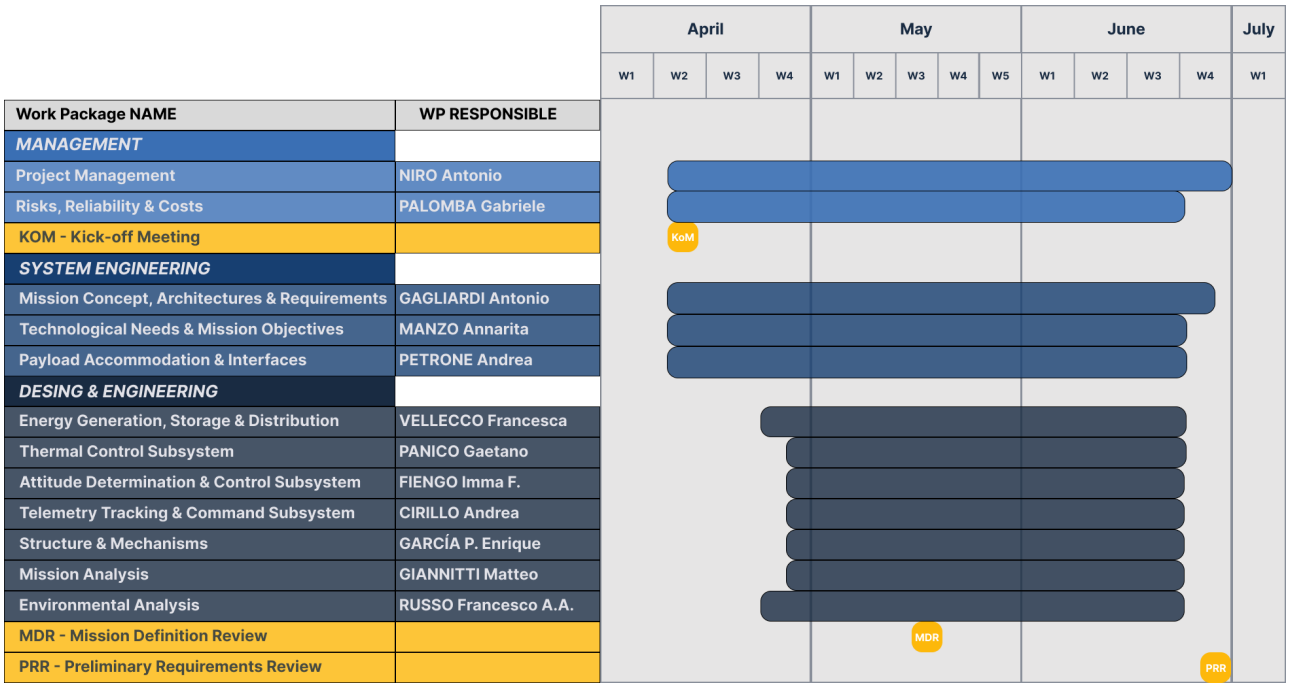

Work Package NAME	WP RESPONSIBLE
MANAGEMENT	
Project Management	NIRO Antonio
Risks, Reliability & Costs	PALOMBA Gabriele
KOM - Kick-off Meeting	
SYSTEM ENGINEERING	
Mission Concept, Architectures & Requirements	GAGLIARDI Antonio
Technological Needs & Mission Objectives	MANZO Annarita
Payload Accommodation & Interfaces	PETRONE Andrea
DESING & ENGINEERING	
Energy Generation, Storage & Distribution	VELLECCO Francesca
Thermal Control Subsystem	PANICO Gaetano
Attitude Determination & Control Subsystem	FIENGO Imma F.
Telemetry Tracking & Command Subsystem	CIRILLO Andrea
Structure & Mechanisms	GARCÍA P. Enrique
Mission Analysis	GIANNITTI Matteo
Environmental Analysis	RUSSO Francesco A.A.
MDR - Mission Definition Review	
PRR - Preliminary Requirements Review	

Figure 8.3: Gantt chart

8.4 Team description and organization chart

AMPERE team consists of fifteen members organized to cover the twelve WPs outlined in Section 8.2. Each team member, team leader excluded, is in charge of at least one among work packages and nodes, with assignments carefully determined based on individual expertise, preferences, and optimal workload distribution throughout the project timeline. This organization is shown in Figure 8.4.

The assignment process balanced technical capabilities with project scheduling to prevent resource overallocation during critical phases. Members responsible for early-phase work packages that conclude sooner are strategically assigned additional responsibilities in later project stages. Similarly, those with cross-domain expertise are placed in complementary WPs with staggered timelines.

This workload-balanced approach ensures consistent team productivity while leveraging each member's unique skillset at the most appropriate project phases, all under the elected leadership of Pietro Di Sarno.

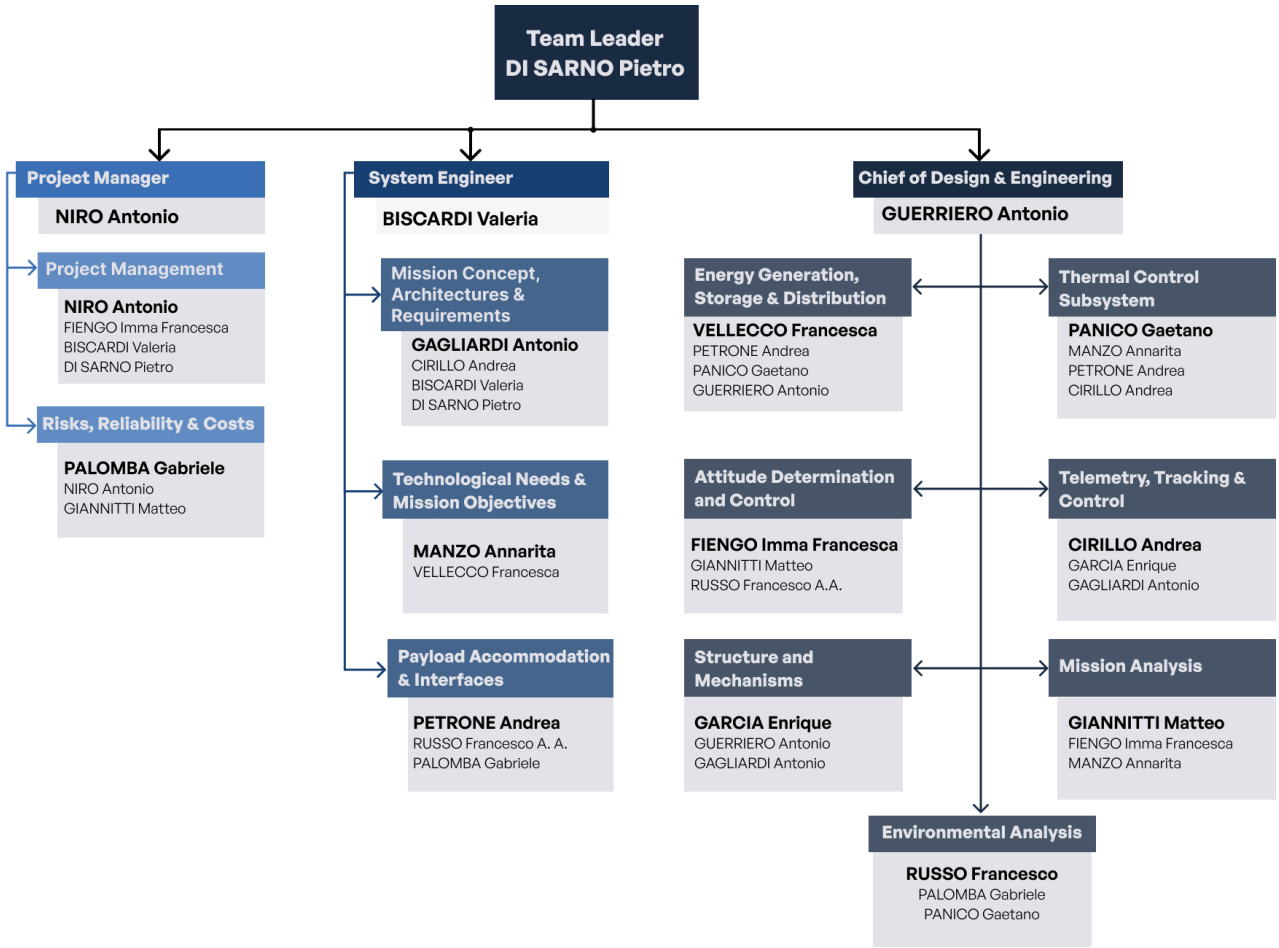

Figure 8.4. Organizational chart

8.4.1 Team members

In this Section, a photocard of each team member is presented along with her or his assignments in terms of responsibilities and WPs.

DI SARNO Pietro
Team Leader

<u>Actively working in:</u>
Project Management;
Mission Concept, Architecture & Requirements.

NIRO Antonio
Project Manager;
Project Management Responsible
<u>Actively working in:</u>
Risks, Reliability & Costs.

BISCARDI Valeria
System Engineer

<u>Actively working in:</u>
Project Management;

GUERRIERO Antonio
Design & Engineering Chief

<u>Actively working in:</u>
Energy Generation, Storage & Distribution;
Structure & Mechanisms.

CIRILLO Andrea
Telemetry, Tracking & Command Subsystem
Responsible
<u>Actively working in:</u>
Mission Concept, Architecture & Requirements;
Thermal Control Subsystem.

FIENGO Imma Francesca
Attitude Determination & Control Subsystem Responsible

<u>Actively working in:</u>
Project Management;
Mission Analysis.

GAGLIARDI Antonio
Mission Concept, Architecture & Requirements Responsible
Actively working in:
Telemetry, Tracking & Command Subsystem;
Structure & Mechanisms.

GARCÍA Enrique Palomares
Structure & Mechanisms Responsible
Actively working in:
Telemetry, Tracking & Command Subsystem.

GIANNITTI Matteo
Mission Analysis Responsible

Actively working in:
Attitude Determination & Control Subsystem;
Risks, Reliability & Costs.

MANZO Annarita
Technological Needs & Mission Objectives Responsible
Actively working in:
Thermal Control Subsystem;
Mission Analysis.

PALOMBA Gabriele
Risks, Reliability & Costs Responsible
Actively working in:
Payload Accommodation & Interfaces;
Environmental Analysis.

PANICO Gaetano
Thermal Control Subsystem Responsible
Actively working in:
Energy Generation, Storage & Distribution;
Environmental Analysis.

PETRONE Andrea
Payload Accommodation & Interfaces Responsible
Actively working in:
Energy Generation, Storage & Distribution;
Thermal Control Subsystem.

RUSSO Francesco Antonio Aldo
Environmental Analysis Responsible
Actively working in:
Payload Accommodation & Interfaces;
Attitude Determination & Control Subsystem.

VELLECCO Francesca
Energy Generation, Storage & Distribution Responsible
Actively working in:
Technological Needs & Mission Objectives.

8.5 Name and logo concept

The AMPERE mission represents a groundbreaking initiative to establish the Moon's first dedicated charging station, captured in our mission emblem. The circular logo showcases ESA's Argonaut at its centre, serving as lander. The prominent solar panel depicted to the right of the lander represent the core technology that will convert solar energy into sustainable power for future lunar missions. The "AMPERE" acronym arcs across the top of the badge, breaking down into "Autonomous Moon Power and Environmental Research Element" along the bottom curve, highlighting the dual objective of the mission.

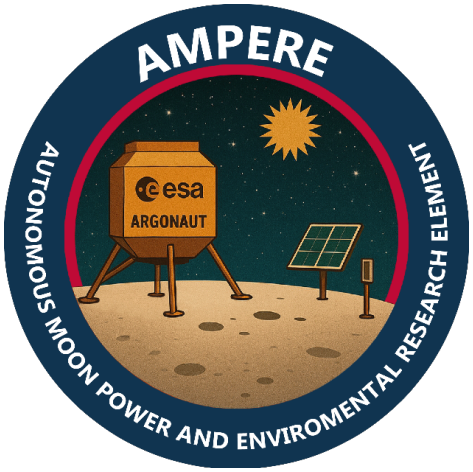

Figure 8.5: Mission logo

The environmental monitoring aspect of our mission is represented by the sensors visible alongside the solar array, which will collect critical data on radiation levels, temperature variations, and illumination at our chosen landing site. The golden sun shining in the starry backdrop symbolizes our primary energy source, while the cratered lunar surface beneath the lander grounds our ambitious mission in the realistic challenges of the lunar environment. Together, these elements illustrate AMPERE's commitment to advancing lunar infrastructure while expanding our scientific understanding of Earth's closest celestial neighbour.

9 Task 1 Scientific needs, constraints and mission requirements

9.1 Technological needs

9.1.1 Potential beneficiaries

From the very beginnings of the earliest space missions, the Moon has consistently been a primary objective for numerous space agencies globally. However, while the initial lunar missions had essentially a pioneering nature, nowadays, most space agencies and private companies are focused on long-term human colonization. This long-term vision entails the sustainable utilization of lunar resources while maintaining continuous exploration, with the eventual establishment of a lunar base serving as a critical stepping stone towards Mars colonization [R.D. 40]. This pathway is being undertaken by both governmental agencies and private sector enterprises. The most significant lunar project is Artemis led by National Aeronautics and Space Administration (NASA), which also involves both public international agencies like ESA, Japan Aerospace Exploration Agency (JAXA), and private companies such as SpaceX, Blue Origin, and Intuitive Machines. Specifically, ESA's involvement in the Artemis program is part of the broader Terrae Novae program. This initiative encompasses both robotic and human exploration, with the goal of guiding Europe's human journey into the Solar System and bringing the benefits of exploration back to society [R.D. 40]. Figure 9.1 outlines the sequential phases of the Artemis mission, which ends with the establishment of the Artemis base camp [R.D. 41].
However, new entities are emerging within the space landscape. China occupies a central role, notably in lunar exploration through the Chang'e program, which is an ongoing series of robotic missions designed to ensure the establishment of a lunar base, the International Lunar Research Station (ILRS), around 2035. Furthermore, this initiative sees the involvement of other countries. This includes Russia, a well-established space power, as well as numerous nations such as Pakistan, Venezuela, and South Africa, who will be making their first contributions to human lunar exploration. The Chang'e program positions itself as a competitor to the Artemis program [R.D. 42]. The idea of building a lunar base is also shared by the Japanese private company Ispace [R.D. 52]. This confirms the trend of increasing commercialization in the space sector. Additionally, new nations are joining the pursuit of lunar exploration. Countries like the United Arab Emirates, Turkey, and South Korea have announced their own lunar research programs planned for the next decade.[R.D. 44], [R.D. 45] and [R.D. 46].

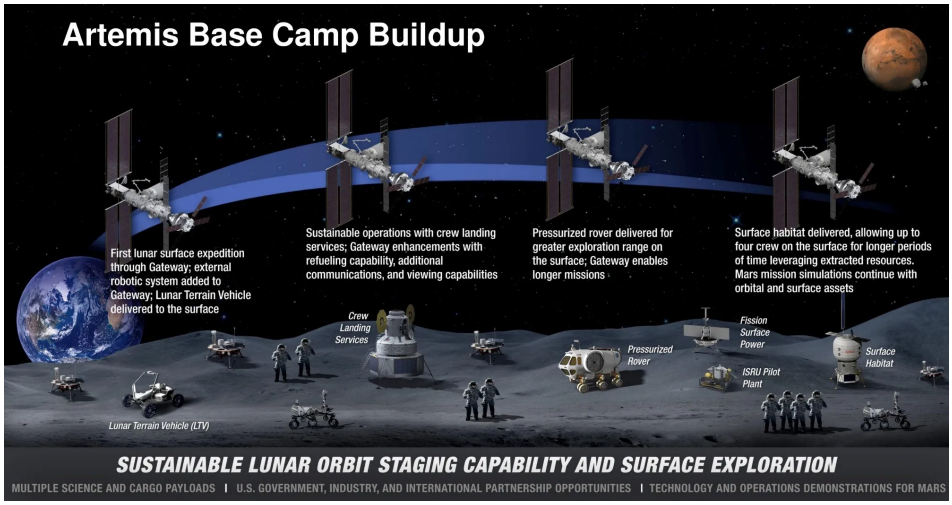

Figure 9.1: The Artemis pathway to lunar base development [R.D. 40]

9.1.2 Power needs and potential users

As outlined above, the establishment of a lunar base is the ultimate objective of lunar exploration. In general, the progression of such lunar mission includes the subsequent phases [R.D. 48]: the first step is robotic exploration, followed by human deployment initiation. Subsequently, the human expansion starts until self-sufficiency is reached. Finally, a full lunar economy, more in-depth scientific studies, and In-Situ Resource Utilization (ISRU) are established. This pathway aligns with the milestones defined within Artemis and the China's Lunar Exploration programs [R.D. 48]. Following these endeavours, the power needs naturally increase, leading to an evolution of power-supply systems, as detailed in [R.D. 41].

AMPERE mission will operate within a context where robotic assets, rovers and landers, are already well-established, at a time when human continuous presence will be about to begin. Therefore, Table 9.1, reports some preliminary average power ranges related to these robotic and early human operations.

Power consuming unit	Active power range (kW)	Survival power range (kW)
ISRU: demonstration	3 to 7	0.5 to 1
ISRU: pilot	7 to 20	1 to 2
ISRU: production	20 to 100	2 to 5
Unpressurized electric rover	1 to 3	0.2 to 0.5
Small pressurized crewed rover	3 to 7	0.5 to 1
Large pressurized crewed rover	7 to 20	1 to 3
Small rover	< 1	< 0.2
Large rover	1 to 7	0.5 to 1
Small robotic lander	< 1	< 0.2
Medium robotic lander	1 to 3	0.2 to 0.5
Large robotic lander	3 to 7	0.5 to 1
Communication system	0.3 to 1 per transmitter	N/A
Lunar nighttime operation and heating systems	1 to 2	N/A
Sensors and other supporting equipment	2 to 10	N/A

Table 9.1: Users preliminary average powers ranges. [R.D. 48]

9.1.3 Operational needs

In the last years, the renewed interest in the Moon has highlighted the need for more recent and comprehensive data on the lunar environment. The lunar surface is characterized by extreme conditions, such as significant thermal excursions between day and night, intense radiation, and the presence of regolith (lunar dust). whose understanding is decisive for the success of future missions. Environmental and operational challenges vary significantly depending on the specific lunar region under consideration: while models for lunar topography and illumination are relatively up-to-date for the equatorial regions, thanks to data from the Lunar Orbiter Laser Altimeter (LOLA) [R.D. 92], the Lunar Reconnaissance Orbiter (LRO), and enhanced by various teams of researchers, the lunar poles' environment presents a complex topography poorly defined by current data, leaving certain regions entirely unknown. Moreover, the models currently available for describing the lunar regolith, thermal conditions, and radiation exposure still rely heavily on data from the Apollo missions (1961 - 1972) and on statistical projections [R.D. 93]. Compounding this issue, the data we currently possess are becoming increasingly obsolete for accurately forecasting the environmental landscape of the most attractive regions over the next decade. These limitations impede the initiation of advanced missions, such as the establishment of permanent lunar bases [R.D. 92],[R.D. 96]. For these reasons, AMPERE mission aims also to employ various sensors, whose detailed description is provided in Section 10.7.2 to significantly contribute to the characterization of the lunar environment, and in particular of the South Pole (see Section 10.1). The data collected will be made available to potential beneficiaries of the AMPERE program to create a shared database that can be accessed to ensure the success of future missions around the power station.

9.2 Mission objectives

Following the analysis of highly intensive activities planned for the coming years, the necessity of building a power station has become clear to support these operations. Table 9.2 and Table 9.3 list AMPERE Primary Mission Objectives (PMOs) and AMPERE Secondary Mission Objectives (SMOs), respectively. Some of these objectives remind to the ones referred to the NASA's Moon to Mars architecture [R.D. 97]. In contrast, a set of objectives echoes the Global Exploration Roadmap defined in 2024 by the International Space Exploration Coordination Group's (ISECG) [R.D. 98]. This group includes the primary international space agencies and companies, which have articulated a common vision for space exploration through 2050, involving activities in low-Earth orbit, on the Moon and on Mars. Among the primary objectives the need to develop a feasible power station, able to generate and supply power to potential users for a long-term period, is outlined. This power will be provided to the user through standard specifications. The fostering of this standardization simplifies the transfer of power from the system to the users and eases the design of their onboard electronics. In the secondary objectives, instead, other fundamental key topics are addressed. Firstly, the lack of information related to the lunar environment, broadly described in Section 9.2, highlights the need to improve our knowledge about it. This improvement will be implemented using environmental sensors that must ensure accurate

functioning. Secondly, the assurance of scalability and evolvability are provided to guarantee the system applicability and benefit for a range of future missions, in accordance with Task 4 of the SoW [A.D. 1]. Other important secondary objectives involve ensuring continuous support for human life and uninterrupted robotic functions, respectively. This becomes particularly vital during the initial stages of lunar exploration, when our power station will operate to enable and support increased activities on the lunar surface. Following this, another key strategic concept centres on the proactive leveraging of European space resources, a logical step given the AMPERE mission's European origin. This involves utilizing existing communication networks, lander technologies, and rover capabilities to actively promote and strengthen the European space sector, thereby fostering its expansion and competitive edge internationally. A further important objective is to guarantee the global welfare. This will be achieved through the implementation of the lunar base, a project that will sparkle both the scientific research and the technological discoveries, incentivizing the international collaboration. The presence of our power station seeks to promote the industrial growth and advancement. In fact, this system is expected to stimulate industrial activities, leading to increased technological innovation and the development of new markets for utilizing local resources. This will directly enhance Earth's economic and industrial strengths. Finally, the importance of outer space colonization is outlined. Promoting activities focused on lunar and planetary colonization is essential for advancing human exploration, and our lunar endeavour is a decisive leap in this larger space program that culminates with the settlement of Mars. Indeed, the purpose of this program is to inspire innovation and cultivate international collaboration for humanity's future beyond Earth.

PMO ID	Title	Primary mission objective	Justification	References
AMP-PMO-01	System feasibility	To test the feasibility of a lunar power generation and distribution system	Demonstrating the feasibility of the system by the leverage of existing models is crucial for the sake of the mission. A reliable and efficient power infrastructure is not merely a support system, but a fundamental prerequisite for all future lunar activities.	[A.D. 1]
AMP-PMO-02	Long-term duration power generation	To generate long-duration power (months to years) for external users supporting continuous robotic/human operations	Generating long-duration power for external users is paramount for enabling continuous robotic and human operations and for realizing the full potential of lunar exploration and development, a critical objective that directly addresses Task 4 of the SoW.	[A.D. 1], [R.D. 97]
AMP-PMO-03	Long-term duration power supply	To provide long-duration power (months to years) for external users supporting continuous robotic/human operations	Providing long-duration power for external users is paramount for enabling continuous robotic and human operations and for realizing the full potential of lunar exploration and	[A.D. 1], [R.D. 97]

			development, a critical objective that directly addresses Task 4 of the SoW.	
AMP-PMO-04	Standard specifications	To foster the definition of standard specifications for the generation and distribution of power for lunar users	Establishing common standards for voltage, frequency, connection interfaces, and safety protocols will streamline the design, development, and manufacturing of power generation and distribution systems. New power sources and users can be integrated more easily and predictably, avoiding the complexities and costs associated with disparate, proprietary systems, making lunar operations more economically viable in the long run.	[A.D. 1], Open literature

Table 9.2: AMPERE primary mission objectives

SMO ID	Title	Secondary mission objectives	Justification	Reference
AMP-SMO-01	Environmental models validation & enhancement	Validation and enhancement of the existing lunar environmental models	Due to the insufficient accuracy of the existing lunar environmental models, their improvement is paramount to guarantee the safety and success of future lunar missions, enable the sustainable utilization of lunar resources, identify potential habitable areas, and advance our fundamental scientific understanding of the Moon. Improving the precision and reliability of these models will significantly mitigate risks, optimize resource management, ensure human colonization, and unlock new scientific discoveries in the lunar environment.	[A.D. 1]
AMP-SMO-02	Environmental sensors functioning assessment	Ensure the correct functioning of the environmental sensors	Environmental sensors are crucial to the definition and characterization of the lunar environment. Hence, their assessment is essential to ensure the accuracy and reliability of the data, guaranteeing both the success of lunar missions and the advancement of lunar science.	[A.D. 1]
AMP-SMO-03	Scalability	To check the possible scalability of the system	In accordance with the Task 4 reported in the SoW, scalability ensures that the system can grow in response to increased demand or evolving requirements.	[A.D. 1], [R.D. 97]
AMP-SMO-04	Evolvability	To ensure the evolvability of the system	In accordance with the Task 4 reported in the SoW, evolvability guarantees the system ability to adapt and incorporate future technological advancements.	[A.D. 1], [R.D. 97]
AMP-SMO-05	Human survival	To simplify human survival on the Moon	Simplifying human survival on the Moon is a challenging but essential goal. A lunar power station is a key enabler for this objective, providing the energy necessary for resource utilization, scientific research, technological development, and long-term sustainability.	[A.D. 1], [R.D. 97]

AMP-SMO-06	Robotic operations	To support robotic operations on the Moon	Continuous and well-powered robotic operations will dramatically enhance lunar science and will strongly take part in human settlement. Therefore, the power station will have a crucial key role to provide power to drive these robotic activities.	[A.D. 1], [R.D. 97]
AMP-SMO-07	European resources valorisation	To exploit European resources in several mission phases	The development and utilization of European space-related resources will act as a catalyst for innovation, fostering the creation of new enterprises, and the expansion of existing ones, within the European space sector. This will lead to technological advancements, the creation of high-skilled employment opportunities, and the overall enhancement of Europe's space capabilities. Furthermore, it will solidify Europe's position as a key player in the global space arena.	[A.D. 1], [R.D. 40]
AMP-SMO-08	Global welfare	To pursue global welfare supporting the future establishment of an international lunar station	Establishing an international lunar station will foster global cooperation and advance global welfare by enabling shared scientific research, technological innovation, and sustainable resource use.	[A.D. 1], [R.D. 98]
AMP-SMO-09	Industrial enhancement	To ensure industrial growth and expansion	The presence of our power station on the Moon will hopefully help to drive technological innovation, create new markets, and open opportunities for lunar resource utilization directly on the Moon surface. Stimulating economic development will position industries at the forefront of space exploration, ultimately benefiting Earth’s economy and global industrial capabilities.	[A.D. 1], [R.D. 98]
AMP-SMO-10	Outer space colonization	To promote the importance of activities focused on the colonization of	Promoting activities focused on lunar and planetary colonization is essential for advancing human exploration.	[A.D. 1], [R.D. 98]

		the Moon and beyond	By emphasizing these efforts, we want to inspire innovation, foster international collaboration, and lay the groundwork for humanity's future beyond Earth.	

Table 9.3: AMPERE secondary mission objectives

9.3 Mission constraints

All the Mission Constraints (MCs) listed in Table 9.4 have been selected in compliance with the SoW [A.D. 1] and Clarification No.1 [A.D. 9]. AMPERE mission will be launched into orbit through a single Ariane 6 launch, scheduled no earlier than 2035. As an Italian mission, the landing on the lunar surface will be carried out using the LDE developed by ESA. The mission falls under Category IIb of the COSPAR Planetary Protection Policy [A.D.2], because all the considered landing sites are located south of 79°S latitude, as specified in Section 10.1[A.D. 2]. The constraints related to the mass and volume of the LPS derive from the SoW [A.D. 1] and are compatible with the dimensions of the LDE. The constraint regarding the landing site originates from Clarification No.1 [A.D. 9]. The temperature and daytime/nighttime cycle survival constraints are derived from the analysis of the SoW [A.D. 1]. The communication constraint is defined considering the European context of the mission, with the intention of maximizing the use of European resources available at the time of the mission, echoing the mission objectives.

MC ID	Name	Description	Reference
AMP-C-01	Launch	The mission shall be realized using a single, dedicated Ariane 6 launch.	[A.D. 1]
AMP-C-02	Landing	The mission shall exploit ESA's Argonaut LDE for landing.	[A.D. 1]
AMP-C-03	Mission period	The mission shall start post-2035.	[A.D. 1]
AMP-C-04	Planetary protection	The mission shall be in accordance with the Planetary Protection Policy guidelines applicable to Category IIb missions.	[A.D. 1], [A.D. 2]
AMP-C-05	Payload Volume	LPS volume shall be characterized by a height of 1.8 m and a maximum base area equal to 4.0 m^2	[A.D. 1], [A.D. 9]
AMP-C-06	Payload Mass	LPS mass shall not exceed 800 kg.	[A.D. 1], [A.D. 9]
AMP-C-07	Self-sufficiency after landing	The LPS shall be fully independent from the LDE after landing.	[A.D. 1], [A.D. 9]
AMP-C-08	Landing Site	The landing site shall be compliant with the Clarification No.1 guidelines.	[A.D. 9]
AMP-C-09	Day/night cycle survival	The LPS shall be engineered to survive and function during the harsh conditions of the lunar day/night cycle.	[A.D. 1]
AMP-C-10	Minimum allowed temperature	LPS shall operate at extreme temperature fluctuations up to a minimum of –150 °C.	[A.D. 1]
AMP-C-11	Communication System	As a first choice, the LPS shall rely on existing resources and European services for communications and navigation.	[A.D. 1]

Table 9.4: AMPERE mission constraints

10 Task 2 System architecture and overall feasibility

10.1 Landing sites

10.1.1 Possible landing sites

The entirety of the Moon's surface arouses significant scientific and commercial interest. However, whereas the equatorial zone was historically the primary area of focus for missions like the Apollo program [R.D. 98], the Poles are now considered the most promising candidates for future endeavours. This shift in focus is driven by several important factors. The favourable lighting conditions in certain polar areas and the presence of Permanently Shadowed Regions (PSRs) stand out as the most important. These two factors are both determined by the Moon's small rotational axial tilt of only 1.54°. This property explains the reason for the near-constant presence of the Sun on the polar horizons, unlike the equatorial regions which experience approximately 14 Earth days of illumination followed by nearly 14 Earth days of darkness [R.D. 94]. This allows to identify regions which face darkness only for a few days. On the other hand, due to the near-perpendicular orientation of the lunar rotational axis, the Sun never rises more than 1.54° above the horizon in the polar regions. This, combined with the highly irregular polar topography, leads to the creation of PSRs. These permanently shadowed areas are of great interest to scientists due to the potential presence of water ice and hydroxyl molecules, trapped by the extremely low temperatures within them. The South Pole holds greater appeal than the North Pole for lunar exploration because it boasts a larger number of PSRs and a more attractive geological past. A key feature of this region is the Aitken basin, recognized as the Solar System's largest impact basin. Moreover, the lunar regolith at the South Pole is older than any samples retrieved from the Apollo missions. This older age significantly boosts the interest of geologists who aim to understand the early evolution of the Solar System [R.D. 100]. The mentioned illumination conditions highlight several challenges for human colonization at the South Pole and are very complex to model because they depend on many factors such as the local topography, the slight seasons changes, the height above ground and the lunar precessional cycle. Therefore, a study period covering a full 18.6-year lunar precessional cycle is being conducted to consider all seasonal and orbital illumination effects. Additionally, illumination conditions are defined at several heights (see Section 11.7). The low elevation of the Sun presents another significant challenge, resulting in very long shadows that could impede power station operations and complicate future crewed missions [R.D. 101]. Considering these factors, a trade-off analysis is conducted to evaluate potential landing sites. The most promising locations are localized in the region of interest displayed in Figure 10.1. A more detailed view of the landing sites, defined in Table 10.1, is shown in Figure 10.2. More detailed images are presented in Section 11.7. All these sites are below 88° of longitude, hence, they are circumscribed by the inner yellow circle in Figure 10.2. Initially, all these sites belonged to the Artemis III candidate landing sites list until 2024 [R.D. 102], [R.D. 103]. Nowadays, only Rim De Garlache (D) remains in this list. However, the other four sites, despite their recent removal from the program's list, continue to captivate the scientific community due to their location near PSRs and their geological composition. Moreover, they also offer advantages for engineering purposes, which include the illumination conditions, the slope, the time in shadow, the average Earth visibility, and the average soil temperature [R.D. 103], [R.D. 104]. The last parameters are crucial for the landing site selection of AMPERE mission: they are evaluated using data collected in a 20-year period (2017-2037) [R.D. 95], [R.D. 96]. Notably, the average maximum illumination and longest shadow duration are defined at a height of 2 m (in the Table 10.1 is reported as @ 2 m AGL, which stands for at 2 m Above Ground Level) to account for the upward deployment of solar arrays above the system's maximum height of 1.8 m [A.D. 9]. Furthermore, the longest time in shadow is evaluated in Earth hours, [R.D. 103], [R.D. 104], which means that in Earth days is defined as in Equation (10.1):

$$T_{Earth\ days} = \frac{T_{hours}}{24} \tag{10.1}$$

The choice of soil conditions is also dictated by [A.D. 9]. A detailed environmental analysis is available in Section 11.7.

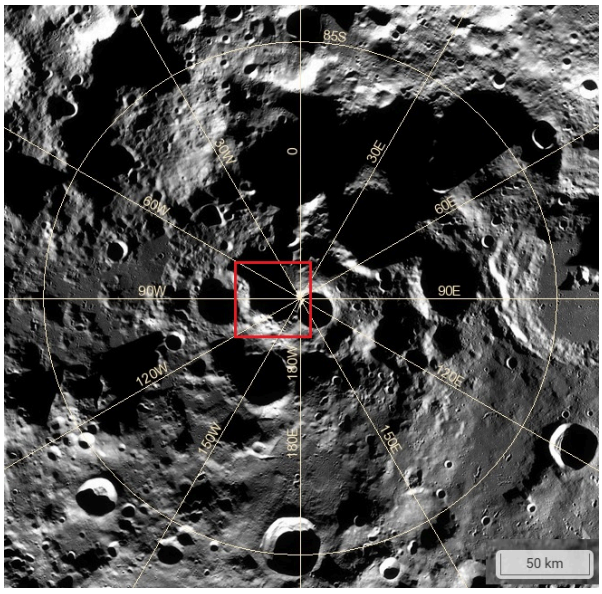

Figure 10.1: Region of interest [R.D. 105]

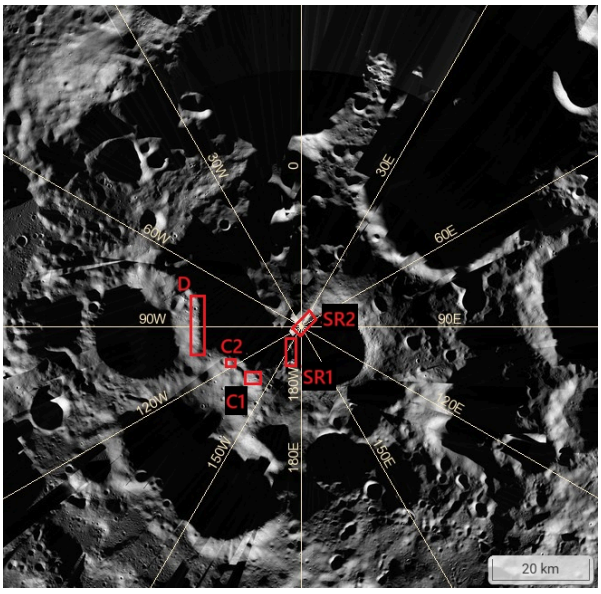

Figure 10.2: Landing sites [R.D. 105]

Name	Sel. lat	Sel. lon	Avg. slope	Avg. max illumination @ 2 m AGL	Longest time in shadow @ 2 m AGL ($T_{Earthdays}$)	Avg. Earth visibility	Avg. temp (K)
Connecting Ridge (C1)	-89.4°	-136.2°	11.5°	88.0 %	4.7	30%	132
Connecting Ridge (C2)	-89.3°	-113.8°	10.6°	78.0 %	6.9	31%	153
Rim of De Garlache crater (D)	-89.0°	-87.5°	14.0°	80.0 %	6.3	44%	167
Shackleton Ridge 1 (SR1)	-89.8°	-156.1°	11.1°	84.3%	2.8	29%	130
Shackleton Ridge 2 (SR2)	-89.7°	-163.2°	6.0°	73.9 %	2.8	29%	130

Table 10.1: Candidate landing sites. "SEL" stand for selenographic.

10.1.2 Landing site selection

10.1.2.1 Preliminary analysis

Based on the findings of WP 3.7, reported in Section 11.7, and on the users' potential interests, a preliminary choice of the landing site is done. This evaluation is based on four parameters, each carrying a specific weight, as reported in Table 10.3. Given a landing site, a number from 1 to 5 is assigned for each parameter. The numbers are associated with the attributes reported in the following Table 10.2:

Number	1	2	3	4	5
Description	Bad	Poor	Acceptable	Good	Excellent

Table 10.2: Possible attributes and numbers for landing site evaluation's parameters

The assigned number is then multiplied by the weight of that parameter and subsequently added to the weighted scores of other parameters for that landing site. A higher total score indicates a better region, and a ranking is created based on these scores. Note that the "morphology" term includes the slopes and the presence of boulders, while the "other environmental conditions" term includes dust, average temperature, radiation and moonquakes evaluation.

Parameter	Weight	C1	C2	D	SR1	SR2
Illumination & shadows conditions	0.45	4	3	3	5	4
Morphology	0.25	4	4	1	2	3
Potential users' interests	0.15	4	4	5	4	4
Other environmental conditions	0.15	3	4	5	2	2
Total	1	3.85	3.55	3.10	3.65	3.45
Ranking		1	3	5	2	4

Table 10.3: Landing sites ranking evaluation

By this preliminary analysis, C1 and SR1 have reached the highest score among all candidates. Therefore, these landing sites have become key drivers in the trade-off analysis across various mission concepts. This analysis is performed in Section 10.4.

10.2 Alternative mission concepts definition

Mission characterization is the initial stage of selecting and defining a space mission, its aim is to identify the most suitable overall approach from the various available options to successfully carry out the mission [A.D. 10]. The unconstrained number of mission options is huge, so during the initial concept exploration phase technological needs, mission objectives and constraints have been defined: a preliminary analysis of these elements enabled the identification of four mission concepts, which were then translated into four alternative architectures. These latter will subsequently undergo a trade-off analysis to determine the baseline solution.

A set of operational assumptions has been maintained across all configurations:

- All configurations are characterized by the same descending and landing profile, enabled by the Argonaut lander.
- All architectures are designed to generate and provide power during the lunar day and to survive the lunar night.
- All configurations include the same set of environmental and monitoring sensors (LSM), described in detail in Section 10.7 of this document.
- All architectures are equipped with a defined functional and mechanical interface between the LDE and the LPS, whose design, development and implementation are outside the scope of this project [A.D. 9].

The four concepts, referred to as MoonStation, MoonGrid, MoonProbe and MoonRover, represent different approaches in terms of the deployment, positioning, and management of the LPM and LSM.

10.2.1 Concept #1: MoonStation

MoonStation foresees the deployment of a single autonomous assembly, integrating both the LPM and the LSM which constitutes the secondary payload: this centralized integration results in a unified scientific unit hosting all sensing elements, which simplifies system interfacing, reduces harnessing complexity, and enables tight structural integration. However, this proximity also necessitates careful sensor layout planning to avoid field-of-view obstruction, thermal cross-coupling, and electromagnetic interference.

The main goal of this mission concept is to prioritize energy generation and storage, with an emphasis on maximizing reliability and robustness. Therefore, this architecture incorporates rollable solar panels, which although not optimal in terms of volume efficiency, are the technology that offers the best performance in energy production. As a result, MoonStation can generate up to 6 kW (To Be Confirmed, TBC), representing the highest power output among the considered architectures. To meet this goal, a series of technical choices has been made.

A ramp-based deployment mechanism has been selected, and the station is integrated on a structure made by a wheeled cart and a braking system. The wheels are not intended for active mobility on lunar surface, after landing, but serve as an aid during the deployment phase. The station indeed is designed to be fully stationary, remaining fixed at the location where it is released by the ramp.

MoonStation is also characterized by a straightforward operational profile with minimal complexity. No onboard users are foreseen to autonomously dock with and recharge from the station; instead, the entire available mass is allocated to energy production.
However, this does not preclude the station's ability to support future external users, in fact MoonStation is equipped with two kinds of interfaces:

- A Laser interface system, designed to manage and distribute high amounts of energy without physical interaction up to 50 meters [R.D. 127].
- A wireless charging unit, particularly suited for use by astronauts during surface operations [R.D. 126].

These interfaces have been included based on the consideration that, given MoonStation's high power output, the energy losses which come with these kinds of technologies would have minimal impact on the station's efficiency.
In this mission scenario any future user must physically reach the station to recharge, meaning that the assembly must be deployed in a clearly identifiable and easily accessible location. The proposed landing site for this concept includes two options, C1 and SR1, both of which offer environmental and operational characteristics well aligned with the station's needs.
An overview of the MoonStation architecture is provided in Table 10.4, preliminary design solutions are detailed in Section 11.

Concept's name	MoonStation
Number of stations	1
Elements	(LPM+LSM)
Integration	Unique assembly
Panels technology	Rollable panels
Landing site	C1/SR1
Lunar mobility	No
Deployment mechanism	Ramp + wheeled cart
Secondary payload	Entire LSM
Power production	6 kW (TBC)
Energy storage capability	75 kWh (TBC)
On board user	None
Self-sufficiency	Yes
Interface	Laser/wireless

Table 10.4: MoonStation's architecture

10.2.2 Concept #2: MoonGrid

MoonGrid foresees the deployment of three autonomous power stations, each equipped with its own energy generation and storage units, along with a dedicated environmental monitoring suite. In this mission scenario, the concept of a single charging station evolves into a lunar microgrid, capable of simultaneously serving the needs of three potential users. An inter-station communication system enables coordinated energy management and operational efficiency.
The focus of this mission concept is to prioritize user's satisfaction, not only by introducing functional redundancy and enhancing overall system reliability in case of a failure in one of the nodes, but also by equipping each station with unique features, enabling the opportunity to test different technologies and assess variations in their energy production efficiency.

- MoonGrid-1 is equipped with fixed solar panel technology, selected to maximize system robustness, and includes a tether-based interface.
- MoonGrid-2 is equipped with rollable solar panel technology, aimed at maximizing power generation, and includes a fixed female dock interface.
- MoonGrid-3 is equipped with thin-film solar panel technology, optimized to minimize the volume, and includes a fixed male dock interface.

The choice to implement multiple interfaces reflects MoonGrid's commitment to developing a system with inherent flexibility and universality, ensuring that a diverse range of future users can meet charging compliance requirements.

Each station will be delivered as a unique assembly via a dedicated deployment mechanism, which includes two options, the Davit system [R.D. 272] or the Egress system [R.D. 8]: both rely on a combination of cables and tensioning mechanisms which allow for safe and passive release. Considering this, differently to the previous configuration, each station is equipped with a wheel-based mobility system that enables autonomous and automated repositioning: once deployed, the distributed units collectively form a decentralized microgrid, meaning that any future user must physically reach the station to recharge. It's important to underline that each of the three stations, relying on its own generated power, effectively acts as a user of itself.
Another key feature of MoonGrid is its sensors' architecture: each station is equipped with a distinct set of environmental sensors. This deliberate distribution minimizes measurement interference and increases the diversity and quality of the collected data.
The power level generated by each station is significantly lower than in all other configurations, limited to 0.5 kW of electrical power (TBC), yet this should not be considered entirely as a drawback, as from a future reuse perspective MoonGrid stands out as the concept most suitable for integration into upcoming missions, successfully aligning with AMPERE's mission objectives of evolvability and scalability.
The mission is planned to operate within the C1 landing site, whose characteristics are well-suited for spatial distribution and surface accessibility.
An overview of MoonGrid architecture is provided in Table 10.5, preliminary design solutions are detailed in Section 11.

Concept's name	MoonGrid#1	MoonGrid#2	MoonGrid#3
Number of stations	3		
Elements	(LPM+LSM)	(LPM+LSM)	(LPM+LSM)
Integration	Unique assembly	Unique assembly	Unique assembly
Inter-stations communication	Yes		
Panels technology	Fixed panels	Rollable panels	Thin-film solar panels
Landing site	C1		
Lunar mobility	Yes	Yes	Yes
Deployment mechanism	Davit system/ Egress	Davit system/ Egress	Davit system/ Egress
Secondary payload	Dust sensor Langmuir probe Pyranometer	Magnetometer Ion-electron Spectrometer Neutral-mass Spectrometer Temperature sensors	Radiation monitor Dosimeter
Power production	0.5 kW (TBC)	0.5 kW (TBC)	0.5 kW (TBC)
Energy storage capability	23 kWh (TBC)	23 kWh (TBC)	23 kWh (TBC)
On board user	None		
Self-sufficiency	Yes	Yes	Yes
Interface	Tether	Fixed female dock	Fixed male dock

Table 10.5: MoonGrid's architecture

10.2.3 Concept #3: MoonProbe

MoonProbe involves the presence of two separate elements: the LPM and a small rover equipped with a part of the environmental sensors which constitute the LSM.
The main goal of this mission concept is to test, through the presence of the rover, the capacity to provide power to a physical user. From a technical and operational point of view this is realized by transferring part of the mass and volume available to the LPM to the small rover: the power produced by MoonProbe's station will be limited to 4 KW (TBC), but this loss is widely compensated by the fact that the rover, in its role as an active user, responds optimally to two primary objectives of the AMPERE mission, long-term duration power supply (AMP-PMO-03) and standard specifications assessment (AMP-PMO-04).

The power provided by the LPM to the rover will serve to feed the sensors that will be on board. The choice of which elements of the LSM to place on the rover was practical: sensors that benefit from dynamic positioning or spatial sampling are mounted on the rover, while those requiring stable, long-term acquisition are hosted on the stationary platform. This split enables a clear functional division between static and mobile sensing, maximizing data coverage while reducing mutual interference. It also facilitates redundant measurement opportunities, as certain parameters can be sampled in different locations for comparison and validation.
For the deployment phase, it is foreseen that both elements will be released on board a unique structure, hence a ramp-based deployment mechanism has been selected. As with MoonStation, also MoonProbe is integrated on a structure made by a wheeled cart and a braking system. In this case, while the station is designed to be fully stationary, remaining fixed at the location where it is released by the ramp, in a subsequent phase of the mission the small rover will descend from the wheeled cart, reaching the lunar soil.
In this mission scenario once the measurement operations have been carried out, within a range of movement to be defined later, once the system approaches the end of its available power supply, the rover will return to the station and recharge itself through a wireless interface [R.D. 126]. The choice to adopt such a system is clearly dictated by the absence of physical connections, which allows not only operational ease, but also fast and efficient recharging. Moreover, MoonProbe will be also equipped with a fixed dock, to meet the needs of future potential users and fulfil standard specifications assessment.
Even in this case the proposed landing site includes two options, C1 and SR1, both of which offer environmental and operational characteristics well aligned with the station's needs.
An overview of the concept is provided Table 10.6, preliminary design solutions are detailed in Section 11.

Concept's name	MoonProbe	
Asset	Power Station	Rover
Number of stations	1	
Elements	LPM + LSM (partial)	Rover+ LSM (partial)
Integration	Separated	
Inter-stations communication	Yes	
Panels technology	Rollable Panels	
Landing site	C1/SR1	
Lunar mobility	No	
Deployment mechanism	Ramp	
Secondary payload	Radiation monitor Dosimeter Magnetometer Pyranometer Temperature sensors	Ion-electron spectrometer Neutral-mass spectrometer Langmuir Probe Dust sensor
Power production	4 KW (TBC)	N/A
Energy storage capability	70 KWh (TBC)	297 W/h
User	LSM (partial)	User
Self-sufficiency	Yes	None, it depends on the LPM
Interface	Dock + Wireless	

Table 10.6: MoonProbe's architecture

10.2.4 Concept #4: MoonRover

MoonRover foresees the integration of the entire assembly, comprising the LPM and LSM, onto a mobile autonomous rover. As already seen for MoonStation, this shared approach of centralized integration streamlines interfacing, minimizes wiring complexity, and supports strong structural cohesion. Nonetheless, the compact layout demands meticulous sensor placement to mitigate risks of obstructed fields of view, thermal interactions, and electromagnetic interference. As a result, sensor operations must be organized in duty cycles: high-power instruments are activated intermittently to conserve energy, while passive sensors remain continuously active where feasible. This mission

concept aims to maximize operational flexibility, enabling the recharge of users distributed across different locations, especially those unable to autonomously reach the station.
Once passively released from the lander, via a deployment mechanism to be chosen between the Davit or the Egress system [R.D. 272][R.D. 273], MoonRover becomes immediately operational: the integrated sensors start collecting environmental data during the exploration phase, while the power station simultaneously accumulates energy. Upon reaching an optimal charge level, the unit can navigate to the location of the user, which in this case is stationary. The energy interaction is therefore reversed compared to the previous concepts; however, it requires reliable navigation capabilities and an optimized energy management strategy to balance both mobility demands and power delivery.
MoonRover is characterized by a significantly lower power output compared to other configurations, amounting to 2.5 kW (TBC). This outcome is understandable, considering that a substantial portion of the energy generated by the solar panels is used by the rover itself for mobility. For this reason, the choice of solar panel technology was made to optimize energy production: this configuration employs thin-film solar panels, which can be stored more efficiently due to their nature, allowing for a greater usable surface area within the same volume, which means more power production.
The user interface is dual: there are a fixed dock and a tether, a more suitable interface for an astronaut who needs to recharge a scientific instrument.
Since this configuration is compliant with missions requiring dynamic support and adaptability to evolving scenarios, it was selected the C1 landing site, whose characteristics are well-suited for spatial distribution and surface accessibility.
An overview of the concept is provided in Table 10.7, preliminary design solutions are detailed in Section 11.

Concept's name	MoonRover
Number of stations	1
Elements	(LPM+LSM)
Integration	Unique assembly
Panels technology	Thin-film solar panels
Landing site	C1
Lunar motion	Yes
Deployment mechanism	Davit system/ Egress
Secondary payload	Entire LSM
Produced energy	2.5 kW (TBC)
Energy storage capability	60 kWh (TBC)
On board user	No
Self-sufficiency	Yes
Interface	Tether/ dock (TBC)

Table 10.7: MoonRover's architecture

10.3 Preliminary mass budget, expected power production and energy storage capability

In order to perform a preliminary estimation of the power that can be generated and stored by the power station, it was first necessary to determine the percentage of mass allocated to the EGSD system. This required a comprehensive analysis of the mass budget, including all subsystems. To that end, data gathered from previous missions [R.D. 106] [R.D. 255] and other available technical references [R.D. 3], which enabled us to establish a nominal reference mass budget. In Table 10.8 the reference ranges obtained from relevant documents are shows. In Table 10.9 the selected baseline mass budget designed to address the first of the concepts, namely MoonStation, is presented. As explained later, it was subjected to a feasibility check to assess its viability. Based on the updated values of MoonStation, shown in Figure 10.3, the mass budgets for all the other concepts have subsequently been derived, incorporating feedback and considerations from the responsible of the design's WPs for the individual subsystems.

Subsystem	Mass % range
EGSD	45% - 60%
Deployment mechanism	15% - 25%

Structure & Mechanisms	5% - 10 %
TCS	8% - 12%
Secondary payload	1% - 5%
TT&C	5% - 10%
ADCS	1% - 3%

Table 10.8: Mass percentage ranges derived from similar missions

Subsystem	Mass (%)	Mass (kg)
EGSD	54.0%	345.6
Deployment mechanism	23.0%	147.2
Structure & Mechanisms	5.0%	32
TCS	9.0%	57.6
Secondary payload	2.0%	12.8
TT&C	5.0%	32.0
ADCS	2.0%	12.8
Total mass without margin		640.0
Harness	5.0%	32.0
System margin	20%	128.0
Total mass		800.0

Table 10.9: MoonStation's preliminary baseline mass budget

As shown in Table 10.9 the baseline mass budget allocation has been divided among the following subsystems: EGSD, deployment mechanism, Structure & Mechanisms, TCS, secondary payload, TT&C, ADCS. The percentages in the table are all referenced to the nominal mass of 640 kg. In particular, the harness and system margin are calculated as 5% and 20% of the nominal mass, respectively [R.D. 107]. Compared to the classical subdivision of spacecraft subsystems, several key differences can be noted. Instead of separating the EPS and the primary payload, a single representative subsystem, EGSD, has been defined. This subsystem is responsible for both the generation and storage of energy for system survival, traditionally the role of the EPS, and for supplying power to the users, in this case associated with the payload. This explains the significant mass allocation assigned to this subsystem. Moreover, the Structure & Mechanisms subsystem does not encompass the entire structural and mechanical domain as commonly defined. Rather, it is limited to elements such as hold-down devices, bonding structures, panel and antenna rotation mechanisms, structural support components, and similar items. A separate subsystem, deployment mechanism, has been introduced to account for the mass of the wheeled cart and/or rover, depending on the selected concept, as well as the deployment system, including ramps, Egress mechanisms, and other related hardware. This distinction enables a more accurate assessment of mass allocation variability, distinguishing between structural components, which primarily depend on required redundancies, and deployment mechanisms, which vary according to the specific technology implemented.

The preliminary mass budget analysis has begun with the development of a baseline configuration for the MoonStation concept. This has been selected as the initial reference case because it represented the simplest architecture among the proposed options, enabling the team to establish a clear and realistic starting point for mass allocation across all subsystems. As shown in Table 10.9, the MoonStation mass budget has been carefully designed to balance the requirements of the key subsystems, while prioritizing the allocation for the EGSD subsystem. This has ensured that the power station could fulfil its core function of generating and storing sufficient energy for system survival and payload operation. Following the creation of this baseline, the mass budget has undergone an initial feasibility review to verify compliance with mission constraints and to confirm that each subsystem could deliver its intended functionality within the allocated mass. This review has included feedback from the responsible teams for each subsystem, ensuring that critical aspects, such as structural integrity, thermal control, deployment mechanisms, and communications, were appropriately covered. An updated mass budget for MoonStation has consequently been obtained and it served as the foundation for deriving the mass budgets of the remaining concepts: MoonProbe, MoonGrid, and MoonRover. Rather than initiating separate detailed mass estimations for each configuration, a logical and qualitative approach has been applied. Starting from the MoonStation allocation, the mass of specific subsystems has been adjusted based on the

distinctive features and operational requirements of each concept. For instance, concepts featuring mobile platforms, such as MoonProbe's small rover or MoonGrid's multiple rovers, have required increased mass allocations for the Deployment mechanism and TCS. This reflected both the added mechanical complexity and the need to dissipate higher thermal loads associated with additional equipment or sustained movement. Similarly, structures and mechanisms mass allocations were adapted according to the number of modules or mobility features integrated into the architecture. These adjustments were driven by reasoned engineering judgement and qualitative comparisons rather than separate bottom-up sizing exercises. The process ensured internal coherence between concepts while respecting the total available mass and the system margin philosophy applied across all configurations. The final preliminary mass budgets for all concepts are illustrated in Figure 10.3. The figure provides a clear comparison of subsystem mass allocations for each configuration, enabling stakeholders to appreciate how the different architectural choices impacted overall mass distribution. The percentages in the figure are all referenced to the nominal mass of 640 kg.

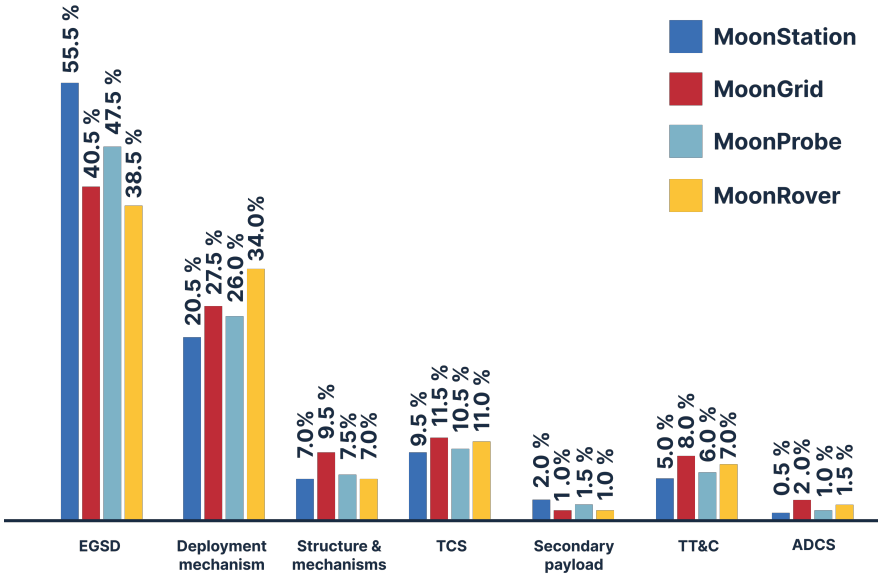

Figure 10.3: Preliminary mass budgets for the different concepts

Regarding the deployment mechanism, MoonStation shows the lowest percentage, as it uses a simple wheeled cart and ramp system. MoonProbe presents a larger mass than MoonStation due to the inclusion of a small rover. In MoonGrid, the increase is more significant, stemming from the use of three rovers. Finally, MoonRover requires the highest mass, as it employs a rover comparable in size to the Lunar Roving Vehicle (LRV) [R.D. 106], which involves a substantially heavier and more complex structure. From the perspective of Structure & Mechanisms, MoonStation and MoonRover are lighter, as they are based on a single-module configuration. In contrast, MoonProbe and MoonGrid incorporate multiple modules, and thus require multiple mechanisms, resulting in a greater mass allocation. Thermal control also varies across the different concepts: starting from the minimum configuration in MoonStation, mass increases in MoonProbe to meet the needs of the small rover and further rises in MoonGrid due to the presence of three rovers. MoonRover presents an intermediate value, since higher dissipation must be considered due to the continuous movement of the main rover.

As for the secondary payload, MoonStation provides the greatest available space, whereas in the other architecture, the space is progressively reduced to accommodate the inclusion of rovers. The TT&C subsystem sees an increase in mass according to the number of redundancies required, which are essential to ensure reliable and efficient communication both between the various rovers and between the rovers and the main station. Regarding the ADCS, the lowest value is found in MoonStation, since the station is fixed. The value increases in the other concepts, which require the use of mobile elements such as rovers. In particular, the highest value is observed in MoonGrid, due to system redundancy introduced by the presence of three rovers. Lastly, the EGSD subsystem, while meeting the minimum requirement in all configurations, takes up all the remaining available mass. It has the largest allocation in MoonStation and MoonProbe.

Following this analysis, it is therefore possible to show how much energy can be produced and stored in the different configurations. The results are shown in Figure 10.4, where energy (red) and power (blue) are represented on the same graph. The x-axis shows the modules, while the y-axis displays the different concepts.

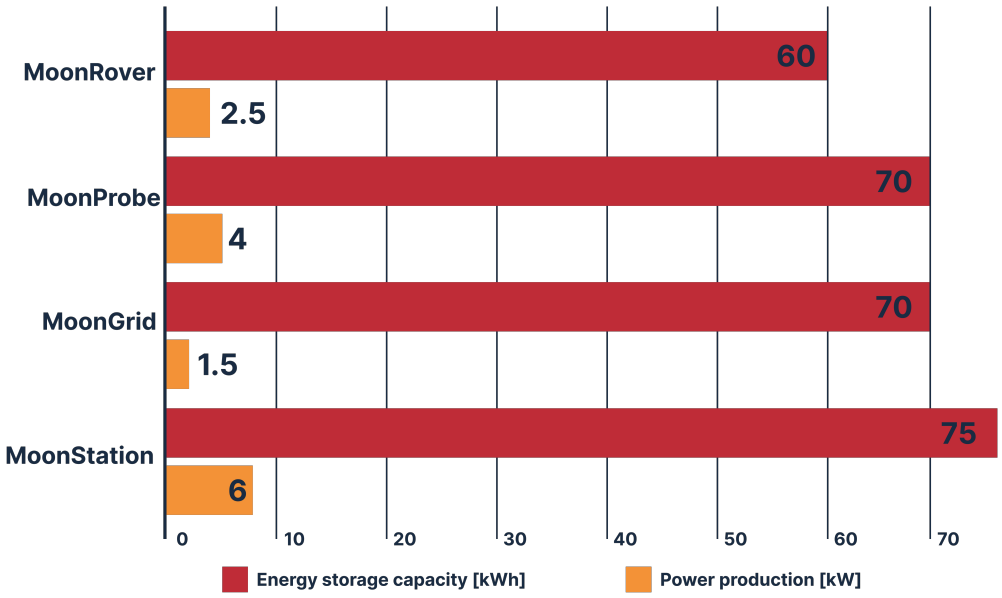

Figure 10.4: Expected power production and energy storage capacity

10.4 Trade-off analysis and baseline concept selection

In the following sections AMPERE*'s* mission concepts are evaluated through a structured trade-off analysis, allowing the selection of the most appropriate baseline mission architecture. Identifying the key system design drivers that influence the overall mission architecture represents the first step of this process. For the AMPERE mission, the following design drivers have been defined:

- costs
- expected returns (derived from the risk analysis)
- reliability
- technical feasibility
- mission objectives achievable
- market differentiation

The identified drivers have been translated into six trade-off parameters, as shown in Table 10.10. The premise of the trade-off analysis is that each concept is assigned a score for each parameter. An overall score for each concept is then calculated as the weighted average of its individual scores, using the weights listed in Table 10.10 which reflect the relative importance of each parameter. The better a concept performs against a given driver, the higher its score for the relative parameter is, and consequently, the concept with the highest overall weighted score is deemed the most favourable.

Each parameter ranges from 0 to 1, where 1 represents the most favourable case. To facilitate the interpretation of the scores used in and resulting from the trade-off analysis, dark green indicates the best result, light green the second best, light red the third, and dark red the lowest performing among the four concepts. Moreover, when a parameter's value for a given concept is the highest among the four concepts, it is indicated in bold in the trade-off tables.

Parameter	Evaluation description	Weight
Costs	Evaluation of total mission cost, properly normalized so that higher values are assigned to cheaper solutions	0.05
Expected returns	Quantitative risk analysis	0.10
Reliability	Measure of system robustness and likelihood of successful operation over the mission lifetime	0.15
Technical score	Quantification of the overall technological feasibility and robustness of each mission concept	0.30
Mission objectives	Degree to which the concept fulfils defined Mission Objectives	0.30
Market differentiation	Evaluation of the concept's uniqueness and strategic value in a competitive space market	0.10
Total		1

Table 10.10: Trade-off parameters

10.4.1 Costs trade-off analysis

To evaluate the value of the "Costs" parameter in support of the trade-off analysis, a preliminary cost estimate has been prepared for each mission concept, incorporating a qualitative complexity assessment. The results are expressed in euros (EUR) and then normalized from 0 to 1, so that the most economical solution receives a higher score, consistently with the other Trade-off drivers. The QuickCost model (NASA) [R.D. 1] has been used to obtain first-order cost estimates for each mission concept. This parametric model relies on key mission parameters such as:

- Dry mass [kg]
- Average power consumption [in Watts, at Beginning of Life (BoL)]
- Data transmission percentile [data %]
- Expected mission lifetime [months]
- New [%]
- Planetary [0,1]
- Authorization To Proceed (ATP, in Years)
- Instruments complexity [%]
- Team experience [from 1 to 4]

To generate conservative estimates, a worst-case approach was applied, considering:

- + 41% cost margin based on the model Standard Error of Estimate (SEE) [R.D. 1]
- + 9% ground segment cost adjustment
- + 5% per year for mission operation.

The following data are assumed equal for the four concepts:

- Dry mass = 800 kg
- Data transmission percentile = 0.15
- Mission life = 12 months
- Planetary = 1
- ATP = 2032
- Team experience = 2

The difference is in the values shown in Table 10.11.

Data	MoonStation	MoonGrid	MoonProbe	MoonRover
Power	500	1000	600	1000
New	0.7	1.2	1	1.1
InstrComp%	0.5	0.7	0.6	0.8

Table 10.11 Power, New, InstrComp data for QuickCost Model

Costs have been inflated from FY2010 USD to FY2035 EUR, using cumulative inflation indices on the USD and a USD/EUR exchange rate assumed equal to the FY2025 (set at an average of 0.88). More specifically Year over Year (YoY) USD

inflation data from 2010 to 2025 are taken from [R.D. 108] while from FY2025 to FY2025 the YoY inflation has been considered as the average of the previous 15 years, resulting in a cumulative inflation of 93.82%. The base QuickCost (QC) cost is evaluated and for the cost analysis the worst-case scenario is used (i.e. the base cost plus the SEE).

	MoonStation	MoonGrid	MoonProbe	MoonRover
Base QC cost (Mln USD FY2010)	11.56	30.26	19.67	27.24
SEE	4.74	12.41	8.07	11.17
Worst case (Mln USD 2010)	18.58	48.65	31.62	43.79
Worst case (Inf adj., Mln USD)	36.02	94.28	61.28	84.86
Worst case (Inf adj., Mln EUR)	31.70	82.97	53.93	74.68

Table 10.12: Estimated mission cost with QuickCost tool. Results are in millions of USD or EUR

In Table 10.12 the first row called "Base Cost" shows the output from the QuickCost Formula [R.D. 2] in millions of 2010 USD. Then worst and best cases are found using the SEE of 41% and considering then the ground segment and mission operation adjustment as well as the inflation and the EUR-USD exchange. The final values of cost are the "Worst case (Inf adj, Mln EUR)". MoonStation (dark green cell) is the less expensive between the four concepts, while MoonGrid (dark red cell) is the most expensive one.

To complement the numerical estimation, a Complexity-Based cost Index (CBI) has been computed for each architecture. This approach allows the assessment of relative mission complexity, based on NASA's methodology for early-phase concept discrimination. The following key cost drivers have been selected for each concept:

- Payload complexity
- Architecture complexity
- Operation complexity
- Technology TRL
- Heritage

Each driver has been rated from 1 (low complexity) to 5 (high complexity) and converted into a point score using an exponential scale, as shown in Equation (10.1).

$$Score = 2^{Level} \tag{10.1}$$

This approach guarantees a score ranging from a minimum of 2 to a maximum of 32 and penalizes the excessive complexity of the architectures. A special consideration shall be made for the TRL, heritage and feedforward drivers:

- Higher TRL and Heritage reduce complexity, hence lower the score
- Feedforward potential increases complexity, so higher the score.

For each concept, the concept CBI score is the sum of all driver scores.

	MoonStation		MoonGrid		MoonProbe		MoonRover	
Driver	Level	Score	Level	Score	Level	Score	Level	Score
Payload complexity	2	4	4	16	3	8	4	16
Architecture complexity	2	4	5	32	3	8	4	16
Operation complexity	2	4	4	16	3	8	4	16
Technology TRL (inverse)	1	2	4	16	2	4	2	4
Heritage	2	4	4	16	3	8	2	4
Total score	18		96		36		56	
QC with CBI (mln €)	31.70		442.51		107.85		232.34	

Table 10.13: Concepts CBI scores

Table 10.13 enhance the difference between MoonStation and MoonGrid, resulting in a MoonGrid cost completely out of scale. To anchor the complexity scores to actual cost values, the concept with the lowest complexity and a reliable QuickCost estimate (MoonStation) has been selected as reference.

The cost for all other concepts has been derived by scaling proportionally based on their CBI score, as shown in Equation (10.2).

$$Cost_i = Cost_{QC,ref} \cdot \left(\frac{CBI_i}{CBI_{ref}} \right) \quad (10.2)$$

This hybrid approach enables CBI-based cost differentiation while retaining a realistic cost baseline.
This cost is then divided by 700 (mln €) representing the upper value of the ESA's Class II mission costs and complemented to 1. The scores from 0 to 1 of the four concepts are shown in Table 10.14.

Concept	MoonStation	MoonGrid	MoonProbe	MoonRover
Cost score	0.95	0.37	3.85	0.67

Table 10.14: Costs scores for each concept

MoonStation has the higher score, followed by MoonProbe. The second concept, MoonGrid, is heavily penalized by its complexity.

10.4.2 Expected returns trade-off analysis

Risk management is an essential part of the planning process for any mission, especially space missions. Proper risk management during the preliminary phases of mission design ensures the minimization of critical issues during the subsequent production and operation phases.
For this reason, a preliminary risk analysis has been carried out, evaluating every proposed concept using both qualitative and quantitative approaches.
The aim of this study is to produce quantifiable results that could support the trade-off analysis, using reference scales and methodologies derived from [A.D. 10], [R.D. 1], [R.D. 3],[R.D. 4], [R.D. 109] and [R.D. 110]. Table 10.15 and Table 10.16 show, respectively, likelihood and impact scales that have been adopted.

Likelihood			
Bin	Qualitative definition	Mission [%]	Implementation [%]
A	Very Low	<5	>10
B	Low	5-15	>25
C	Moderate	15-25	>50
D	High	25-50	>70
E	Very high	>50	>100

Table 10.15: Likelihood scale

Impact				
Bin	Qualitative definition	Nominal impact (in terms of mission objectives)	Mission [% of lost mission objectives]	Implementation [% of exploited resources]
1	Negligible	Virtually no loss	1	1
2	Low	Acceptable loss	1-20	20
3	Moderate	Measurable loss, but still manageable	20-50	60
4	High	Unacceptable loss	50-90	100
5	Catastrophic	Complete loss	100	120

Table 10.16: Impact scale

These reference scales have been used to develop a tool for the qualitative assessment of the risk priority distribution related to the AMPERE Mission Concepts, also known as fever chart (Table 10.17).

E	E1	E2	E3	E4	E5
D	D1	D2	D3	D4	D5
C	C1	C2	C3	C4	C5
B	B1	B2	B3	B4	B5
A	A1	A2	A3	A4	A5
LIKELIHOOD / IMPACT	1	2	3	4	5

Table 10.17: Fever chart

Table 10.17 highlights a clear contrast between the different layers, which visually supports the ranking of risks using a priority-based approach. For clarity, Table 10.18 shows how to mitigate risks based on the obtained rank.

Risk index	Priority	Description	Action
A1-A2-A3-B1-B2-C1	Lowest	Acceptable risk	No action required
A4-B3-C2-D1-E1	Low	Acceptable risk	No further action other than monitoring
A5-B4-B5-C3-D2-E2	Moderate	Unacceptable risk	Mitigation action shall be implemented to avoid aggravation of the risk.
C4-C4-D3-D4-E3	High	Unacceptable risk	Management shall be notified. Aggressive countermeasures shall be applied.
D5-E4-E5	Highest	Unacceptable risk	

Table 10.18: Risk priority levels and corresponding actions

10.4.2.1 Preliminary risk analysis

A preliminary risk analysis is necessary to emphasize the differences between the mission concepts, as well as to really highlight the areas where additional human and intellectual resources should be concentrated.
Although the mission concepts may be characterized by different risks or root causes all of them share common risk areas. Below is a list of the identified risk areas and corresponding risks:

- ADCS: Failure to maintain nominal attitude
- DEPL: Failure to achieve correct deployment
- EGSD: Failure of the EGSD system
- ENV: Failure to survive the lunar night
- MA: Failure to achieve the nominal, expected landing
- PAY: Insufficient results
- RVR: Failure of the autonomous infrastructure
- TCS: Inability to mitigate lunar temperatures
- TT&C: Communication failure
- USN: Failure to provide the expected services

These risk areas identify mission risks; furthermore, the RVR risk area applies only to Concepts 3 and 4. Moreover, an additional risk area identifies an implementation risk common to every concept:

- MSN: Failure in mission design reliability

It is to be noted that implementation risks do not have any weight in the expected returns computation, but they do appear as possible risks on the fever charts.
At the end of the risk analysis process, two results have been generated:

- a visual representation of the risks of the different concepts, displayed on a fever chart, which could also serve in the trade-off analysis.
- a numerical estimation of the expected returned objectives, as explained in [R.D. 1] and [A.D. 10], that will take part in the weighted ranking explained in Section 10.4.

Tables from Table 10.20 to Table 10.23 are the risk indices of the four mission concepts. Table 10.19 shows the common risks for all the proposed architectures. Each risk area and corresponding risk are followed by their root causes, the responsible WP or node for the cause, Likelihood (L), Impact (I) and the start dates marking when the WP or node began addressing the root cause. These start dates correspond to the dates in the Gantt chart (Section 8.3) indicating when each WP begins its activities. Additionally, when a node is present, it is considered to start working at T0. Multiple WPs may be responsible for a given root cause. Finally, all end dates have been omitted, as they coincide with the MDR.

Risk area	Risk	Root causes	Responsible WPs or nodes	L	I	Start date
MA	Failure in achieving the nominal, expected landing	Fail before landing	WP 3.6	A	5	T0 + 3 weeks
		Error in the descending phase	WP 3.6	C	3	T0 + 3 weeks
		Critical landing	WP 3.6	C	5	T0 + 3 weeks
		Missed target landing point	WP 3.6	B	4	T0 + 3 weeks
PAY	Insufficient results	Failure of the payload sensors	WP 3.5 WP 2.3	C	2	T0

Table 10.19: Common risks for every architecture

Risk area	Risk	Root causes	Responsible WPs or nodes	L	I	Start date
ENV	Failure to survive lunar environment	Undesired mechanical effects of lunar dust	WP 3.7 WP 3.5	D	4	T0 + 2 weeks
		Triboelectric charging of outer surfaces due to lunar dust	WP 3.7 WP 3.5	D	3	T0 + 2 weeks
		Dangerous phenomena related to radiation	WP 3.7 WP 3.5	C	3	T0 + 2 weeks
		Meteoroid impact	WP 3.7 WP 3.5	E	4	T0 +2 weeks
		Moonquakes	WP 3.7	B	2	T0 + 2 weeks
		Thermal stress affecting structures	WP 3.2 WP 3.7	E	4	T0 + 2 weeks
		Non-sufficient light exposure	WP 3.7 WP 3.1	C	5	T0 + 2 weeks
		Lander damages	WP 3.5 WP 3.7	C	3	T0 + 3 weeks
ADCS	Failure to keep nominal asset	Computational errors	WP 3.3 WP 3.4	C	3	T0 + 3 weeks
		Sun sensors low accuracy	WP 3.3	C	2	T0 + 3 weeks
		Sun sensors failure	WP 3.3	B	4	T0 + 3 weeks
EGSD		Battery failure	WP 3.1	B	5	T0 + 2 weeks

	Failure of the EGSD system	Solar array failure	WP 3.1	C	5	T0 + 2 weeks
		Failure to properly distribute power	WP 3.1	B	4	T0 + 2 weeks
		Inadequate solar array sizing	WP 3.1	C	4	T0 + 2 weeks
		Fuel cells failure	WP 3.1	C	5	T0 + 2 weeks
		Tanks leakage	WP 3.1	C	4	T0 + 2 weeks
		Tanks rupture	WP 3.1	B	5	T0 + 2 weeks
DEPL	Failure to achieve correct deployment	Tipping over	WP 3.5 WP 3.3	C	5	T0 + 3 weeks
		Failure of the deployment architecture/structure	WP 3.5	C	5	T0 + 3 weeks
		Deployment solution doesn't function properly	WP 3.5	B	5	T0 + 3 weeks
MA	Failure in achieving the nominal, expected landing	Failure before landing	WP 3.6	A	5	T0 + 3 weeks
		Error in the descending phase	WP 3.6	C	3	T0 + 3 weeks
		Critical landing	WP 3.6	C	5	T0 + 3 weeks
		Missed target landing point	WP 3.6	B	4	T0 + 3 weeks
TT&C	Communication failure	Obstructed/faulty link between Moonlight and power station	WP 3.4	B	3	T0 + 3 weeks
		Data corruption	WP 3.4	B	4	T0 + 3 weeks
		TT&C subsystem failure	WP 3.4	B	4	T0 + 3 weeks
TCS	Inability to mitigate lunar temperatures	Temperature control failure	WP 3.2	C	5	T0 + 3 weeks
		Temperature range wider than anticipated	WP 3.2 WP 3.7	B	3	T0 + 3 weeks
USN	Failure to provide the expected services	Failure to protect user interfaces	WP 3.5 WP 2.3	C	4	T0
		Insufficient energy provision	WP 3.1	C	4	T0 + 2 weeks
		Failure to provide meaningful support	WP 2.2	C	3	T0
PAY	Insufficient results	Failure of the payload sensors	WP 2.3 WP 3.5	C	2	T0
MSN	Resources overrun	Failure to respect mass margins	Design node	C	5	T0
		Failure to respect volume margins	WP 2.3	C	5	T0
		Low TRLs	Design node	D	4	T0

Table 10.20: MoonStation risk index

Risk area	Risk	Root causes	Responsible WPs or nodes	L	I	Start date
ENV	Failure to survive lunar environment	Undesired mechanical effects of lunar dust	WP 3.7 WP 3.5	E	4	T0 + 2 weeks
		Electric/charging effects due to dust	WP 3.7 WP 3.5	D	3	T0 + 2 weeks
		Dangerous phenomena related to radiation	WP 3.7 WP 3.5	C	3	T0 + 2 weeks
		Meteoroid impact	WP 3.7 WP 3.5	E	3	T0 + 2 weeks
		Moonquakes	WP 3.7	B	2	T0 + 2 weeks
		Thermal stress affecting structures	WP 3.2 WP 3.7	E	3	T0 + 3 weeks
		Non-sufficient light exposure	WP 3.7 WP 3.1	C	5	T0 + 2 weeks
		Lander damages	WP 3.5 WP 3.7	C	3	T0 + 3 weeks
ADCS	Failure to keep nominal asset	Computational errors	WP 3.3 WP 3.4	C	3	T0 + 3 weeks
		Sun sensors low accuracy	WP 3.3	C	2	T0 + 3 weeks
		Sun sensors failure	WP 3.3	B	4	T0 + 3 weeks
EGSD	Failure of the EGSD system	Battery failure	WP 3.1	C	5	T0 + 2 weeks
		Solar array failure	WP 3.1	C	5	T0 + 2 weeks
		Failure to properly distribute power	WP 3.1	C	4	T0 + 2 weeks
		Inadequate solar array sizing	WP 3.1	D	4	T0 + 2 weeks
		Fuel cells failure	WP 3.1	C	5	T0 + 2 weeks
		Tanks leakage	WP 3.1	C	4	T0 + 2 weeks
		Tanks rupture	WP 3.1	B	5	T0 + 2 weeks
DEPL	Failure to achieve correct deployment	Tipping over	WP 3.5 WP 3.3	B	5	T0 + 3 weeks
		Failure of the deployment architecture/structure	WP 3.5	D	5	T0 + 3 weeks
		Deployment solution doesn't function properly	WP 3.5	C	5	T0 + 3 weeks

MA	Failure in achieving the nominal, expected landing	Fail before landing	WP 3.6	A	5	T0 + 3 weeks
		Error in the descending phase	WP 3.6	C	3	T0 + 3 weeks
		Critical landing	WP 3.6	C	5	T0 + 3 weeks
		Missed target landing point	WP 3.6	B	4	T0 + 3 weeks
TT&C	Communication failure	Obstructed/faulty link between Moonlight and power station	WP 3.4	A	3	T0 + 3 weeks
		Data corruption	WP 3.4	C	4	T0 + 3 weeks
		TT&C subsystem failure	WP 3.4	B	4	T0 + 3 weeks
TCS	Inability to mitigate lunar temperatures	Temperature control failure	WP 3.2	D	5	T0 + 3 weeks
		Temperature range wider than anticipated	WP 3.2 WP 3.7	B	3	T0 + 3 weeks
USN	Failure to provide the expected services	Failure to protect user interfaces	WP 3.5 WP 2.3	D	4	T0
		Insufficient energy provision	WP 3.1	D	3	T0 + 2 weeks
		Failure to provide meaningful support	WP 2.2	C	3	T0
PAY	Insufficient results	Failure of the payload sensors	WP 2.3 WP 3.5	C	2	T0
MSN	Resources overrun	Failure to respect mass margins	Design node	C	5	T0
		Failure to respect volume margins	WP 2.3	C	5	T0
		Low TRLs	Design node	D	4	T0

Table 10.21: MoonGrid risk index

Risk area	Risk	Root causes	Responsible WPs or nodes	L	I	Start date
ENV	Failure to survive lunar environment	Undesired mechanical effects of lunar dust	WP 3.7 WP 3.5	E	4	T0 + 2 weeks
		Electric/charging effects due to dust	WP 3.7 WP 3.5	D	4	T0 + 2 weeks
		Dangerous phenomena related to radiation	WP 3.7 WP 3.5	C	3	T0 + 2 weeks
		Meteoroid impact	WP 3.7 WP 3.5	D	3	T0 + 2 weeks
		Moonquakes	WP 3.7	B	1	T0 + 2 weeks

		Thermal stress affecting structures	WP 3.2 WP 3.7	D	3	T0 + 3 weeks
		Non-sufficient light exposure	WP 3.7 WP 3.1	C	5	T0 + 2 weeks
		Lander damages	WP 3.5 WP 3.7	C	3	T0 + 3 weeks
ADCS	Failure to keep nominal asset	Computational errors	WP 3.3 WP 3.4	C	3	T0 + 3 weeks
		Sun sensors low accuracy	WP 3.3	C	2	T0 + 3 weeks
		Sun sensors failure	WP 3.3	B	4	T0 + 3 weeks
EGSD	Failure of the EGSD system	Battery failure	WP 3.1	B	5	T0 + 2 weeks
		Solar array failure	WP 3.1	C	5	T0 + 2 weeks
		Failure to properly distribute power	WP 3.1	B	4	T0 + 2 weeks
		Inadequate solar array sizing	WP 3.1	C	4	T0 + 2 weeks
		Fuel cells failure	WP 3.1	C	5	T0 + 2 weeks
		Tanks leakage	WP 3.1	C	4	T0 + 2 weeks
		Tanks rupture	WP 3.1	B	5	T0 + 2 weeks
DEPL	Failure to achieve correct deployment	Tipping over	WP 3.5 WP 3.3	B	5	T0 + 3 weeks
		Failure of the deployment mechanism	WP 3.5	C	5	T0 + 3 weeks
		Deployment solution doesn't function properly	WP 3.5	C	4	T0 + 3 weeks
MA	Failure in achieving the nominal, expected landing	Failure before landing	WP 3.6	A	5	T0 + 3 weeks
		Error in the descending phase	WP 3.6	C	3	T0 + 3 weeks
		Critical landing	WP 3.6	C	5	T0 + 3 weeks

		Missed target landing point	WP 3.6	B	4	T0 + 3 weeks
TT&C	Communication failure	Obstructed/faulty link between moonlight and power station	WP 3.4	A	3	T0 + 3 weeks
		Data corruption	WP 3.4	C	4	T0 + 3 weeks
		TT&C subsystem failure	WP 3.4	B	4	T0 + 3 weeks
TCS	Inability to mitigate lunar temperatures	Temperature control failure	WP 3.2	D	5	T0 + 3 weeks
		Temperature range wider than anticipated	WP 3.2 WP 3.7	C	3	T0 + 3 weeks
USN	Failure to provide the expected services	Failure to protect user interfaces	WP 3.5 WP 2.3	C	2	T0
		Insufficient energy provision	WP 3.1	C	2	T0 + 2 weeks
		Failure to provide meaningful support	WP 2.2	B	1	T0
PAY	Insufficient results	Failure of the payload sensors	WP 2.3 WP 3.5	C	2	T0
RVR	Failure of the autonomous moon rover	Rover sensors failure	WP 3.3	A	3	T0 + 3 weeks
		Inadequate protection to the lunar environment	WP 3.5	B	3	T0 + 3 weeks
		Poor planning of the chosen path	WP 3.6 WP 3.7	C	2	T0 + 3 weeks
		Communication failure	WP 3.4	C	2	T0 + 3 weeks
		Avary and subsequent loss of the rover	WP 3.3 WP 3.4	B	3	T0 + 3 weeks
MSN	Resources overrun	Failure to respect mass margins	Design node	C	5	T0
		Failure to respect volume margins	WP 2.3	D	5	T0
		Low TRLs	Design node	D	4	T0

Table 10.22: MoonProbe risk index

Risk area	Risk	Root causes	Responsible WPs or nodes	L	I	Start date
ENV	Failure to survive lunar environment	Undesired mechanical effects of lunar dust	WP 3.7 WP 3.5	E	5	T0 + 2 weeks
		Electric/charging effects due to dust	WP 3.7 WP 3.5	E	4	T0 + 2 weeks
		Dangerous phenomena related to radiation	WP 3.7 WP 3.5	C	3	T0 + 2 weeks
		Meteoroid impact	WP 3.7 WP 3.5	D	3	T0 + 2 weeks
		Moonquakes	WP 3.7	B	3	T0 + 3 weeks
		Thermal stress affects structures	WP 3.2 WP 3.7	D	3	T0 + 2 weeks
		Non-sufficient light exposure	WP 3.7 WP 3.1	B	3	T0 + 3 weeks
		Lander damages	WP 3.5	B	3	T0 + 3 weeks
ADCS	Failure to keep nominal asset	Computational errors	WP 3.3 WP 3.4	C	3	T0 + 3 weeks
		Sun sensor accuracy low	WP 3.3	C	2	T0 + 3 weeks
		Sun sensor failure	WP 3.3	B	4	T0 + 2 weeks
EGSD	Failure of the EGSD system	Battery failure	WP 3.1	C	5	T0 + 2 weeks
		Solar array failure	WP 3.1	C	5	T0 + 2 weeks
		Failure to properly distribute power	WP 3.1	C	4	T0 + 2 weeks
		Inadequate solar array sizing	WP 3.1	D	4	T0 + 2 weeks
		Fuel cells failure	WP 3.1	C	5	T0 + 2 weeks
		Tanks leakage	WP 3.1	C	4	T0 + 2 weeks
		Tanks rupture	WP 3.1	C	5	T0 + 3 weeks
DEPL	Failure to achieve correct deployment	Tipping over	WP 3.5 WP 3.3	D	5	T0 + 3 weeks
		Failure of the deployment architecture/structure	WP 3.5	D	5	T0 + 3 weeks
		Deployment solution doesn't function properly	WP 3.5	C	4	T0 + 3 weeks
MA	Failure in achieving the nominal, expected landing	Fail before landing	WP 3.6	A	5	T0 + 3 weeks
		Error in the descending phase	WP 3.6	C	3	T0 + 3 weeks
		Critical landing	WP 3.6	C	5	T0 + 3 weeks
		Missed target landing point	WP 3.6	B	4	T0 + 3 weeks

TT&C	Communication failure	Obstructed/faulty link between moonlight and Station	WP 3.4	A	2	T0 + 3 weeks
		Data corruption	WP 3.4	C	4	T0 + 3 weeks
		TT&C subsystem failure	WP 3.4	B	4	T0 + 3 weeks
TCS	Inability to mitigate lunar temperatures	Temperature controls failure	WP 3.2	D	5	T0 + 3 weeks
		Temp range wider than anticipated	WP 3.2 WP 3.7	C	3	T0 + 2 weeks
USN	Failure to provide the expected services	Failure to protect user interfaces	WP 3.5 WP 2.3	C	2	T0
		Insufficient energy Provision	WP 3.1	C	2	T0 + 2 weeks
		Failure to provide meaningful support	WP 2.2	B	1	T0
PAY	Insufficient results	Failure of the payload sensors	WP 3.5 WP 2.3	C	2	T0
RVR	Failure of the autonomous moon roaming station	Rover sensors failure	WP 3.5	A	3	T0 + 3 weeks
		Inadequate protection to the lunar environment	WP 3.5	B	3	T0 + 3 weeks
		Poor planning of the chosen path	WP 3.6	C	2	T0 + 3 weeks
		Communications failure	WP 3.4	C	2	T0 + 3 weeks
		Avary and subsequent loss of the entire station	WP 3.3 WP 3.4	B	5	T0 + 3 weeks
		Unexpected coupling between inertia forces and possible changes in geometry	WP 3.5	D	4	T0 + 3 weeks
MSN	Resources overrun	Failure to respect mass margins	Design node	C	5	T0
		Failure to respect volume margins	WP 2.3	D	5	T0
		Low TRLs	Design node	E	5	T0

Table 10.23: MoonRover risk index

Starting from the values of likelihood and impact in the risk indices, it is possible to obtain, for each concept, the likelihood and impact for each risk area, through a weighted average as detailed [R.D. 109]. These results were then reported on the fever charts, Figure 10.5, to visually track the severity of risks.

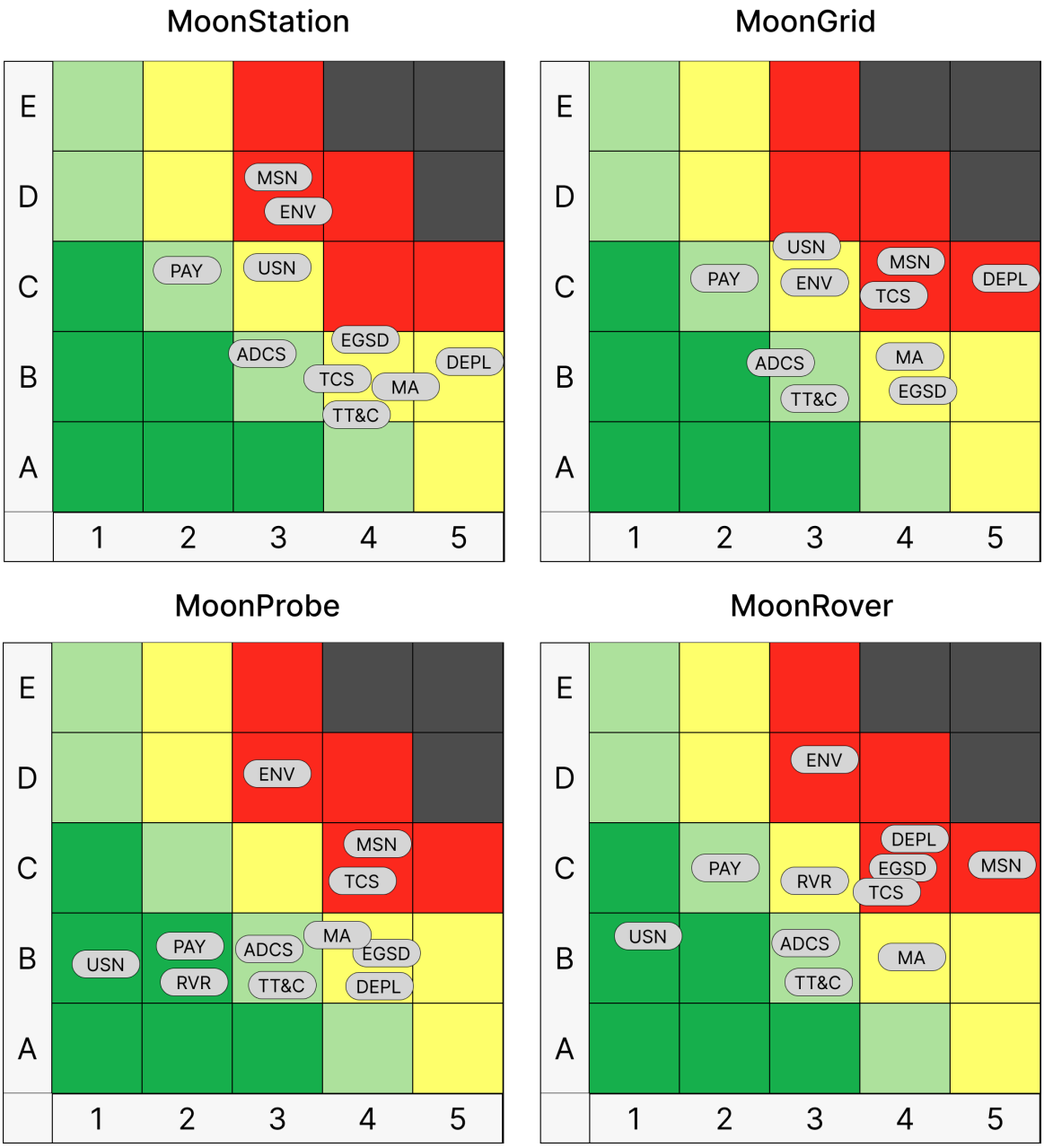

Figure 10.5: MoonStation, MoonGrid, MoonProbe, MoonRover fever charts

With the help of the aforementioned tools, a quantitative analysis has been conducted. The obtained results are exposed in Table 10.24 and have been obtained by applying the approach presented in [R.D. 1].

Concept	Expected return E [%]
MoonStation	0.78
MoonGrid	0.82
MoonProbe	0.83
MoonRover	0.87

Table 10.24: Mission concepts expected returns

Even though, from a purely visual standpoint, one might infer that MoonProbe carries the lowest risk exposure, a more rigorous assessment leads to a different conclusion. In fact, as Table 10.24 demonstrates, MoonRover exhibits a more

balanced risk profile, thereby reducing overall risk severity, which perfectly concludes with MoonRover as the concept that overall is the one showing a balance in terms of risks.

10.4.3 Preliminary reliability trade-off analysis

A qualitative reliability assessment has been carried out for the four mission concepts, to evaluate the score for the "Reliability" parameter in support of the trade-off analysis.
The analysis has been performed qualitatively by assigning, for each configuration and for each WP listed in Table 10.25 a reliability score. This score is an integer from 1 to 4 (the more reliable the subsystem, the closer the score is to 4), based on a preliminary idea of the output that the WP is expected to produce.
WP 2.3 Payload Accommodation & Interfaces and all design WPs, except WP 3.6 Mission Analysis, have been selected because only for these packages the impact of design choices on reliability varies from concept to concept. Mission Analysis has not been included since the same sequence of operations is envisaged for every concept.

WP	MoonStation	MoonGrid	MoonProbe	MoonRover
2.3: Payload	3	1	**4**	2
3.1: EGSD	3	**4**	3	2
3.2: TCS	**4**	1	3	2
3.3: ADCS	**4**	3	**4**	2
3.4: TT&C	**4**	2	3	**4**
3.5: STR&MEC	3	1	**4**	2
3.7: Environment	**4**	2	**4**	3
Score	25	14	25	17

Table 10.25: Reliability values for each concept

Once the scores have been collected and summed for each concept, final values between 0 and 1 have been assigned through appropriate scaling for each configuration. The scaling has been performed by assigning a value of 1 to the concept with the highest total score and adjusting the others proportionally, according to Equation (10.3):

$$Reliability\ Score_i = \frac{Reliability_i}{max_{i=1,..,4}\ Reliability_i} \qquad (10.3)$$

In this equation, the subscript i, which takes all integer values from 1 to 4 (inclusive), denotes the i-th concept, where 1 corresponds to MoonStation, 2 to MoonGrid, 3 to MoonProbe, and 4 to MoonRover.

Concept	Reliability	Reliability score
MoonStation	25	1.00
MoonGrid	14	0.56
MoonProbe	25	1.00
MoonRover	17	0.68

Table 10.26: Reliability and reliability score for each concept

Based on the preliminary reliability trade-off analysis, MoonStation and MoonProbe are identified as the most reliable mission architectures, each achieving the highest total reliability score. This outcome highlights their consistent robustness across multiple subsystems. From a qualitative standpoint, both concepts scored higher in Payload Accommodation & Interfaes, TCS and Structure & Mechanisms, indicating a lower susceptibility to design-related failures. These results make MoonStation and MoonProbe (dark green cell) the most favourable options from a reliability perspective in this early design phase.

10.4.4 Technical score trade-off analysis

The technical score has been determined by evaluating the performance of all relevant design node WPs and the system node WP 2.3, Payload Accommodation & Interfaces. The WPs selected for the technical score evaluation are those that feature distinct design solutions for each concept, thereby contributing to the differentiation of the technical score across the various concepts.

The rationale for the inclusion of WP 2.3, Payload Accommodation & Interfaces, is that the secondary payload selection depends on the specific mission concept, in terms of sensors' mass, placement and power consumption.
In particular, the Mission Analysis WP has not been included, since all four concepts involve a South Pole landing, albeit at different sites, and therefore the related design solutions are identical and do not represent a source of differentiation.
To ensure a consistent comparison across the different concepts, each WP has been asked to produce a technical score derived by combining two parameters: Technical Implementation Effort (TIE) and confidence. This dualistic approach enables the integration of both technical insight and epistemic uncertainty.
TIE reflects the expected engineering burden for a given WP solution within a specific mission concept; it combines, for instance, the resource demands (mass, power, volume trade-offs) and development complexity (novel algorithms or control laws, mechanical designs).
To ensure that each WP could generate a TIE value aligned with its intrinsic characteristics, the following procedure has been adopted by each of the WP responsible:

- One or more relevant TIE parameters for each WP have been identified.
- For each concept, a score between 0 and 1 has been assigned to each parameter, such that higher values reflect simpler solutions.
- To each parameter a weight has been assigned based on its relative importance.
- Through the weighted average of all TIE parameters, each WP responsible can determine an appropriate TIE value for each concept.

Confidence represents the degree of knowledge each WP has about the technologies or specific architecture elements, based on existing models, TRL and prior spaceflight applications for the given element. To measure confidence, each WP responsible has been asked to assign a score from 1 to 3, where:

- 1 denotes no available information
- 2 denotes an intermediate level of understanding
- 3 denotes a fully established technology

These two parameters are then combined to yield the technical score of each concept for each WP, derived with the approach defined as per Equation (10.4).

$$technical\ score = TIE * \frac{confidence}{3} \qquad (10.4)$$

The technical score formula ensures that the resulting value lies between 0 and 1.
The specific assignment of TIE and confidence is detailed in the following subsections, each pertaining to a single WP.
In Table 10.27, the resultant technical scores are weighted with the relative importance of each WP with the respect to the overall mission.

WP	Weight	MoonStation	MoonGrid	MoonProbe	MoonRover
EGSD	0.35	0.49	0.15	**0.50**	0.16
TCS	0.20	**0.42**	0.14	0.37	0.32
ADCS	0.05	**0.76**	0.23	0.40	0.73
TT&C	0.05	**0.53**	0.12	0.38	0.44
Structure & Mechanisms	0.25	0.54	0.37	**0.58**	0.39
Environment	0.05	**0.71**	0.27	0.48	0.53
Secondary Payload	0.05	**0.51**	0.13	0.49	0.20
Total	1	0.52	0.21	0.48	0.31

Table 10.27: Resultant technical scores of each WP for each concept and related weights

The chosen weights mirror the mission's focus on generating and distributing energy: EGSD leads with 35%, while Structure & Mechanisms comes in at 25% since this WP encompasses deployment subsystem, mechanical interfaces and any weakness of these mechanisms would jeopardize panel unfurling. TCS follows at 20%, reflecting the critical challenge of maintaining batteries, electronics and moving parts within operational temperature windows in the face of extreme lunar swings.
ADCS, TT&C, Environment and Secondary Payload remain at 5% each because the technical feasibility impacts of each of these WPs on the mission are comparable, and lower than that of the other WPs.

From Table 10.27, it is evident that MoonStation and MoonProbe record the highest technical scores, although MoonStation's is slightly higher.

10.4.4.1 Energy Generation, Storage & Distribution

To compute the TIE associated with the EGSD, five key parameters have been considered: energy production, storage capability, user interface design, power consumed by subsystems, and energy dissipation mechanisms. Energy production and storage capability originate from the same driver, as both are directly influenced by the mass allocated to each configuration. In the MoonStation and MoonProbe concepts, a larger share of the mass budget is allocated to the EGSD system, enabling more robust on-board resources. In contrast, MoonRover assigns a smaller percentage of mass to the EGSD, thereby limiting its available resources. Finally, in MoonGrid, the mass allocated to the EGSD must be distributed among three rovers, each requiring its own electrical subsystem, which reduces their individual capacity for power generation and energy storage. User interface design considers the number of interfaces required for each configuration: one for MoonStation and MoonRover, two for MoonProbe, and three for MoonGrid. Power consumed by subsystems assesses how energy-demanding each configuration is. MoonGrid and MoonRover are the most energy-intensive architectures, as they must provide power for mobility, leaving less energy available for potential users. The energy dissipation mechanism evaluates how each configuration manages any excess energy produced by the system. Ideally, in MoonRover, surplus energy could be used to power the rover's motors; in MoonProbe, it could be used to recharge the LSM rover. In contrast, in the MoonStation and MoonGrid configurations, dissipation technologies may be required to release excess energy as heat.
The scores are presented in Table 10.28.

Parameter	Weight	MoonStation	MoonGrid	MoonProbe	MoonRover
Energy production	0.30	0.80	0.20	0.70	0.40
Storage capability	0.30	0.80	0.70	0.80	0.50
User interface design	0.05	0.90	0.50	0.80	0.90
Power consumed by subsystems	0.20	0.90	0.50	0.80	0.20
Energy dissipation mechanism	0.15	0.20	0.40	0.70	0.80
TIE		0.74	0.46	**0.76**	0.48

Table 10.28: TIE evaluation for EGSD

Considering for each concept the TIE and the confidence values based on the definition of confidence provided in Section 10.4.4, the final score associated with each configuration is shown in Table 10.29. The darkest green cell corresponds to the concept with the highest final score.

	MoonStation	MoonGrid	MoonProbe	MoonRover
TIE	0.74	0.46	**0.76**	0.48
Confidence	**2**	1	**2**	1
Final score	0.49	0.15	0.50	0.16

Table 10.29: Final score evaluation for EGSD

10.4.4.2 Thermal Control Subsystem

To evaluate the TIE associated with the TCS, three main evaluation criteria have been defined: environmental effects, thermal size, and thermal elements.
The environmental effects criterion accounts for the impact of external conditions, primarily solar illumination, on thermal control. Configurations involving mobile structures, such as MoonGrid and MoonRover, are disadvantaged under this criterion, as their movement can lead to significant variations in solar exposure. In contrast, stationary architectures like MoonStation and MoonProbe are preferred, as they offer at least one fixed element between the LPM and LSM, resulting in more predictable and stable thermal conditions.
The thermal size principle considers the physical space available for installing TCS components. Architectures that provide more area for thermal hardware are considered more favorable, as they offer greater flexibility in system design and capacity.
Lastly, the thermal elements criteria evaluate the type and variety of thermal control components that can be integrated within each configuration. Some configurations, such as MoonGrid and MoonProbe, present limitations in this regard,

restricting the range of thermal elements that can be implemented on the payload and, therefore, potentially constraining thermal performance.
This multi-criteria approach provides a comprehensive basis for comparing the thermal control feasibility of each mission architecture, ensuring that both environmental conditions and technical constraints are considered in the design process.
The scores are presented in Table 10.30.

Parameter	Weight	MoonStation	MoonGrid	MoonProbe	MoonRover
Environmental effects	0.50	0.60	0.30	0.50	0.40
Thermal size	0.25	0.50	0.80	0.70	0.40
Thermal elements	0.25	0.80	0.30	0.50	0.70
TIE		**0.63**	0.43	0.55	0.48

Table 10.30: TIE evaluation for TCS

Considering for each concept the TIE and the confidence values based on the definition of confidence provided in Section 10.4.4, the final score associated with each configuration is shown in Table 10.31. The darkest green cell corresponds to the concept with the highest final score.

	MoonStation	MoonGrid	MoonProbe	MoonRover
TIE	**0.63**	0.43	0.55	0.48
Confidence	**2**	1	**2**	**2**
Final score	0.42	0.14	0.37	0.32

Table 10.31: Final score evaluation for TCS

10.4.4.3 Attitude determination and control subsystem

To evaluate the TIE associated with the ADCS across the four proposed architectures six parameters have been considered: mass, power, integration, (Central Processing Unit) CPU demand, controllability, and complexity.
Architectures requiring fewer or simpler sensors, such as MoonStation, are favored, as they result in a lighter and more power-efficient design. Conversely, systems involving mobile or distributed elements, like MoonGrid, impose a larger mass and power footprint, leading to lower scores.
Integration reflects how easily the ADCS can be accommodated within the architecture. Fixed, centralized systems are inherently easier to integrate than smaller and moving configurations.
The CPU demand accounts for the onboard computational effort required for attitude estimation, navigation and control. Simpler architectures, which rely on coarse attitude knowledge and absence of navigation, are awarded higher scores. In contrast, rovers or dynamic platforms, which demand real-time navigation and precise control, incur a heavier computational load.
Controllability measures how easily the system can achieve and maintain correct orientation, pointing and planned path in case of mobile elements. Since no actuator is present, static platforms like MoonStation are awarded negatively, a higher score is giver to the platforms with mobile elements. In MoonGrid case a lower score is attributed with respect to the MoonProbe because of simpler rover paths.
Finally, complexity encompasses the overall difficulty of implementation, from sensor integration to software development and fault management. Architectures that rely on passive systems and well-established sensor suites are considered less complex and therefore more favourable. Conversely, the inclusion of stereo vision systems, navigation algorithms, or active orientation mechanisms increases the implementation burden.
The scores are presented in Table 10.32.

Parameter	Weight	MoonStation	MoonGrid	MoonProbe	MoonRover
Mass	0.10	1.00	0.20	0.60	0.70
Power	0.10	1.00	0.20	0.60	0.70
Integration	0.10	0.80	0.20	0.40	0.70
CPU	0.25	1.00	0.20	0.50	0.60
Controllability	0.25	0.20	0.60	0.80	0.90

Complexity	0.20	0.90	0.40	0.60	0.70
TIE		**0.76**	0.34	0.61	0.73

Table 10.32: TIE evaluation for ADCS

Considering for each concept the TIE and the confidence values based on the definition of confidence provided in Section 10.4.4, the final score associated with each configuration is shown in Table 10.33. The darkest green cell corresponds to the concept with the highest final score.

	MoonStation	MoonGrid	MoonProbe	MoonRover
TIE	**0.76**	0.34	0.61	0.73
Confidence	**3**	2	2	**3**
Final score	0.76	0.23	0.40	0.73

Table 10.33: Final score evaluation for ADCS

10.4.4.4 Telemetry, tracking & command subsystem

The evaluation of the TIE of the four concepts for TT&C subsystem is based on three parameters: hardware resources, communication architecture, and system integration and mobility. Hardware resources parameter includes the physical and operational burden of the TT&C subsystem in terms of mass, volume, and onboard resource consumption (e.g., power, processing, thermal load), which directly affects system integration and platform sizing. Communication architecture reflects the structural complexity of the TT&C links, including the number of nodes, the type of communication, i.e. Lunar Surface to Lunar Orbit (LS-to-LO), LS-to-LS, and the dynamic or static nature of the elements involved. System integration and mobility captures the integration complexity between distributed or mobile elements, accounting for synchronization needs, tracking during movement, and the planning of time-sensitive interactions such as rendezvous or coordinated data collection.
Based on these considerations the scores are presented in Table 10.34.

Parameter	Weight	MoonStation	MoonGrid	MoonProbe	MoonRover
Hardware resources	0.15	0.90	0.20	0.70	0.80
Communication architecture	0.50	0.70	0.30	0.50	0.60
System integration and mobility	0.35	0.90	0.50	0.60	0.70
TIE		**0.80**	0.36	0.57	0.67

Table 10.34: TIE evaluation for TT&C

Considering for each concept the TIE and the confidence values based on the definition of confidence provided in Section 10.4.4, the final score associated with each configuration is shown in Table 10.35. The darkest green cell corresponds to the concept with the highest final score.

	MoonStation	MoonGrid	MoonProbe	MoonRover
TIE	**0.80**	0.36	0.57	0.67
Confidence	**2**	1	**2**	**2**
Final score	0.53	0.12	0.38	0.44

Table 10.35: Final score evaluation for TT&C

10.4.4.5 Structure and mechanisms

To evaluate the TIE of the different configurations of the AMPERE mission, four parameters have been selected: proximity to LDE, size, power required and operational stability. The proximity to LDE penalizes solutions where the payload is released too close to the lander (MoonStation and MoonProbe), favoring architectures capable of positioning themselves farther away due to the mobility of the station (MoonGrid and MoonRover). Size considers the overall bulk of the structure, in terms of mass and volume: compact and easier-to-integrate configurations are preferred. Power required measures the amount of energy required for the deployment: more efficient and passive solutions are preferred overactive and motorized systems. Operational stability reflects potential issues related to oscillation and instability that may arise when using these deployment mechanisms. Higher scores are awarded to architectures that ensure greater stability. Finally, the parameter complexity has been considered, which represents how involved and

intricate the system is: solutions using a wheeled cart and a ramp are preferred with respect to the ones using a rover and a Davit/Egress deployment mechanism.
The scores are presented in Table 10.36.

Parameter	Weight	MoonStation	MoonGrid	MoonProbe	MoonRover
Proximity to LDE	0.20	0.40	0.90	0.70	1.00
Size	0.20	0.30	0.60	0.30	0.60
Power required	0.20	0.30	0.60	0.30	0.60
Operational stability	0.20	0.80	0.50	0.80	0.40
Complexity	0.20	0.90	0.20	0.80	0.30
TIE		0.54	0.56	**0.58**	**0.58**

Table 10.36: TIE evaluation for Structure & Mechanisms

Considering for each concept the TIE and the confidence values based on the definition of confidence provided in Section 10.4.4, the final score associated with each configuration is shown in Table 10.37. The darkest green cell corresponds to the concept with the highest final score.

	MoonStation	MoonGrid	MoonProbe	MoonRover
TIE	0.54	0.56	**0.58**	**0.58**
Confidence	**3**	2	**3**	2
Final score	0.54	0.37	0.58	0.39

Table 10.37: Final score evaluation for Structure & Mechanisms

10.4.4.6 Environmental Analysis

To evaluate the TIE, although lunar environmental contextualization should consider other aspects such as surface temperature, radiation, moonquakes, meteoroids impact, these elements are assumed to affect the entire lunar South Pole in a broadly uniform way or not demanding for AMPERE mission requirements and needs.
The characteristics of the potential landing sites which play a key role when evaluating the different architectures are illumination condition, morphology and dust. flatter areas are more suitable for systems where mobility is required as they offer better illumination conditions and favourable morphology, while static solutions are more adaptable: for this reason, MoonGrid and MoonRover scored higher in these categories. Dust impact must be considered, too: since the lunar regolith is very fine and corrosive, consequently infiltration and damage to the structures are likely. Also, solar panels can be covered by dust due to deposition or strong electromagnetic interactions. Therefore, scores are low across all the architectures: MoonGrid and MoonRover score lower as wheels provide motion but, at the same time, are most affected by these effects.
The scores are presented in Table 10.38.

Parameter	Weight	MoonStation	MoonGrid	MoonProbe	MoonRover
Illumination condition	0.65	0.80	0.90	0.80	0.90
Morphology	0.25	0.50	0.80	0.60	0.70
Dust	0.10	0.60	0.20	0.50	0.40
TIE		0.71	**0.81**	0.72	0.80

Table 10.38: TIE evaluation for Environmental Analysis

Considering for each concept the TIE and the confidence values based on the definition of confidence provided in Section 10.4.4, the final score associated with each configuration is shown in Table 10.39. The darkest green cell corresponds to the concept with the highest final score.

	MoonStation	MoonGrid	MoonProbe	MoonRover
TIE	0.71	**0.81**	0.72	0.80
Confidence	**3**	1	2	2
Final score	0.71	0.27	0.48	0.53

Table 10.39: Final score evaluation for Environmental Analysis

10.4.4.7 Payload Accommodation & Interfaces

The evaluation of the TIE is based on three parameters: architecture interface, sensor implementation, and technological complexity. Architecture interface represents the effort required to define and implement the interface between the selected configuration and the LDE. Sensor implementation refers to the effort associated with the physical layout of the sensors, i.e. their placement on the LPM across the different configuration options, considering accommodation requirements in terms of available mass and volume. Lastly, technological complexity describes the degree of miniaturization required for the sensors, considering that extreme miniaturization, relative to the dimensions of the LPM, leads to increased technological and industrial complexity. The scores are presented in Table 10.40.

Parameter	Weight	MoonStation	MoonGrid	MoonProbe	MoonRover
Architecture interface	0.3	0.9	0.2	0.7	0.7
Sensor implementation	0.3	0.6	0.7	0.8	0.6
Technological complexity	0.4	0.8	0.3	0.7	0.5
TIE		**0.77**	0.39	0.73	0.59

Table 10.40: TIE evaluation for Payload Accommodation & Interfaces

Considering for each concept the TIE and the confidence values based on the definition of confidence provided in Section 10.4.4, the final score associated with each configuration is shown in Table 10.41. The darkest green cell corresponds to the concept with the highest final score.

	MoonStation	MoonGrid	MoonProbe	MoonRover
TIE	**0.77**	0.39	0.73	0.59
Confidence	**2**	1	**2**	1
Final score	0.51	0.13	0.49	0.20

Table 10.41: Final Score evaluation for Payload Accommodation & Interfaces

10.4.5 Mission objectives trade-off analysis

In Table 10.42, scores ranging from 0 to 1 are assigned to each mission objective to reflect how well each mission concept meets the strategic goals of the AMPERE mission. Not all the mission objectives have been considered for this analysis, but only those that are met by the concepts to varying extents and are therefore a basis for conducting the trade-off. A set of weights reflecting the relative importance of each Objective has been defined (see Table 10.42), for each concept, the final score is then obtained by computing the weighted sum of the individual scores using these weights.

The most important objectives for the AMPERE mission are long-term power generation and supply, which are taken into account in AMP-PMO-02 and AMP-PMO-03 and have been assigned the highest weights (0.20 and 0.25, respectively).

Other factors are system feasibility (considered in AMP-PMO-01, with a weight of 0.10) which considers the feasibility of implementation within the given constraints of launch, landing, and deployment and the standard specifications (AMP-PMO-04), which considers the definition of standard specifications for the generation and distribution of power for lunar users.

Another impactful objective is the validation and enhancement of existing lunar models (AMP-SMO-01), due to their current inaccuracy. The inclusion of scalability and evolvability (AMP-SMO-03 and AMP-SMO-04, with a weight of 0.05 each) reflects the ambition to build an infrastructure capable of adapting to future needs, such as supporting additional users, varying energy demands, or international contributions to the lunar ecosystem.

Finally, robotic operations (AMP-SMO-06, with a weight of 0.05) focus on the system's ability to support automated assembly, an important factor in the absence of consistent human presence.

The final score for each concept is calculated as the weighted sum of the individual scores across all objectives.

Mission objective	Weight	MoonStation	MoonGrid	MoonProbe	MoonRover
AMP-PMO-01	0.15	**0.90**	0.40	**0.90**	0.60
AMP-PMO-02	0.20	**0.90**	0.30	0.80	0.50

AMP-PMO-03	0.25	0.80	0.30	**1.00**	0.50
AMP-PMO-04	0.15	0.70	**1.00**	0.90	0.60
AMP-SMO-01	0.10	0.70	**0.90**	**0.90**	0.80
AMP-SMO-03	0.05	0.80	**0.90**	0.80	0.40
AMP-SMO-04	0.05	0.80	**0.90**	**0.90**	0.50
AMP-SMO-06	0.05	0.70	0.70	0.70	**0.80**
TOTAL	1	0.81	0.56	0.89	0.57

Table 10.42: Mission objectives scores for trade-off analysis

The final scores based on the mission objectives show that MoonProbe achieves the highest score. From a qualitative standpoint, the presence of the rover that recharges at the fixed energy station results in very high scores for the mission objectives related to energy generation, distribution and standard interfaces. The same rover, equipped with sensors, enables a more accurate environmental analysis. In contrast, MoonStation receives a lower score since it does not include a rechargeable user, and sensing is limited to instruments mounted on the fixed platform. MoonGrid and MoonRover report the lowest and nearly identical scores, primarily because the amount of energy available to an external user is limited (which is the reason why they do not receive high scores for the first three primary mission objectives), although they perform reasonably well with respect to the secondary mission objectives.

10.4.6 Market differentiation trade-off analysis

As reported in Table 10.43, market differentiation assesses each concept's ability to stand out in the lunar payload services sector by offering distinctive features, strategic advantages, and clear value propositions that appeal to future customers and partners.

Concept	Market differentiation
MoonStation	0.20
MoonGrid	0.90
MoonProbe	0.80
MoonRover	0.60

Table 10.43: Market differentiation scores for trade-off analysis

MoonStation scores 0.2, as its single-station architecture offers little novelty and thus weak competitive appeal. MoonGrid scores 0.9, thanks to its innovative grid that can be tailored to diverse client needs and easily expanded for larger networks. MoonProbe scores 0.8, leveraging its unique rover-station docking demonstration to showcase cutting-edge robotic integration, while still targeting a relatively specialized market segment. MoonRover scores 0.6, reflecting a solid but less differentiated offering, the integrated mobile power-rover, that combines proven technologies in a single platform without radically new capabilities.

10.4.7 Trade-off analysis results

The results of the trade-off analysis led in the previous sections are presented in Table 10.44.

Parameter	Weight	MoonStation	MoonGrid	MoonProbe	MoonRover
Costs	0.05	**0.95**	0.37	0.85	0.67
Expected return	0.10	0.78	0.82	0.83	**0.87**
Reliability	0.15	**1.00**	0.56	**1.00**	0.68
Mission objectives	0.30	0.81	0.56	**0.89**	0.57
Technical score	0.30	**0.52**	0.21	0.48	0.31
Market differentiation	0.10	0.20	**0.90**	0.80	0.60
Total	1	0.69	0.51	0.77	0.55

Table 10.44: Results for trade-off analysis

The concept with the highest overall score is MoonProbe, as it does not show any significantly lower value than the others across the system design drivers. The same applies to MoonStation, except for market differentiation driver, which is the reason it ranks below MoonProbe.
MoonGrid and MoonRover are the lowest performing, with nearly identical scores; MoonGrid performs worse in terms of cost, reliability and technical score, but achieves a much higher score in market differentiation.
Following the trade-off analysis, MoonProbe has been selected as the preferred concept for the mission.

10.4.8 Final landing site

The final landing site associated with the most compelling architecture is C1. For more detailed information see Section 11.7.

10.5 Baseline concept definition

As a result of the trade-off analysis, MoonProbe has been selected as the baseline concept and is further developed in the following sections in terms of concept of operations, requirements and technical design. As previously introduced, MoonProbe is composed of two main modules: a recharging power station and a demonstrator rover, both equipped with a wide set of environmental sensors. It is foreseen that both the modules will be deployed together from Argonaut via a dedicated ramp mechanism, to ensure a controlled positioning on the lunar surface and to avoid interferences during nominal operations.
To enhance clarity and understanding of the mission structure and its components, a renewed nomenclature is introduced and adopted from this point onward.

Firstly, it is important to underline that during orbital, descent and landing phases, when the modules are accommodated on Argonaut's mounting plate, AMPERE is referred to as the LPS.
The LPS, consequently, consists of three main elements known as Eagle, Scott and PDS:

- Eagle is the core of AMPERE's mission, being the module housing the recharging power station. Its structure, a honeycomb aluminium wheeled cart, acts as a stable mechanical base and integration platform for the other elements. Specifically, Eagle includes:
  - The LPM, composed of solar arrays, lithium-ion batteries and Regenerative Fuel Cells (RFCs) to generate and storage power.
  - The Lunar Sensor Module -Stationary (LSM-S), which is the portion of the sensor suite intended for stable accommodation. The detailed sensor list is provided in the Section 10.7.3.
  - The Rover Delivery System (RDS), a mechanism based on winches and cables, used to safely lower the rover onto the lunar surface. The system also handles the deployment of the wireless charging interface, enabling rover recharging when docked.

- Scott is the mobile demonstrative rover, designed within a 24U CubeRover [R.D. 54] volume and equipped with a mobility system, driving wheels and a GNC subsystem. Its integration onto Eagle (detailed in Section 10.7) not only facilitates the first descent from Argonaut, but also the second deployment on lunar's surface.
  During orbital, descent and landing phases Scott is housed underneath the Eagle wheeled cart and remains stowed until landing. Once Eagle module is landed, the RDS handles its controlled deployment. Scott also hosts the Lunar Sensor Module-Mobile (LSM-M), which is the subset of environmental sensors optimized for dynamic operations and tolerant of rover-induced perturbations.

- The PDS consists of 5 foldable panels and 5 pairs of motorized hinges that articulate the panels into a continuous surface ramp, enabling Eagle, while housing Scott, to descend from Argonaut to the lunar surface. Eagle is mechanically secured in place on the second panel by a locking system consisting of 4 Kevlar cables and 8 thermal knives. Another component essential for ramp unfolding operations is a battery, which provides the energy required to power the hinges and the knives. A detailed description of PDS mechanism and LPS accommodation on the LDE is provided in Section 10.7 and 11.5.

A preliminary representation of Eagle and Scott is given in Figure 10.6 and Figure 10.7 (not in scale).

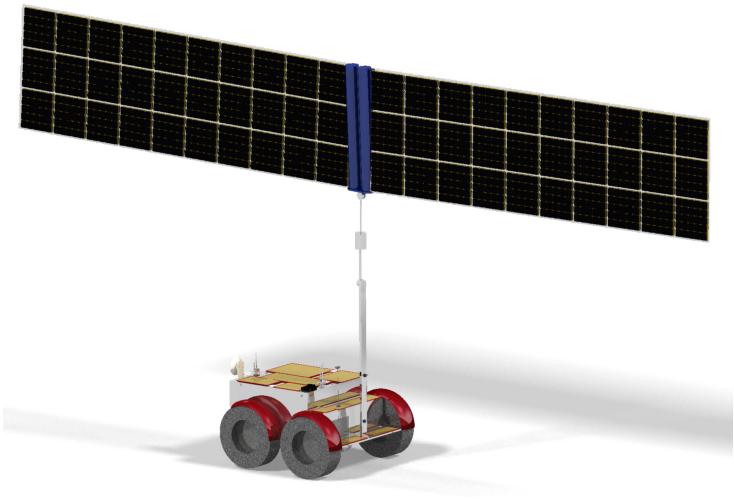

Figure 10.6: Eagle module

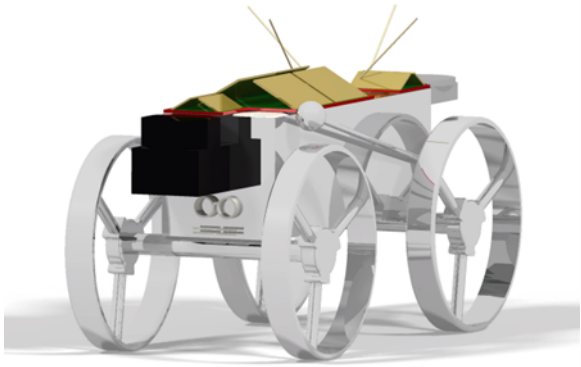

Figure 10.7: Scott module

10.6 ConOps

10.6.1.1 Mission phases

The AMPERE mission, embarked on ESA's Argonaut lander, follows a set of rigorously defined operational phases, mirroring ESA's mission architecture guidelines [A.D. 7] to ensure safe deployment, automated system activation and attainment of its scientific and technological goals. The adopted convention is to consider a 'day' as an Earth Day. It is underlined that the duration of the Nominal Day Operations phase (NOMDOP) and the Nominal Night Operations phase (NOMNOP) has been derived according to analyses led by the WP.3.7. After the end of the Secondary Deployment phase (SD), an alternation of daytime and nighttime with a cyclic variation has been observed. Therefore, the durations presented refer only to the total amount of days with respective daytime and nighttime conditions within the 354-daytime span. An overview of the mission phases throughout the 1-year operational lifetime of the AMPERE mission, from LLO to disposal, is reported in Table 10.45.

Mission phase	Description	Start date	Duration	Success criteria
Lunar Orbit Insertion (LOI)	Controlled insertion into a polar low lunar orbit, verification of orbital parameters and health-check of all spacecraft systems to ensure readiness for descent toward the selected landing site.	t_0	4.5 days	Orbital elements within defined tolerances; all subsystems nominal.

Descent & Landing (D&L)	The phase begins with the Periselene Lowering Burn (PLB), which places the vehicle on an elliptical trajectory with a periselene of 30 km, followed by an autonomous descent through key waypoints (brake burn, pitch-up manoeuvre, powered descent and diverts, vertical descent and landing) to a soft touchdown within the target ellipse, with no ground-in-the-loop communications.	t_0 + 4.5 days	0.05 day (1.15 hours)	Touchdown inside the landing ellipse; residual velocities within specifications; structural integrity confirmed.
Post-Landing Initialization (PLI)	Immediate autonomous boot-up of critical subsystems (EGSD, TT&C) and re-establishment of the Earth link to validate AMPERE status.	t_0 + 4.55 days	0.5 day	EGSD and communication subsystems active; first housekeeping telemetry received on ground; nominal parameters.
Primary Deployment (PD)	TT&C subsystem communication with Moonlight to command PDS battery activation and ramp unfolding. Subsequent deployment of Eagle module, housing Scott, via the PDS integrated ramp, precise placement on the surface and mechanical integrity checks under lunar gravity.	t_0 + 5.05 days	0.08 days (2 hours)	PDS ramp successfully unfolded, Eagle module correctly positioned and fixed; no mechanical or structural anomalies detected, akin to Chang'e-4's Yutu-2 deployment [R.D. 55].PDS ramp successfully unfolded, Eagle module correctly positioned and fixed; no mechanical or structural anomalies detected, akin to Chang'e-4's Yutu-2 deployment [R.D. 55][R.D. 55].
Commissioning (COM)	Functional verification and calibration of all AMPERE subsystems, margin-testing under expected load profiles, and formal readiness confirmation for surface operations.	t_0 + 5.13 days	0.5 day	All systems operate within defined performance envelopes, green light for nominal surface mission.
Secondary Deployment (SD)	Lowering of Scott, already charged from the Eagle module, initial checkout and calibration, and release to commence the rover's first traverse.	t_0 + 5.63 days	0.08 days (2 hours)	Scott deployed and mobile; first traverse successfully completed.

Nominal Day Operations (NOMDOP)	The LPM generates and distributes electrical power to support all surface activities, including periodic recharging of Scott and to operate its own full suite of subsystems (communications, data handling, etc.). Meanwhile, Scott conducts autonomous traverses to predefined science targets, collects and caches data, then returns periodically for recharge and data uplink, reflecting long-duration power strategies pioneered by solar arrays [R.D. 56].Meanwhile, Scott conducts autonomous traverses to predefined science targets, collects and caches data, then returns periodically for recharge and data uplink, reflecting long-duration power strategies pioneered by solar arrays [R.D. 56][R.D. 56].	N/A	298 days	Continuous power generation and delivery from LPM; regular Scott recharges; continuous communications; autonomous Scott traverses and data collection; scientific objectives met.
Nominal Night Operations (NOMNOP)	The LPM's solar arrays are inactive during the lunar night, while the Regenerative Fuel Cell System (RFCS) remains operational to support the active portion of the TCS responsible for thermal regulation under extreme nighttime conditions. Scott periodically returns to the LPM to recharge using the energy stored in the onboard lithium batteries.	N/A	56 days	Continuous thermal control of critical subsystems; reliable power supply from stored energy; successful periodic Scott recharging; system survival and readiness for resumption of daytime operations.
End-of-Life & Disposal (EOL&D)	Final data uplink to the Earth, primary subsystems shutdown and transition to inert state, attending command to start Task 4 operations, as described in Section 11.9, for planetary protection and hardware preservation for future inspection or reuse.	t_0 + 360 days	5 days	Primary subsystems passivation; all data sent; full compliance with ESA planetary-protection and reuse guidelines; hardware intact.

Table 10.45: AMPERE mission phases

10.6.1.2 System modes

AMPERE's system modes describe the configuration states and operational behaviours of the three modules involved in the mission: PDS, Eagle and Scott. Their relative operative modes are described respectively in Table 10.46, Table 10.47 and Table 10.48.

Code	Mode name	Brief description
PDS-STBY	Standby mode	PDS on board the LDE in standby, waiting for commands.
PDS-DEP	Deployment mode	PDS enabled: battery supplies for ramp unfolding, monitoring of deployment mechanical cycle.

Table 10.46: PDS modes.

Code	Mode name	Brief description
EAGLE-CRS	Cruise mode	EGSD and TT&C powered by Argonaut; Scott and PDS powered off; OBC active only for telemetry transmission.
EAGLE-DESN	Descend mode	Controlled descent of Eagle housing Scott along the PDS ramp: ramp kinematics, structural load monitoring and constant descending velocity control.
EAGLE-COMM	Surface initial commissioning	After touchdown, primary calibration of all Eagle subsystems, PDS awaiting commands.
EAGLE-RDEP	Rover deployment	Eagle initiates the controlled release of Scott.
EAGLE-CHG	Power supply mode	Energy storage dedicated to rover recharge only; solar panels oriented for optimal solar incidence.
EAGLE-PGEN	Power generation mode	Full power generation mode: solar panels deployment and sun-pointing oriented; energy routed to primary bus.
EAGLE-SECCOMM	Secondary commissioning mode	After ramp descend, secondary calibration of all Eagle subsystems, Scott and RDS awaiting commands.
EAGLE-SENSOR	Environmental mode	Operation of LSM-S environmental sensors.
EAGLE-INTL	Interlink mode	Inter-modules communication: Eagle acts as a relay between Scott and Moonlight for telemetry data.
EAGLE-SAFE	Safe mode	Safety configuration: minimum power budget, locked mechanisms, emergency link only. Sensors in standby.
EAGLE-NIGHT	Night mode	During lunar night, Eagle resists cold and lack of illumination by activating its heating system.
EAGLE-EOL	End-of-life	Entire system in standby, only telemetry data available.

Table 10.47: Eagle modes.

Code	Mode name	Brief description
SCOTT-OFF	Power off mode	Scott powered off while on board Eagle during descent, landing and PDS deployment.
SCOTT-P&REL	Power on and release	Scott powers up and is ready for a controlled release via RDS.
SCOTT-COMM	Commissioning	Functional check of environmental sensors (LSM-M).
SCOTT-NEM	Navigation environmental mode	Autonomous navigation thought a straight path in both forward and return directions.
SCOTT-EMD	Environmental mode day	Static environmental data acquisition with LSM-M during daytime.
SCOTT-EMN	Environmental mode night	Static environmental data acquisition with LSM-M during nighttime.
SCOTT-RCG	Recharge mode	Scott receives power from Eagle.
SCOTT-UPL	Uplink mode	Uplink of collected environmental data to Moonlight.
SCOTT-INTL	Interlink mode	Inter-modules communication: telemetry data uploaded to Eagle.
SCOTT-SAFE	Safe mode	Minimum power: only critical systems are on, battery maintenance, periodic communications.
SCOTT-NIGHT	Night mode	During lunar night, Scott resists cold and lack of illumination by activating its heating system.
SCOTT-EOL	End-of-life	Scott takes shelter under Eagle; battery discharge, progressive shutdown of all subsystems.

Table 10.48: Scott modes.

Since each mode is applicable to different mission phases, Figure 10.8 has been introduced to facilitate the estimation of power budgets and duty cycles during the design phase, by indicating which operational mode is active in each phase.

			Mission phases								
			LOI	D&L	PLI	PD	COM	SD	NOMDOP	NOMNOP	EOL&D
	PDS	Standby Mode	■	■	■		■	■	■	■	■
		Deployment Mode				■					
	EAGLE	Cruise Mode	■	■							
		Surface Initial Commissioning Mode			■						
		Descend Mode				■					
		Secondary Commissioning Mode					■				
		Power Generation Mode							■		
		Rover Deployment						■			
		Power Supply Mode							■	■	
		Environmental Mode							■	■	
		Interlink Mode							■	■	
		Night Mode								■	
		Safe Mode	■	■	■	■	■	■	■	■	■
		End-of-Life									■
	SCOTT	Power off Mode	■	■	■	■	■				
		Power on and Release						■			
		Commissioning						■			
		Environmental Mode Day							■		
		Environmental Mode Night								■	
		Navigation Environmental Mode							■		
		Recharge Mode							■	■	
		Uplink Mode							■	■	
		Interlink Mode							■	■	
		Night Mode								■	
		Safe Mode	■	■	■	■	■	■	■	■	■
		End-of-Life									■

Figure 10.8: Mission phases and system modes interception

10.7 Payload Accommodation & Interfaces

10.7.1 Introduction

The objective of the Payload Accommodation & Interfaces WP is primarily to identify the necessary accommodation and interface solutions for AMPERE. The term accommodation refers to the space that must be allocated within Argonaut to safely house the LPS. The term interface refers to all components that must be included to ensure proper integration onboard the LDE. This section will also focus on the selection of the LSM to guarantee proper monitoring of the lunar environment.

10.7.2 Preliminary LSM selection

As discussed in Sections 9.1.3 and 11.7, local environmental monitoring is essential to support long-term presence at the lunar South Pole. Therefore, a preliminary selection of the LSM has been primarily driven by the need to update existing environmental data in this specific region and to properly characterize it through a sufficiently comprehensive set of parameters. In support of this, several key lunar environmental parameters are selected for monitoring. In particular, the mission foresees the observation of ionizing radiation levels, in order to assess the cumulative exposure experienced by electronic systems and, prospectively, by human crews. Ambient temperature and thermal gradients will also be monitored to enable the characterization of the lunar thermal environment under varying exposure conditions. Another parameter of interest is the presence of electrostatic charging and local plasma, as these phenomena affect the LPM surface behaviour and contribute to the levitation of regolith particles. This is complemented by the observation of lunar dust distribution and dynamics, since dust is one of the most critical degradation factors for optics, mechanical joints, exposed surfaces and connectors. In addition, the mission includes the monitoring of the exospheric composition of neutral particles, due to their scientific value and potential relevance for future ISRU applications. Measurements of the local magnetic field will also be collected to better understand the interaction with the solar wind and to investigate the geological structure of the landing region. To complement these

observations, the inclusion of a sensor for incident solar irradiance is planned. Based on these considerations, nine sensor types have been selected, as listed in Table 10.49.

Environmental parameter	Sensor type
Ionizing radiation	Dosimeter, radiation monitor
Ambient temperature	Temperature sensor
Plasma and charged particles	Langmuir probe, ion-electron spectrometer
Lunar dust	Dust sensor
Exospheric composition of neutral species	Neutral mass spectrometer
Magnetic field	3-axis magnetometer
Solar irradiance	Pyranometer (TBC)

Table 10.49: LSM components

The selection of two sensors for ionizing radiation, as for plasma and charged particles, is justified by their complementarity. For the former, the dosimeter records the accumulated dose over time, while the radiation monitor provides real-time detection of variations, including transient events such as Solar Particle Events (SPE) and Galactic Cosmic Rays (GCR). For the latter, the Langmuir probe measures bulk plasma properties (e.g. density and potential), whereas the ion-electron spectrometer characterizes energy and species distribution. [R.D. 8] and [R.D. 11] are representative of such dual approach, as in it are proposed sensors' architectures which employ the above-defined instruments for these specific environmental parameters.
As sensors are never deployed independently but always integrated, on the LPM or on board a rover, across all proposed architectures, compactness and low mass and low power are essential requirements. The aim is to select sensors with a high TRL and established flight heritage in lunar or analogous space environments, in order to ensure a high overall maturity level for the sensing package and reduce integration risks. For solar irradiance measurement, a single broadband pyranometer is preferred over three separate Ultraviolet (UV), visible and Infrared (IR) sensors, to minimize mass and volume. Although pyranometers lack direct space heritage, this trade-off may be considered acceptable, acknowledging a lower TRL for this subsystem. The remaining sensor types have been not only on their scientific relevance but also on their demonstrated performance in space missions. The radiation monitor and dosimeter types proposed align with those considered in [R.D. 8] and [R.D. 11] having strong heritage from ESA's European Radiation Sensor Array (ERSA) Gateway studies and the European Data Relay System - Satellite C (EDRS-C) satellite for the monitor and from the Standard Radiation Environment Monitor (SREM) for the dosimeter. The dosimeter technology could be based on Radiation Sensing Field Effect Transistors (RADFETs), known for their compact size and cumulative dose measurement capabilities. This technology has been validated in several ESA flights and characterized in [R.D. 111]. It is currently offered by commercial providers such as Varadis. The dust sensor, based on impact analysis or micro-imaging, draws heritage from multiple missions, including Cassini's Cosmic Dust Analyzer, Rosetta's Grain Impact Analyzer and Dust Accumulator (GIADA) and the Micro-Imaging Dust Analysis System (MIDAS) instrument. Similarly, the Langmuir probe and ion-electron spectrometer technologies have both been flown on Rosetta, with further development exemplified by Peregrine Ion-Trap Mass Spectrometer (PITMS), a miniaturized ion-trap mass spectrometer for the Moon developed in collaboration between ESA and NASA [R.D. 112]. The neutral mass spectrometer is a well-established instrument class with flight heritage from missions such as Jupiter Icy Moons Explorer (JUICE) mission. A miniaturized version for CubeSat of this instrument type has also been developed by NASA [R.D. 113]. For temperature sensing, the most widely adopted technologies in lunar applications are Resistance Temperature Detectors (RTDs) [R.D. 114] and thermocouples (used in Apollo missions), due to their robustness, accuracy and compatibility with vacuum and thermal cycling conditions. Lastly, for magnetic field monitoring, compact three-axis magnetometers flew on Rosetta, Venus Express and more recently the MAIGRET instrument aboard ESA's ExoMars.

10.7.3 Final LSM selection

Following an initial assessment, the LSM has been selected for MoonProbe. In addition to the drivers highlighted in the previous Section 10.7.2, the final selection has been focused on identifying Commercial Off-The-Shelf (COTS) solutions. Wherever not feasible, efforts have been directed to leveraging the design and heritage of sensors previously employed

in similar missions. These have been chosen to meet mission constraints and requirements while maximizing the use of sensors already proven effective in both static and mobile lunar environments.

10.7.3.1 Final LSM-S selection

The choice to position the LSM-S components on the Eagle platform is primarily driven by the specific environmental and operational requirements of such sensors. These include the necessity for a stable environment and the elimination of movement, ensuring optimal functionality. The LSM-S consists of:

- Varadis RADFET Module RM-VT01-A: it is entirely passive and measures the total ionizing dose within a range from 1 cGy to 1 kGy [R.D. 57], making it highly suitable for the mission's duration and ensuring high sensitivity. The module incorporates two RADFETs, which provide local redundancy, along with a readout circuit requiring minimal power consumption. Currently, this module is part of the Deep Space Radiation Probe (DSRP) mission onboard the lunar lander Hakuto-R [R.D. 58].
- New Generation Radiation Monitor (NGRM): developed by ESA as the successor to SREM, this advanced system features significant improvements in resolution, reduced mass and volume, and enhanced energy efficiency. It has already been deployed on prominent ESA missions such as EDRS-C and Sentinel-6 [R.D. 59][R.D. 60].
- Bartington Mag566: a 3-axis fluxgate magnetometer, detailed in [R.D. 61], has also been selected as the sensor for the upcoming Lunar Vertex mission, scheduled for launch by 2026 and it will be hosted aboard the Nova-C lander [R.D. 62]. The decision to employ two magnetometers, as previously implemented in missions such as Rosetta and Venus Express, is made to ensure redundancy and enhance the precision of magnetic field measurements.
- Honeywell Thin Film Platinum RTD - HRTS Series: it is a RTD, specifically a Platinum Resistance Thermometer (PRT) with a nominal resistance value of 1000 Ohm [R.D. 63], extensively validated and successfully employed in Martian environments as well as on terrestrial satellites [R.D. 64]. AMPERE employs four of these temperature sensors to achieve a more comprehensive assessment of the lunar thermal environment.

Details about these sensors are provided in Table 10.50. A conservative mass of 300g, based on studies of sensors with similar characteristics [R.D. 82], is also accounted for the boom instrument, which is not listed in Table 10.50. This component supports the two magnetometers.

Sensor	Mass without margins [kg]	Nominal power w/o margins [W]	Volume [mm^3]	TRL
RM-VT01-A	0.060	0.020 (read-out)	2.9 x 2.8 x 1.1	7
NGRM	1.17	1.00	132 x 67.9 x 150	8
Mag566	0.054	0.070	42 x 20 x 52	8
RTD	0.12	0.0040 (read-out)	4.8 x 313 x 1.95	7

Table 10.50: LSM-S components list

10.7.3.2 Final LSM-M selection

Scott is equipped with a suite of environmental sensors designed to analyze the plasma environment and charged particles, detect neutral particles in the exosphere and monitor solar radiation as well as lunar dust. These include:

- Ion and Electron Spectrometer (IES): it is part of the Rosetta Plasma Consortium (RPC) and consists of two electrostatic plasma analyzers, one for ions and electrons, which share common entrance aperture. The three-dimensional plasma distributions will be used to investigate the interaction of the solar wind with the Moon [R.D. 65][R.D. 66].
- Miniaturized Ion and Neutral Mass Spectrometer (INMS) for CubeSat: this component has been utilized in various Cubesat missions, such as ExoCube and Dellingr [R.D. 113].
- Radio Anatomy of Moon Bound Hypersensitive ionosphere and Atmosphere - Langmuir Probe (RAMBHA-LP): it is a sensor that forms part of the RAMBHA instrumentation aboard the lander of the Chandrayaan-2 and Chandrayaan-3 missions. The sensor consists of a metallic spherical probe with a titanium nitride coating on its surface, measuring 5 cm in diameter. It is mounted at the end of a non-conductive boom to prevent the plasma sheath effect in the Moon's plasma environment. Additionally, it is equipped with front-end electronics, a spring-assisted deployment mechanisms, a dust-protection subsystem and a hold release mechanism based on a shape-memory alloy-based actuator [[R.D. 67][R.D. 68][R.D. 69]
- Solar Radiation and Dust Sensor (SRDS): derived from the RDS of the Mars Environmental Dynamics Analyzer (MEDA) onboard the Perseverance rover, this instrument is selected for Scott due to its proven success and optimization for mobile platforms. The presence of a solar panel on Eagle could have compromised

measurements, whereas Scott's mobility maximizes solar exposure. The SRDS in AMPERE serves as a combined tool designed to measure solar irradiance and the reflectance from lunar regolith dynamically lifted during Scott's movement. Studies on the optical properties of lunar dust, particularly its reflection and scattering characteristics, have shown that sunlight can be effectively reflected and measured to provide meaningful data [R.D. 70][R.D. 71][R.D. 72]. The primary aim of the RDS is to determine the optical depth, single scattering albedo and phase function of dust particles based on seasonal and local time variations. These findings will help estimate particle size and their refractive index. Additionally, it is tasked with characterizing the solar radiation environment on the lunar surface, including its seasonal and daily fluctuations. This functionality is achieved through an array of eight zenithal photodiodes covering from UV to Near Infrared (NIR) range and seven lateral photodiodes positioned at different azimuth angles, all operating at a fixed wavelength of 750 nm ± 10 nm [R.D. 73]. This wavelength, already utilized on spacecraft like Clementine, has been confirmed to exhibit moderate and stable reflectance from the regolith [R.D. 74].

The Table 10.51 below highlights some of the key specifications.

Sensor	Mass w/o margins [kg]	Nominal power w/o margins [W]	Volume [mm^3]	TRL
IES	1.04	1.85	139 x 121 x 64 (sensor), Ø 146 x h 101 (electronic box)	7
INMS	0.57	1.80	130 x 100 x 100	7
RAMBHA-LP	1.10	3.00	/	8
SRDS	1.00	2.30	120x120x120	7

Table 10.51: LSM-M components list.

LSM-M, as well as LSM-S, requires to be shielded from lunar dust to prevent contamination that could distort measurements and damage sensitive surfaces. Additionally, thermal insulation and mechanical protection are necessary. These requirements can be achieved through the use of environmental protection technologies such as Multi-Layer Insulation (MLI), potting and encapsulation resins.

10.7.4 LSM operations

To establish the operational sequence of the LSM on both Eagle and Scott, various subsystem modes have been identified and linked to the corresponding system modes. Table 10.52 and Table 10.53 outline the results and provide detailed information about the characteristics of subsystem modes for LSM-S and LSM-M (see Section 10.6), respectively.

LSM-S mode	Description	Nominal power w/o margins [W]		Associated system modes
Off	The sensors are turned off, meaning they do not perform measurements and do not consume power.	RM-VT01-A	0	EAGLE-CRS EAGLE-DESN EAGLE-CHG EAGLE-PGEN EAGLE-INTL EAGLE-NIGHT EAGLE-EOL
		NGRM	0	
		Mag566	0	
		RTD	0	
Standby	The sensors are in standby mode to ensure the safe positioning and security of Eagle.	RM-VT01-A	0	EAGLE-SAFE
		NGRM	0.30	
		Mag566	0.04	
		RTD	0	
Science mode	The sensors operate at full capacity and are capable of gathering data effectively. Additionally, a continuous read-out of the two passive sensors is considered.	RM-VT01-A	0.02	EAGLE-COMM EAGLE-RDEP EAGLE-SECCOMM EAGLE-SENSOR
		NGRM	1.00	
		Mag566	0.07	
		RTD	0.004	

Table 10.52: LSM-S subsystem modes.

LSM-M mode	Description	Nominal power without margins [W]		Associated system modes
Off	The sensors are turned off, meaning they do not perform measurements and do not consume power.	IES	0	SCOTT-OFF SCOTT-P&REL SCOTT-RCG SCOTT-UPL SCOTT-INTL SCOTT-EOL
		INMS	0	
		Langmuir Probe (LP)	0	
		SRDS	0	
Standby	The sensors are in standby mode to ensure the safe positioning and security of Scott.	IES	0.56	SCOTT-SAFE
		INMS	0.54	
		LP	0.90	
		SRDS	0.69	
Science mode	The sensors operate at full capacity and are capable of gathering data effectively, both in a fixed position and by utilizing mobility.	IES	1.85	SCOTT-COMM SCOTT-NEM SCOTT-EMD
		INMS	1.80	
		LP	3.00	
		SRDS	2.30	
Night science mode	Only the IES is activated to collect data both while stationary and in motion, whereas all other sensors remain deactivated.	IES	1.85	SCOTT-NIGHT SCOTT-EMN
		INMS	0	
		LP	0	
		SRDS	0	

Table 10.53: LSM-M subsystem modes.

The decision to operate only the IES during the night hours is not solely intended to reduce Scott's energy consumption. It is also because lunar plasma environment does not completely vanish during the nocturnal period. Therefore, nighttime data collection is valuable for analyzing differences between diurnal and nocturnal plasma behavior and detecting transient phenomena that may occur. In contrast, the LP, which directly measures electron density and plasma potential, can remain powered off during the lunar night due to the substantial reduction in plasma density observed during this period. The use of the IES and the ineffectiveness of RAMBHA-LP in night mode are corroborated in [R.D. 68] and [R.D. 75].

10.7.5 LPS accommodation

It is essential that the LPS not only fits on the LDE without exceeding a surface area of 4 m² and a height of 1.8 m as specified in [A.D. 9], but also that each component is properly integrated within Eagle and Scott. The components have been arranged in such a way that the center of mass prevents any tipping over during the descent of Eagle while housing Scott. This configuration also avoids any overturning of Eagle and Scott during their operational phases. Moreover, to prevent interference and ensure correct functionality, all subsystems and equipment are strategically positioned to avoid any potential conflicts or collisions that could result in critical failures. This careful arrangement is essential to safeguarding the operational integrity of the LPS, ensuring uninterrupted performance of mission-critical tasks, including power generation, communication and scientific observations. The following accommodation is based on the requirements that the design WPs have outlined, shown in Section 10.13.

10.7.5.1 Scott accommodation

The wireless interface is positioned on the top of the rover to enable charging via the Eagle wireless interface.
Regarding Guidance, Navigation and Control (GNC), the two stereo-configured cameras are mounted on the forward-facing side, inclined upward at an angle of 49.42° relative to the ground's normal and 20 cm from the ground (see Figure 11.40), with the Light Emitting Diodes (LEDs) positioned below to ensure optimal vision. The ten Coarse Sun Sensors (CSSs) are arranged in pairs on the lateral and upper surfaces of Scott, providing comprehensive angular coverage and sensor redundancy. To minimize the effects of translational displacements and ensure more accurate attitude measurements, the Inertial Measurement Units (IMUs) should be placed near the center of mass. With respect to TT&C, a critical requirement for the Ultra High Frequency (UHF) and S-band antennas is their placement on opposite sides. This configuration minimizes coverage issues and mitigates the risk of communication blackouts.

Concerning TCS, the heaters are strategically located near the batteries. Given that the batteries operate at an efficiency of 90%, most of the available energy is electrical, therefore this energy can be converted into heat by the heaters to maintain thermal survivability. An area of 0.1 m² is also allocated on the upper side of Scott to accommodate the installation of the radiator and ensure proper dissipation of excess heat, as well as the opening of its blade louvers.
In terms of LSM-M, LP should be mounted at the tip of a 0.5-meter boom, initially stowed and deployed after Scott's touchdown. This ensures an elevated and isolated position, minimizing electromagnetic disturbances from the rover and avoiding plasma interference. The IES is to be installed on Scott's body with a Field Of View (FOV) sufficient to sample plasma flows and cover both the sky and the surface. Similarly, the INMS requires an unobstructed FOV to monitor the lunar exosphere but is positioned internally due to its higher thermal sensitivity, with an opening towards the exosphere. The SRDS is also mounted externally on Scott's body to maintain direct access to solar radiation and reflections from the regolith.
Regarding Scott's 1 kg payload, a volume of 1U (10 cm x 10 cm x 10 cm) is allocated, aligning with the remaining available space on the rover and the CubeSat standard, which suggests a mass between 1 and 1.33 kg per unit [R.D. 76]. This choice is also consistent with modular approaches already adopted by other lunar rovers in advanced stages of development, which accommodate scientific payloads within a 1U format [R.D. 77]. The payload's specific position within Scott is left to the discretion of the end user, allowing flexibility based on the payload's nature and operational requirements.
The final internal and external configuration is shown in Figure 10.9.

Figure 10.9: Scott internal and external configuration.

10.7.5.2 Eagle accommodation

The radiation shield encompasses the entire structure of the Eagle, except for the antennas, Scott, wireless and dock interfaces, radiators, solar panels, LSM-S, CSSs and Fine Sun Sensors (FSSs).
Scott is positioned on the underside of the Eagle to facilitate its deployment onto the lunar surface via its RDS, as well as the wireless interface which is externally and lower-mounted to be lowered via the winch. Meanwhile, the dock interface is intended to be placed on the external rear lower section of Eagle, enabling easier energy collection for future users.
Regarding EGSD, the panels, initially arranged in their stowed configuration, must be deployed in such a way that their deployment mechanism remains unhindered and unobstructed by other components of Eagle during its operation. Additionally, the solar panels, in this initial configuration, are positioned as close to the base as possible to ensure the center of mass remains low during Eagle's descent down the ramp. Another critical consideration is the placement of the three RFCS tanks, the heaviest components of the mission. These tanks should be positioned at the rear of Eagle to comply with the requirement that the center of mass remains within the range specified in Section 11.3 for descent. Furthermore, since these tanks are pressurized and to facilitate fluid flow under low gravity, they must be arranged vertically. Regarding the ADCS system, the IMU needs to be installed following the same considerations used for Scott. Additionally, the FFSs should be placed at the base of the cylinders of the solar panels to ensure direct visibility of the Sun and proper panels deployment. As for the TT&C system, the Ka-band antenna must be positioned at the outer edge to avoid being obstructed by the solar panels. At the same time, it should remain free to rotate in both azimuth and elevation. In addition to this, there are two S-band and two UHF antennas, which follow the same general principles as outlined by Scott. However, each individual Low Gain Antenna (LGA) must be placed strategically to achieve omnidirectional coverage. In terms of TCS, the same considerations used for Scott apply to the heaters, which now need

to be positioned near the fuel cells. Additionally, an overall area of 1.5 m² is allocated on the upper side of the radiation shield to accommodate the radiators and ensure proper dissipation of excess heat, as well as the opening of its blade louvers. In terms of LSM-S, the two magnetometers should be mounted on a 1-meter-long, non-conductive boom. This configuration is similar to that used in the Rosetta and Venus Express missions. One magnetometer is positioned at the tip of the boom, while the other is placed 50 cm from the tip. The boom must be oriented away from the solar panels' field of view and directed away from the direction of maximum magnetic disturbance. Moreover, one RTD is mounted on the boom at a height of 1.2 meters from the lunar surface for an offset measurement, while the remaining three are distributed on the lateral faces of the radiation shield at a lower height, allowing for data collection from different orientations. Both NGRM and RM-VT01-A must be fully exposed to incoming and reflected environmental radiation without any radiation shielding or obstructions. It is essential that these components remain free from electromagnetic interference. Additionally, they must not be covered by the solar panels to ensure exposure to both cosmic radiation and direct sunlight. Therefore, they are positioned on the upper side of the radiation shield.
The final internal and external configuration is shown in Figure 10.10.

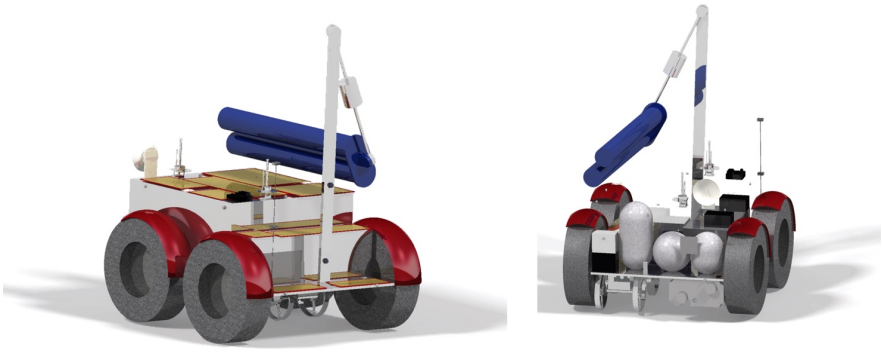

Figure 10.10: Eagle internal and external configuration.

10.7.5.3 LDE accommodation

AMPERE requires an octagonal mounting plate to physically connect the LPS to the LDE. This plate facilitates the accommodation of the LPS on the LDE. Considering the volume constraints specified by [A.D. 9], a total surface area of 4 m^2 with a maximum allowable height of 1.8 m is available on the plate. The allocated volume for the LPS is defined as a parallelepiped, where the base is a rectangle formed by one side of the octagon of 1.68 m and another of 2.38 m, ensuring that the base area corresponds to the available 4 m^2, and the height is 1.8 meters. The PDS must be installed on one of the eight sides of the mounting plate. Meanwhile, Eagle is positioned vertically and attached securely to the ramp from launch all the way through to lunar landing. It remains fixed in place by the locking system designed for the deployment sequence. Eventually, the battery used to deploy the ramp must be installed on the mounting plate, within the remaining space of the parallelepiped. The final LPS configuration on the LDE is illustrated in Figure 10.11.

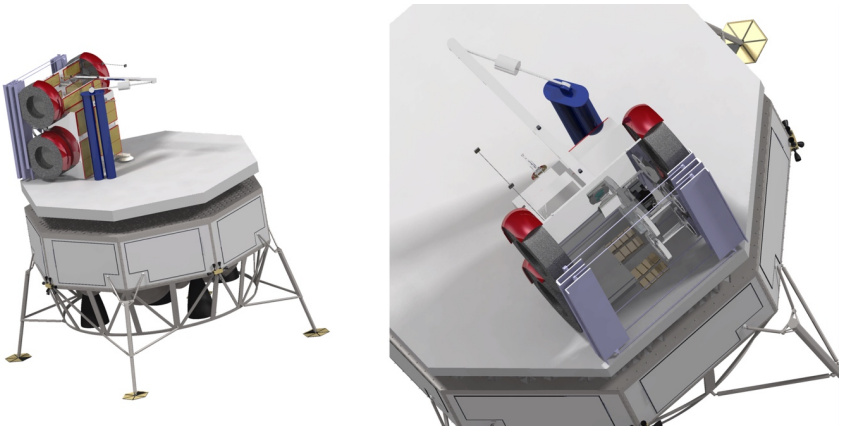

Figure 10.11: LPS configuration on the LDE

10.7.6 LPS interface with LDE

According to [A.D. 9], a mechanical and electrical connection is assumed to exist between the LDE and the LPS, ensuring compatibility for all necessary mission operations until deployment on the lunar surface. Its functionality is considered guaranteed throughout the descent, landing, and pre-deployment phases. Through this interface, the LDE supplies both power and housekeeping data to the LPS, up to the moment of separation. However, no thermal exchange occurs across the interface, as both the underside of the LPS and the corresponding LDE mounting surface are thermally isolated. Consequently, all thermal control requirements shall be managed using AMPERE's power resources. The LDE's Main Power System (MPS) is responsible for supplying power to the LPS during all mission phases until separation, while TT&C ensures a minimum data rate of 2 Mbps from the LDE to ground. The interfaces with the LDE are not included within the LPS bulk.

10.7.6.1 LPS power and data interfaces with LDE

According to Section 11.4.4.4 and Section 11.10, the LDE is required to provide a peak power availability of 47.9 W and a data transmission rate of 2.63 Mbps during the cruise mode. To achieve this, it must support the SpaceWire communication protocol outlined in standard [R.D. 78], which provides a bidirectional data rate of up to 200 Mbps and complies with streamlined harness requirements, as specified in [R.D. 36]. Additionally, Eagle's next generation OBC is fully compatible with this protocol. SpaceWire is widely recognized and frequently implemented in proven space missions [R.D. 79]. Regarding the power system, the MPS of the LDE must operate at a voltage of 28 VDC, adhering to the specifications of the PCDU described in Section 11.1.4.5. The associated cabling and connectors must comply with standards [R.D. 80] and [R.D. 81], respectively. Axon provides an extensive range of ESA-compliant American Wire Gauge (AWG) 24 or 26 cables and rectangular micro-D connectors specifically designed for space applications, meeting the previous two standards. Furthermore, the recommended micro-D connectors align with those specified in the SpaceWire standard.

10.8 Final risk assessment

For the final risk assessment of the chosen concept MoonProbe, a more detailed approach has been used. In particular, the risks that characterize this concept have been, where needed, expanded or modified. A notable example is the MA risk: in a preliminary analysis it has been considered a mission risk, from now onward it will be treated as an implementation risk. The reason for the change stands in the fact that said risk, and the relative Root Causes (RCs), only truly affect the margins that have been individuated. On a more general note, the bulk of the risk analysis after the MDR has been individuating the necessary mitigation actions for the expressed risks and the result of said actions. Two iterations of the mitigation strategy have been conducted: the first lists the design choices adopted between iterations 2 and 3, the second those relative to iteration 4. The first mitigation ended three weeks after the MDR, the second after two more weeks.

It should be highlighted that continuous improvement of design, revision and study are the baseline, primary mitigation actions. Therefore, when a mitigation action could be described as direct result of one of these three it has been simply omitted in the making of Table 10.54. In such cases N/A has been written as a placeholder.

Area	Risk	Root cause	WP	L	I	Mitigation 1	L	I	Mitigation 2	L	I
ENV	Failure to survive lunar environment	Lunar dust causes abrasion of the structure	3.5 3.7	E	4	Use of anti-dust actuators	C	3	Revision of working time	B	3
		Triboelectric effects due to dust alterate properties of the system	3.5 3.7	D	4	Use of anti-dust actuators	B	3	Revision of working time	A	3
		Radiative phenomena change the physical properties of the systems	3.5 3.7	C	3	Addition of a 1.5 mm thick radiation and micro-meteorite protective layer	B	3	N/A	B	3

		Micro-meteoroid impact	3.5 3.7	D	3	Addition of a 1.5 mm thick radiation and micro-meteorite protective layer	B	3	N/A	A	3
		Moonquakes	3.7	B	1	N/A	A	1	N/A	A	1
		Structures experience early failure, or fatigue due to thermal stress	3.5 3.7	D	3	Careful selection of thermal control components	C	3	N/A	B	3
		Non-sufficient light exposure	3.1 3.7	C	5	Iterations of codes for lunar environment with new inputs	B	4	Codes constantly improved	A	4
		Dust moved by the argonaut lander, or its plume, causes sandblasting	3.5 3.7	C	3	System deployed at an adequate distance, via ramp	A	3	N/A	A	3
ADCS	Failure to keep nominal attitude	Miscalculations of the Centre of Mass (CoM)	3.3 3.4	C	3	Computer-aided computation of finalized CoM	B	3	N/A	A	3
		Attitude sensors inaccuracy	3.3	C	2	Selection of specialized sensors; redundant design	B	2	N/A	A	2
		Sensors failure	3.3	B	4	Selection of specialized sensors; redundant design	A	3	N/A	A	3
EGSD	Failure of the EGSD system	Failure of the battery component	3.1	B	5	Revise design, battery workload can be distributed appropriately in case of failure of one of them	B	3	Complete study of charge-discharge cycles	A	3
		Lower battery capacity than anticipated	3.1	B	3	Revision of design, adoption of high-performance batteries.	B	2	N/A	A	2
		Failure of one of the solar panels	3.1	C	5	Change of the Solar Arrays (SAs) configuration	B	4	Implementation of multiple	A	4

									SAs, deployed horizontally		
		Failure to properly distribute power among subsystems	3.1	B	5	Implementation of commercial PCDU unit	A	5	PCDU tailored to our mission	A	5
		Inadequate solar array sizing	3.1	C	4	Revision of design	A	3	Higher margins considered	A	3
		Fuel cells failure	3.1 3.2	C	5	Implementation of PEM RFCS	B	5	Higher estimated TRL during mission timeframe	B	5
		Failure to deploy SAs	3.1 3.5	B	5	Change of the SAs deployment configuration	B	4	Final changes in SAs deployment solutions	A	4
		Tanks leakage	3.1	C	4	Revision of design	B	4	N/A	B	4
		Tanks rupture	3.1	B	5	Revision of design	A	5	N/A	A	5
DEPL	Failure to achieve correct PDS deployment and descent	Tipping over	3.3 3.5	B	5	Proper mass distribution; increase of the ramp rails length via an additional plate per each one	A	5	Redesign of the ramp rails using four longer plates and an overhang plate	A	5
		Failure of the deployment architecture	3.5	C	5	Increase of the ramp rails length via an additional plate per each one	A	5	Addition of lateral guides; slip-resistant coating added to the last three plates of each rail; redundant motorized hinges	A	5
		Components are too close to the lunar surface while deploying	3.5	B	4	Geometric, computer-aided visualizations used to ensure Scott's safety	A	4	Finalization of Scott's positioning	A	3
		Exceedingly high velocity of Eagle descent down the ramp	3.5	C	4	Study of possible controlled	B	4	Implementation of a breaking system for	A	4

						descent solutions			the wheeled cart		
TT&C	Communication failure	Obstructed/faulty link between Moonlight and Eagle	3.4	A	3	Redundancy; implementation of different antennas	A	2	N/A	A	2
		Data-rate miscomputed	3.4	C	2	Evaluation of necessary data-rate	A	2	N/A	A	2
		Data corruption	3.4	C	4	Use of backup material	C	2	N/A	B	2
		TT&C subsystem components fail	3.4	B	4	Redundancy; change of the initial components in favour of better ones	A	3	N/A	A	3
TCS	Failure of the TCS system	Temperature controls failure	3.2	D	5	Implementation of multiple thermal control components, such as: heaters, radiator and multilayer	C	5	Iteration of components characteristic; smart multilayer addition	B	5
		Temperature range of the components wider than anticipated	3.2 3.7	C	3	Implementation of high TRL components, with known thermal characteristics	A	3	N/A	A	3
USN	Failure to provide the expected services	Failure to protect Eagle-to-user interfaces	2.3 3.5 3.1	C	2	Implementation of removable protection for Eagle-to-user interfaces	B	2	N/A	B	2
		Insufficient energy generation	3.1	C	2	Revision of produced energy computation	B	2	N/A	B	2
		Market request overestimated	2.2	B	3	Study of future lunar missions that would benefit from AMPERE's services	A	3	N/A	A	3
PAY	Insufficient results	Failure of Eagle sensors	2.2	C	2	Integration of high TRL, flight-proven sensors	B	2	N/A	B	2
		Inadequate sensor allocation	2.2	C	2	Geometric and computer-aided allocation simulations	B	2	N/A	B	2

RVR	Scott's failure	Failure of Scott's sensors	2.2	A	3	Use of high TRL, flight-proven sensors	A	3	N/A	A	3
		Inadequate protection to the lunar environment	3.1 3.5	B	3	Implementation of removable dust cover	A	3	N/A	A	3
		Poor planning of the chosen path	3.6	C	2	Implementation of a hazard detection and avoidance strategy	B	2	Definitive planning of the path	A	2
		Inability to illuminate path during night	3.3	E	3	Addition of LEDs	B	3	N/A	A	3
		Failure of communications between Eagle and Scott	3.4	C	2	Redefinition of data exchange cycles, added UHF antenna for redundancy	B	2	Implementation of a reliable omnidirectional antenna	B	2
		Scott's critical subsystems failure	Design Node	D	3	Implementation of temperature control components; better definition of battery performances	B	2	N/A	A	2
		Avary and subsequent loss of Scott	3.3 3.6	B	3	Implementation of a hazard detection and avoidance strategy; high TRL components considered	B	3	N/A	B	3

Table 10.54: Risk register of MoonProbe's mission risks

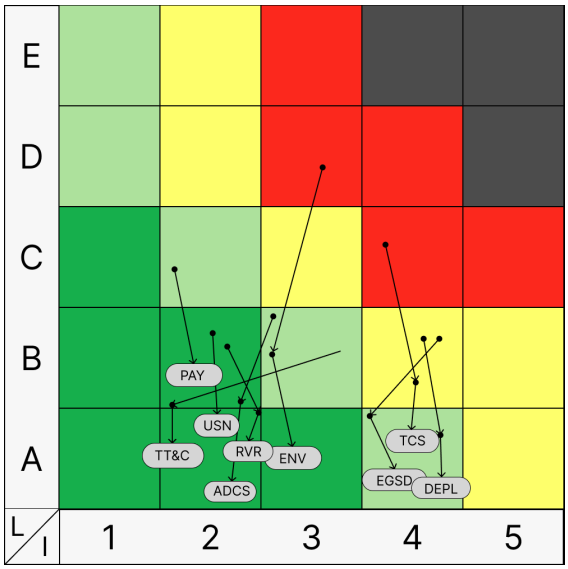

Figure 10.12: Finalized fever chart

For implementation risks, which can be found in the following Table 10.55 mitigations have not been defined as the cumulative results of every other mitigation action clearly affect them. As stated in Table 10.56, the probability of exceeding the dedicated resources is less than 10%.

Area	Risk	Root cause	L	I		L	I		L	I
TECH	Technology risk	Failure to respect mass margins	3	5		2	5		1	5
		Failure to respect volume margins	4	5		2	5		1	5
		Effective TRLs lower than anticipated	4	4		2	3		2	3
MA	Errors in the manoeuvre	Wrongly defined manoeuvre	2	4		1	4		1	4
		Wrongly defined Δv	2	4		1	4		1	4

Table 10.55: Risk register of MoonProbe's implementation

Expected returns	At MDR	After mitigations
	0.83	0.955
Resources overrun	>60%	<10%

Table 10.56: Finalized expected returns and probability of exceeding assigned resources

10.8.1 Expected productivity risk analysis

Fever charts are an effective tool for analysing risks associated with various concepts and for highlighting the effects of mitigations during the early stages of project planning, but they may prove inadequate when a more complex or detailed analysis is required. A way to deliver reliable, quantitative results tailored to a specific mission concept is through the Expected Productivity Risk Analysis (EPRA) approach. While traditional approaches do not consider the physical attributes of subsystems and their components, the EPRA accounts for the very real possibility that they may not operate under nominal conditions indefinitely. With the EPRA it is possible to simulate how the expected productivity varies in time with respect to the possible states the components can function in [R.D. 83].

It is important to note that this approach could be highly complex so, to use it in a way that still represents the early-stage state of our proposal, a number of simplifying assumptions have been made:

- Each subsystem and its components will be in the nominal state before and during deployment;
- It is possible to complete an objective -the expected output of the component- both in a nominal and degraded state, albeit at different rates;

- The degraded state has been defined as the state in which a subsystem yields half the results that it would yield in the nominal state;
- Given the nature of the mission, it is impossible to repair any subsystem or components;
- Each subsystem is considered independently, so that the failure of one or more components does not affect the probability of failure of any other;
- The probability to go from one state to the other is estimated based on the data provided by the different subsystems responsibles and the reliability data that has been estimated;

Two analyses have been conducted: the first one uses time steps of one week over a three-year period, the second uses daily time steps over a year timespan. As shown in Figure 10.13 the expected productivity at the end of the time frame considered for our mission is approximately 67% of the expected nominal productivity. These results have been obtained by integrating the "EPRA path-dependent modelling approach" [R.D. 84].

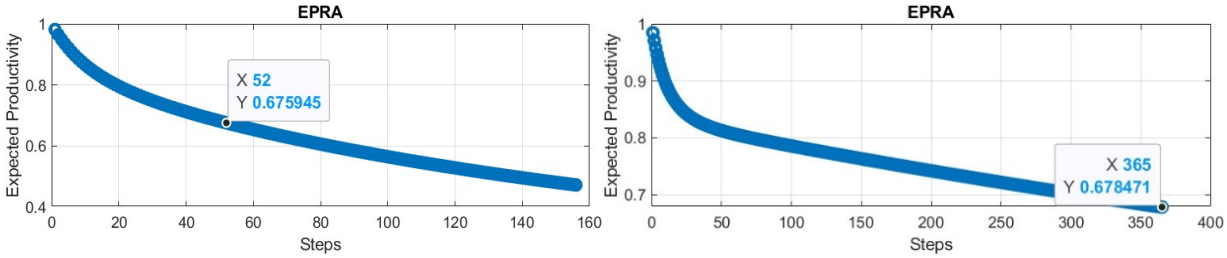

Figure 10.13: EPRA with one week time-step over three years (left) and with one daytime step over one year (right)

Although the simulations have yielded promising results, it is important to emphasize that, given the assumptions, this analysis is only loosely representative of the work conducted so far. Further modifications and improvements shall be made to ensure that a preliminary analysis such as this can adequately represent subsequent developments within the AMPERE mission.

10.9 Final Reliability Estimation

This Section discusses the preliminary reliability analysis of the AMPERE mission for the chosen architecture MoonProbe. It is important to clarify that the mission is defined as failed when at least one primary objective is not achieved. This definition has been used to build the corresponding fault tree, as shown in Figure 10.14.

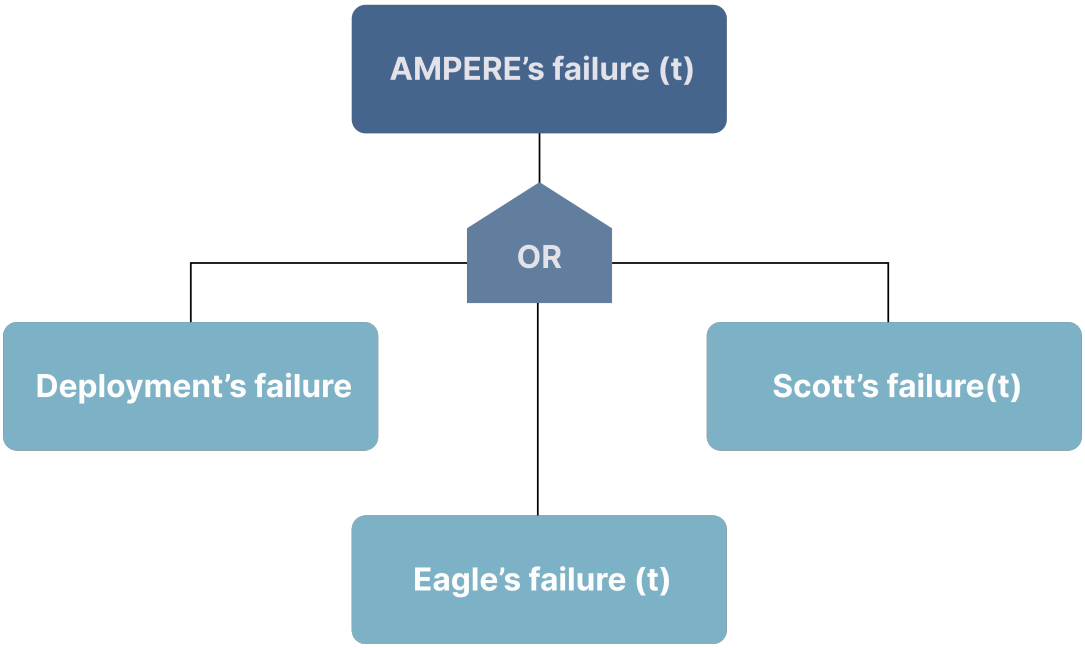

Figure 10.14: AMPERE's fault tree

The fault tree depicted above indicates that:

- due to a failed deployment of Eagle housing Scott down the ramp, the mission may fail before AMPERE's operational time begins;
- the mission may fail at any point during its operational life due to a failure of Eagle, as such failure prevents the achievement of any of the primary objectives;
- the mission may fail at any point during its operational life due to a failure of Scott, which specifically compromises the fulfillment of objectives AMP-PMO-01 and AMP-PMO-03.

It should be noted that the only factor considered in addition to the failure of Eagle and Scott is the failure of the deployment. Although there are other events whose occurrence would terminate the mission before surface operations on the Moon begin (such as a catastrophic landing), these are beyond AMPERE's scope and are therefore ignored. It should also be noted that the operational time starts immediately after the completion of the deployment.
At this point, the following rule in Equation (10.5) must be recalled:

$$P(A \cup B \cup C) = 1 - P(\overline{A} \cap \overline{B} \cap \overline{C}) \tag{10.5}$$

And if these events are assumed to be stochastically independent, it is possible to state, as in Equation (10.6), that:

$$1 - P\left(\overline{A} \cap \overline{B} \cap \overline{C}\right) = 1 - P(\overline{A})P(\overline{B})P(\overline{C}) \tag{10.6}$$

Consequently, it can be concluded that the probability of an AMPERE failure is given by Equation (10.6):

$$P(AMPERE's\ failure\ at\ t) = F_T(t) = 1 - P(successful\ deployment) \cdot R_{EAGLE}(t) \cdot R_{SCOTT}(t) \tag{10.6}$$

Where:

- T is the random variable representing the operational time of the AMPERE mission, and *t* is a generic realization of it;
- $F_T(t)$ is the unreliability of the AMPERE mission at the generic operational time *t*;
- $R_{EAGLE}(t)$ is the reliability of Eagle at the generic operational time *t*;
- $R_{EAGLE}(t)$ is the reliability of Scott at the generic operational time *t*.

The value of P(successful deployment) is the result of a risk analysis and is set equal to 0.99. To estimate the two reliabilities of Eagle and Scott, it is necessary to logically model their functioning and then assign an appropriate reliability distribution to each subsystem, along with suitable parameters for those distributions.
For this preliminary analysis, for the sake of simplicity, only Weibull distributions have been used. Specifically, the values from [R.D. 85] have been taken as a starting point and then adjusted using appropriate scaling factors to adapt the data, originally referring to Earth-orbiting satellites, to a lunar mission like AMPERE. Both the shape parameter (β) and the scale parameter (α) have been degraded by 20% to make the reliability estimates more conservative. This adjustment accounts for the harsher environmental conditions on the lunar surface compared to Earth orbit, which are expected to negatively impact system reliability. The values used are summarized Table 10.57 :

Name	β	α(years)
FSS	0.5745	3064.8
CSS	0.5745	3064.8
Structure & Mechanisms	0.2848	17046996.8
TCS	0.2848	17046996.8
Cameras	0.7099	6386.4
LEDs	0.7099	6386.4
Battery	0.5968	6186.4
Fuel cells	0.5968	6186.4
Solar array	0.3228	1572694.4
Electrical distribution	0.40168	135417.6

TT&C	0.3151	320785.6
OBC	0.7099	6386.4

Table 10.57: Values of α and β used

The following logical scheme shown in Figure 10.15 is used for both Eagle and Scott:

Figure 10.15: Logic diagram for Eagle and Scott

These subsystems have been arranged in series, as the failure of any individual unit would result in the failure of the whole system. Among these subsystems, only ADCS and EGSD exhibit reliability differences depending on whether Eagle or Scott is considered, as shown in Figure 10.16:

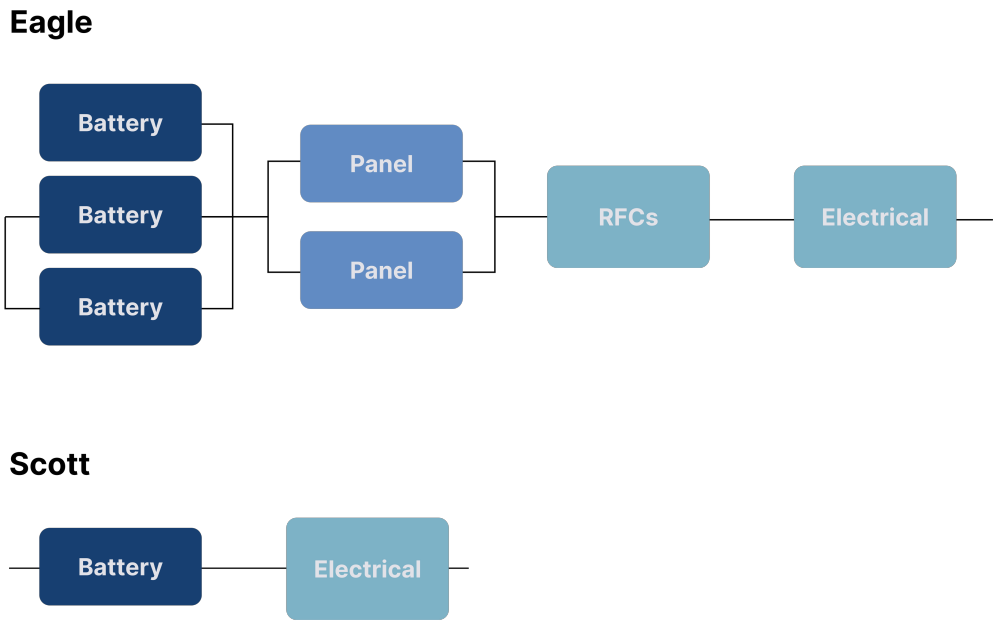

Figure 10.16: Logic diagrams of the EGSD systems for Eagle and Scott

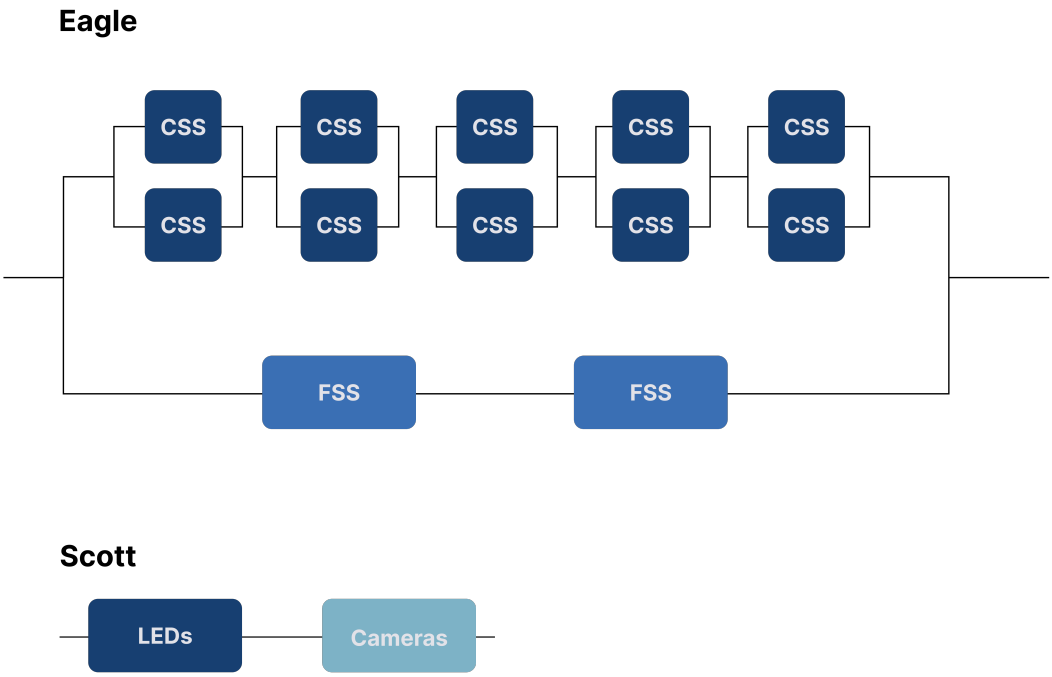

Figure 10.17: Logic diagram for ADCS of Eagle and Scott

It is noted that the logic schemes used to model the EGSD and ADCS subsystems in detail are derived from the operational principles of these subsystems, and considering the minimum set of components required to perform the tasks essential for the mission's functionality. For example, although multiple batteries are installed on Eagle, they are connected in parallel, so that if one battery fails, the remaining units are still capable of meeting the mission requirements. At this point, all the necessary information is available to calculate the reliability of AMPERE. This calculation has been performed in MATLAB, yielding the following results:

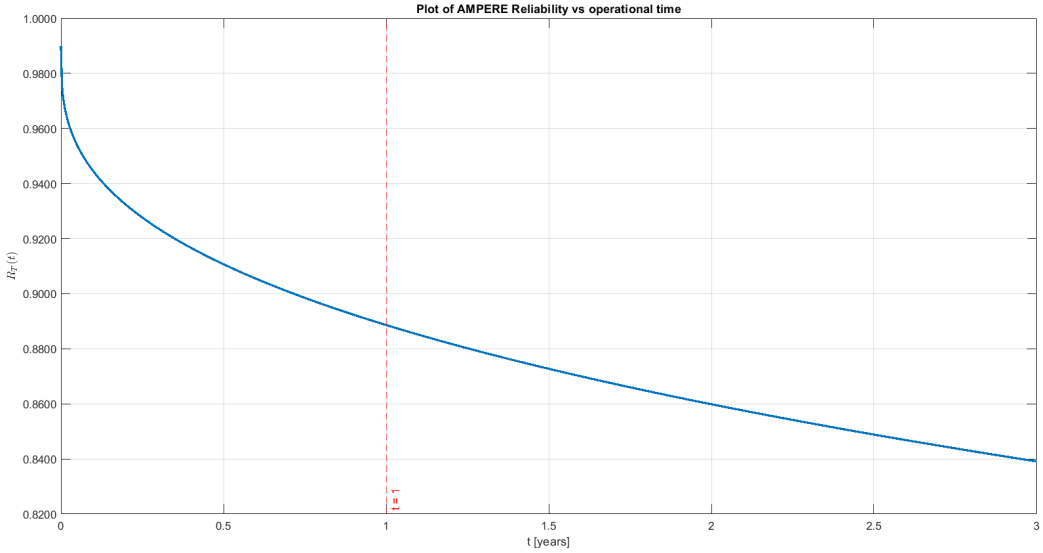

Figure 10.18: AMPERE's reliability

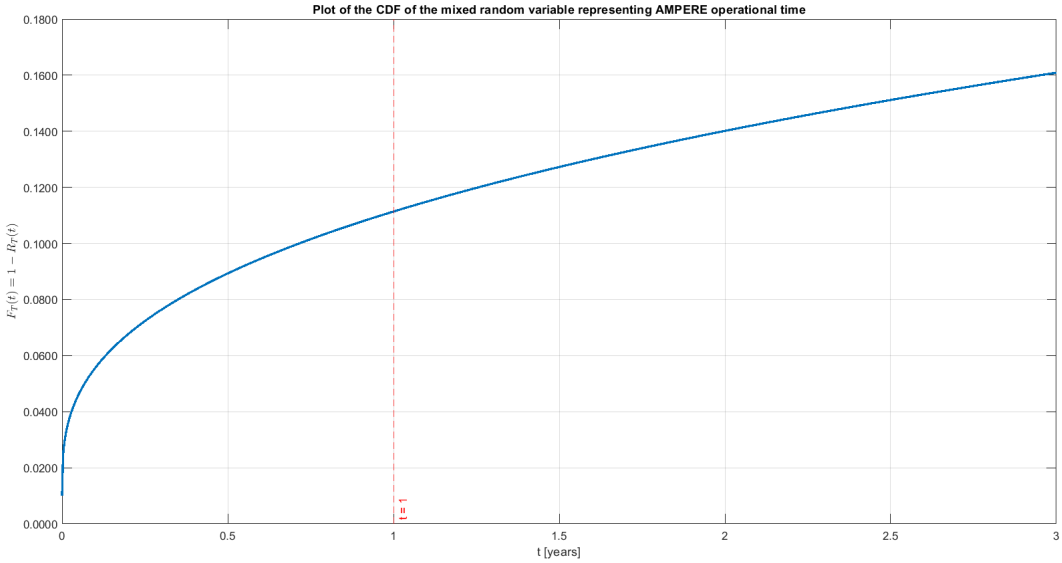

Figure 10.19: AMPERE failure probability.

It should be noted that the random variable T, which represents the operational time of the AMPERE mission, is a mixed random variable with a probability mass of 0.01 at $t = 0$. Consequently, unlike continuous random variables, the initial value of reliability is not 1, but $1 - 0.01$.
It can be observed from the graph that the probability that the operational time exceeds 1 year (which is the operational duration of interest for the AMPERE mission) is 88.86%. This is considered a reasonable value for a lunar, unmanned mission with no direct predecessors

10.10 Final Cost Analysis

The detailed cost analysis of AMPERE mission is provided in this Section, with a more precise estimation of the mission costs for the selected MoonProbe concept. A first estimation was conducted using QuickCost model for Eagle, Scott module, while the PDS module cost is estimated in a second phase, where the NASA Instrument Cost Model (NICM) model [R.D. 86] for the three modules composing LPS, considering each subsystem specifically.
The QuickCost input parameters are explained in Section 10.4.1. With respect to the preliminary analysis, the costs are divided between the Eagle and Scott module, then summed to have the total cost.

Data	Eagle	Scott	Unit
Dry Mass	499.0	41.4	Kg
Power	1630	40	W
Data%	0.25	0.15	0 to 100%
Life	14	14	Months
New	0,7	0,7	28% to 130%
Planetary?	1		[0,1]
Year ATP	2032		Year
InstrComp%	0,8	0,7	0 to 100%
Team experience	2		1 to 4
Total cost (USD FY2010)	14.62	2.34	
Total cost (EUR FY2038)	49.46	9.22	

Table 10.58: Eagle and Scott cost with QC model

Following the detailed design phase, notable variations can be observed in key parameters such as dry mass (kg) and power (W) when compared to the values utilized in the previous cost estimation. Given the current system TRL assessment (Section 11.8) the percentage of new has been individually determined for each module, reflecting the varying degrees of technological heritage and development maturity across the AMPERE subsystems. The life parameter has been update to 14 months for the Eagle module to include phase F11 or phase F12 (i.e. the disposal, see Section 10.6.1.1). Furthermore, the ATP milestone, marking the commencement of Phase B activities, has been updated to 2032 in accordance with the AMPERE master schedule Section 10.12. Total costs from the QuickCost model results in USD FY2010 and are firstly converted to EUR FY2010 with the exchange rate of USD/EUR = 0.711 as of 01/01/2010 and then adjusted for a cumulative inflation of 85.99% up to 2038 (end of Phase E) calculated as described in Section 10.4.1 Total cost of Eagle plus Scott comes out to 58.58 million EUR FY2038. PDS module's cost has not been estimated with QuickCost. Further analysis has been made using NICM [R.D. 86] carefully choosing correct Cost Estimating Relationship (CER) for each subsystem. Data inserted in CER are from Section 11.9 and 11.10. Costs resulting from the NICM model are in USD FY2004, and they are converted to EUR 2038, using the same strategy used in the preliminary analysis (i.e. using EUR/USD exchange of 01/01/2004 [R.D. 88], EUR inflation data up to 2025 from [R.D. 87], and inflation from 2025 to 2038 is the average of the of the 10 previous years). Cumulative inflation from 2004 to 2038 for the Euro zone is 131.72%.

Module	Subsystem	Input parameters	Cost (USD FY2038)
PDS		Mechanical mass (kg); power (in W)	2.42
EAGLE	EGSD	Electronics mass (kg); design life (months)	373.01
	RDS	Mechanical mass (in kg); power (in W)	0.10
	STR&MEC	Mechanical structural mass(kg); power (in W)	16.14
	TCS	Thermal mass (kg); design life (months)	179.74
	SENSORS	Sensors mass (in kg); power (in W)	3.24
	TT&C	Subsystem mass (in kg) power (in W)	15.51
	ADCS	Mass (in kg); power (in W)	2.11
SCOTT	EPS	Electrical mass (in kg); design life (in months)	2.59
	GNC-Mobility	Mass (in kg); power (in W)	0.80
	GNC-Sensors	Mass (in kg); power (in W)	5.31
	STR&MEC	Structure mass (in kg); power (in W)	0.79
	SENSORS	Sensors mass (in kg); power (in W)	5.07
	TCS	Thermal mass (in kg); design life (in months)	32.41
	TT&C	Subsystem mass (in kg); power (in W)	0.35

Table 10.59: Instruments cost with NICM

The sum of the cost of LPS is: 204.62 millions (EUR FY2038).
Additional costs are necessary:

Cost	Input parameter	Result (FY2038)

Management cost	Total instrument cost	52.31
System engineering cost	Total instrument cost	60.95
Product assurance cost	Total instrument cost	118.59
Integration and test cost	Total instrument cost	36.36
Total additional cost	/	215.90

Table 10.60: Additional cost with NICM

AMPERE's total mission cost is shown in Table 10.61, as the sum of the three modules cost plus the additional costs.

Module	Cost EUR (FY2038)
Eagle	590.71
PDS	2.42
Scott	46.40
Additional	54.96
Total	627.11

Table 10.61: AMPERE total estimated mission cost

10.11 Verification

A preliminary verification plan for the AMPERE mission has been defined, based on [R.D. 89] and [R.D. 90], with the scope of demonstrating, through a dedicated process, that the deliverable system meets its specified requirements, can sustain its operational role throughout the project lifecycle and maintains its integrity and performance during all key phases of the mission. The verification program has been derived considering the full system lifecycle, including models, development and integration timelines, verification tools and project milestones, following an iterative approach based on technical, costs reduction and schedule considerations. As a first step, the following verification stages have been selected for AMPERE, based on its specific characteristics:

- Qualification
- Acceptance
- Pre-flight
- In-orbit
- Post landing

Qualification and acceptance shall be completed before launch during phase D (Section 10.12): during the qualification stage, verification must confirm that the design, including its safety margins, satisfies all applicable requirements, using hardware and software that accurately represent the product configuration in terms of design and materials. In particular, the qualification program is developed with consideration of the product category and its heritage, as specified in [R.D. 90]. The acceptance stage serves the purpose of verification but applies less conservative margins and is executed only after completing a successful qualification campaign. While pre-flight, in-orbit and post landing stages are out of the scope of the study, it is noted that the pre-flight stage is needed to confirm that the system is ready for launch, the in-orbit stage is done during the commissioning shortly after launch, while the post landing stage, particularly relevant for AMPERE, shall address the product integrity and performance after the orbiting phase.

10.11.1 Product categories

AMPERE's model philosophy and testing activities have been established based on the product categories outlined in Table 10.62. Each subsystem or equipment item is categorized according to its expected TRL as of the current date.

Cat.	Description	Qualification program	TRL
A	Off the shelf product without modifications and: - subjected to a qualification test programme at least as severe as that imposed by the actual project specifications including environment. - produced by the same manufacturer or supplier and using the same tools and manufacturing processes and procedures.	None	8-9

B	Off the shelf product without modifications. However, it has been subjected to a qualification test programme less severe or different to that imposed by the actual project specifications (including env ironment).	Delta qualification programme, decided on a case-by-case basis.	6-7
C	Off the shelf product with design modifications. Modification includes changes to design, parts, materials, t ools, processes, procedures, supplier or manufacturer.	Delta or full qualification programme (including testing), decided on a case-by-case basis depending on the impact of the modification.	4-5
D	Newly designed and developed product.	Full qualification programme.	1-3

Table 10.62: Product categories according to TRL

10.11.2 Model philosophy

For the AMPERE mission, the adoption of a hybrid model philosophy has been identified as the most suitable choice, driven by the different TRLs of all the subsystems and instruments comprising the mission. Indeed, the hybrid philosophy is a verification approach that combines elements of both the prototype and protoflight models and it is typically adopted when parts of the system involve new designs or critical functions. This strategy offers a balanced trade-off between risk, cost, and schedule, allowing parallel activities and better accommodation of delivery timelines. This approach, therefore, facilitates a differentiated strategy among the different subsystem verification activities. The selection of models for AMPERE's philosophy was guided by recommendations regarding the use of model combinations commonly employed for the progression of TRL, as outlined in [R.D. 91].

The following models have been used at system level:

- Structural and Thermal Model (STM): the STM serves as a representative prototype of the flight model in both structural and thermal aspects, enabling comprehensive qualification testing of the structure and thermal subsystems. For this purpose, all the remaining components are substituted with dummy counterparts.
- Electrical and Functional Model (EFM): the EFM serves as an electrical and functional representation but is unsuitable for Electromagnetic Compatibility (EMC) testing since it does not accurately reflect the equipment's placement within the flight configuration.
- Protoflight Model (PFM): the PFM serves as the final flight model and undergoes a hybrid testing campaign that falls between the qualification and acceptance levels.

At equipment and subsystem level, a combination of the following models has been introduced for each item based on its heritage:

- Development Model (DM): a DM is utilized during the creation of new designs or in instances requiring significant redesigns. It is essential for equipment that is entirely newly developed to meet the specific requirements of the mission.
- Engineering Model (EM) or Engineering Qualification Model (EQM): an EM serves as a representative prototype in terms of Form, Fit and Function (FFF), yet it does not incorporate high-reliability components or full redundancy. Its primary purpose is to facilitate electrical and functional verification processes. Conversely, an EQM is entirely representative of a flight-ready model and is additionally suited for EMC testing as well as environmental testing. When conducting a full qualification campaign, one of these models should be employed to assess and validate the required component.
- Suitcase model: a suitcase model is utilized to evaluate the performance of Radio Frequency (RF) receivers and transmitters, along with the data handling subsystem.
- PFM or Flight Model (FM): the final product designed for flight will be classified as either a PFM or an FM, depending on the results of prior qualification testing.

The structure of AMPERE's model philosophy is illustrated in Figure 10.20. Specific qualification tests in the critical areas are carried out on dedicated models. In these areas only acceptance testing is performed on the PFM. The EM/EQM equipment that successfully completes its respective testing campaigns is subsequently utilized in the EFM system-level model, and the same applies to the PFM/FM equipment. STM provides structural and thermal qualification at system level, using integrated dummy components.

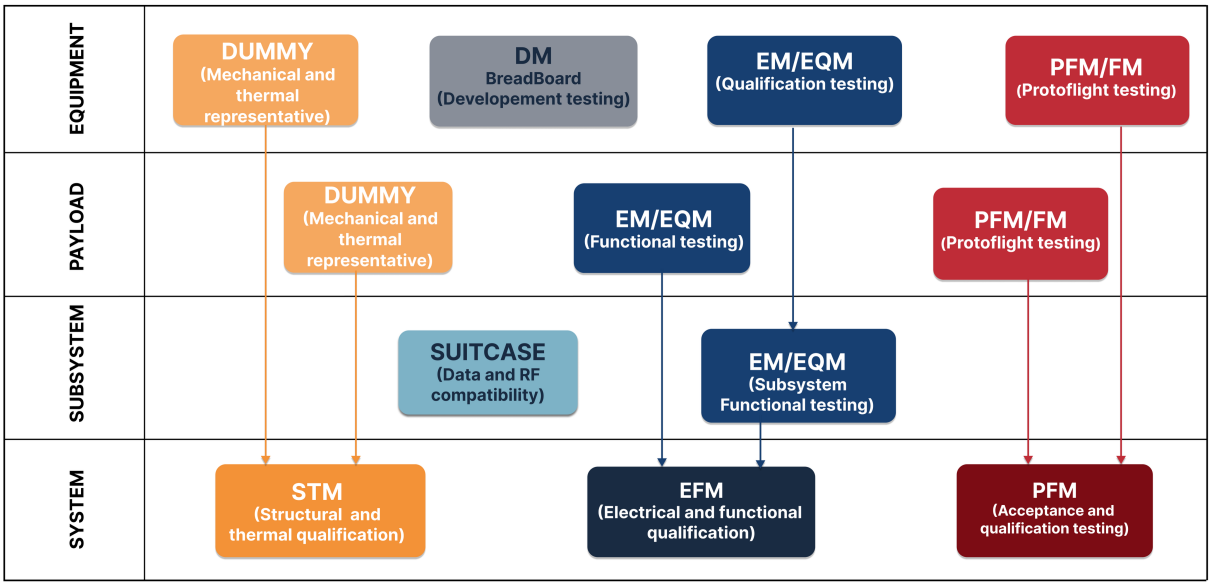

Figure 10.20: Model philosophy structure

10.11.3 Hardware matrix

The hardware matrices for Eagle, including PDS, and separately for Scott are shown in the following Table 10.63 and Table 10.64.

ID	Item	Cat.	Equipment/Subsystem level				System level			Remarks
			DM	EM/ EQM	Suit.	FM/ PFM	STM	EFM	PFM	
STR& MEC	Wheels	A	/	/	/	/	4	/	4	
	Cart's plate	C	/	/	/	1	1	/	1	
	Brakes actuator	C	/	/	/	1	1	/	1	
	Solar array drive electronics	B	/	/	/	/	1	/	1	
	Pointing mechanism	A	/	/	/	/	1	/	1	
	Solar array drive mechanism	A	/	/	/	/	1	/	1	
	Solar array deployment	D	1	/	/	1	1	/	1	
	Radiation shield	C	/	/	/	1	1	/	1	
TT&C	Ka-band antenna	B	/	/	1	1	1*	1^^	1	*Dummy ^^ Refurbished from suitcase model
	Ka-band transceiver	B	/	/	2	2	2*	2^^	2	
	Ka-band amplifier	B	/	/	2	2	2*	2^^	2	
	Ka-band diplexer	A	/	/	2	2	2*	2^^	2	
	S-band antenna	A	/	/	2	2	2*	2^^	2	
	S-band transponder	A	/	/	2	2	2*	2^^	2	
	OBC	A	/	/	1	1	1*	1^^	1	
	UHF antenna	B	/	/	2	2	2*	2^^	2	
	UHF transceiver	A	/	/	2	2	2*	2^^	2	
TCS	Generator for Electrodynamic Dust Shield (EDS)	A	/	/	/	/	1	/	1	** Refurbished from STM
	EDS	A	/	/	/	/	1	/	1	
	MLI Teflon	A	/	/	/	/	1	/	1	
	MLI mylar + Vacuum-Deposited Aluminium (VDA)	A	/	/	/	/	1	/	1	
	Heater	A	/	/	/	/	2	2**	2	
	Loop heat pipe	B	/	/	/	/	6	6**	6	

	Radiator	C	/	/	/	/	1	1**	1	
	Temperature sensor	A	/	/	/	/	3	/	3	
	MLI smart	C	/	/	/	/	1	1**	1	
EGSD	Solar panel	B	/	1	/	1	1*	1^	1	*Dummy ^From equipment EQM
	RFCS	C	/	1	/	1	1*	1^	1	
	Battery	A	/	/	/	1	1*	1	1	
	PCDU	C	/	1	/	1	1*	1^	1	
	Wireless interface	B	/	1	/	1	1*	1^	1	
	Dock interface	B	/	/	/	1	1*	1	1	
	Connector	B	/	/	/	1	1*	1	1	
ADCS	IMU	C	/	1	/	1	1*	1^	1	*Dummy ^From equipment EQM
	Inclinometer	C	/	1	/	1	1*	1^	1	
	CSS	A	/	/	/	10	10*	10	10	
	FSS	A	/	/	/	2	2*	2	2	
RDS	Drop-release system	B	/	/	/	1	1	/	1	
	Winch + worm gear + motor + Dyneema cables	B	/	/	/	1	1	/	1	
LSM_S	RADFET	B	/	1	/	1	1*	1^	1	*Dummy ^From equipment EQM
	Magnetometer	A	/	/	/	2	2	2	2	
	Boom	A	/	/	/	1	1*	1	1	
	RTD	B	/	4	/	4	4*	4^	4	
	Radiation monitor	A	/	/	/	1	1	1	1	
PDS	Ramp	C	/	/	/	1	1	/	1	
	Hinges	C	/	/	/	1	1	/	1	
	Thermal knives	B	/	/	/	/	8	/	8	
	Kevlar cables	B	/	/	/	/	4	/	4	
	Ramp actuator moog965	C	/	/	/	1	1	/	1	
	Ramp actuator cubemars	C	/	/	/	1	1	/	1	
	Reduction unit	C	/	/	/	1	1	/	1	
	Reduction unit moog965	C	/	/	/	1	1	/	1	
	Slip resistant material	D	1	/	/	1	1	/	1	
	Battery	A	/	/	/	/	1	/	1	

Table 10.63: Eagle and PDS hardware matrix

ID	Item	Cat.	Equipment/Subsystem level				System level			Remarks
			DM	EM/ EQM	Suit.	FM/ PFM	STM	EFM	PFM	
TT&C	UHF antenna	B	/	/	1	1	1*	1^^	1	*Dummy ^^ Refurbished from Suitcase Model
	UHF transceiver	A	/	/	1	1	1*	1^^	1	
	S-band antenna	A	/	/	1	1	1*	1^^	1	
	S-band transceiver	A	/	/	1	1	1*	1^^	1	
	S-band diplexer	A	/	/	1	1	1*	1^^	1	
	OBC	A	/	/	1	1	1*	1^^	1	
	Lunar Communication and Navigation Services (LCNS) unit	B	/	/	1	1	1*	1^^	1	
STR& MEC	Astrobotic Cuberover system	A	/	/	/	/	/	/	1	
GNC	IMU	C	/	2	/	2	2*	2^	2	*Dummy ^From equipment
	CSS	A	/	/	/	10	10*	10	10	
	Camera	A	/	/	/	2	2*	2	2	

	Astrobotic Cuberover system	A	/	/	/	/	/	/	1	EQM
	LED	A	/	/	/	16	/	/	16	
LSM_M	IES	B	/	1	/	1	1*	1^	1	*Dummy ^From equipment EQM
	INMS	B	/	1	/	1	1*	1^	1	
	SRDS	B	/	1	/	1	1*	1^	1	
	Langmuir probe	A	/	/	/	1	1*	1	1	
	Boom	A	/	/	/	1	1*	1	1	
TCS	Generator for EDS	A	/	/	/	/	1	/	1	** Refurbished from STM
	EDS	A	/	/	/	/	1	/	1	
	MLI Teflon	A	/	/	/	/	1	/	1	
	MLI mylar + VDA	A	/	/	/	/	1	/	1	
	Loop heat pipe	B	/	/	/	/	2	2**	2	
	Radiator	C	/	/	/	/	1	1**	1	
	Temperature sensor	A	/	/	/	/	2	/	2	
	Heaters	A	/	/	/	/	2	2**	2	
	MLI smart	C	/	/	/	/	1	1**	1	
EPS	Battery	A	/	/	/	1	1*	1	1	*Dummy ^From equipment EQM
	Wireless interface	B	/	1	/	1	1*	1^	1	
	PCDU	B	/	1	/	1	1*	1^	1	

Table 10.64: Scott hardware matrix

10.12 Master schedule

The master schedule for a space mission represents a plan that defines all essential activities, timelines, and resources necessary for the success of the mission. It serves as a supporting structure for project management and coordination, ensuring that the mission implementation proceeds according to the established timeline, preventing delays and facilitating cooperation among all involved parts.

The AMPERE mission schedule follows seven different phases according to the ECSS standard [A.D. 4] each characterized by both closing and intermediate milestones. The schedule covers the entire duration of the mission, form April 9, 2025, to July 1, 2039, for a total of 14 years, 2 months and 22 days and it's shown in Figure 10.21 where the yellow marks are standard milestones while red marks represent the AMPERE mission specific milestones.

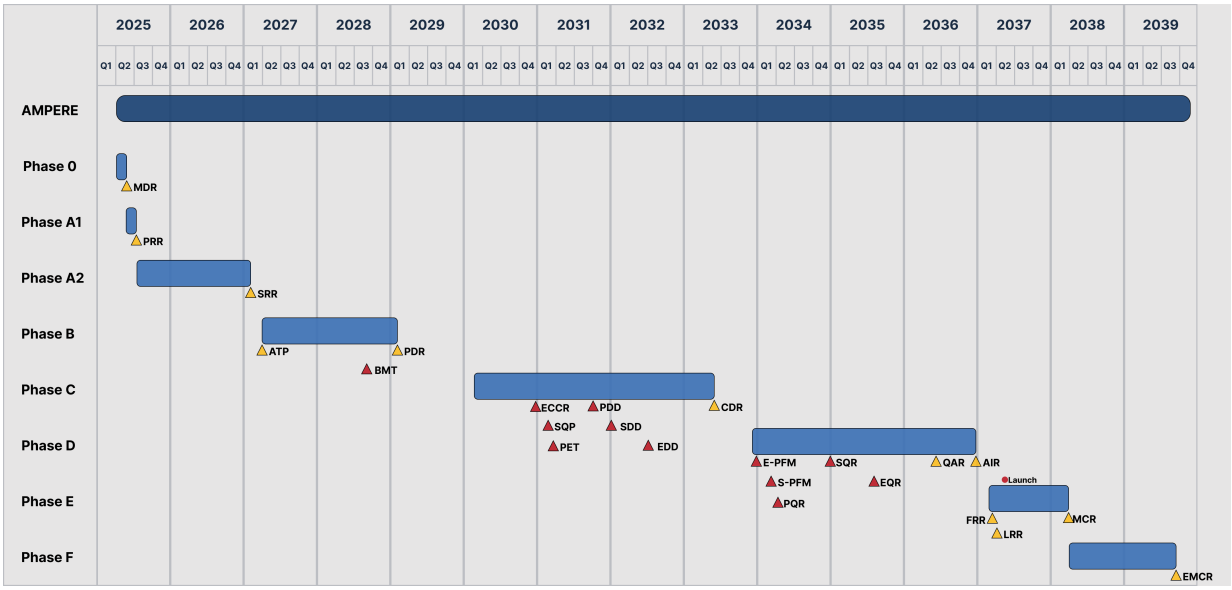

Figure 10.21: Master schedule

The milestones are structured to follow a Go/No-Go logic after certain key milestones (acronyms are provided in Table 10.66). PDS, Eagle and Scott modules undergo different design, production, and qualification processes based on their design complexity and component TRL levels. PDS has the lowest TRL components (TRL 3), which is why it requires breadboard testing and validation activities. Eagle and Scott modules both operate at TRL 5, representing more mature technologies. Scott must pass a dedicated design completion milestone (SDD) in Phase C. Eagle requires multiple critical milestones including ECCR, EDD, and EQR between Phase C and D due to its system complexity. The entire LPS system will undergo design and qualification phases once the three modules are integrated.
The phases are as follow:

- Phase 0 (38 days from April 9, 2025, to May 16, 2025):
  This represents the mission analysis and preliminary definition phase concluding with the Mission Definition Review (MDR). This phase establishes the mission concept and feasibility study.
- Phase A1 (48 days from May 17, 2025 to July 4, 2025):
  Here mission requirement foundations are established. The Preliminary Requirements Review (PRR) represents the culminating milestone where initial mission requirements and constraints are defined and validated against feasibility assessments from Phase 0.
- Phase A2 (575 days from 5 July, 2025 to January 31, 2027):
  Here the complete mission requirements baseline and detailed system architecture are established. The System Requirements Review (SRR) serves as a critical milestone where the finalized System Requirements Document, complete Mission Analysis Report, and System Architecture Document are validated. During this phase, particular attention is given to EAGLE critical components assessment and SCOTT supplier selection strategy. The phase also produces the Interface Control Document (ICD) in preliminary form.
- Phase B (670 days from April 1, 2027 to January 31, 2029):
- The preliminary design phase transforms the established requirements into concrete system architecture and preliminary designs across all subsystems. This phase is characterized by intensive design activity where the System Design Document and preliminary Software Design Document are developed, along with complete Interface Control Documents that define all system interfaces. The Authorization-to-Proceed (ATP) milestone marks the formal start of design activities. The PDS Breadboard Module Test (BMT) is critical for validating PDS low-TRL components (TRL 3) in a representative environment, providing essential technology maturation data. The Preliminary Design Review (PDR) serves as the phase-closing milestone where all preliminary designs are validated and approved for detailed development.
- Phase C (1248 days from March 1, 2030 to July 31, 2033):
  The longest and most complex phase of the mission, Phase C represents the most challenging period of the AMPERE mission due to the convergence of multiple critical design activities and the varying TRL levels of the three main modules. The PDS module continues to require intensive development, while Eagle and Scott modules with TRL 5 components follow more mature development paths. The EAGLE Critical Components Review (ECCR) serves as the first major milestone for critical component validation. The System Qualification Plan Approval (SQP) ensures all qualification strategies are validated before proceeding. Module-specific milestones include the PDS EM Test (PET) for electromagnetic compatibility validation, critical for low-TRL component integration, and the PDS Design Done (PDD) milestone completing PDS development after extensive technology maturation activities. The SCOTT Design Done (SDD) milestone marks the completion of SCOTT module detailed design while the Eagle Design Done (EDD) represents the completion of Eagle module design activities. The Critical Design Review (CDR) serves as the phase-closing milestone where all detailed designs across all modules are validated and frozen for production
- Phase D (1125 days from November 1, 2033 to November 31, 2036):
  This phase is critical due to the manufacturing and qualification risks associated with flight hardware production. The EAGLE module continues to drive the critical path through its component qualification tests requiring a 10-month period for all critical components, followed by a 6-month assembly and integration period demanding precision manufacturing techniques. The flight qualification tests represent the final 1-month intensive testing period, culminating in the EAGLE Qualification Review (EQR), which serves as the most critical milestone determining overall mission viability. A safety buffer of one additional month has been implemented after EQR specifically for risk mitigation purposes. The system integration timeline requires 8 months due to the complex interfaces between PDS, EAGLE, and SCOTT modules, comprehensive end-to-end testing requirements for lunar landing systems, ground segment integration and validation needs, and the necessity to verify all operational procedures before final acceptance. Two critical Go/No-Go decision points are

established in Phase D: the EAGLE Go/No-Go at month 6 based on EQR results where mission continuation depends entirely on successful EAGLE qualification, and the System Go/No-Go at month 11 representing the final system readiness assessment before launch campaign preparation begins.

- Phase E (396 days from March 1, 2037 to April 1, 2038):
  This phase is critical due to the manufacturing and qualification risks associated with flight hardware production. All three modules undergo intensive qualification testing with module-specific timelines reflecting their development maturity levels. The PDS module, having matured from TRL 3 to flight-ready status through Phase C activities, undergoes comprehensive PFM testing and validation, culminating in the PDS Qualification Review (PQR) where final acceptance criteria are verified. Eagle and Scott modules, building on their TRL 5 foundation, proceed through their respective qualification programs with the Eagle PFM Test (E-PFM) focusing on critical system performance validation, followed by the Scott PFM Test (S-PFM) for Scott module verification. The Scott Qualification Review (SQR) validates Scott module readiness for integration, while the EAGLE Qualification Review (EQR) represents the most critical milestone in Phase D, serving as a major Go/No-Go decision point where overall mission viability is determined based on Eagle module performance. The system-level integration activities commence following successful module qualifications, with the comprehensive Qualification and Acceptance Review (QAR) ensuring all integrated system requirements are met. The Test Readiness Review (TRR) validates that all testing protocols and procedures are properly established and verified before final integration activities. The Argonaut Integration Review (AIR) represents the culminating milestone of Phase D, where the complete integration of LPS on Argonaut system is validated and approved for launch campaign preparation.
- Phase F (455 days from April 2, 2038 to July 1, 2039):
  The final phase encompasses extended mission operations and comprehensive mission closure activities following the completion of primary lunar surface operations. More specifically phase F is divided into more sub-phases, explained in detail in Section 11.9, that last for a total of 12 months and that will address task 4 [A.D. 1]. The Extended Mission Close-out Review (EMCR) serves as the final milestone where all mission objectives are assessed against achieved results, lessons learned are documented, and scientific data packages are finalized. The extended duration ensures adequate time for thorough analysis of mission data, preparation of final scientific publications, and documentation of operational procedures and anomalies encountered during the mission.

Phase	Start date	End date	Duration (Days)	Closing MS
0	09/04/25	17/05/25	38	MDR
A1	17/05/25	04/07/25	48	PRR
A2	05/07/25	31/01/27	575	SRR
B	01/04/27	30/01/29	670	PDR
C	01/03/30	31/07/33	1248	CDR
D	01/11/33	30/11/36	1125	AR
E	01/03/37	01/04/38	396	MCR
F	02/04/38	01/07/39	455	ECMR

Table 10.65: Mission phases

Milestone	Milestone Full name	Phase	Date	Status
KoM	Kick-off Meeting	0	09/04/25	Passed
MDR	Mission Definition Review	0	16/05/25	Passed
PRR	Preliminary Requirements Review	A1	04/07/25	Doing
SRR	System Requirements Review	A2	31/01/27	Planned
ATP	Authorization-To-Proceed	B	01/04/27	Target
BMT	PDS Breadboard Module Test	B	01/09/28	Planned
PDR	Preliminary Design Review	B	30/01/29	Planned
ECCR	Eagle Critical Components Review	C	31/12/30	Planned

SQP	System Qualification Plan Approval	C	01/03/31	Planned
PET	PDS EM Test	C	30/04/31	Planned
PDD	PDS Design Done	C	30/09/31	Planned
SDD	Scott Design Done	C	31/01/32	Planned
EDD	Eagle Design Done	C	30/06/32	Planned
CDR	Critical Design Review	C	31/07/33	Planned
E-PFM	Eagle PFM Test	D	31/12/33	Planned
S-PFM	Scott PFM Test	D	01/03/34	Planned
PQR	PDS Qualification Review	D	01/04/34	Planned
SQR	Scott Qualification Review	D	31/12/34	Planned
EQR	Eagle Qualification Review	D	31/06/35	Planned
QAR	Qualification Review	D	31/07/36	Planned
TRR	Test Readiness Review	D	30/11/36	Planned
AIR	Argonaut Integration Review	D	31/12/36	Planned
FRR	Flight Readiness Review	E	15/03/37	Planned
LRR	Launch Readiness Review	E	25/03/37	Planned
Launch	Launch	E	29/03/37	Planned
LOI	Lunar Orbit Insertion	E	01/04/37	Planned
LL	Lunar Landing	E	05/04/37	Planned
MCR	Mission Close-out Review	E	01/04/38	Planned
EMCR	Extended Mission Close-out Review	F	01/07/39	Planned

Table 10.66: Mission milestones

10.13 Requirements

The following Sections present the AMPERE requirements, based on a 4-level structure, as shown in the specification tree (Figure 10.22).

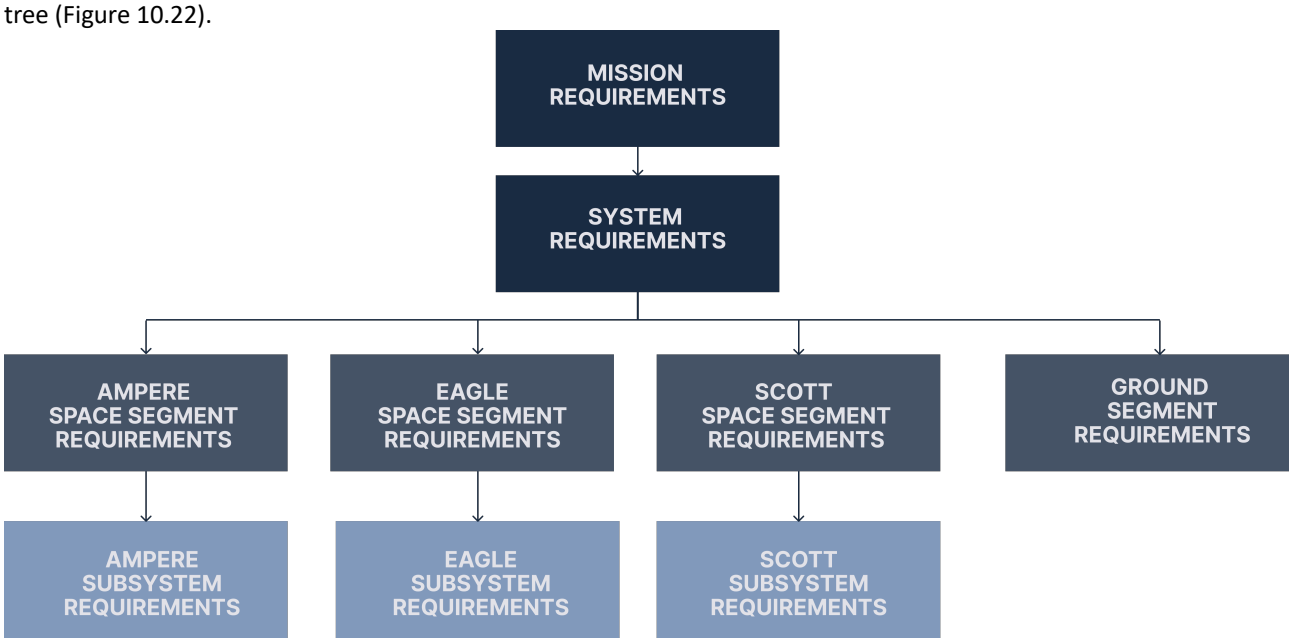

Figure 10.22: AMPERE specification tree

Each requirement is uniquely identified by an alphanumeric ID code, made by 6 letters and 4-digit numbers, where the first 3 letters represent the interested element (AMP for AMPERE, EGL for Eagle and SCT for Scott) and the other 3 the requirement level (MIS, SYS, SSE, GSE, SUB). The number is in the format “0010” and defines every single requirement. The requirements have been defined as belonging to different types, which include mission, functional, operational,

interface, performance, design, environment, product assurance and verification. Note that the types listed in the tables are represented by abbreviations. Each requirement is enriched with the designation of a key person, who is responsible for ensuring that the requirement is fulfilled by the end of the mission. Moreover, the chosen verification method is also indicated for each requirement, selected among the following: R = Review, A = Analysis, I = Inspection, T = Test.

10.13.1 Mission requirements

AMPERE's mission requirements are presented in Table 10.67. They have been directly derived from AMPERE's mission objectives and mission constraints, as by definition mission requirements are related to a task, a function, a constraint, or an action induced by the mission scenario.

REQ. ID	Short Name	Requirement	Type	Ver. Meth.	Key Person
AMP-MIS-0010	System feasibility	The mission shall be able to demonstrate the feasibility of a lunar power generation and distribution system.	Miss.	R, A, T	Team leader
AMP-MIS-0020	Critical sub-system power	AMPERE shall provide the power levels to support all planned mission operations.	Fun.	R, A, T	Design chief
AMP-MIS-0030	User power demand	AMPERE shall be capable of generating power to support the activities of users included in the following categories: rovers, scientific instruments, and astronauts, during surface operations.	Func.	R, T	Design chief
AMP-MIS-0040	Long term operations	AMPERE shall be capable of generating and providing sustained power to external users over long duration (from months to years), supporting continuous robotic and human operations.	Oper.	R, A	Design chief
AMP-MIS-0050	Standards establishment	The mission shall foster the definition of standard specifications for the generation and distribution of power for lunar users.	Miss.	R	System engineer
AMP-MIS-0060	Models validation	The mission shall acquire lunar environmental data to validate and refine existing lunar environmental models.	Miss.	R, A	System engineer
AMP-MIS-0070	Environmental sensors	AMPERE shall guarantee the correct functioning of the environmental sensors.	Fun.	R, A, T	System engineer
AMP-MIS-0080	Scalability	AMPERE shall be designed for scalability to meet future power needs.	Oper.	R, A	Design chief
AMP-MIS-0090	Evolvability	AMPERE shall be designed for evolvability to meet future technological integrations.	Oper.	R, A	System engineer
AMP-MIS-0100	Launch	The mission shall be implemented using a dedicated Ariane 6 launch.	Miss.	R	Team leader
AMP-MIS-0110	Land	AMPERE shall utilize ESA's Argonaut LDE to transport its payloads to the lunar surface.	Miss.	R	Team leader
AMP-MIS-0120	Lander interface	AMPERE shall be compatible with the Argonaut LDE, adhering to the applicable interface standard, physical connection and data exchange format.	Miss.	R, A	System engineer

AMP-MIS-0130	Lunar Payload System	AMPERE shall be housed as the LPS within ESA's Argonaut LDE.	Miss.	R	Team leader
AMP-MIS-0140	Deployment	AMPERE shall be equipped with a deployment mechanism to enable its release from the LDE after lunar landing.	Oper.	R, A	Design Chief
AMP-MIS-0150	Start date	The mission start date shall be scheduled post-2035.	Miss.	R	System engineer
AMP-MIS-0160	Start illumination	The mission shall start within a time window where solar illumination is at a level capable of initiating power generation.	Miss.	R	Design chief
AMP-MIS-0170	Planetary protection	AMPERE shall be compliant with the COSPAR Planetary Protection Guidelines applicable to Category IIb Missions [A.D. 2].	Miss.	R	System engineer
AMP-MIS-0180	LPS maximum allowed volume	AMPERE shall have a maximum height of 1.8 meters, a base area of 4.0 m^2.	Fun.	R, A	Design chief
AMP-MIS-0190	LPS maximum allowed mass	AMPERE shall have a total mass not exceeding 800 kg.	Fun.	R, A	Design chief
AMP-MIS-0200	Temperature endurance	AMPERE shall be capable of operating at extreme temperature fluctuations up to a minimum of –150 °C.	Fun.	R, A, T	Design chief
AMP-MIS-0210	Post-landing autonomy	AMPERE shall operate fully autonomously from LDE in terms of energy production and storage, communications and surface operations after landing.	Oper.	R, A, T	Design chief
AMP-MIS-0220	Communications services	AMPERE shall, as a first choice, utilize existing resources and European services to perform communications and navigation.	Miss.	R, A	Team leader
AMP-MIS-0230	Landing site	AMPERE's landing site shall be selected to operate safely and effectively at the lunar south pole, within the landing site criteria defined in [A.D. 9]	Miss.	R, A	System engineer

Table 10.67: AMPERE mission requirements

10.13.2 System requirements

The system requirements of AMPERE mission are shown in Table 10.68.

Req. ID	Short name	Requirement	Type	Parent requirement	Ver. meth.	Key person
AMP-SYS-0010	LPS composition	The LPS, accommodated on Argonaut's LDE, shall be composed of three different elements: Eagle, Scott and PDS.	Miss.	AMP-MIS-0130	A, R	Team leader
AMP-SYS-0020	Eagle composition	The Eagle module shall include a wheeled cart acting as the structural platform, housing the LPM, the LSM-S, the RDS and initially accommodating Scott.	Miss.	AMP-MIS-0130, AMP-MIS-0140	A, R	System engineer
AMP-SYS-0030	Lunar Power Module	The LPM shall demonstrate the generation and provision of	Fun.	AMP-MIS-0010, AMP-MIS-0120	A, R	Team leader

		electrical power to support surface operations at the lunar South Pole.				
AMP-SYS-0040	Lunar Sensor Module	The LSM shall perform environmental monitoring by acquiring local surface and atmospheric data at the lunar South Pole.	Fun.	AMP-MIS-0060, AMP-MIS-0120	A, R	System engineer
AMP-SYS-0050	LSM division	LSM shall be divided in two elements: LSM-S and LSM-M.	Miss.	AMP-MIS-0060, AMP-MIS-0120	A, R	System engineer
AMP-SYS-0060	Scott description	Scott shall be a mobile rover designed to host and transport the LSM-M to perform environmental measurements.	Fun.	AMP-MIS-0120, AMP-MIS-0190	A, R	System engineer
AMP-SYS-0070	Payload Delivery System	The Eagle module, while housing Scott, shall be deployed via a PDS that includes a ramp.	Oper.	AMP-MIS-0120, AMP-MIS-0190	A, R	Design chief
AMP-SYS-0080	Safe ramp descent	The PDS shall be able to support all the loads during the descent of Eagle, while housing Scott, to ensure a safe deployment.	Fun.	AMP-MIS-0120, AMP-MIS-0190	A, R	Str. & Mech. responsible
AMP-SYS-0090	Safe separation	The PDS shall ensure the safe positioning of Eagle, while housing Scott, at a safe distance from Argonaut to prevent any interference or damage during subsequent operations.	Fun.	AMP-MIS-0120, AMP-MIS-0190	A, R	Str. & Mech. responsible
AMP-SYS-0100	Rover Delivery System	RDS shall enable the safe deployment of Scott and charging interface platform from the Eagle module to the lunar surface.	Miss.	AMP-MIS-0140	A, R	Design chief
AMP-SYS-0110	Scott charging	Scott shall be deployed on the lunar surface fully charged and capable of supporting initial operations.	Oper.	AMP-MIS-0020, AMP-MIS-0210	T	Design chief
AMP-SYS-0120	Daytime convention	Daytime shall be defined as any period during which the local solar elevation angle remains positive for a duration exceeding 1 hour (Earth time).	Oper.	AMP-MIS-0160	R	Design chief
AMP-SYS-0130	Nighttime convention	Nighttime shall be defined as any period during which the local solar elevation angle remains negative for a duration exceeding 1 hour (Earth time).	Oper.	AMP-MIS-0160	R	Design chief
AMP-SYS-0140	Power output threshold	The LPM shall be equipped with solar panels capable of generating 1630 W of continuous power during daytime to ensure the operation of all onboard subsystems.	Perf.	AMP-MIS-0010, AMP-MIS-0030	A, R, T	Design chief
AMP-SYS-0150	Scott survival power	Scott shall provide a power budget of 40 W to support the operation of all onboard subsystems.	Perf.	AMP-MIS-0020, AMP-MIS-0210	A, R, T	Design chief

AMP-SYS-0160	Battery capacity threshold	The LPM shall include an energy storage system with a capacity of 4884 Wh to perform Scott's recharge and support all its operations.	Fun.	AMP-MIS-0020, AMP-MIS-0040	A, R, T	Design chief
AMP-SYS-0170	Long term operations	The LPM shall provide continuous electrical power to the LSM, subsystems and potential users for 1 Earth year.	Fun.	AMP-MIS-0040	A, R, T	Design chief
AMP-SYS-0180	Interface standards	AMPERE shall foster the definition of standard specifications for the recharging interface.	Miss.	AMP-MIS-0050	A, R	System engineer
AMP-SYS-0190	Reference standards	AMPERE shall use Scott as a demonstrative user to validate and support the definition of a dedicated interface specification.	Fun.	AMP-MIS-0050	A, R, T	System engineer
AMP-SYS-0200	Interface accessibility	AMPERE's charging interface shall be positioned to ensure suitable access for Scott.	Inter.	AMP-MIS-0050	A, R	Design chief
AMP-SYS-0210	Power supply demonstration	AMPERE shall demonstrate to be able to provide power energy to Scott.	Fun.	AMP-MIS-0030, AMP-MIS-0050	T	System engineer
AMP-SYS-0220	LDE interfaces	The interface between AMPERE and Argonaut LDE shall be implemented in accordance with [A.D. 9]	Miss.	AMP-MIS-0120	A, R	System engineer
AMP-SYS-0230	Launcher compliance	Space and ground segments shall be compliant with mission deployment by Ariane 6.	Miss.	AMP-MIS-0100	R	Team leader
AMP-SYS-0240	Solar irradiance measurement	The LSM shall perform in-situ solar irradiance measurements.	Fun.	AMP-MIS-0060, AMP-MIS-0070	A, R	System engineer
AMP-SYS-0250	Temperature measurement	The LSM shall perform in-situ measurements of the thermal properties of the lunar surface.	Fun.	AMP-MIS-0060, AMP-MIS-0070	A, R	System engineer
AMP-SYS-0260	Plasma measurement	The LSM shall perform in-situ plasma density measurements.	Fun.	AMP-MIS-0060, AMP-MIS-0070	A, R	System engineer
AMP-SYS-0270	Cumulative radiation dose measurement	The LSM shall perform in-situ cumulative radiation dose measurements of the environment throughout the mission.	Fun.	AMP-MIS-0060, AMP-MIS-0070	A, R	System engineer
AMP-SYS-0280	Lunar dust measurement	The LSM shall perform in-situ lunar dust measurements.	Fun.	AMP-MIS-0060, AMP-MIS-0070	A, R	System engineer
AMP-SYS-0290	Exospheric composition measurement	The LSM shall perform in-situ exospheric composition of neutral species measurements.	Fun.	AMP-MIS-0060, AMP-MIS-0070	A, R	System engineer
AMP-SYS-0300	Magnetic field measurement	The LSM shall perform in-situ magnetic field measurements.	Fun.	AMP-MIS-0060, AMP-MIS-0070	A, R	System engineer
AMP-SYS-0310	Ionizing radiation measurement	The LSM shall perform in-situ ionizing radiation measurement.	Fun.	AMP-MIS-0060, AMP-MIS-0070	A, R	System engineer
AMP-SYS-0320	Local plasma composition	The LSM shall perform in-situ plasma composition measurements.	Fun.	AMP-MIS-0060, AMP-MIS-0070	A, R	System engineer

AMP-SYS-0330	Survivability	AMPERE shall be designed to survive in different severe environmental conditions throughout the entire mission duration.	Env.	AMP-MIS-0010, AMP-MIS-0020, AMP-MIS-0030	A, R	Design chief
AMP-SYS-0340	Landing date	The nominal start date of the AMPERE mission shall be April 1st, 2037, at 16:00 UTC, with a flexibility of 30 days.	Miss.	AMP-MIS-0140	R	Design chief
AMP-SYS-0350	Landing site	The landing site shall have the following coordinates: - 89.40 S - 137 W	Env.	AMP-MIS-0230	A, R	Env. An. responsible
AMP-SYS-0360	Expected returns	AMPERE expected returns shall be higher than 95%.	Prod. Assur.	AMP-MIS-0010, AMP-MIS-0020, AMP-MIS-0030	A, R	Project manager
AMP-SYS-0370	Reliability	AMPERE reliability shall be higher than 85%.	Prod. Assur.	AMP-MIS-0010, AMP-MIS-0020, AMP-MIS-0030	A, R	Project manager
AMP-SYS-0380	Costs	AMPERE cost budget shall be lower than EUR 630 mln.	Prod. Assur.	AMP-MIS-0010, AMP-MIS-0020, AMP-MIS-0030	A, R	Project manager
AMP-SYS-0390	TRL	The TRL for all AMPERE's equipment shall be higher than 6 by the start of Phase C.	Fun.	AMP-MIS-0040	A, R	System engineer
AMP-SYS-0400	Communication	AMPERE shall use Moonlight as a communication relay between the Moon and the Earth.	Miss.	AMP-MIS-0220	R	Design chief
AMP-SYS-0410	Mission phases	AMPERE shall comply with the operational mission phases which shall follow in chronological order as defined below: 1. LOI - Lunar Orbit Insertion 2. D&L - Descent and Landing 3. PLI - Post - Landing Initialization 4. PD - Primary Deployment 5. COM - Commissioning 6. SD - Secondary Deployment 7. NOMDOP - Nominal Day Operations 8. NOMNOP-Nominal Night Operations 9. EOL&D - End-of-Life and Disposal	Miss.	AMP-MIS-0210	R	System engineer
AMP-SYS-0420	Verification plan	AMPERE verification plan shall adopt a hybrid model philosophy, in accordance with [A.D. 7][R.D. 90].	Ver.	AMP-MIS-0010	R	System engineer

Table 10.68: AMPERE system requirements

10.13.3 Ground segment requirements

The ground segment requirements of the AMPERE mission are shown in Table 10.69.

Req. ID	Short name	Requirement	Type	Parent requirement	Ver. meth.	Key person
AMP-GSE-0010	Eagle scientific data	Eagle shall transmit scientific data to Moonlight using the Ka-band.	Des.	AMP-SYS-0400	A, R	TT&C responsible
AMP-GSE-0020	Eagle telemetry data	Eagle shall transmit telemetry and telecommand data to Moonlight using the S-band.	Des.	AMP-SYS-0400	A, R	TT&C responsible
AMP-GSE-0030	Eagle telemetry data rate	The telemetry data rate from Eagle to Moonlight shall be in the range [10 Kbps - 300 Kbps].	Perf.	AMP-SYS-0400	A, R	TT&C responsible
AMP-GSE-0040	Eagle scientific data rate	The scientific data rate from Eagle to Moonlight shall be in the range [5 Mbps - 100 Mbps].	Perf.	AMP-SYS-0400	A, R	TT&C responsible
AMP-GSE-0050	Scott scientific data	Scott shall transmit scientific data to Moonlight using the S band.	Des.	AMP-SYS-0400	A, R	TT&C responsible
AMP-GSE-0060	Scott telemetry data rate	The scientific data rate from Scott to Moonlight shall be 125 kbps.	Des.	AMP-SYS-0400	A, R	TT&C responsible
AMP-GSE-0070	Scott LCNS data	Scott shall transmit LCNS data to Moonlight using the S band.	Des.	AMP-SYS-0400	A, R	TT&C responsible
AMP-GSE-0080	Threshold link budget	The communication link between AMPERE and Moonlight shall ensure a link budget of 3 dB.	Perf.	AMP-SYS-0400	A, R	TT&C responsible
AMP-GSE-0090	Eagle communication window	AMPERE shall guarantee a communication window between Eagle and Moonlight of 18 hours per day.	Fun.	AMP-SYS-0400	A, R	TT&C responsible
AMP-GSE-0100	Threshold D&L data rate	The LDE's ground communication system shall support a data rate of 2 Mbps during the D&L phase.	Perf.	AMP-SYS-0400, AMP-SYS-0410	A, R	TT&C responsible

Table 10.69: AMPERE ground segment requirements

10.13.4 Space segment requirements

In the following Table 10.70, Table 10.71 and Table 10.72, are shown respectively the space segment requirements for AMPERE, regarding requirements in common within all the modules, Eagle and Scott.

Req. ID	Short name	Requirement	Type	Parent requirement	Ver. meth.	Key person
AMP-SSE-0010	Shielding	AMPERE shall be equipped with a shield, during the entire mission lifetime, to reduce radiations incidence and to prevent meteorites impact.	Env.	AMP-SYS-0330	A, R	Env. An. responsible
AMP-SSE-0020	Illumination after landing	The landing site shall experience a continuous daytime period ranging from 74 to 104 days, starting from the landing date.	Env.	AMP-SYS-0350	A, R	Env. An. responsible
AMP-SSE-0030	Illumination conditions	The worst-case illumination conditions shall include 5 consecutive days of nighttime followed by 7 consecutive days of daytime.	Env.	AMP-SYS-0350	A, R	Env. An. responsible
AMP-SSE-0040	Landing site slope	The landing site slope shall not exceed 8°.	Env.	AMP-SYS-0350	A, R	Env. An. responsible
AMP-SSE-0050	Temperature range	LPS shall be capable of operating and surviving within a temperature range of 273 K to 313 K during LOI and D&L phases.	Env.	AMP-SYS-0330	A, R	TCS responsible
AMP-SSE-0060	LLO duration	AMPERE shall remain in LLO for a duration between 4 and 14 days.	Oper.	AMP-SYS-0410	A, R	Miss. An. responsible
AMP-SSE-0070	Landing site	The LLO shall include the Landing Site (LS) within the orbital plane.	Oper.	AMP-SYS-0410	A, R	Miss. An. responsible
AMP-SSE-0080	LLO parameters	The LLO shall have the following orbital parameters: - Altitude: 100 km - Eccentricity: 0 - Inclination: 90° - Right ascension of the ascending node: 302.69° - Argument Of Periapsis (AOP): 0°	Oper.	AMP-SYS-0410	A, R	Miss. An. responsible
AMP-SSE-0090	True anomaly	The initial and final true anomaly of the LLO, from which the Hohmann transfer is initiated, shall be 73.68°.	Oper.	AMP-SYS-0410	A, R	Miss. An. responsible
AMP-SSE-0100	AOP perilune	The AOP of the perilune shall be 254.28°.	Oper.	AMP-SYS-0410	A, R	Miss. An. responsible
AMP-SSE-0110	Hommann transfer perilune	The perilune of the Hohmann transfer orbit shall be located 30 km above the lunar surface.	Oper.	AMP-SYS-0410	A, R	Miss. An. responsible
AMP-SSE-0120	Descent phase begin	The descent phase shall begin at the periapsis of the Hohmann transfer orbit.	Oper.	AMP-SYS-0410	A, R	Miss. An. responsible
AMP-SSE-0130	Descent phase	The descent phase shall be divided into the following four sub-phases: - Braking Burn (BB) - Pitch-Up (PU)	Oper.	AMP-SYS-0410	A, R	Miss. An. responsible

		- Powered Descent and Diverts (PDD) - Vertical Descent and Landing (VDL)				
AMP-SSE-0140	BB thrust	During the BB phase, the thrust shall be 18000 N.	Oper.	AMP-SYS-0410	A, R	Miss. An. responsible
AMP-SSE-0150	BB descent angle	During the BB phase, the descent pith angle shall remain constant at 27.72°.	Oper.	AMP-SYS-0410	A, R	Miss. An. responsible
AMP-SSE-0160	PU altitude	The PU phase shall begin at an altitude of 675.58 meters above the lunar surface.	Oper.	AMP-SYS-0410	A, R	Miss. An. responsible
AMP-SSE-0170	PU pitch angle	During the PU phase, the pitch angle shall transition from 27.72° to 90°.	Oper.	AMP-SYS-0410	A, R	Miss. An. responsible
AMP-SSE-0180	PU angular velocity	During the PU phase, the pitch angular velocity shall be 5 degrees per second.	Oper.	AMP-SYS-0410	A, R	Miss. An. responsible
AMP-SSE-0190	PDD altitude	The PDD phase shall reduce altitude from 500 meters to 30 meters above the lunar surface.	Oper.	AMP-SYS-0410	A, R	Miss. An. responsible
AMP-SSE-0200	VDL altitude	The VDL phase shall start at an altitude of 30 meters and continue down to the lunar surface at a constant velocity.	Oper.	AMP-SYS-0410	A, R	Miss. An. responsible
AMP-SSE-0210	LLO to HTO delta-V	The total delta-V for the transfer from LLO to Hohmann Transfer Orbit (HTO) shall be 0.016 km/s.	Miss.	AMP-SYS-0410	A, R	Miss. An. responsible
AMP-SSE-0220	Descent phase delta-V	The total delta-V for the descent phase shall be 2.20 km/s.	Miss.	AMP-SYS-0410	A, R	Miss. An. responsible
AMP-SSE-0230	Descent phase duration	The descent phase shall not exceed a duration of 15 minutes.	Oper.	AMP-SYS-0410	A, R	Miss. An. responsible
AMP-SSE-0240	Hohmann transfer and descend duration	The duration from the start of the Hohmann transfer manoeuvre to the end of the descent phase shall not exceed 1 hour and 10 minutes.	Oper.	AMP-SYS-0410	A, R	Miss. An. responsible
AMP-SSE-0250	PDS description	The PDS shall consist of: - 5 foldable, hinged panels - 5 couples of motorized hinges - 8 thermal knives - 4 Kevlar cables - A Lithiated Nickel Cobalt Aluminum (LNCA) battery	Fun.	AMP-SYS-0070, AMP-SYS-0080, AMP-SYS-0090	A, R	Str. & Mech. responsible
AMP-SSE-0260	LDE power	The LDE shall guarantee a 47.90 W of power energy to sustain LPS orbit operations.	Perf.	AMP-SYS-0210	A, R	Payload Acc. & Int. responsible
AMP-SSE-0270	LDE data rate	The LDE shall guarantee a dedicated data rate of 2.63 Mbps to the LPS for the uninterrupted communication of telemetry data.	Perf.	AMP-SYS-0210	A, R	Payload Acc. & Int. responsible
AMP-SSE-0280	LDE telemetry interface	Data transfer shall be ensured by the SpaceWire communication protocol.	Des.	AMP-SYS-0210	A, R	Payload Acc. & Int. responsible

AMP-SSE-0290	System level verification	At system level, qualification and acceptance shall be performed using the PFM, representative of the final flight configuration.	Verif.	AMP-SYS-0400	R, T	Payload Acc. & Int. responsible
AMP-SSE-0300	Subsystem level verification	At subsystem level, qualification shall be performed using the EQM.	Verif.	AMP-SYS-0420	R, T	Payload Acc. & Int. responsible
AMP-SSE-0310	Payload level verification	At payload level, functional verification shall be conducted using EMs or PFMs, with acceptance testing executed on the flight-configured PFMs.	Verif.	AMP-SYS-0420	R, T	Payload Acc. & Int. responsible
AMP-SSE-0320	Equipment level verification	At equipment level, verification shall be performed using DMs for early functional validation and STM for mechanical and thermal compliance.	Verif.	AMP-SYS-0420	R, T	Payload Acc. & Int. responsible
AMP-SSE-0330	LPS accommodation	The LPS shall occupy a volume of 1683 mm × 1800 mm × 2376 mm on the LDE's mounting plate.	Inter.	AMP-SYS-0220	R, A	Payload Acc. & Int. responsible
AMP-SSE-0340	PDS accommodation	The PDS shall be installed on one of the eight sides of the octagonal mounting plate, occupying the full 1683 mm edge length of that side.	Inter.	AMP-SYS-0220	R, A	Payload Acc. & Int. responsible
AMP-SSE-0350	Eagle accommodation	Eagle, while housing Scott, shall be accommodated on the PDS until landing, secured in place by the Kevlar cables.	Inter.	AMP-SYS-0220	R, A	Payload Acc. & Int. responsible

Table 10.70: AMPERE space segment requirements

Req. ID	Short name	Requirement	Type	Parent requirement	Ver. meth.	Key person
EGL-SSE-0010	ADCS	Eagle shall be equipped with ADCS capable of providing the navigation data to guarantee a correct ramp descent and safe lunar surface positioning.	Fun.	AMP-SYS-0021, AMP-SYS-0330	A, R	ADCS responsible
EGL-SSE-0020	ADCS components	ADCS shall be made up by: - IMU - Inclinometer - 10 CSSs - 2 FSSs	Fun.	AMP-SYS-0021, AMP-SYS-0330	A, R	ADCS responsible
EGL-SSE-0030	TCS	Eagle shall be equipped with a TCS capable of withstanding the lunar environment and ensuring nominal operation of all subsystems.	Fun.	AMP-SYS-0021, AMP-SYS-0330	A, R	TCS responsible
EGL-SSE-0040	Internal temperature	The TCS shall maintain the internal temperature in the range of [273 K – 320 K].	Env.	AMP-SYS-0021, AMP-SYS-0330	A, R	TCS responsible
EGL-SSE-0050	TCS components	The TCS shall be made up by: - MLI - Smart Multilayer Insulation (SMLI) - Radiator - 2 heaters	Fun.	AMP-SYS-0021, AMP-SYS-0330	A, R	TCS responsible

		- 6 loop heat pipes - 5 temperature sensors				
EGL-SSE-0060	EDS	Eagle shall be equipped with an EDS to protect the MLI and radiator from thermo-optic degradation caused by dust accumulation.	Fun.	AMP-SYS-0021, AMP-SYS-0330	A, R	TCS responsible
EGL-SSE-0070	TT&C	Eagle shall be equipped with a TT&C subsystem capable of ensuring continuous and accurate data exchange with Scott to ensure continuous and accurate data exchange.	Fun.	AMP-SYS-0400	A, R	TT&C responsible
EGL-SSE-0080	TT&C components	The TT&C subsystem shall be made up by: - Ka antenna - 2 Ka transceivers - 2 Ka amplifiers - 2 Ka diplexers - 2 S-band antennas - 2 S- band transponders - 2 UHF antennas - 2 UHF transceivers	Fun.	AMP-SYS-0400	A, R	TT&C responsible
EGL-SSE-0090	LPM components	LPM shall be made up by: - 2 rollable solar panels - RFCS - 3 Li-ion batteries - PCDU - Wireless interface - Dedicated charging system for future potential users, called the Lunar Experiment Support System and Handling (LESSH) - Battery Charging Module (BCM)	Fun.	AMP-SYS-0140, AMP-SYS-0160	A, R	EGSD responsible
EGL-SSE-0100	RDS elements	The RDS shall be composed of two elements: - a winch for wireless interface deployment; - a release mechanism for Scott deployment.	Fun.	AMP-SYS-0100	A, R	Str. & Mech. responsable
EGL-SSE-0110	Wireless interface accommodation	The wireless interface shall be positioned on the bottom side of Eagle.	Inter.	AMP-SYS-0200		Payload Acc. & Int. responsible
EGL-SSE-0120	Wireless interface position	The wireless interface, through the winch, shall be lowered until it reaches a vertical distance of 35 cm from lunar surface to enable charging.	Inter.	AMP-SYS-0200		Payload Acc. & Int. responsible
EGL-SSE-0130	LESSH BCM accommodation	The LESSH BCM shall be mounted on the bottom-rear section of the Eagle module.	Inter.	AMP-SYS-0200		Payload Acc. & Int. responsible
EGL-SSE-0140	Structure	Eagle shall be equipped with a structural support and release system,	Fun.	AMP-SYS-0021, AMP-SYS-0330	A, R	Str.& Mech. responsible

		capable of withstanding the expected static and dynamic loads, including a wheeled cart and RDS.				
EGL-SSE-0150	Mechanisms	Eagle shall be equipped with the following mechanisms to support the subsystems operations: - Solar Array Drive Electronics (SADE) - Solar Array Drive Mechanism (SADM) - Antenna pointing mechanism - Any secondary mechanism.	Fun.	AMP-SYS-0021, AMP-SYS-0330	A, R	Str. & Mech. responsible
EGL-SSE-0160	LSM-S components	LSM-S shall be equipped with the following environmental sensors: - RADFET - 2 magnetometers - 4 resistance temperature detectors - NGRM.	Fun.	AMP-SYS-0250, AMP-SYS-0260, AMP-SYS-0270, AMP-SYS-0300	A, R	Payload Acc. & Int. responsible
EGL-SSE-0170	OBC	Eagle shall be equipped with an OBC to ensure reliable management and processing of mission data.	Fun.	AMP-SYS-0021	A, R	TT&C responsible

Table 10.71: Eagle space segment requirements

Req. ID	Short name	Requirement	Type	Parent requirement	Ver. meth.	Key person
SCT-SSE-0010	GNC	Scott shall be equipped with a GNC subsystem capable of performing mobility operations on lunar surface.	Fun.	AMP-SYS-0060	A, R	ADCS responsible
SCT-SSE-0020	GNC subsystem components	GNC subsystem shall be made up by: - 2 IMUs - 2 stereo cameras with 16 LEDs - 10 CSSs	Fun.	AMP-SYS-0060	A, R	ADCS responsible
SCT-SSE-0030	TCS	Scott shall be equipped with a TCS capable of withstanding the lunar environment and ensuring nominal operation of all subsystems.	Fun.	AMP-SYS-0330	A, R	TCS responsible
SCT-SSE-0040	Internal temperature	The TCS shall maintain the internal temperature in the range of [263 K – 313 K].	Env.	AMP-SYS-0330	A, R	TCS responsible
SCT-SSE-0050	TCS components	The TCS shall be made up by: - MLI - SMLI - Radiator - 2 heaters - 2 loop heat pipes - 2 temperature sensors	Fun.	AMP-SYS-0330	A, R	TCS responsible
SCT-SSE-0060	EDS	Scott shall be equipped with an EDS to protect the MLI and radiator from thermo-optic degradation caused by dust accumulation.	Fun.	AMP-SYS-0330	A, R	TCS responsible
SCT-SSE-0070	TT&C	Scott shall be equipped with a TT&C subsystem capable of establishing a reliable interlink with Eagle to enable	Fun.	AMP-SYS-0400	A, R	TT&C responsible

		continuous and accurate data exchange.				
SCT-SSE-0080	TT&C components	The TT&C subsystem shall be made up by: - UHF antenna - S-band transceiver - S-band antenna - Diplexer - Global Navigation Satellite System (GNSS) antenna - GNSS receiver	Fun.	AMP-SYS-0400	A, R	TT&C responsible
SCT-SSE-0090	EPS	Scott shall be equipped with an EPS capable of storing energy to operate all subsystems, perform surface operations and execute recharge cycles provided by Eagle.	Fun.	AMP-SYS-0150, AMP-SYS-0160	A, R	EGSD responsible
SCT-SSE-0100	EPS components	The EPS shall be made up by: - Li-ion battery - PCDU - Wireless interface	Fun.	AMP-SYS-0150	A, R	EGSD responsible
SCT-SSE-0110	Mobility	Scott shall be equipped with Astrobotic Cuberover's mobility system, capable of withstanding with navigation and data acquisition operations.	Fun.	AMP-SYS-0060	A, R	Str. & Mech. responsible
SCT-SSE-0120	LSM-M components	LSM-M shall be equipped with the following environmental sensors: - Ion electron mass spectrometer - Ion and neutral mass spectrometer - Solar radiation and dust sensor - Langmuir Probe	Fun.	AMP-SYS-0250, AMP-SYS-0260, AMP-SYS-0270, AMP-SYS-0290, AMP-SYS-0300, AMP-SYS-0310, AMP-SYS-0320	A, R	Payload Acc. & Int. responsible
SCT-SSE-0130	OBC	Scott shall be equipped with an OBC to ensure correct management and utilization of mission data.	Fun.	AMP-SYS-0060	A, R	TT&C responsible
SCT-SSE-0140	Scott payload	Scott shall reserve a 1U volume to host a potential future user payload.	Des.	AMP-SYS-0060	A, R	Payload Acc. & Int. responsible

Table 10.72: Scott space segment requirements

10.13.5 Subsystem requirements

In the following Table 10.73,Table 10.74 and Table 10.75 are shown respectively the subsystem requirements for AMPERE, regarding requirements in common within all the modules, Eagle and Scott.

Req. ID	Short name	Requirement	Type	Parent requirement	Ver. meth.	Key person
AMP-SUB-0010	Radiation level threshold	AMPERE shall withstand a total radiation level less than or equal to $5x10^3$ rad.	Env.	AMP-SSE-0010	A, R	Env. An. responsible
AMP-SUB-0020	Shielding thickness	AMPERE's shielding shall have a thickness of 1.5 mm.	Des.	AMP-SSE-0010	A, R	Env. An. responsible
AMP-SUB-0030	Shielding material	AMPERE's shielding shall be made of aluminium.	Des.	AMP-SSE-0010	A, R	Env. An. responsible
AMP-SUB-0040	PDS battery	PDS battery shall have a capacity of 345.5 Wh to support the unfolding and folding of the ramp.	Perf.	AMP-SSE-0250	A, R	Str. & Mech. responsible
AMP-SUB-0050	PDS battery mass	PDS battery shall have a mass of 3.72 kg.	Des.	AMP-SSE-0250	A, R	Str. & Mech. responsible
AMP-SUB-0060	PDS ramp material	The ramp shall be made by aluminium honeycomb beams, covered with Carbon Fiber Reinforced Polymer (CFRP) sandwich strips.	Des.	AMP-SSE-0250	A, R	Str. & Mech. responsible
AMP-SUB-0070	PDS load managing	The ramp shall be capable of managing a 725 kg structural load.	Perf.	AMP-SSE-0250	A, R	Str. & Mech. responsible
AMP-SUB-0080	PDS length	The ramp shall have a 6.84 meters length.	Des.	AMP-SSE-0250	A, R	Str. & Mech. responsible
AMP-SUB-0090	PDS weight	The PDS shall have a total mass not exceeding 69.71 kg.	Des.	AMP-SSE-0250	A, R	Str. & Mech. responsible
AMP-SUB-0100	PDS inclination	The ramp shall have an inclination of 26 degrees with respect to the local lunar surface.	Des.	AMP-SSE-0250	A, R	Str. & Mech. responsible

Table 10.73: AMPERE subsystem requirements

Req. ID	Short name	Requirement	Type	Parent requirement	Ver. meth.	Key person
EGL-SUB-0010	CoM	The centre of mass of Eagle shall be located x_{cm} behind the front wheel's contact point with the ground and h cm above the ground to prevent tipping and wheels slipping during ramp descent.	Des.	EGL-SSE-0010, EGL-SSE-0020	A, R	ADCS responsible
EGL-SUB-0020	CoM coordinates	The CoM coordinates x_{cm} and h_{cm} shall be defined to satisfy the following condition: $1.48\,x_{cm} - 0.55\,m < h_{cm} < 1.48\,x_{cm} - 0.02\,m$	Des.	EGL-SSE-0010, EGL-SSE-0020	A, R	ADCS responsible
EGL-SUB-0030	Friction coefficient first segment	The static friction coefficient between the ramp and the wheels shall be 1.1 in the first ramp segment to ensure that Eagle starts moving under maximum slope conditions.	Perf.	EGL-SSE-0010, EGL-SSE-0020	A, R	ADCS responsible

EGL-SUB-0040	Friction coefficient second segment	The static friction coefficient between the ramp and the wheels in the last three ramp segments shall be < 0.67 to ensure that Eagle starts moving under maximum slope conditions.	Perf.	EGL-SSE-0010, EGL-SSE-0020	A, R	ADCS responsible
EGL-SUB-0050	Final velocity	Eagle shall have zero velocity immediately upon reaching the end of the ramp.	Perf.	EGL-SSE-0010, EGL-SSE-0020	A, R	ADCS responsible
EGL-SUB-0070	IMU	The IMUs shall provide attitude and acceleration measurements.	Fun.	EGL-SSE-0010, EGL-SSE-0020	A, R	ADCS responsible
EGL-SUB-0080	CSS	The CSSs shall be positioned two on each side of the main body to provide estimation of the Sun direction in any orientation.	Fun.	EGL-SSE-0010, EGL-SSE-0020	A, R	ADCS responsible
EGL-SUB-0090	FSS	The FSSs shall be co-aligned with the solar panel pointing mechanism.	Fun.	EGL-SSE-0010, EGL-SSE-0020	A, R	ADCS responsible
EGL-SUB-0100	FSS accuracy	The FSSs shall provide an angular accuracy ≤ 0.10° in determining the Sun direction.	Perf.	EGL-SSE-0010, EGL-SSE-0020	A, R	ADCS responsible
EGL-SUB-0110	Inclinometer	The inclinometer shall measure the slope.	Fun.	EGL-SSE-0010, EGL-SSE-0020	A, R	ADCS responsible
EGL-SUB-0120	OBC data managing	The next generation OBC shall be capable of managing and storing at least 1 Gbit of data per Earth Day.	Perf.	EGL-SSE-0170	A, R	TT&C responsable
EGL-SUB-0130	Radiator mass	The radiator shall have a mass of 16.50 kg.	Des.	EGL-SSE-0030, EGL-SSE-0050	A, R	TCS responsible
EGL-SUB-0140	Radiator surface	The radiator shall have a surface area of 1.50 m^2.	Des.	EGL-SSE-0030, EGL-SSE-0050	A, R	TCS responsible
EGL-SUB-0150	Radiator starting temperature	The radiator shall begin deployment at 273 K.	Oper.	EGL-SSE-0030, EGL-SSE-0040, EGL-SSE-0050	A, R	TCS responsible
EGL-SUB-0160	Radiator hysteresis	The radiator shall exhibit a thermal hysteresis of 20 K for deployment, being fully open at 293 K.	Perf.	EGL-SSE-0030, EGL-SSE-0040, EGL-SSE-0050	A, R	TCS responsible
EGL-SUB-0170	Radiator closed emissivity	The radiator shall have an emissivity of 0.05 when in closed configuration.	Perf.	EGL-SSE-0030, EGL-SSE-0040, EGL-SSE-0050	A, R	TCS responsible
EGL-SUB-0180	Radiator open emissivity	The radiator shall have an emissivity of 0.64 when in open configuration.	Perf.	EGL-SSE-0030, EGL-SSE-0050	A, R	TCS responsible
EGL-SUB-0190	Radiator absorptivity	The radiator shall have an absorptivity of 0.14.	Perf.	EGL-SSE-0030, EGL-SSE-0050	A, R	TCS responsible
EGL-SUB-0200	MLI composition	The MLI shall be composed of: - Outer layer of Teflon - Kapton substrates - Inner layer of VDA	Des.	EGL-SSE-0030, EGL-SSE-0050	A, R	TCS responsible
EGL-SUB-0210	Heaters consume	The heaters shall consume a total constant power of 180 W during nighttime operations.	Perf.	EGL-SSE-0030, EGL-SSE-0040, EGL-SSE-0050	A, R	TCS responsible
EGL-SUB-0220	SMLI	The SMLI shall be a smart material, positioned upon the MLI, capable of changing its thermal properties between daytime and nighttime.	Des.	EGL-SSE-0030, EGL-SSE-0050	A, R	TCS responsible

EGL-SUB-0230	SMLI emissivity	The SMLI shall have an emissivity in a variable range from 0.64 to 0.065.	Perf.	EGL-SSE-0030, EGL-SSE-0050	A, R	TCS responsible
EGL-SUB-0240	SMLI absorptivity	The SMLI shall have an absorptivity of 0.10.	Perf.	EGL-SSE-0030, EGL-SSE-0050	A, R	TCS responsible
EGL-SUB-0250	EDS threshold	The activation of the EDS shall occur when the accumulated dust level is higher than 11%	Perf.	EGL-SSE-0060, EGL-SSE-0030, EGL-SSE-0050	A, R	TCS responsible
EGL-SUB-0260	Solar panels mass	The total mass of the solar panels shall be 50 kg.	Des.	EGL-SSE-0090, EGL-SSE-0150	A, R	EGSD responsible
EGL-SUB-0270	Solar panels dimensions	The dimensions of each solar panel shall be 5.42 m × 1.60 m × 0.0020 m.	Des.	EGL-SSE-0090, EGL-SSE-0150	A, R	EGSD responsible
EGL-SUB-0280	RFCS total mass	The RFC shall have a total mass of 139.38 kg.	Des.	EGL-SSE-0090	A, R	EGSD responsible
EGL-SUB-0290	RFCS tanks	The RFCS shall include 3 tanks: - One for oxygen (O_2) - One for hydrogen (H_2) - One for water (H_2O)	Des.	EGL-SSE-0090	A, R	EGSD responsible
EGL-SUB-0300	O_2 tank volume	The O_2 tank shall have a volume of 0.01 m^3.	Des.	EGL-SSE-0090	A, R	EGSD responsible
EGL-SUB-0310	O_2 stored mass	The stored O_2 shall have a mass of 9.74 kg.	Perf.	EGL-SSE-0090	A, R	EGSD responsible
EGL-SUB-0320	H_2 tank volume	The H_2 tank shall have a volume of 0.02 m^3.	Des.	EGL-SSE-0090	A, R	EGSD responsible
EGL-SUB-0330	H_2 stored mass	The stored H_2 shall have a mass of 1.22 kg.	Perf.	EGL-SSE-0090	A, R	EGSD responsible
EGL-SUB-0340	H_2O tank dimensions	The H_2O tank shall have a volume of 0.01 m^3.	Des.	EGL-SSE-0090	A, R	EGSD responsible
EGL-SUB-0350	Electrolysis	The RFCS shall complete the electrolysis process, achieving a full recharge, within 7 days.	Perf.	EGL-SSE-0090	A, R	EGSD responsible
EGL-SUB-0360	Li-ion battery mass	The Li-ion battery shall have a mass of 23.40 kg.	Des.	EGL-SSE-0090	A, R	EGSD responsible
EGL-SUB-0370	Li-ion battery dimensions	The Li-ion battery shall have dimensions of 364 mm × 203 mm × 98 mm.	Des.	EGL-SSE-0090	A, R	EGSD responsible
EGL-SUB-0380	PCDU mass	The PCDU shall have a mass of 16 kg.	Des.	EGL-SSE-0090	A, R	EGSD responsible
EGL-SUB-0390	PCDU dimensions	The PCDU shall have dimensions of 805 mm × 430 mm × 260 mm.	Des.	EGL-SSE-0090	A, R	EGSD responsible
EGL-SUB-0400	Sun incidence angle	The solar panels shall operate with a Sun incidence angle within the range of -1.50° to +1.50°.	Perf.	EGL-SSE-0090, EGL-SSE-0150	A, R	EGSD responsible
EGL-SUB-0410	Solar power density	The solar panels shall have a power density of 100 W/kg.	Perf.	EGL-SSE-0090, EGL-SSE-0150	A, R	EGSD responsible
EGL-SUB-0420	Solar panels efficiency	The efficiency of the solar panels shall be 30%.	Perf.	EGL-SSE-0090, EGL-SSE-0150	A, R	EGSD responsible
EGL-SUB-0430	Solar cells number	The number of solar cells per panel shall be 2528.	Des.	EGL-SSE-0090, EGL-SSE-0150	A, R	EGSD responsible
EGL-SUB-0440	Solar panel output voltage	Each solar panel shall generate a voltage output of 105 V.	Perf.	EGL-SSE-0090, EGL-SSE-0150	A, R	EGSD responsible

EGL-SUB-0450	RFCS output	The RFCS shall be able to generate 48 KWh of chemical energy to ensure system survival during 120 consecutive hours of nighttime.	Perf.	EGL-SSE-0090	A, R	EGSD responsible
EGL-SUB-0460	Wireless interface	The wireless charging interface shall consist of a power transmitter and a transmitter coil.	Inter.	EGL-SSE-0090, EGL-SSE-0110, EGL-SSE-0120	A, R	EGSD responsible
EGL-SUB-0470	Transmitter mass	The power transmitter shall have a mass of 3 kg.	Des.	EGL-SSE-0090, EGL-SSE-0110	A, R	EGSD responsible
EGL-SUB-0480	Transmitter dimensions	The power transmitter shall have dimensions of 200 mm × 200 mm × 40 mm.	Des.	EGL-SSE-0090, EGL-SSE-0110	A, R	EGSD responsible
EGL-SUB-0490	Transmitter coil diameter	The transmitter coil shall have a diameter of 210 mm.	Des.	EGL-SSE-0090, EGL-SSE-0110	A, R	EGSD responsible
EGL-SUB-0500	Transmitter coil mass	The transmitter coil shall have a mass of 210 g.	Des.	EGL-SSE-0090, EGL-SSE-0110	A, R	EGSD responsible
EGL-SUB-0510	Energy transfer rate	The wireless interface shall support an energy transfer rate of 125 W/h.	Perf.	EGL-SSE-0090, EGL-SSE-0110	A, R	EGSD responsible
EGL-SUB-0520	Charging duration	The charging process of Scott shall require 2 hours to complete from 20% to 100%.	Perf.	EGL-SSE-0090, EGL-SSE-0110	A, R	EGSD responsible
EGL-SUB-0530	LESSH BCM dimensions	The LESSH BCM unit shall have dimensions of 500 mm × 250 mm × 100 mm.	Des.	EGL-SSE-0090, EGL-SSE-0110	A, R	EGSD responsible
EGL-SUB-0540	LESSH BCM weight	The LESSH BCM unit shall have a mass of 9.40 kg.	Des.	EGL-SSE-0090, EGL-SSE-0110	A, R	EGSD responsible
EGL-SUB-0550	LESSH BCM charge time	The LESSH BCM system shall charge a compatible user device from 20% to 100% in 4 hours.	Perf.	EGL-SSE-0090, EGL-SSE-0130	A, R	EGSD responsible
EGL-SUB-0560	LESSH BCM charging method	The charging method shall support: -A current range from 0 A to 9.40 A -A voltage range from 24 V to 33.60 V	Inter.	EGL-SSE-0090, EGL-SSE-0130	A, R	EGSD responsible
EGL-SUB-0570	Cart dimensions	The cart shall have dimensions of 1223 mm × 1780 mm × 20 mm.	Des.	EGL-SSE-0140	A, R	Str. & Mech responsable
EGL-SUB-0580	Cart materials	The cart shall be made by a sandwich structure with the following layers: - one honeycomb aluminium internal layer - two carbon fiber external layers	Des.	EGL-SSE-0140	A, R	Str. & Mech. responsable
EGL-SUB-0590	Wheels diameter	The wheels of the wheeled cart shall have a 818 mm diameter.	Des.	EGL-SSE-0140	A, R	Str. & Mech. responsable
EGL-SUB-0600	Wheels locking system	The wheels shall be secured to the ramp using four Kevlar cables, one at each corner.	Fun.	EGL-SSE-0140, EGL-SSE-0150	A, R	Str. & Mech. responsable
EGL-SUB-0610	RADFET	The cumulative radiation dose of the space environment shall be measured by the RADFET RM VT-01.	Perf.	EGL-SSE-0160	A, R	Payload Acc. & Int. responsible
EGL-SUB-0620	RADFET accuracy	The RADFET shall measure the cumulative radiation dose ranging from 1 cGy to 1 kGy.	Perf.	EGL-SSE-0160	A, R	Payload Acc. & Int. responsible

EGL-SUB-0630	RADFET mass	The RADFET shall have a mass of 0.06 kg.	Des.	EGL-SSE-0160	A, R	Payload Acc. & Int. responsible
EGL-SUB-0640	RADFET dimensions	The RADFET shall have maximum external dimensions not exceeding 2.9 mm × 2.8 mm × 1.1 mm.	Des.	EGL-SSE-0160	A, R	Payload Acc. & Int. responsible
EGL-SUB-0650	Magnetometers	The magnetic field shall be measured by two magnetometers MAG566.	Perf.	EGL-SSE-0160	A, R	Payload Acc. & Int. responsible
EGL-SUB-0660	Magnetometers accuracy	Each magnetometer shall have a measuring range of ± 100µT.	Perf.	EGL-SSE-0160	A, R	Payload Acc. & Int. responsible
EGL-SUB-0670	Magnetometers mass	The magnetometer shall have a mass of 0.054 kg.	Des.	EGL-SSE-0160	A, R	Payload Acc. & Int. responsible
EGL-SUB-0680	Magnetometers dimensions	The magnetometer shall have maximum external dimensions not exceeding 42 mm × 20 mm × 52 mm.	Des.	EGL-SSE-0160	A, R	Payload Acc. & Int. responsible
EGL-SUB-0690	Magnetometers accommodation	The two magnetometers shall be mounted on a boom with a length of 1 m to achieve the required magnetic cleanliness level.	Inter.	EGL-SSE-0160	A, R	Payload Acc. & Int. responsible
EGL-SUB-0700	Temperature sensors	Lunar surface thermal properties shall be measured using RTD sensors of the High-Resolution Temperature Sensor (HRTS) series.	Des.	EGL-SSE-0160	A, R	Payload Acc. & Int. responsible
EGL-SUB-0710	Temperature sensors accuracy	The RTD shall provide a measurement accuracy of ± 0.30 K.	Perf.	EGL-SSE-0160	A, R	Payload Acc. & Int. responsible
EGL-SUB-0720	Temperature sensors dimensions	The RTD shall have maximum external dimensions not exceeding 4.8 mm × 313 mm × 1.95 mm.	Des.	EGL-SSE-0160	A, R	Payload Acc. & Int. responsible
EGL-SUB-0730	Temperature sensors mass	The RTD shall have a mass not exceeding 0.12 kg.	Des.	EGL-SSE-0160	A, R	Payload Acc. & Int. responsible
EGL-SUB-0740	NGRM	The real-time ionizing radiation level shall be measured using the NRGM.	Des.	EGL-SSE-0160	A, R	Payload Acc . & Int. responsible
EGL-SUB-0750	NGRM accuracy	The NRGM shall provide energy measurements within the following ranges: - Electrons: 0.10-7 MeV - Protons: 2-200 MeV - Ions (LET): 0.10-10 MeV·cm²/mg	Perf.	EGL-SSE-0160	A, R	Payload Acc. & Int. responsible
EGL-SUB-0760	NGRM dimensions	The NGRM shall have maximum external dimensions not exceeding 132 mm × 67.9 mm × 150 mm.	Des.	EGL-SSE-0160	A, R	Payload Acc. & Int. responsible
EGL-SUB-0770	NGRM mass	The NGRM shall have a mass not exceeding 1.17 kg.	Des.	EGL-SSE-0160	A, R	Payload Acc. & Int. responsible

Table 10.74: Eagle subsystem requirements

Req. ID	Short name	Requirement	Type	Parent requirement	Verif. method	Key person
SCT-SUB-0010	Scott dimensions	Scott shall have dimensions equivalent to 24U.	Des.	SCT-SSE-0110	A, R	Str. & Mech. responsable
SCT-SUB-0020	Scott mass	Scott shall have a total mass of 41.30 kg.	Des.	SCT-SSE-0110	A, R	Str. & Mech. responsable
SCT-SUB-0030	Scott wheels	Scott shall be equipped with Astrobotic wheels having a maximum diameter of 350 mm.	Des.	SCT-SSE-0110	A, R	Str. & Mech. responsable
SCT-SUB-0040	OBC	The OBC shall be a GomSpace Nanomind A3200.	Des.	SCT-SSE-0130	A, R	TT&C responsable
SCT-SUB-0050	OBC data handling	The OBC shall be capable of managing and storing a minimum of 40 Mbit of data per day, including scientific measurements and telemetry.	Perf.	SCT-SSE-0130	A, R	TT&C responsable
SCT-SUB-0060	UHF band	Scott shall transmit scientific data to Eagle via UHF.	Inter.	SCT-SSE-0070, SCT-SSE-0080	A, R	TT&C responsable
SCT-SUB-0070	Scientific data rate	The scientific data rate from Scott to Eagle shall be 38.90 kbps.	Perf.	SCT-SSE-0070, SCT-SSE-0080	A, R	TT&C responsable
SCT-SUB-0080	Traverse path	The mobility system shall be designed to follow a straight path in both forward and return directions.	Fun.	SCT-SSE-0010, SCT-SSE-0020	A, R	ADCS responsible
SCT-SUB-0090	Hazards detection	Scott shall stop every 1 meter along the straight path to perform hazards detection.	Oper.	SCT-SSE-0010, SCT-SSE-0020	A, R	ADCS responsible
SCT-SUB-0100	GNC cameras	The cameras resolution shall be > 1 megapixel.	Perf.	SCT-SSE-0020	A, R	ADCS responsible
SCT-SUB-0110	EDS threshold	The activation of the EDS shall occur when the accumulated dust level is higher than 11%.	Oper.	SCT-SSE-0030, SCT-SSE-0050, SCT-SSE-0060	A, R	TCS responsible
SCT-SUB-0120	Radiator mass	The radiator shall have a mass of 1.10 kg.	Des.	SCT-SSE-0030, SCT-SSE-0050	A, R	TCS responsible
SCT-SUB-0130	Radiator surface	The radiator shall have a surface area of 0.10 m^2.	Des.	SCT-SSE-0030, SCT-SSE-0040, SCT-SSE-0050	A, R	TCS responsible
SCT-SUB-0140	Radiator starting temperatur e	The radiator shall begin deployment at 273 K.	Oper.	SCT-SSE-0030, SCT-SSE-0040, SCT-SSE-0050	A, R	TCS responsible
SCT-SUB-0150	Radiator hysteresis	The radiator shall exhibit a thermal hysteresis of 20 K for deployment, being fully open at 293 K.	Perf.	SCT-SSE-0030, SCT-SSE-0040, SCT-SSE-0050	A, R	TCS responsible
SCT-SUB-0160	Closed radiator emissivity	The radiator shall have an emissivity of 0.05 when in closed configuration.	Perf.	SCT-SSE-0030, SCT-SSE-0040, SCT-SSE-0050	A, R	TCS responsible
SCT-SUB-0170	Radiator open emissivity	The radiator shall have an emissivity of 0.64 when in open configuration.	Perf.	SCT-SSE-0030, SCT-SSE-0040, SCT-SSE-0050	A, R	TCS responsible
SCT-SUB-0180	Radiator absorptivity	The radiator shall have an absorptivity of 0.14.	Perf.	SCT-SSE-0030, SCT-SSE-0040, SCT-SSE-0050	A, R	TCS responsible

SCT-SUB-0190	MLI composition	The MLI shall be composed by: - Outer layer of Teflon - Kapton substrates - Inner layer of VDA	Des.	SCT-SSE-0030, SCT-SSE-0040, SCT-SSE-0050	A, R	TCS responsible
SCT-SUB-0200	Heaters consume	The heaters shall consume a constant power of 8 W during nighttime operations.	Perf.	SCT-SSE-0030, SCT-SSE-0040, SCT-SSE-0050	A, R	TCS responsible
SCT-SUB-0210	SMLI	The SMLI shall be a smart material, positioned upon the MLI, capable of changing its thermal properties between day and night phases.	Des.	SCT-SSE-0030, SCT-SSE-0040, SCT-SSE-0050	A, R	TCS responsible
SCT-SUB-0220	SMLI emissivity	The SMLI shall have an emissivity in a variable range from 0.64 to 0.24.	Perf.	SCT-SSE-0030, SCT-SSE-0040, SCT-SSE-0050	A, R	TCS responsible
SCT-SUB-0230	SMLI absorptivity	The SMLI shall have an absorptivity of 0.10.	Perf.	SCT-SSE-0030, SCT-SSE-0040, SCT-SSE-0050	A, R	TCS responsible
SCT-SUB-0240	Battery capacity	The Li-Ion battery shall have a 297 Wh capacity.	Perf.	SCT-SSE-0090, SCT-SSE-0100	A, R	EGSD responsible
SCT-SUB-0250	Wireless interface	The wireless charging interface shall consist of a onboard charger and a receiver coil.	Inter.	SCT-SSE-0090, SCT-SSE-0100	A, R	EGSD responsible
SCT-SUB-0260	Onboard charger mass	The power transmitter shall have a mass of 0.40 kg.	Des.	SCT-SSE-0120	A, R	TT&C responsible
SCT-SUB-0270	Onboard charger dimensions	The power transmitter shall have dimensions of 104 mm × 104 mm × 28 mm.	Des.	SCT-SSE-0120	A, R	TT&C responsible
SCT-SUB-0280	Receiver coil diameter	The transmitter coil shall have a diameter of 132 mm.	Des.	SCT-SSE-0090, SCT-SSE-0100	A, R	EGSD responsible
SCT-SUB-0290	Receiver coil mass	The power transmitter shall have a mass of 0.09 kg.	Des.	SCT-SSE-0090, SCT-SSE-0100	A, R	EGSD responsible
SCT-SUB-0300	IES	The plasma composition shall be measured using the IES.	Des.	SCT-SSE-0120	A, R	Payload Acc. & Int. responsible
SCT-SUB-0310	IES accuracy	The IES shall provide an angular resolution of 5°× 22.50° for electrons and 5° × 45° for ions.	Perf.	SCT-SSE-0120	A, R	Payload Acc. & Int. responsible
SCT-SUB-0320	IES energy range	The IES shall cover an energy range from 1 eV/e to 22 keV/e, with an energy resolution of 4%.	Perf.	SCT-SSE-0120	A, R	Payload Acc. & Int. responsible
SCT-SUB-0330	IES dimensions	The IES shall have maximum external dimensions not exceeding 139 mm × 121 mm × 64 mm.	Des.	SCT-SSE-0120	A, R	Payload Acc. & Int. responsible
SCT-SUB-0340	IES mass	The IES shall have a mass not exceeding 1.04 kg.	Des.	SCT-SSE-0120	A, R	Payload Acc. & Int. responsible
SCT-SUB-0350	INMS	The exospheric composition of neutral species shall be measured using the INMS for CubeSat applications.	Des.	SCT-SSE-0120	A, R	Payload Acc. & Int. responsible
SCT-SUB-0360	INMS density	The INMS shall support a density dynamic range of approximately 10^5.	Perf.	SCT-SSE-0120	A, R	Payload Acc. & Int. responsible

	dynamic range					
SCT-SUB-0370	INMS mass dynamic range	The INMS shall support a mass dynamic range from 1 to 40 atomic mass units (amu).	Perf.	SCT-SSE-0120	A, R	Payload Acc. & Int. responsible
SCT-SUB-0380	INMS dimensions	The INMS shall have maximum external dimensions not exceeding 130 mm x 100 mm x100 mm.	Des.	SCT-SSE-0120	A, R	Payload Acc. & Int. responsible
SCT-SUB-0390	INMS mass	The INMS shall have a mass not exceeding 0.57 kg.	Des.	SCT-SSE-0120	A, R	Payload Acc. & Int. responsible
SCT-SUB-0400	SRDS	The solar irradiance and dust level shall be measured using the SRDS.	Des.	SCT-SSE-0120	A, R	Payload Acc. & Int. responsible
SCT-SUB-0410	SRDS spectral range	The SRDS shall be capable of measuring radiative properties within the spectral range from 100 to 1400 nanometers, covering the UV to near-IR domains.	Perf.	SCT-SSE-0120	A, R	Payload Acc. & Int. responsible
SCT-SUB-0420	SRDS dimensions	The SRDS shall have maximum external dimensions not exceeding 120 mm × 120 mm × 120 mm.	Des.	SCT-SSE-0120	A, R	Payload Acc. & Int. responsible
SCT-SUB-0430	SRDS mass	The SRDS shall have a mass not exceeding 1.0 kg.	Des.	SCT-SSE-0120	A, R	Payload Acc. & Int. responsible
SCT-SUB-0440	Langmuir Probe	The plasma density shall be measured using a Langmuir probe.	Des.	SCT-SSE-0120	A, R	Payload Acc. & Int. responsible
SCT-SUB-0450	Langmuir Probe	The Langmuir Probe shall be capable of measuring plasma densities in the range of 10 to 10^4 particles per cubic centimetre.	Perf.	SCT-SSE-0120	A, R	Payload Acc. & Int. responsible
SCT-SUB-0460	Langmuir Probe dimensions	The Langumir Probe shall have maximum external dimensions not exceeding 50 mm × 50 mm × 70 mm.	Des.	SCT-SSE-0120	A, R	Payload Acc. & Int. responsible
SCT-SUB-0470	Langmuir Probe mass	The Langumir Probe shall have a mass not exceeding 1.10 kg.	Des.	SCT-SSE-0120	A, R	Payload Acc. & Int. responsible
SCT-SUB-0480	Langmuir Probe accommodation	The Langmuir Probe shall be mounted on a boom with a length of 0.50 meters to avoid plasma sheath effects in the lunar plasma environment and to reduce electromagnetic interference.	Inter.	SCT-SSE-0120	A, R	Payload Acc. & Int. responsible

Table 10.75: Scott subsystem requirements

11 Task 3 Space segment and lunar payload design

11.1 Energy Generation, Storage & Distribution

11.1.1 State-of-the-art analysis

An analysis of past and upcoming missions was conducted to evaluate different technologies and identify potential components of the EGSD system across the various AMPERE configurations.
Four technologies of solar panels have been considered for AMPERE's mission: rigid solar arrays, Roll-Out Solar Arrays (ROSAs), membrane solar arrays and deployable mast solar arrays.

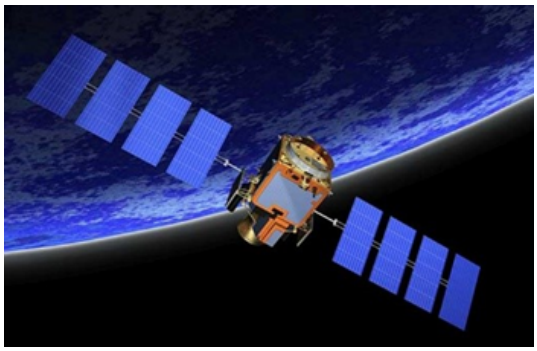

Figure 11.1: Rigid solar arrays [R.D. 115]

Rigid solar arrays, shown in Figure 11.1, represent the conventional choice for solar-powered missions. Numerous variants are available, developed by well-established manufacturers and exhibiting high TRLs. This kind of technology has been successfully employed in lunar missions, such as the Apollo program's Apollo Lunar Surface Experiments Package (ALSEP) and the Chang 'e landers [R.D. 116], [R.D. 117]. Their high reliability in energy production makes them a strong candidate for the AMPERE configurations. However, one challenge that may arise involves the stowed volume of the arrays during the transfer phase: most of the available panels can be stacked on top of each other and then deployed through hinges, but this could prove insufficient to comply with the requirements of volume presented in the SoW [A.D. 1].
Recent advancements in solar cells technology have led to the development of multi-junction solar cells, which should guarantee an efficiency of 22-25% depending on the combined materials (e.g., InGaAs, GaInP), higher than the earlier silicon cells, which typically reached around 15% [R.D. 118].

Figure 11.2: Deployed ROSA [R.D. 119]

NASA's ROSA, shown in Figure 11.2, is a type of deployable flexible solar panel designed for space applications. Unlike traditional rigid panels, ROSAs can be rolled up for launch and unrolled once in space, using composite structures that provide lightweight construction, compact stowage, and ease of deployment. This type of panel has demonstrated excellent performance and has already been used on the International Space Station (ISS), where it is called ISS Roll Out Solar Array (iROSA). Scalability and versatility are among its key advantages [R.D. 119].

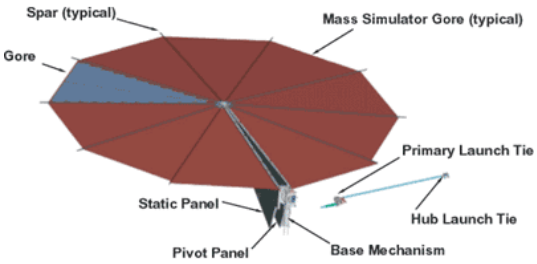

Figure 11.3: Membrane solar array [R.D. 120]

The Membrane Solar Array (MSA), shown Figure 11.3, is a type of deployable solar panel, characterized by its flexible, membrane-like structure. Unlike traditional rigid panels, MSAs can be folded for compact storage and later deployed in situ, which makes them suitable for missions requiring lightweight and space-saving solutions [R.D. 3].

Figure 11.4: Deployable mast solar array [R.D. 3]

The deployable mast solar array, shown in Figure 11.4, is a system composed of hinged blanket segments, deployed and kept in tension by an extendable central mast. This technology remains under development and much of its detailed information is under Non-Disclosure Agreement (NDA). The deployable mast, coupled with next-generation flexible solar cells, ensures the scalability of the design [R.D. 3].

As an alternative to solar energy, Radio-Isotope Thermoelectric Generators (RTGs) have also been considered. Although previous lunar missions, such as Apollo and Chang'e, successfully employed RTGs, this solution has been deemed unsuitable for AMPERE for both safety and technical reasons. Despite their long operational lifetime (exceeding 10 years), RTGs have much lower power density (~15 W/kg) compared to modern solar arrays (~70 W/kg), which would result in a prohibitively high system mass to meet AMPERE's power requirements. Additionally, the overall cost of RTGs is generally higher [R.D. 118], [R.D. 121], [R.D. 122], [R.D. 123].

In the context of energy storage, lithium-ion (Li-ion) batteries have been analysed during the trade-off study. These batteries are widely used in space systems due to their high energy density, flight heritage, and relatively mature TRL. Typically, they serve as buffer systems or operate during eclipse phases [R.D. 3], [R.D. 118]. However, in the context of AMPERE, where energy must be stored for multiple Earth days of nighttime, Li-ion batteries become less suitable. The total mass required to store the necessary energy over such extended periods would be prohibitive, significantly exceeding the mass budget allocated for the energy system. Additionally, the degradation associated with long-term cycling and temperature fluctuations on the lunar surface further limits their applicability. As a result, despite their maturity and simplicity, lithium-ion batteries were not selected as the sole energy storage solution.

RFCSs have also been assessed as a complementary energy system to solar panels. RFCSs operate by coupling a conventional fuel cell with an electrolyser in a closed-loop system. During the daytime phase, power produced by the solar panels is used to run the electrolyser, which splits water (H_2O) into hydrogen (H_2) and oxygen (O_2). These gases are stored in separate tanks. During the nighttime, the stored gases are fed into the fuel cell, which recombines them to produce electricity and water. The process is reversible, and the water produced is recirculated into the system. This technology has been previously studied for lunar applications and is currently under development by multiple space agencies. Due to their ability to store energy and to operate during the lunar night, RFCs are considered well suited for missions with extended eclipse durations. Although RFCSs current TRL is lower compared to conventional battery storage, ongoing advancements suggest a promising trajectory for near-future deployment. Considering AMPERE's mass and energy requirements, RFCSs are likely to represent the baseline solution, in combination with high-efficiency solar panels for daytime generation and Li-ion batteries for nighttime operations. This configuration enables long-duration energy storage with higher specific energy than typical Li-ion batteries and reduces performance loss associated with repeated battery cycling [R.D. 3], [R.D. 124]. The PCDU and user power interfaces are designed to ensure efficient energy

transfer and system compatibility. Several interface options are being explored: laser power beaming, wireless charging, tethers, docks (male and female) [R.D. 3], [R.D. 125], [R.D. 126].
Laser power beaming is an optimal solution for long-distance charging: the station is placed on an elevated area, where it can receive radiation from the Sun, which is then used to form the laser beam, while the user is in a different region (e.g., a PSR). The beam is pointed towards the user, equipped with a photovoltaic receiver tuned to the laser wavelength, converting energy into electricity. In the reference paper, the distance considered between the source and the receiver was 50 m, but it may be possible to demonstrate that the system could be improved considering hundreds of meters [R.D. 127]. Wireless charging systems enable power transfer without physical connectors, using magnetic coupling. Due to the harsh environment, classic connectors may degrade quickly, while wireless pads can be designed to resist the abrasiveness of the lunar regolith [R.D. 128], [R.D. 129].
Tethers can be employed to provide robust connection for power and data and are particularly recommended when EVA (Extra Vehicular Activities) are planned [R.D. 130]. Docking mechanisms ensure a reliable mechanical and electrical connection between spacecraft. The male component usually includes guiding or alignment pins, while the female side contains sockets or capture mechanisms to receive and secure the incoming dock. A potential complication when employing these systems lies in their interaction with the environment [R.D. 131]. However, all these solutions require further technical analysis to ensure compatibility, reliability, and ease of integration.

11.1.2 Preliminary design considerations supporting concept selection

For MoonStation and MoonProbe the primary design driver is maximizing energy production. To achieve this, the rollable solar arrays, such as ROSA or equivalent commercial solutions, have been chosen as the baseline solution, due to their mass-to-power ratio and compact stowage configuration.
In MoonGrid, the mission aims to test various technologies. Each rover will be equipped with a different type of solar panel: the first will feature rigid solar panels, the second a membrane solar array, and the third a rollable panel.
For MoonRover, the chosen solution in terms of solar array is the membrane, as it optimizes volume usage and is better suited for a mobile platform, where compactness and mechanical flexibility are essential.
Regarding the interfaces, laser or wireless chargers are considered for MoonStation. Each rover from MoonGrid will adopt a different technology to support the objective of testing multiple solutions: rover 1 will use a tether, rover 2 a male docking mechanism, and rover 3 a female docking mechanism. MoonProbe will be equipped with a dual interface, consisting of a dock for potential future users and a wireless charger for the LSM rover. For MoonRover, the interface options under consideration include tether and/or dock. These interface choices may be revised based on the outcomes of further technical assessments.

11.1.3 Final design

As a result of the trade-off analysis, the baseline solution is MoonProbe. As specified in Section 11.1.2, this configuration features rollable solar arrays, Li-ion batteries dedicated exclusively to charging Scott and a system of RFCs for Eagle's night survival, plus a Li-ion battery for the rover. In addition, a stack of Lithiated Nickel Cobalt Aluminum Oxide cells has been used to deploy PDS during PDS-DEP. After the last iteration, the power budget for the mission has been produced (see Section 11.9). The energy/power calculations presented in the following paragraphs are based on the assumption of 168 hours of daytime followed by 120 hours of nighttime, which represents the worst-case scenario. During daytime, three modes have to be overlapped: EAGLE-PGEN, EAGLE-INTL and EAGLE-SENSOR. Of these, the most demanding is the first one, where the panel has to provide power to the bus and the components of Eagle, while simultaneously giving energy to the electrolyser of the RFCS and recharging the battery used to restore the capacity of Scott's accumulator. Summing the peak power need for each phase, the consumption amounts to ~1630 W. This value has been employed to evaluate the solar panel design, including a system margin of 20% and various losses (details in Section 11.1.4.3). During nighttime, the phases that overlap are EAGLE-NIGHT, EAGLE-INTL and EAGLE-SENSOR. The energy in this timeframe is provided by the RFCS. In this case, the energy needed by the subsystems has been calculated considering the duty cycle of each component: a total energy of ~15256 Wh in 120h (127 W continuous) is deemed necessary to the survival of Eagle. Further details are provided in the next Section. Also, the phase EAGLE-CHG has to be added during both daytime and nighttime. This does not affect the solar arrays and the RFCS sizing, because the power demand is met by Eagle's battery pack. An important assumption is that all the batteries are at full capacity at the moment of landing and that the RFCS is ready to operate in Fuel Cell (FC) mode (Section 11.1.4.2) to supply for the phases before the deployment of the ROSAs.

11.1.4 Components

11.1.4.1 Battery sizing

PDS battery: to satisfy the power request of the mode PDS-DEP, a stack of Lithiated Nickel Cobalt Aluminum Oxide (12Ah Space Cell) cells produced by EAGLEPITCHER has been sized. The characteristics of the single cell are shown in Table 11.1 [R.D. 132].

Nominal cell weight	465 g
Dimensions	71 mm (L) x 25.3 mm (W) x 113.1 mm (H)
Nominal voltage	3.6 V
Nominal capacity	12 Ah
Max constant discharge current	96 A
Operating temperature	253.15 K to 333.15 K

Table 11.1: Characteristics of PDS single cell

As shown in Table 11.2, during this mode, there are three different components that require energy in sequence (more details provided in Section 11.5:

Component	Total operating time	Energy required
4 Thermal knives	150 seconds	4.2 Wh
3 CubeMars AK80-8	90 seconds	30.9 Wh
Moog 965	180 seconds	42.5 Wh

Table 11.2:Components requiring energy during PDS-DEP

The total energy required is 77.6 Wh. Considering an efficiency of 85%, the energy the battery has to supply is 91.3 Wh. Since the components need a voltage of 28V, a configuration of 8 cells in series has been employed. The final topology of the cell stack is 8s1p, with a total capacity of 345.6 Wh and a mass of 3.7 kg. The discharge of this battery stack is ≈ 26%.

Scott's battery: as highlighted in the power budget in (Section 11.9), Scott's complete cycle lasts nine hours. Of these, two hours are allocated for charging Scott's battery (SCOTT-RCG mode), while the remaining seven hours are divided differently, depending on the illumination conditions. The operations are represented by the overlapping of different modes:

- Movement in daytime→ SCOTT-NEM, SCOTT-INTL
- Acquisition in daytime→ SCOTT-EMD, SCOTT-INTL, SCOTT-UPLINK
- Movement in nighttime→ SCOTT-NIGHT, SCOTT-INTL
- Acquisition in nighttime→ SCOTT-EMN, SCOTT-INTL, SCOTT-UPLINK

In daytime acquisition mode, the rover has more active sensors and collects more data with respect to nighttime acquisition mode. The rover's total power consumption during the operations and their duration in hours are shown in Table 11.3.

Daytime	Power consumption	Duration
Movement mode	~40 W	2h
Acquisition mode	~32 W	5h

Nighttime	Power consumption	Duration
Movement mode	~40 W	3h
Acquisition mode	~30 W	4h

Table 11.3: Daytime (on the left) and nighttime (on the right) power consumption

The rover's batteries have been selected considering its dimensional constraints and energy demands. Following a comprehensive market analysis, the 28-300 Battery Module (28 V Li-ion) from Dragonfly Aerospace, whose characteristics are summarized in Table 11.4, has been identified as the most suitable option. This module will require further modification to enable wireless charging (see 11.1.4.4). In addition, a 20% state-of-charge threshold was established as a permanent operational constraint [R.D. 133].

Topology	9s4p
Chemistry	LFP
Nominal voltage	29.7 V
Design capacity	297 Wh
EoC voltage	32 V
Mass	4.8 kg
Dimensions	350 (L) x 108 (W) x 115 mm (H)
Protection	Over/under voltage

Table 11.4: Scott's battery characteristics

During daytime, Scott has to be recharged 19 times; during nighttime, the number of recharges lowers to 14. This amounts to a total of 66 hours of recharge on a 288-hour period.
Eagle's battery: this battery pack has been sized based on key aspects of Scott's operative cycle. To ensure a high TRL and adequate capacity, the Li-ion rechargeable battery ABSL produced by EnerSys has been selected. It provides significant energy density with a lower-than-average mass and footprint, and it has already been employed for Lunar missions. Considering the capacity of Scott's accumulator and the frequency of its recharge, three of the ABSL batteries have been placed in parallel. Each one presents the characteristics summarized in Table 11.5.[R.D. 134]

ABSL cell	18650 E35
Configuration	8s16p
Nameplate capacity	1628 Wh
Maximum discharge current (continuous)	25 A
Nominal voltage	29 V
Voltage range	24-33.6 V
Footprint x height	364 mm x 203 mm x 98 mm
Weight	7.8 kg

Table 11.5: Eagle's single battery characteristics

Considering that Scott is recharged every seven hours, during periods of illumination Eagle's batteries experience micro-discharge cycles, as they charge Scott and are subsequently recharged by the solar array. Conversely, during nighttime, when the solar panels are inoperative, the batteries undergo intermittent discharges down to 20% of their total capacity. This threshold has been established for safety reasons. As a result, the primary contributor to battery wear is the deep discharge that occurs for approximately 120 hours out of every 288-hour period in the worst-case scenario. However, the Li-ion technology ensures that the performances of the batteries will be in the optimal range for a period that exceeds the mission considered lifetime [R.D. 135].

11.1.4.2 Regenerative fuel cells system

The selected technology for the RFCS is the Proton Exchange Membrane (PEM). These RFCs are advanced electrochemical devices that enable highly efficient energy storage and conversion. In this system, a proton-conducting polymer membrane serves as the core component, allowing the device to operate in both FC and Electrolyser (ELY) modes. In FC mode, hydrogen and oxygen are combined to generate electrical power and water, while in ELY mode, electrical energy is used to split water into hydrogen and oxygen. These chemical components are stored in separate tanks. This dual functionality allows PEM RFCS to provide a robust and compact solution for long-duration energy storage and generation. Moreover, the PEM FC - PEM ELY combination has higher TRL compared with other alternatives, even though still under development [R.D. 3], [R.D. 136]. A schematic representation of PEM RFCS is provided in Figure 11.5.

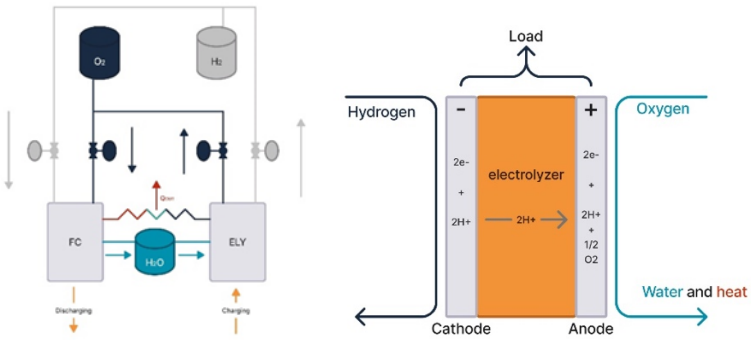

Figure 11.5: Schematic representation of PEM RFCS

For AMPERE mission, calculations have been carried out to produce an estimate of the power needed and of the energy stored into the RFCS. The solar panels provide energy to the RFCS in ELY mode during daytime. The tanks of the system have been sized so that there is no need to activate the ELY mode in nighttime, since the hydrogen and oxygen stored are sufficient to supply power for the entire 120 hours period. An overview of the parameters used for the computations can be found in Table 7.[R.D. 3] [R.D. 137]. It is important to note that the RFCS are employed only for Eagle's nighttime survival.

Efficiency RFCS	0,50
Efficiency electrolyser	0,85
Stack power density	550 W/kg
Tanks material density (Aluminium)	2,70 g/cm³

Table 11.6: RFCS parameters

For the sizing of the RFCS, Eagle's average energy request of 127 W (for 120 hours) has been considered (see Section 11.1.3). Taking into account losses from the RFCS to the components, a value of 200 W has been used to size the system. To supply this amount of constant electrical output, the chemical reaction between hydrogen and oxygen must release 48kW of chemical energy. In fact, only half of this energy will be transformed into electrical power. The other half is dispersed in form of heat, due to the efficiency value of the system. However, the thermal energy is not wasted, because it is used by the TCS to balance Eagle's temperature (Section 11.2 for additional details) [R.D. 138][R.D. 139].
Aluminium cylindrical pressure vessels with domed ends, rated at 10 MPa, have been considered for storing hydrogen and oxygen, along with an additional tank for water. In Table 11.7 are listed the masses of the components, in Table 11.8 the dimensions of the tanks. The parameter "L" refers to the length of the cylinder between the two domes [R.D. 140].

Item	Mass
H_2	1.22 kg
Oxygen	9.74 kg
H_2 tank	51.92 kg
O_2 tank	31.04 kg
H_2O tank	34.05 kg
Stack	0.36 kg

Table 11.7: Mass of RFCS component

H_2 tank volume	0.02 m³
O_2 tank volume	0.01 m³
H_2O tank volume	0.01 m³
L H_2 tank	0.32 m
L O_2 tank	0.08 m
L H_2O tank	0.01 m
External diameter H_2 and O_2 tanks	0.30 m

Internal diameter tanks H_2 and O_2	0.22 m
External diameter H_2O tank	0.35 m
Internal diameter H_2O tank	0.27 m

Table 11.8: RFCS components dimensions

The total mass of the RFCS is 140 kg, which includes not only the tanks and the stack, but also the mass of additional components such as pipes and valves (see Figure 11.5). The complexity of the system extends beyond the chemical process itself. In fact, the tanks pose some challenges in the design process. Since lunar gravity is approximately one sixth of the terrestrial, one of the problems is represented by efficiently channelling the liquids towards the nozzles. To reduce the issue, the tanks are placed vertically. Moreover, a Propellant Management Device (PMD) could be used. There are three primary technologies: vanes, sponges and screen channel liquid acquisition devices, but the first represent the most reliable solution for this mission purposes. These vanes, see Figure 11.6, could be added inside the tanks along the walls, to exploit the effect of capillarity and to ensure that only the liquid is taken. This solution will require further assessments [R.D. 140], [R.D. 141].

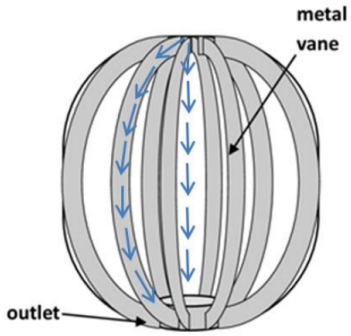

Figure 11.6: Metal vane flow patterns in low gravity [R.D. 141]

11.1.4.3 Solar arrays

Since the aim of the AMPERE mission is to maximize power production, the selection of solar arrays is of paramount importance. The final choice is represented by ROSAs, produced by NASA and Redwire, with a modification in the deployment mechanism. While the original panels are designed to be deployed for the entirety of the mission, AMPERE's ROSAs shall be re-rolled in a cylinder before nighttime (Section 11.5). The panel is composed by a flexible Kapton blanket held in tension by booms. These tubes are constructed of a thin high-strain composite laminate carbon fibre reinforced epoxy, flexible enough to permit them to be flattened and rolled up on a cylindrical mandrel for stowage and stiff enough to provide the energy needed to deploy the whole array. By datasheet, this type of panel has a typical power density that ranges from 100 W/kg to 120 W/kg [R.D. 142], [R.D. 119]. A Sun-tracking and tilting mechanism has been included, to follow the movement of the Sun, as specified in Section 11.5. Since the whole array will have to rotate of 360°, it is fundamental to assume that there is a circumference with a radius of at least 5.42 m around Eagle, free of any physical obstacles that could hinder the panel's rotation. According to WP 3.7, the landing site for AMPERE must be free of large boulders to be compliant with the constraints outlined in the [A.D. 9]. It is therefore assumed that, in this location, there are no physical impediments to the proper operation of the panels.
The solar cells chosen to be mounted on the solar arrays are the 32% efficiency (at 25°C) Quadruple Junction GaAs solar cell (Type: QJ Solar Cell 4G32C-Advanced), produced by Azur Space. The cells will have to undergo some modifications, since they will be mounted on a flexible and thin Kapton blanket, not on a traditional rigid honeycomb panel [R.D. 3][R.D. 143], [R.D. 144]. An overview of solar cell characteristics is provided in Table 11.9.

Dimensions	40 x 80 ± 0.1 mm
Cell area	30.18 cm2
Average weight	≤ 1780 mg
Thickness	110 ± 12 µm
Avg. open circuit voltage (BoL)	3451 mV
Operative voltage V_{op}	2900 mV

Table 11.9: Solar cell characteristics

To compute the power provided by the solar arrays, several assumptions have been made, summarized in Table 11.10:

Assumption	Note
Solar constant S=1450 W/m^2	Provided by WP 3.7
Maximum angle between the sun direction and the normal direction to the panel β=0.2994 rad (including also maximum slope)	Provided by WP 3.7
Degradation calculated at the end of one year of activity =0.001	SPENVIS analysis
Efficiency of the solar cell lowered at 0.30 due to temperature effect	T0 assumed 273 K
Efficiencies related to radiations, thermal cycling, UV damage, imperfections in assembly, contaminations taken from literature.	[R.D. 118]
Ideal power produced by single cell =1.31 W	/
Real power provided by single cell =0.99 W	/
Packaging Factor (PF) =0.88	[R.D. 118]

Table 11.10: List of assumptions for solar array sizing

To provide a total power of 5 kW in these conditions, 5056 solar cells has been deemed necessary. To accommodate the cells, two panels have been designed, for a total area of 17.34 m^2 and a total mass of 50 kg. Each wing measures 1.60 m in height, a structural constraint given by Eagle's dimensions, and 5.42 m in length. The two panels have to be placed perpendicular to Eagle structure to minimize the angle of the solar radiation with respect to the normal of the array. When stowed, the arrays are rolled into separate cylinders. After a first phase of deployment, which places the cylinders in the upward position, the deployment mechanism is activated, unrolling the arrays (more details provided in Section 11.5). As written in Section 11.1.3, the peak power request from Eagle is $\approx 1630\ W$, to be supplied from the solar arrays. This value is the result of the sum of three contributions, presented in the following Figure 11.17.

Contribution	Power inc. 20% system margin	Power transfer efficiency	Value incl. losses
Sum of peak power needs of the subsystem's components during NOMDOP* (inc. PCDU, exc. batteries and RFCS in ELY mode)	499W	From SA to loads (X_d) =0.9[R.D. 118]	554 W
Peak power needed to recharge Eagle's battery pack**	386.81W	From SA to batteries (X_B) =0.8[R.D. 118]	455 W
Peak power needed to supply RFCS in ELY mode***	484W	From SA to RFCS (X_{RFCS}) =0.78	620 W
Total	/	/	1629 W

Table 11.11: Contributions to Eagle peak power consumption during daytime

* Not considering CHG, which relies on Eagle's battery pack.
**To evaluate this contribution, some assumptions have been made. First, the battery pack is considered at the start of the 168-hour period of daytime after the 120 hours of nighttime. For this reason, the State of Charge (SoC) should be at 20%. Furthermore, to achieve a moderate power demand, a 15-hour period is allocated for recharging. Since Scott will also require power during this timeframe, an additional 10% of Eagle's battery capacity has been subtracted to account for its energy consumption. To summarize, it is assumed that the effective SoC is 10% at the beginning of the recharge period and that the capacity must be increased from 10% to 100% over the course of these 15 hours.
***The RFCS is considered as at the end of the FC mode. All the reactants have been transformed into water and the system is ready to operate in ELY mode. The power transfer efficiency has been assumed, since no real data is currently available. Moreover, the "power including 20% system margin" value has been obtained taking into account the efficiency of the electrolyser (Section 11.1.4.2).
In conclusion, considering the peak power consumption in the worst-case scenario, the power available in daytime for an eventual external user of the station amounts to 3370 W, without considering any losses. Figure 11.7 shows an approximate visualization of peak power during NOMDOP and NOMNOP, Figure 11.8 shows approximately the power request available for future user during NOMDOP.

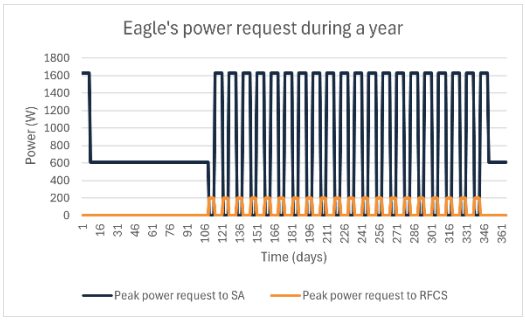

Figure 11.7 : Approximate visualization of peak power request during NOMDOP and NOMNOP

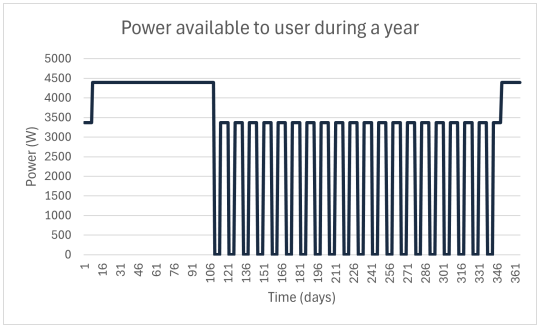

Figure 11.8: Approximate visualization of power available for future user during NOMDOP

11.1.4.4 Charging interfaces

Wireless interface: for recharging Scott's battery, a wireless interface has been chosen, a promising technology currently under development. Designed by Astrobotic in collaboration with NASA and WiBotic, the Ultra Fast Proximity Charger (UFPC) project aims to support robotic missions on the Moon without the need for on-board solar panels or nuclear sources. The UFPC has four components, as shown in Figure 11.9: a power transmitter, a transmitter coil, an on-board charger and a receiver coil.

Figure 11.9: Transmitter, transmitter coil, on board charger, receiver coil (from left to right)

The first two will be mounted on Eagle, while the other two on Scott, which will have to place its receiver in contact with the transmitter, as shown in Figure 11.10. Astrobotic is also developing an algorithm for autonomous docking.

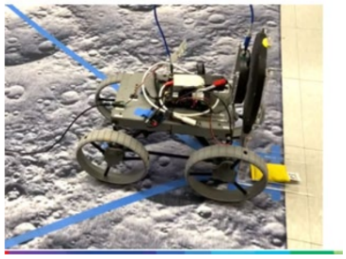

Figure 11.10: Autonomous docking

While the project is still ongoing, the conclusion is expected in 2026, with the system reaching a TRL of 7. Currently, the design has achieved the characteristics shown in Table 11.12. Lightweight and resistant, it appears suitable for the harsh lunar environment. For the computation of the power transmitted via the UFPC, a 10% margin has been considered. [R.D. 147], [R.D. 148]

	Power Transmitter (TR)	Transmitter coil	Onboard Charger (OC)	Receiver coil
Model	125W: OC-125-08-SPC	125W TR	125W: TR-125-DC-SPC	125W OC

Dimensions	200 x 200 x 40 mm	210 mm (diameter)	104 x 104 x 28 mm	132 mm (diameter)
Mass	2.5 kg	420 g	400 g	90 g
Operating temperature range	233.15 K to 343.15 K	73.15 K to 448.15 K	248.15 K to 358.15 K	73.15 K to 448.15 K
Charging current	8 A (125 W)	/	/	/
Voltage	26.6-29.4 VDC (input)	/	12-36 VDC fixed (output)	/

Table 11.12: UFPC characteristics

Docking system: the interface for the future user is represented by the LESSH BCM, developed by NASA (shown in Figure 11.11). It is composed of a 1.5-meter flexible harness, with an EVA-compatible connector and a removable dust cover. Designed specifically for operations at the lunar South Pole, the LESSH BCM provides a safe solution for future astronauts to recharge tools and instrument modules thanks to its power switch. To use this device, the battery to be recharged must be installed inside a LESSH-Placed module, which needs to be integrated directly into the user's design, as depicted in Figure 11.11 [R.D. 130]
The characteristics of the LESSH BCM are shown in Table 11.13.

Mass	9.4 kg
Volume	50 x 25 x 10 cm^3
Charging power	Rated 215W power output (9.4 A output)
Charge time	4 hours from 0% - 100% SoC
Charging method	Constant current 0 A - 9.4A and constant voltage 24V-33.6V (cannot exceed 300W input power limit)
Supported batteries	28V astronaut-rated batteries in LESSH instrument modules
Compatible lunar exploration systems	Human Landing System Sustaining, Orion, Gateway Logistics Module, Gateway, Surface Hab, Transit Hab, Pressurized Rover, Lunar Terrain Vehicle, Cargo Lander

Table 11.13: LESSH BCM characteristics

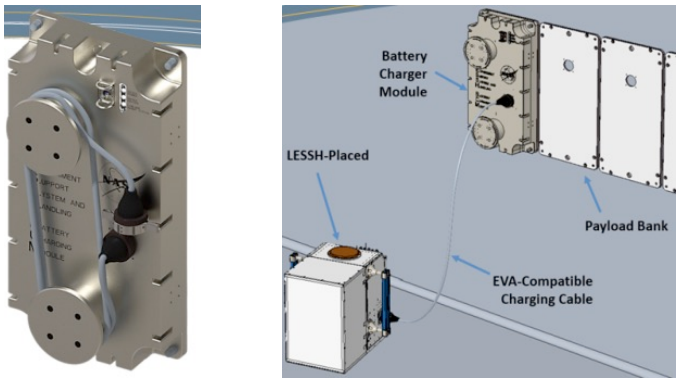

Figure 11.11: LESSH BCM (on the left), LESSH system configuration (on the right)

11.1.4.5 Power Conditioning and Distribution Unit

Eagle's PCDU has been designed considering the complexity of the entire EGSD subsystem. Since no mission like AMPERE has ever been carried out, the design of the PCDU has been inspired by various models, either already existing, but developed for different types of missions, or still under development. An estimated mass of $\approx 16\ kg$ has been considered, and a volume of 805 x 430 x 260 mm^3. Furthermore, a power consumption of 50 W has been considered. The system must manage multiple inputs and outputs, ensuring efficient transfer of power. A dual-bus type has been selected, with a 120VDC regulated and a 28 VDC regulated supply, in accordance with the needs of the components [R.D. 145] [R.D. 3]. During daytime the solar arrays are deployed to supply the required power to the system loads. In this timeframe, as mentioned in before, three key processes occur simultaneously:

- Eagle module's components are active and consume electrical power to support nominal functions;

- Eagle's battery pack is used to recharge Scott and must subsequently be restored to its original SoC to ensure readiness for the next discharge cycle;
- The solar arrays provide electrical power to the RFCs, which operate in electrolysis mode to produce and store chemical energy to be utilized during the nighttime.

The power produced by the solar arrays is managed by the Array Power Regulator (APR) through a Maximum Power Point Tracker (MPPT), a non-dissipative system that dynamically changes the working point of the arrays to extract the exact power needed by the bus, up to the maximum power point. The excess of power is not dissipated, but left on the array side, thus increasing its efficiency. [R.D. 118] The MPPT must be of the "booster" type, to convert the voltage from ~100 V to 120 V. Then, the power is directed towards the battery pack through a Battery Discharge Charge Regulator (BDCR), which protects the accumulators from overcharging, overheating and/or undervoltage; it is directed towards the RFCS through a Regenerative Fuel Cell Regulator (RFCR). This component is expected to be provided by the productor of the RFCS.
Using Direct Current (DC) - DC converters, the voltage is decreased from 120 V to 28 V and then channelled into Latching Current Limiters (LCLs), which are circuit protection devices that limit excessive current flow in an electrical circuit, in situations like overload or short circuits. This is a further step to protect the future user docked at the LESSH BCM (11.1.4.4). Moreover, the 28 VDC is also the channel used to receive power from the LDE until landing.
A schematic representation of the designed PCDU can be seen in Figure 7.

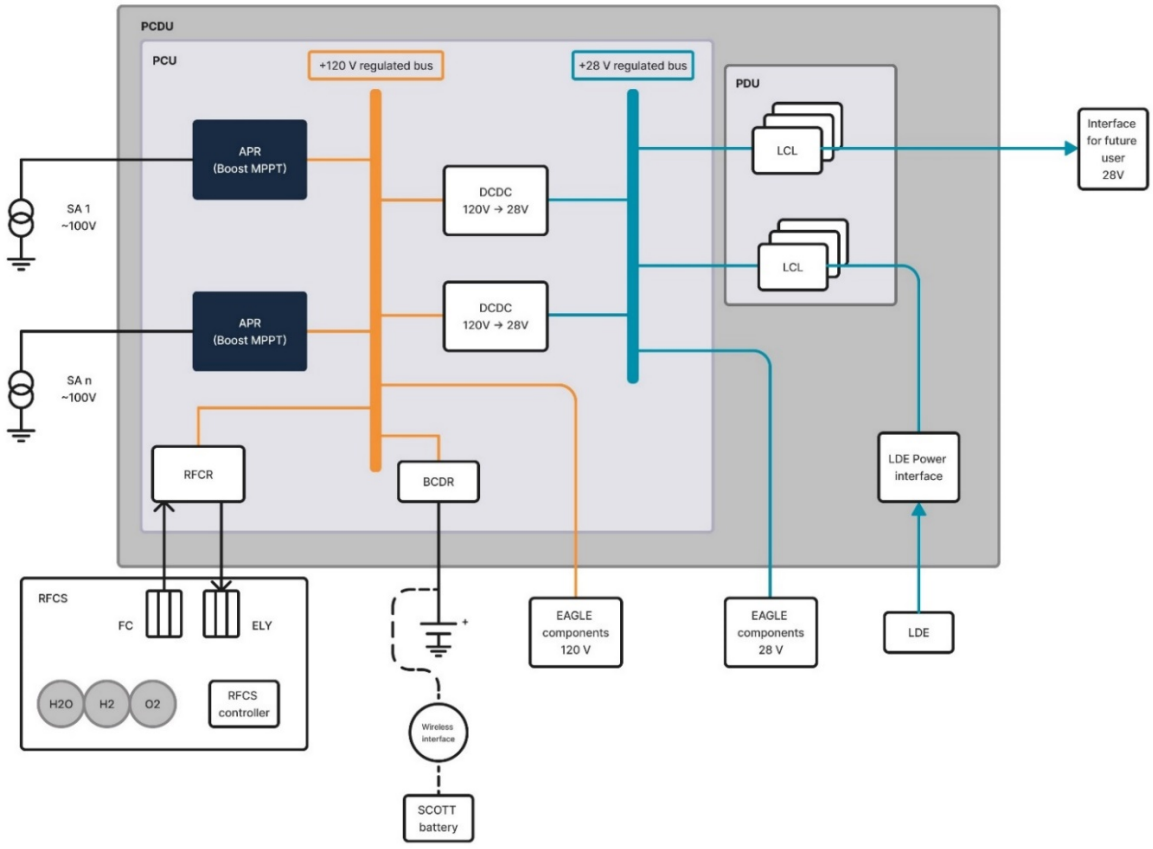

Figure 11.12: Eagle's PCDU scheme

For Scott's PCDU, shown in Figure 11.13, a commercial model commonly used on CubeSats has been chosen, to exploit the expertise gained from previous flights. However, this component will require some modifications, because Scott is not equipped with solar panels and relies solely on its battery to function [R.D. 146]. Scott's PCDU characteristics are provided in Table 11.14.

Figure 11.13: Scott's PCDU

STARBUCK-NANO-PLUS	Value
Mass	148 g
Length x width x height	95.89 mm x 90.17 mm x 20.82 mm
Regulated power buses	3.3V, 5V, and 12V
LCL	10 configurable
Interfaces	12C
Maximum battery voltage	8.2V
Estimated power consumption	1.5 W

Table 11.14: Scott's PCDU characteristics

11.1.4.6 Summary of components and TRL assessment

A summary of the EGSD components and their TRL is shown in Table 11.15.

Component	Mass	TRL	Notes on TRL
Lithiated Nickel Cobalt Aluminum Oxide Space cell (x 8)	3.72 kg	8	Cells employed for various aerospace missions [R.D. 132]
28-300 battery module	4.80 kg	8	TRL 9 from datasheet, but some modifications will be required to allow wireless recharge.
Li-ion Rechargeable Battery ABSL (x 3)	23.40 kg	8	Some modifications will be required to allow wireless recharge.
RFCS	140 kg	4	[R.D. 3]
Solar Panels ROSA	50 kg	5	Currently in use on the ISS but never employed in the lunar environment.
Wireless interface UFPC	3.50 kg	7	TRL 7 expected at the end of 2025, 8 at the end of 2026.
LESSH-BCM	9.40 kg	6	Tests are in progress, planning to end before the start of AMPERE mission.
STARBUCK-NANO-PLUS	0.15 kg	7	Unit commercially available for space applications.
PCDU	16 kg	4	Designed based on existing PCDUs but substantially different.

Table 11.15: **EGSD components and TRL assessment**

11.2 Thermal Control Subsystem

Both during and after the lunar landing, the thermal control subsystem must remain operational, in accordance with the SoW [A.D. 1]. The thermal control subsystem is a fundamental part of the AMPERE mission: it must keep all parts of the LPS within acceptable temperature ranges and protect the LPS from the radiation environment, in order to guarantee the best performance possible and mission success.

11.2.1 State-of-the-art analysis

Several thermal management strategies have been investigated to ensure optimal thermal control. A key consideration is that, depending on the lunar environmental conditions and mission requirements, thermal control can be achieved through passive systems, active systems or a combination of both. The selection of the most suitable configuration will depend on the LPS location, the duration of the operational phase and the need to ensure the proper functioning of all components sensitive to the extreme temperatures on the lunar surface. To ensure that the instruments can operate within the defined temperature range without malfunctions, various thermal control systems must be employed. Thermal insulation for AMPERE can be achieved using MLI [R.D. 149], [R.D. 150]. Due to its favourable optical properties, MLI provides effective thermal shielding and it is a technology widely used in numerous space missions, including lunar missions such as Apollo 11, Volatiles Investigating Polar Exploration Rover (VIPER) [R.D. 151], and the Chang'e missions [R.D. 152].

The lunar South Pole presents extreme conditions: very high temperatures during the lunar day (worst hot case) and very low temperatures during the lunar night (worst cold case). To address these challenges, new types of MLI are being developed and tested, some of which are currently being tested on nanosatellites[R.D. 154]. These materials, known as SMLI, can adjust their emissivity and absorption based on the temperature they encounter [R.D. 155].

Another possible solution is the implementation of a deployable thermal shield mechanism, which would be activated only during the lunar night. However, these last two options may require additional power and have a greater mass compared to traditional MLI [R.D. 156], [R.D. 157].

Subsequently, there are heat dissipation mechanisms known as radiators, which can be either active or passive. This is also a highly effective technology, widely utilized in various lunar missions, for which the amount of heat dissipated increases with the surface area of the radiator [R.D. 151].
Passive radiators rely on an automatic mechanism that opens the grids when high temperatures are reached. Active radiators, on the other hand, operate differently: they are activated only when a signal is received from the OBC or through another instrument, requiring a certain amount of power.
In both cases, radiators exhibit two different emissivity: a high one when the grids are open and a very low one when the grids are closed. However, these thermal control components can present challenges in terms of mass, as larger surfaces are required to dissipate higher power levels, resulting in greater weight [R.D. 153], [R.D. 158], [R.D. 159].
Another piece of technology that plays a crucial role during the lunar night and is widely used is resistive heaters. These lightweight and efficient devices are utilized in missions such as VIPER [R.D. 151].Their operation is based on the Joule effect: they are active mechanisms that convert electrical energy into heat, thus enabling the payload to be warmed when necessary. Resistive heaters are notable for their straightforward design, low cost, and ability to provide targeted and controllable heating. However, their usage demands careful energy management, especially in extreme environments like the lunar night, where maintaining the mission's energy balance is particularly critical [R.D. 149],[R.D. 160].
Recently, a technology that has proven extremely useful both during the lunar day and night is Phase Changing Materials (PCMs). These materials, already employed in specific missions, are completely passive mechanisms based on the melting and solidification of the chosen material [R.D. 161]. During the melting phase, PCM absorbs heat due to its latent heat, stabilizing the temperature for a defined period. Similarly, during solidification, the material releases heat, helping to maintain temperature during critical phases. These systems are particularly valued for their lightweight design and minimal space requirements. However, they cannot serve as a standalone solution for heat dissipation or storage. They must be paired with other thermal management systems, such as radiators or resistive heaters, to ensure comprehensive and reliable thermal control [R.D. 162],[R.D. 163].
Heat transport is essential during both the lunar night and the lunar day, and there are three commonly employed solutions that share similar operating principles. The first is Heat Pipes (HPs), a passive heat transfer mechanism. They are compact in size, but the amount of heat they can transport is relatively limited [R.D. 149]. The second option is Loop Heat Pipes (LHPs), which, unlike HPs, can transport significantly higher amounts of heat. They are slightly larger and result in a modest increase in mass, though they remain relatively lightweight overall [R.D. 164], [R.D. 165], [R.D. 166].
Lastly, Mechanical Loop Heat Pipes (MLHPs) are active systems that weigh over 10 kilograms. These systems are capable of dissipating very high amounts of power. However, they are bulkier and require an external power source to operate the pump, as the fluid movement is driven by the pump rather than temperature and pressure gradients, as occurs in the first two, which are passive systems [R.D. 167], [R.D. 168]. These technologies are widely used in many space missions, including lunar missions such as Chang'e-5 and VIPER, where thermal management is critical for ensuring the functionality and survival of spacecraft components in the harsh lunar environment [R.D. 151], [R.D. 167].
Finally, it is necessary to have instruments capable of monitoring the temperature inside the satellite. Specifically, temperature sensors can be used to detect the equilibrium temperature and are directly connected to the OBC. This connection allows for the automatic activation of specific mechanisms once a certain temperature is reached. Another solution is thermostats, which not only regulate the temperature but can also autonomously activate instruments without necessarily being connected to the OBC. Thermostats are particularly useful in systems where autonomy is critical or when it is desirable to reduce the complexity of the OBC software. However, in the case of temperature sensors, the impact on power and mass is negligible compared to thermostats [R.D. 149].

11.2.2 Preliminary design considerations supporting concept selection

The design of the TCS begins with modelling the environment. The following inputs have been considered:

- Direct solar radiation, Q_{SUN}: the solar radiation is modelled as the one emitted by a black body at $5800\ K$. The intensity of the solar radiation impacting on LPS depends on the distance from the Sun and the solar activity. The solar constant is $S = 1450\ \frac{W}{m^2}$ [R.D. 256].
- Moon infrared radiation, Q_{IR}: the infrared radiation emitted by the moon is assumed as the one emitted by a blackbody, considering multiple temperatures corresponding to those achievable on the lunar surface.
  Table 11.16 shows the values for this radiation computed for the minimum and maximum surface temperatures through the application of the Stefan-Boltzmann law (Equation (11.1)), where σ is the Stefan-Boltzmann constant and T_{Moon} is the surface temperature of the Moon [R.D. 118].

$$q_{IR} = \sigma \cdot T_{Moon}^4 \tag{11.1}$$

Minimum infrared radiation (97.7 K)	Maximum infrared radiation (286.8 K)
$4.91\ \frac{\mathrm{W}}{\mathrm{m}^2}$	$364\ \frac{W}{m^2}$

Table 11.16: Moon infrared radiation

- Moon albedo radiation, Q_{alb}: the radiation emitted by the Sun and reflected by the Moon towards LPS. The albedo irradiance is given as $\alpha_{albedo} \cdot S \cdot k_A$, where α_{albedo} is the albedo coefficient and it is equal to 0.14 [R.D. 3], S is the solar constant and k_A represents the semiempirical corrective factor (≤ 1) and it is given by Equation (11.2) [R.D. 118].

$$k_A = 0.657 + 0.54 \cdot \frac{R_{Moon}}{R_{Moon} + h} - 0.196 \cdot \left(\frac{R_{Moon}}{R_{Moon} + h}\right)^2 \quad (11.2)$$

Additionally, for each phase a dissipated power has been considered according to the required power of the platform. The preliminary thermal model is characterised by the following assumptions:

- The LPS is modelled as an isothermal sphere, whose surface area is assumed to be equal to that of a sphere with a volume corresponding to the total volume of the platform. Its simplicity enables the assessment of critical mission phases by evaluating preliminary WCH and WCC temperatures [R.D. 118].
- The dissipated power (Q_{int}) is computed according to the margin discussed in [R.D. 3].
- The WCH is represented by maximum solar radiation, maximum on-board dissipated power and maximum infrared power emitted by the Moon.
- The WCC is characterized just by the minimum infrared power emitted by the Moon and the minimum on-board dissipated power.

11.2.2.1 Thermal analysis input

Starting from the components of each subsystem, it is possible to establish the upper limit for the minimum temperature and the lower limit for the maximum temperature allowed. Table 11.17 reports the full operating temperature ranges for Eagle components.

Subsystem	Components	Minimum operating temperature [K]	Maximum operating temperature [K]
TT&C	Ka band parabolic antenna	243	343
	Ka band transceiver	248	328
	Ka-band GaN-on-SiC MMIC balanced HPA	248	328
	DPX VC222834 diplexer Ka	223	358
	Anywaves compact S band antenna	153	393
	C/TT-520 S band multimode transponder	263	333
	Next generation OBC	233	343
	UHF system	233	343
TCS	Heaters	208	423
	Radiator	250	440
	EDS	233	523
	Generator for EDS	233	523
	Temperature sensor	208	673
	Loop heat pipes	213	363
STR&MEC	Solar array drive electronics	243	333
	SA deployment	253	323
	Solar array drive mechanism	243	333
	Braking actuators	270	323
	Moog Type 33 biaxial gimbal	243	343
RDS	Drop-release system	208	353
	Winch	233	323
	Worm gear	233	323

	Motor	233	323
	Cable in Dyneema	233	323
ADCS	Inertial measurement unit	233	358
	Coarse Sun sensor	248	343
	Fine Sun sensor	248	343
	Inclinometer	253	343
EGSD	Solar panels	173	408
	Regenerative fuel cells	273	323
	Batteries	268	323
	Wireless interface	233	343
	Dock interface & connectors	243	323
	Power conditioning & distribution unit	243	338
Eagle sensors	RADFET RM VT-01-A	273	320
	MAG566 X 2	241	323
	RTD HTRS	203	533
	NGRM	233	338

Table 11.17: Eagle's on-board components temperature range

As a result, the minimum allowable temperature is set by the RADFET RM VT-01-A and the regenerative fuel cells, both operating down to 273 K. The maximum allowable temperature is also constrained by the RADFET RM VT-01-A, which tolerates up to 320 K. Therefore, it is essential to ensure that all Eagle subsystems operate within the thermal range of [273 K; 320 K].
Table 11.18 reports the full operating temperature ranges for Scott components.

Subsystem	Components	Minimum operating temperature [K]	Maximum operating temperature [K]
TT&C	Antenna UHF ANT430	243	343
	NanoCom AX100	243	358
	PW2022-111	203	373
	Endurosat S band transceiver	253	333
	WiRan Diplexer	233	348
	GomSpace Nanomind Z7000	233	353
	LCNS unit	233	358
TCS	Heaters	208	423
	Radiator	250	440
	Electrodynamic dust shield	233	523
	Generator for EDS	233	523
	Temperature sensor	208	673
	Loop heat pipes	213	363
STR&MEC	Astrobotic CubeRover systems	243	353
EPS	Power conditioning & distribution unit	233	358
	Battery	263	313
	Wireless interface	248	358
ADCS	Inertial measurement unit	233	358
	Coarse Sun sensor	248	343

	Camera	170	343
	LEDs	233	373
Scott sensors	Ion electron sensor	223	363
	Ion and neutral mass spectrometer	263	313
	Solar radiation and dust sensor	233	323
	Langmuir probe	233	323

Table 11.18: Scott's on-board components temperature ranges

Consequently, the minimum allowable temperature is defined by the battery and the ion and neutral mass spectrometer, both of which remain operational down to 263 K. Similarly, the maximum allowable temperature is limited by the same components, which can withstand temperatures up to 313 K. It is therefore critical to maintain all Scott subsystems within the thermal range of [263 K; 313 K]. A temperature range of [273 K; 313 K] is considered during the LLO, descent, and landing phases, since the analysis was carried out for LPS.

11.2.3 Final design of TCS

11.2.3.1 TCS equipment

The use of MLI has been considered (Figure 11.14). The configuration included VDA as the inner layer, a certain number of aluminized Mylar layers and Teflon as the outer layer [A.D. 10], [R.D. 150].

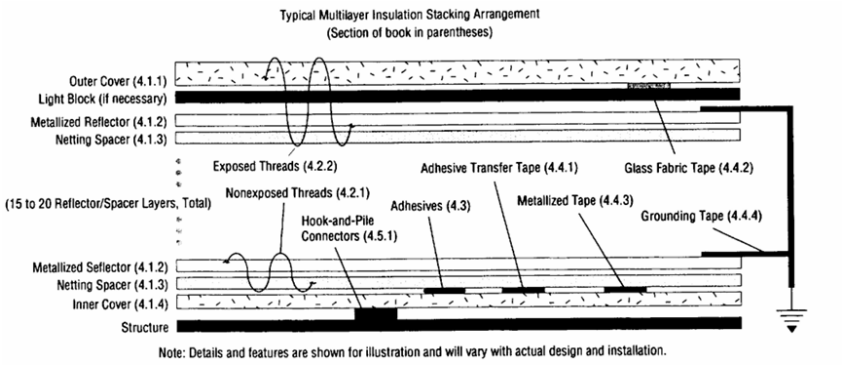

Figure 11.14: Composition of a typical MLI [R.D. 150]

Since 15 layers of aluminized Mylar have been used in previous lunar missions [R.D. 169], the Figure 11.15 shows the resulting effective emissivity of the Mylar which is ~ 0.003.

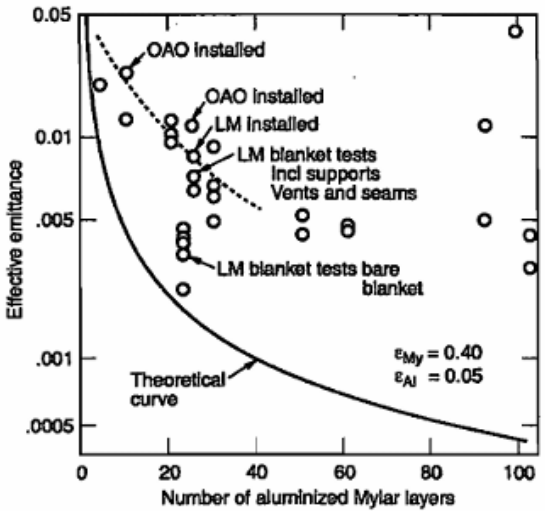

Figure 11.15: Effective emittance vs number of aluminized Mylar layers [A.D. 10]

An additional layer of SMLI has been added on top of the Teflon, which constitutes the outer layer of the classical MLI, allowing the thermo-optical properties to vary during nighttime. Specifically, lightweight electrochromic materials have been used, capable of altering their emissivity through a power impulse [R.D. 155], [R.D. 174]. A thin-film electrochromic device with the structure ITO/WO_3/Ta_2O_5/NiO/Au has been tested, showing an emissivity modulation from 0.64 to 0.057, with an absorptivity of 0.1 [R.D. 122]. To be conservative, since Eagle has larger dimensions compared to Scott, an emissivity variation from 0.64 to 0.065 has been considered for Eagle, and a variation from 0.64 to 0.24 for Scott.
Furthermore, for the temperature calculation during nighttime, due to the low surface temperature of the Moon, heaters have been considered to produce enough heat to ensure the proper functioning of all instruments. The power required by the heaters is defined as the heat supplied directly by the RFCS and the amount of electrical energy provided by the RFCS that is converted into heat through the Joule effect [R.D. 168] [R.D. 170]. The power density of these heaters is $0.8\ \frac{W}{m^2}$ [R.D. 171].
A radiator has been added to enable greater heat dissipation and to stay within the acceptable temperature range during daytime. The radiator is a passive system, based on the opening of two blade louvers (Figure 11.16). Being a passive system, it exhibits an hysteresis cycle of 20 K: it remains fully closed at $T \leq 273\ K$, with an effective emissivity of 0.05 and an absorptivity of 0.14; it is fully open at $T \geq 293\ K$, with an effective emissivity of 0.64 and the same absorptivity (0.14). For temperatures between $273\ K < T < 293\ K$, the emissivity is assumed to vary linearly. This radiator has been designed for the Polar Ice Explorer (PIE) mission, an ISRU exploration mission in the lunar polar regions [R.D. 158].

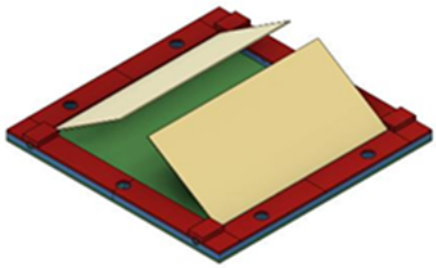

Figure 11.16: Radiator with two blade vane louvers

LHPs are widely used for efficient heat transport in thermal management systems. The working fluid employed is ammonia, chosen for its low freezing point, enabling reliable operation at low temperatures. The general working principle of a LHP is illustrated in Figure 11.17. In the evaporator, ammonia absorbs heat and vaporizes, creating a pressure difference that drives the vapor through the transport lines to the condenser. At the condenser, the vapor releases heat and condenses back into liquid form, which is then returned to the evaporator via a capillary wick structure. This cycle maintains continuous fluid circulation and effective heat transfer [R.D. 165].

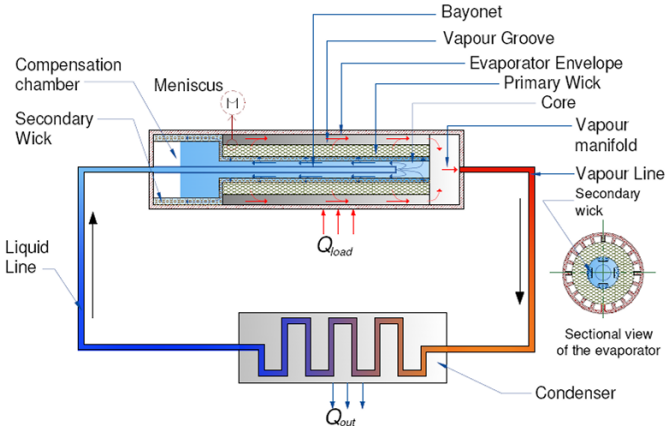

Figure 11.17: Working principle of a loop heat pipe [R.D. 165]

The EDS and its dedicated power generator have been also included to ensure effective dust removal, allowing the thermo-optical properties of both SMLI and radiator to be considered unaffected by the regolith in thermal analyses. The EDS consists of a set of electrodes connected to a generator and arranged to produce a non-uniform electric field,

thereby creating a force gradient that enables the removal of regolith [R.D. 175], [R.D. 176] [R.D. 276].This system has also been used in the lunar Blue Ghost Mission I, as shown in Figure 11.18 [R.D. 177].

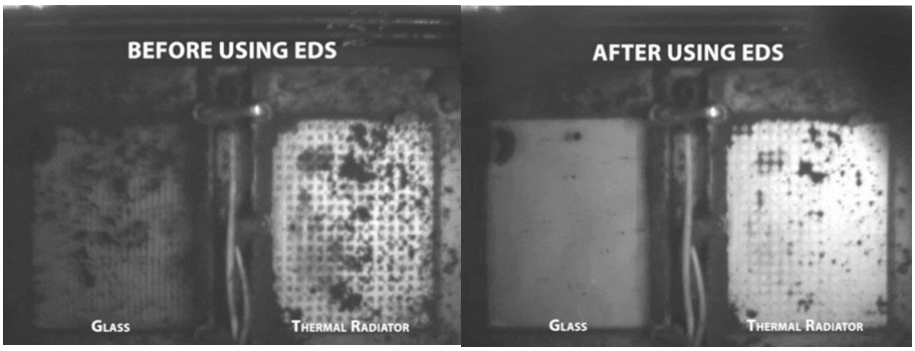

Figure 11.18: Utilization of EDS

Finally, temperature sensors have been incorporated to monitor the system's equilibrium temperature [R.D. 172] . Table 11.19 and Table 11.20 list the component of the TCS final design along with their characteristics, both for Eagle and Scott.

Component	Number of units	Power $[W]$	Total weight $[kg]$
MLI	1	0	1.91
SMLI	1	108.60	2.98
Radiator	1	0	16.50
EDS and generator	1	49.50	8.52
Heaters	2	180.00	$1.27 \cdot 10^{-2}$
LHP	6	0	1.320
Temperature sensor	5	$2.00 \cdot 10^{-3}$	0.035

Table 11.19: Eagle's TCS equipment for final design

Component	Number of units	Power $[W]$	Total weight $[kg]$
MLI	1	0	0.05
SMLI	1	4.02	0.11
Radiator	1	0	1.10
EDS and generator	1	1.61	0.27
Heaters	2	8.00	$3.40 \cdot 10^{-3}$
LHP	2	0	0.44
Temperature sensor	2	$6.70 \cdot 10^{-6}$	0.01

Table 11.20: Scott's TCS equipment for final design

11.2.4 Stady state analysis

Steady-state thermal analysis is essential for predicting the temperature distribution within the LPS once thermal equilibrium is achieved. This analysis ensures that the thermal control subsystem keeps all components within their operational temperature limits under various environmental conditions. A key assumption is that the radiator is not subject to radiation from the surrounding environment [R.D. 149], [R.D. 168]. Temperature variations must be analysed by considering both internal and external heat fluxes across different scenarios, and by balancing them with the emitted thermal radiation (Q_{em}) reported in Equation (11.3).

$$Q_{em} = \sigma \cdot T^4 \cdot (A \cdot \varepsilon + A_{rad} \cdot \varepsilon_{rad}) \tag{11.3}$$

Where:

- σ is the Stefan-Boltzmann constant.
- T is the LPS's temperature.
- A is the area of LPS covered by SMLI.
- ε is the emissivity of the SMLI.
- A_{rad} is the area of the radiator.
- ε_{rad} is the emissivity of the radiator.

For the WCH scenario, the maximum thermal inputs and onboard thermal production are considered in (11.4).

$$Q_{SUN} + Q_{alb} + Q_{IRmax} + Q_{intmax} + Q_{heaters} = Q_{em} \quad (11.4)$$

Where:

- $Q_{SUN} = \alpha \cdot S \cdot A \cdot \cos\theta$, α is the absorptivity of the LPS covered by SMLI and θ is defined as the angle between the direction of the solar rays and the local normal to the surface.
- $Q_{alb} = \alpha_{albedo} \cdot S \cdot k_A \cdot \alpha \cdot F_{sm} \cdot A$, $F_{sm} = \frac{1}{2} \cdot \left[1 - \cos\left(\frac{R_{Moon}}{R_{Moon}+h}\right)\right]$, it is the view factor of the spherical LPS.
- $Q_{IRmax} = \varepsilon_{IR} \cdot q_{IRmax} \cdot A \cdot F_{sm}$, ε_{IR} is the infrared emissivity of the satellite's SMLI.
- $Q_{intmax} = 0.6 \cdot P_{totmax}$, P_{totmax} is the maximum power consumption of the LPS in that phase [R.D. 4].
- $Q_{heaters}$ is the continuous power required by the heaters during nighttime; during daytime it is $0\ W$.

At the end, it is possible to evaluate the temperature for the worst case hot (Equation (11.5)).

$$T_{WCH} = \left(\frac{Q_{SUN} + Q_{alb} + Q_{IRmax} + Q_{intmax}}{\sigma \cdot (A \cdot \varepsilon + A_{rad} \cdot \varepsilon_{rad})}\right)^{\frac{1}{4}} \quad (11.5)$$

For the WCC scenario, only the minimum thermal inputs and onboard thermal production are considered (equation (11.6)).

$$Q_{IRmin} + Q_{intmin} = Q_{em} \quad (11.6)$$

Where

- $Q_{IRmin} = \varepsilon_{IR} \cdot q_{IRmin} \cdot A \cdot F_{sm}$.
- $Q_{intmin} = 0.6 \cdot P_{totmin}$, P_{totmin} is the minimum power consumption of the LPS in that phase [R.D. 4].

At the end, it is possible to calculate the temperature for the WCC (Equation (11.7)).

$$T_{WCC} = \left(\frac{Q_{IRmin} + Q_{intmin} + Q_{heaters}}{\sigma \cdot (A \cdot \varepsilon + A_{rad} \cdot \varepsilon_{rad})}\right)^{\frac{1}{4}} \quad (11.7)$$

11.2.4.1 Steady state analysis for LPS

The analysis has been carried out under the assumption that LPS is fully illuminated during the LLO, descent and landing phases, therefore only the temperature of the WCH has been evaluated. Table 11.21 summarizes the inputs used for this analysis. Moreover, based on WP 3.6 data, it is assumed that LPS is continuously subjected to maximum illumination ($\cos\theta = 1$).

Input parameter	Value [unit]
A	16.53 $[m^2]$
A_{rad}	1.50 $[m^2]$
ε	0.64
ε_{rad}	linearly from 0.05 to 0.64
α	0.10
σ	$5.67 \cdot 10^{-8}$ $[W/K \cdot m^2]$
S	1450.00 $[W/m^2]$
α_{albedo}	0.14
R_{Moon}	1737.40
P_{totmax}	47.90 $[W]$
$\cos\theta$	1
q_{IRmax}	364.00 $[W/m^2]$

Table 11.21: Input parameters for LPS

Figure 11.19 illustrates the variation of the three radiation sources as a function of altitude. It can be inferred that the albedo is negligible compared to the solar radiation and the infrared radiation emitted by the Moon. The solar heat flux (Q_{SUN}) is constant due to the assumption that LPS is continuously subjected to maximum illumination.

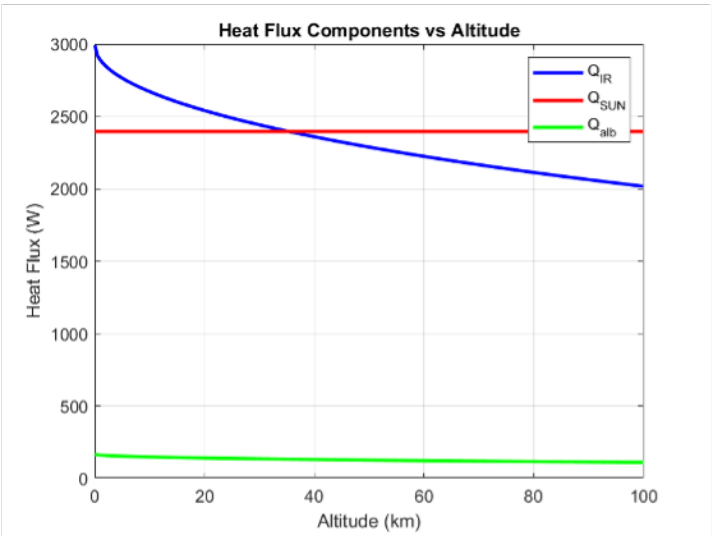

Figure 11.19: Variation of the three radiation sources for LPS with altitude

Thanks to the calculations presented in Section 11.2.4, it is possible to obtain a temperature value for the WCH that varies with altitude (Figure 11.20). Therefore, the minimum temperature value is 288.87 K, while the maximum is 303.96 K, both falling within the range of 273 K to 313 K.

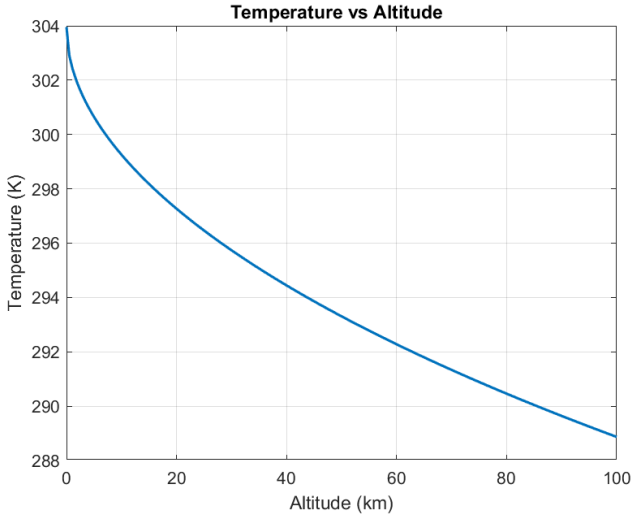

Figure 11.20: Temperature for LPS with altitude

11.2.4.2 Stady state analysis for Eagle and Scott

Since the calculations were carried out over a one-year period, the WCC and WCH for Eagle and for Scott are included within the same set of results. As a result, the outputs directly reflect the minimum and maximum temperature values over the course of the mission year. Table 11.22 summarizes the inputs used for these analyses. Moreover, based on environmental analysis data, it is assumed that Eagle and Scott are continuously subjected to maximum illumination (θ = elevation angle of the Sun). The heaters are operated continuously during the night ($\theta = 0°$). Moreover, the SMLI changes its emissivity during this phase to optimize thermal control.

Input parameter	Value [unit]
A for Eagle	$12.36\ [m^2]$
A for Scott	$0.40\ [m^2]$
A_{rad} for Eagle	$1.50\ [m^2]$
A_{rad} for Scott	$0.10\ [m^2]$
ε for Eagle	0.64 to 0.065
ε for Scott	0.64 to 0.24

ε_{rad}	linearly from 0.05 to 0.64
α	0.10
σ	$5.67 \cdot 10^{-8}$ $[W/K \cdot m^2]$
S	1450.00 $[W/m^2]$
α_{albedo}	0.14
R_{Moon}	1737.40
P_{totmax} for Eagle	1630.00 $[W]$
P_{totmax} for Scott	39.03 $[W]$
P_{totmin} for Eagle	97.70 $[W]$
P_{totmin} for Scott	22.20 $[W]$
$Q_{heaters}$ for Eagle	180.00 $[W]$
$Q_{heaters}$ for Scott	8.00 $[W]$
q_{IRmin}	4.91 $[W/m^2]$
q_{IRmax}	364.00 $[W/m^2]$

Table 11.22: Input parameters for Eagle and Scott

Figure 11.21 illustrates the variation of the three radiation sources as a function of $\cos\theta$. It can be inferred that the albedo is negligible compared to the solar radiation and the infrared radiation emitted by the Moon. The behaviour shown in the figure is related to the fact that, in the absence of illumination, the solar elevation angle θ is equal to 0. Although cos(θ) is equal to 1, this condition represents nighttime in the model. Therefore, during the daytime/nighttime alternation, the angle shifts abruptly from 0 to values greater than 0.

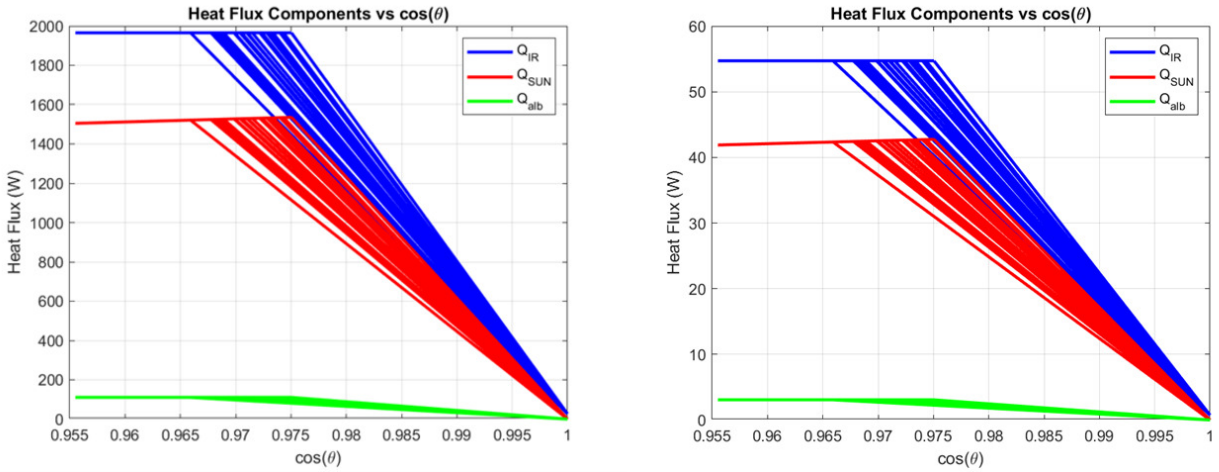

Figure 11.21: Variation of the three radiation sources for Eagle (left) and Scott (right) with $cos(\theta)$.

Thanks to the calculations presented in Section 11.2.4, it is possible to obtain a temperature value that varies with $\cos\theta$ (Figure 11.22). The minimum temperature for Eagle is 278.18 K, and the maximum is 318.00 K, both falling within the range of 273 K to 320 K. In comparison, the minimum temperature for Scott is 266.07 K, and the maximum is 303.54 K, both within the range of 263 K to 313 K. The behaviour shown in the figure is related to the fact that, in the absence of illumination, the solar elevation angle θ is equal to 0. Although cos(θ) is equal to 1, this condition represents nighttime in the model. Therefore, during the daytime/nighttime alternation, the angle shifts abruptly from 0 to values greater than 0.

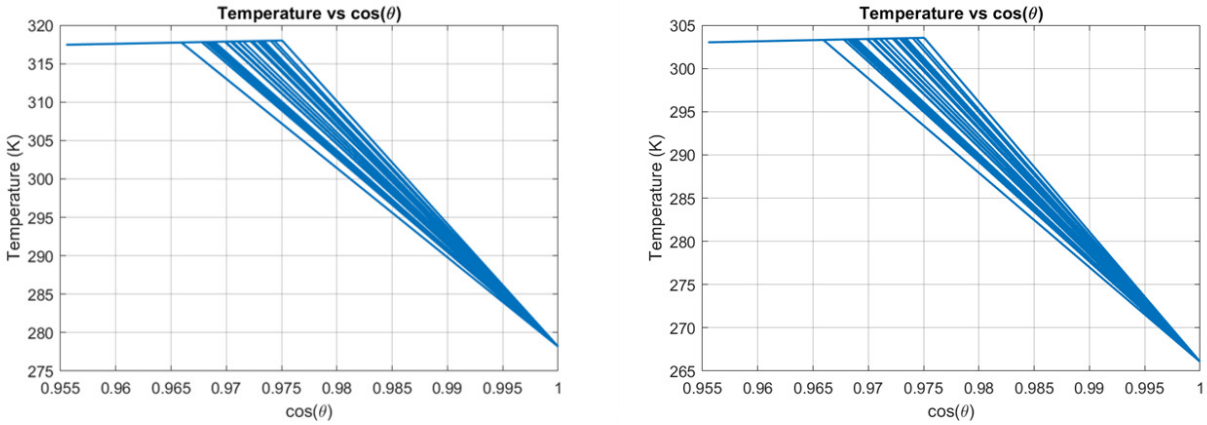

Figure 11.22: Temperature variation for Eagle (left) and for Scott (right) with cos(θ).

11.2.4.3 Steady state analysis for solar panels

Since the panels are operational during the daytime and return to a closed position during the nighttime, the temperature evaluation has been therefore carried out exclusively in the WCH. The temperature calculation Equation has been slightly modified (Equation (11.8)).

$$T_{WCHpanel} = \left(\frac{Q_{SUN} + Q_{alb} + Q_{IRmax} + Q_{intmax} - Q_{el}}{\sigma \cdot (A \cdot \varepsilon + A_{rad} \cdot \varepsilon_{rad})}\right)^{\frac{1}{4}} \quad (11.8)$$

Where

- Q_{el} is the electrical production of solar panels with a given efficiency, it doesn't contribute to the temperature increase, so it must be subtracted.
- $Q_{el} = \eta(T) \cdot S \cdot A_{panel} \cdot \cos\theta$,
- $\eta(T)$ is the efficiency that depends on the temperature and A_{panel} is the total area of solar panels.

In the case of Q_{alb} and Q_{IRmax}, the view factor is different because this is the thermal balance of a panel rather than a sphere. It is given by $[\sin(\frac{R_{Moon}}{R_{Moon}+h})]^2$, where h is the height of the panels. Table 11.23 summarizes the inputs used for this analysis.

Input parameter	Value [unit]
A_{panels}	$17.34\ [m^2]$
ε_{ext}	0.07
ε_{int}	0.50
α_{ext}	0.50
α_{int}	0.41
σ	$5.67 \cdot 10^{-8}\ [W/K \cdot m^2]$
S	$1450\ [W/m^2]$
α_{albedo}	0.14
R_{Moon}	1737.40
Q_{intmax}	$0\ [W]$
q_{IRmax}	$364\ [W/m^2]$

Table 11.23: Input parameters for Steady State Analysis (SSA) for solar panels.

Q_{intmax} is zero, since the deployable panel is not associated with any power dissipated by the Eagle's buses.
In this case, ε_{ext} and α_{ext} are the emissivity and absorptivity, respectively, of the external coating exposed to Q_{SUN}. Conversely, ε_{int} and α_{int} represent the emissivity and absorptivity of the innermost layer, which is exposed to Q_{IRmax} and Q_{alb}. Only the graph of temperature variation as a function of $\cos\theta$ is presented (Figure 11.23), as the radiation profiles follow the same trend as those shown for Eagle in Figure 11.21. Therefore, the maximum temperature value is 390.65 K, while the minimum is 389.65 K, both falling within the range of 173 K to 408 K.

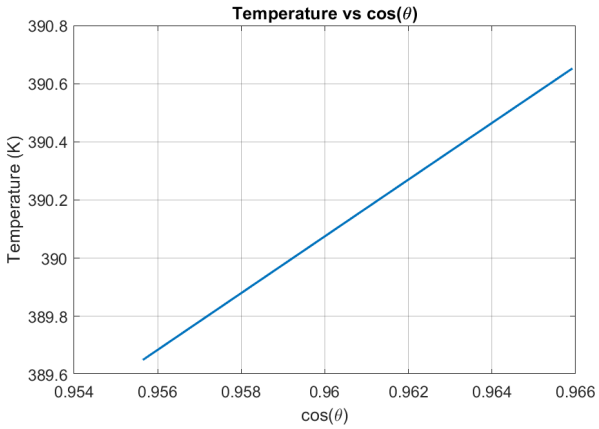

Figure 11.23: Temperature variation for solar panels with cos(θ).

11.2.5 Transient analysis

Transient thermal analysis evaluates how the temperature of a satellite and its components evolve over time in response to both external and internal thermal loads. These thermal loads are calculated using the same methodology as in the steady-state analysis. The simulation covers a one-year period, during which the input parameters remain consistent with those used in the steady-state analyses. This approach provides more accurate results compared to those obtained from steady-state analyses alone. Since an initial temperature condition is required, it is defined as the first value obtained from the steady-state analysis. For each time step the following values are computed:

- $Q_{net} = Q_{SUN} + Q_{alb} + Q_{IR} + Q_{int} + Q_{heaters} - Q_{em}$, it calculates the net heat input/output for the face considering absorbed heat, internal dissipation, radiative loss, flux emitted by the radiator or produced by the heaters.
- $dT = \frac{\Delta t \cdot Q_{net}}{m \cdot c}$, where Δt is a fixed time step set to $900\ s$ for each simulation. This value ensures sufficient accuracy, given the long total simulation period. In the denominator, m and c represent the mass and the specific heat capacity of the LPS, respectively.

At the end of the computation, the temperature of the consecutive time step is found by Equation (11.8).

$$T(i+1) = T(i) + dT(i). \tag{11.9}$$

11.2.5.1 Transient analysis for LPS

The analysis has been carried out under the assumption that LPS is fully illuminated during the LLO, descent and landing phases. For this analysis, LPS has $m = 771.90\ kg$ and $c = 1900\ \frac{J}{kg \cdot K}$. Figure 11.24 illustrates the variation of the three radiation sources as a function of time. It can be inferred that the albedo is negligible compared to the solar radiation and the infrared radiation emitted by the Moon. The solar heat flux (Q_{SUN}) is constant due to the assumption that LPS is continuously subjected to maximum illumination.

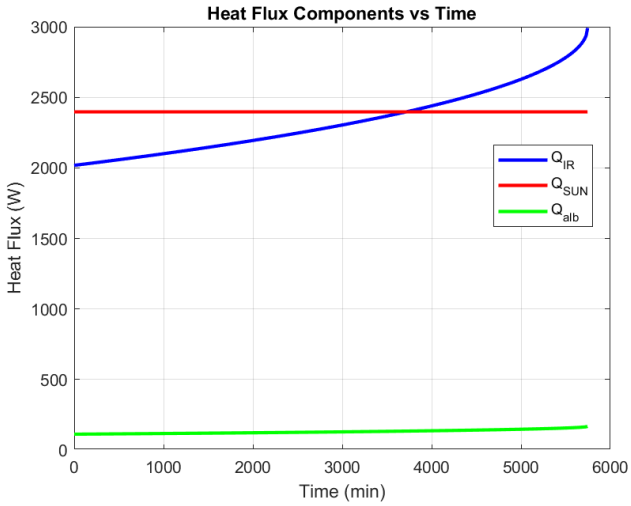

Figure 11.24: Variation of the three radiation sources for LPS over time

Thanks to the calculations presented in Section 11.2.5, it is possible to obtain a temperature value for the WCH that varies with time (Figure 11.25). Therefore, the minimum temperature value is 288.87 K, while the maximum is 300.98 K, both falling within the range of 273 K to 313 K.

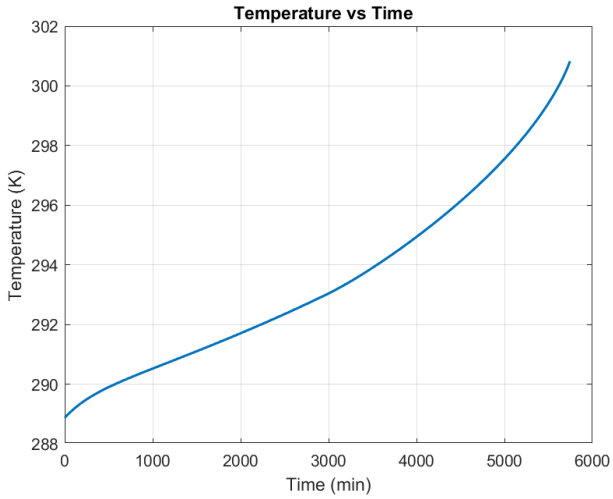

Figure 11.25: Temporal evolution of temperature for LPS

11.2.5.2 Transient analysis for Eagle and Scott

Since the calculations have been carried out over a one-year period, the WCC and WCH for Eagle and for Scott are included within the same set of results. For this analysis, Eagle has $m = 623.75\ kg$ and $c = 700\ \frac{J}{kg \cdot K}$. Instead, Scott has $m = 51.75\ kg$ and $c = 300\ \frac{J}{kg \cdot K}$. Figure 11.26 illustrates the variation of the three radiation sources as a function of time. It can be inferred that the albedo is negligible compared to the solar radiation and the infrared radiation emitted by the Moon. The variation is caused by the alternation between daytime and nighttime.

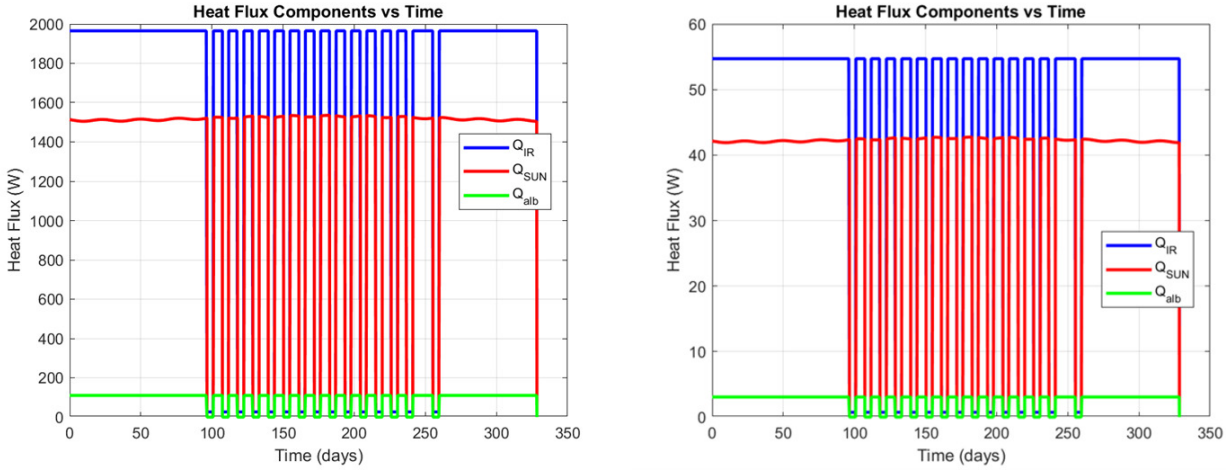

Figure 11.26: Variation of the three radiation sources for Eagle (left) and for Scott (right) over time.

Thanks to the calculations presented in Section 11.2.5 it is possible to obtain a temperature value that varies with time (Figure 11.27). The minimum temperature for Eagle is 274.08 K, and the maximum is 318.01 K, both falling within the range of 273 K to 320 K. In comparison, the minimum temperature for Scott is 264.16 K, and the maximum is 303.54 K, both within the range of 263 K to 313 K.

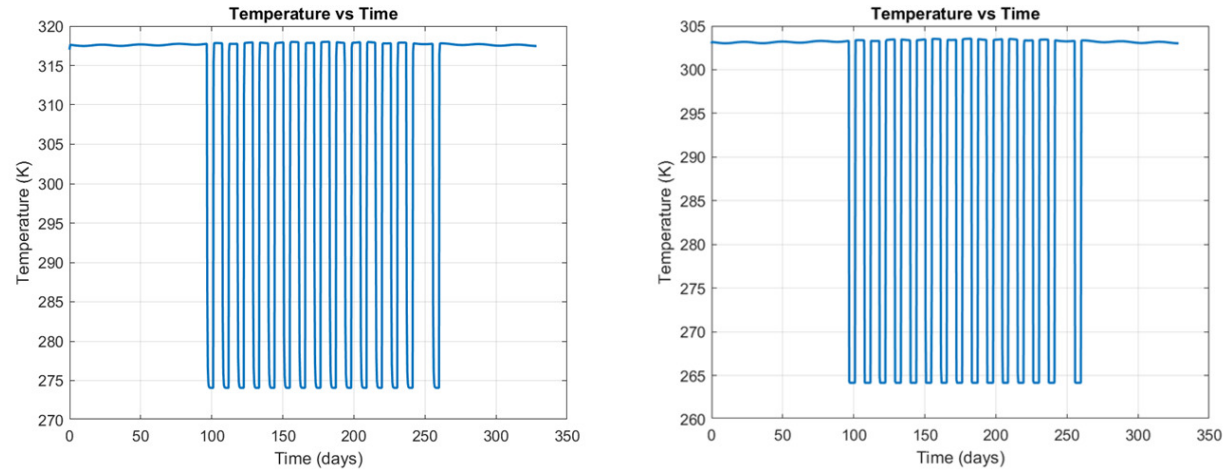

Figure 11.27: Temporal evolution of temperature for Eagle (left) and Scott (right).

11.2.5.3 Transient analysis for solar panels

Since the panels are operational during the daytime and return to a closed position during the nighttime, the temperature evaluation has therefore been carried out exclusively in the WCH. In this case, the formula for Q_{net} also includes the contribution from the electrical production of the solar panels, with all related considerations taken directly from Section 11.2.4.3. For this analysis, solar panels have $m = 66\ kg$ and $c = 900\ \frac{J}{kg \cdot K}$. Only the graph of temperature variation as a function of time is presented (Figure 11.28) as the radiation profiles follow the same trend as those shown for Eagle in Figure 11.26. Therefore, the maximum temperature value is 406.28 K, while the minimum is 305.53 K, both falling within the range of 173 K to 408 K.

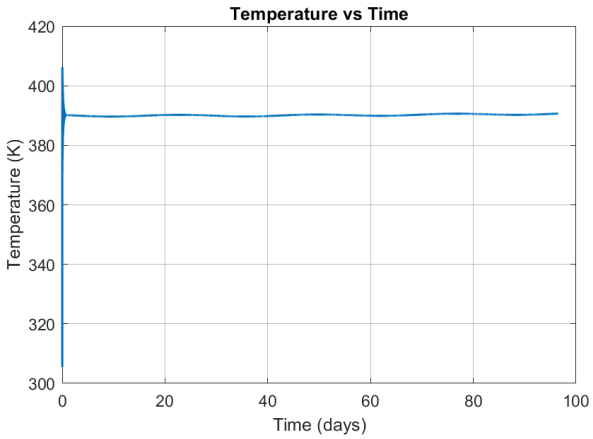

Figure 11.28: Temporal evolution of temperature for solar panels

11.3 Attitude Determination and Control Subsystem

11.3.1 Introduction

In AMPERE mission the ADCS design does not include orbital or descent phases, which are under the responsibility of the LDE [A.D. 9].

For these reasons the involvement of ADCS is limited to:

- the deployment of the LPS;
- the post-deployment phase, to determine if active stabilization is required;
- the operational phase, to ensure the correct orientation for power generation, sensors functionality and, where applicable, system mobility.

11.3.2 State-of-the-art analysis

The analysis of relevant lunar and planetary past missions provides insight into the role and implementation of ADCS for surface payloads. Specifically, this suggests that lunar and, more generally, planetary static surface elements are designed with minimal or no active attitude control post-deployment, relying on mechanical constraints and pre-deployment orientation. As for rovers, they require a GNC system. Typical sensors include Sun sensors, cameras (navigation cameras, obstacle avoidance cameras), IMUs, while actuators mainly include wheels, mast mechanisms. However, such actuators generally belong to other subsystems of the rover [R.D. 249]. Table 11.24 provides a brief overview of ADCS-related solutions employed in relevant missions.

Mission	Year	Payload	Sensors
Apollo 12, 14, 15, 16, 17	1969-1972	Apollo ALSEP (static scientific instruments) [R.D. 250].	Manually adjusted sensors and antenna pointing
Chang'e-3	2013	Yutu-1 (rover) [R.D. 249], [R.D. 254].	4 cameras: 2 navigation cameras, 2 obstacle avoidance cameras 2 Sun sensors 1 IMU 1 laser spot array indicator
Chandrayaan-3	2023	Pragyan (rover) [R.D. 255]	Stereoscopic camera-based 3D vision
VIPER	2025 (cancelled 2024)	VIPER (rover[R.D. 256],[R.D. 257]).	8 cameras: 2 stereo NavCams, 4 HazCams (one per wheel), 2 stereo AftCams 8 lamps for the cameras: 2 NavLights, 6 HazLights 1 star tracker 1 IMU
Mars Exploration Rovers (MERs)	2003	Spirit and Opportunity (rovers) [R.D. 249],[R.D. 258], [R.D. 259]	For each rover: 8 cameras: 2 panoramic cameras, 2 navigation cameras, 4 pairs of hazard avoidance cameras) 1 IMU

Table 11.24: ADCS solutions for past lunar and planetary missions

11.3.3 Preliminary design considerations supporting concept selection

The four concepts presented in Section 10.2 entail different needs from the ADCS. Based on open literature solutions, Section 11.3.2, actuators are considered unnecessary for the current concepts. Specifically, for MoonStation and the stationary unit in MoonProbe, it has been considered that tipping during deployment with ramp and operative phase can be avoided through appropriate Centre of Mass (CoM) placement and mechanical stability. The selection of pointing mechanisms, masts and wheels, both for deployment and mobile elements, remains under the responsibility of WP 3.5. Across all concepts, the baseline sensor suite includes Sun sensors, for solar panel orientation and Sun-tracking, and IMUs, to detect undesired movements after deployment. For concepts involving mobility (MoonGrid, MoonProbe and MoonRover) the position/attitude determination capability, the environmental perception, the path planning and the motion control are essential [R.D. 249]. For these reasons, not only Sun sensors and IMUs, but also stereo cameras are needed to be implemented in the GNC system. Star trackers and illumination systems are not considered necessary, as operations are not expected during the nighttime and the systems are assumed to remain powered down.

In MoonStation an IMU is required to monitor the station's stability and detect any unintentional rotation. A coarse-grade IMU is sufficient for this purpose. Sun sensors are necessary to ensure that solar panels remain correctly oriented toward the Sun.

In MoonGrid each mobile element is equipped with IMUs, Sun sensors and stereo cameras. For this reason, compared to the MoonStation concept, a higher accuracy IMU is necessary.This, together with the inclusion of stereo cameras, while crucial for autonomy, has implications in terms of mass, power and integration, particularly considering the smaller size of the units compared to the larger, stationary platforms in MoonStation and MoonRover.

In MoonProbe the stationary unit adopts the same configuration as in MoonStation. The single mobile element requires the same sensor suite as in MoonGrid, though the GNC requirements are slightly relaxed due to a simpler navigation environment with fewer agents and interactions.

MoonRover combines the features of MoonGrid with the GNC functionalities of mobile elements, like in MoonGrid. Due to the system's larger size, some of the integration constraints seen in MoonGrid may be alleviated.

Table 11.25 contains an overview of the sensors required for each concept. The exact number of sensors is not specified.

Concept\Hardware		IMUs	Pairs of cameras	Sun sensors
MoonStation	LPM + LSM	V (coarse)	X	V
MoonGrid	LPM + LSM 1	V	V	V
	LPM + LSM 2	V	V	V
	LPM + LSM 3	V	V	V
MoonProbe	LPM	V (coarse)	X	V
	LSM	V	V	V
MoonRover	LPM + LSM	V	V	V

Table 11.25: Preliminary ADCS sensors selection for the concepts

11.3.4 Final design

For the selected concept MoonProbe, WP 3.3 has analysed the external disturbance torques acting during the circular orbit and elliptical transfer. In addition, it has studied the descent of Eagle housing Scott from the ramp, with the objective of avoiding tip-over and ensuring that the wheels rolled without slipping. It has been also verified that no tip-over occurred during operations. The sensors required by Eagle during the descent and operational phase have been identified, and a preliminary design of the GNC system for Scott has been also performed.

11.3.4.1 ADCS modes

This paragraph provides an overview of the ADCS modes for MoonProbe. This enables the definition of the ADCS active hardware during the control modes defined in Section 10.6.1.2, both for Eagle and Scott. The ADCS modes are defined also for Argonaut during the LOI and D&L phases, however the hardware selection has not been performed as the required function is assumed to be managed by the LDE [A.D. 9].

11.3.4.1.1 Argonaut ADCS modes

1. Orbit control mode: while Argonaut is orbiting around the Moon, the ADCS of the LDE maintains the z-axis of the Body Reference Frame (BRF), defined in Section 11.5.3.5, anti-parallel to the x-axis of the Orbital Reference Frame (ORF) corresponding to a 270° pitch rotation. The ORF is defined with the z-axis pointing towards the Moon's centre, the y-axis antiparallel to the orbital angular momentum vector and x-axis to complete the right-

handed tern. This orientation ensures that the thrusters are aligned to the correct direction to provide impulsive ΔV, as required by the WP 3.6.

2. Braking burn mode: a pitch rotation of -27.72° (defined in Section 11.6.3.1) is performed with an accuracy <0.01°, to achieve the correct attitude at perilune for the braking burn.
3. Pitch-up manoeuvre mode: the pitch angle varies from 242.28° to 180°, with a pitch rate of 5 °/s [A.D. 9] to start the vertical descent.
4. Vertical descent mode: the ADCS of the LDE maintains a 180° pitch angle to ensure vertical descent.

11.3.4.1.2 Eagle ADCS modes

1. Ramp descent mode: this mode is active during the EAGLE-COMM, EAGLE-DESN, EAGLE-RDEP system modes. The braking torque required to reach the end of the ramp at 0 m/s for safety reasons, is computed using the ramp inclination and landing site slope, measured by an inclinometer, and the acceleration provided by the IMU. Additionally, the IMU provides angular rates, which can be monitored to detect potential tip-over events. The IMU and the inclinometer are on to continuously monitor any tipping or abnormal tilting of Eagle, once on the ground. The CSSs are used to detect approximately the Sun direction. This can be done as the Sun sensors are mounted on each surface of Eagle's plate, excluding the one facing the lunar surface, specifically two per side for redundancy reasons.
2. Second commissioning mode: this mode is active during EAGLE-SECCOM system mode. The inclinometer is standby, as it has already been checked during EAGLE-COMM system mode, the IMU is on to monitor any tipping of Eagle, the FSSs are turned on to be checked.
3. Nominal daytime operation mode: this mode is active during EAGLE-PGEN system mode, apart from the IMU, the inclinometer and the CSSs, the 2 FSSs are active to perform the Sun tracking with an accuracy of 0.1°. During this mode diagnostic use of the CSSs can be made in the event of anomalous power generation. CSSs help distinguish between a failure of the FSSs, resulting in incorrect orientation, and fault in the solar arrays themselves.
4. Idle mode: this mode is active during the EAGLE-NIGHT and EAGLE-SAFE system modes. All the ADCS sensors are standby apart from the CSSs which monitor during the night for the return of solar illumination and the IMU which is off to reduce the power consumption.
5. Off mode: this mode is active during the EAGLE-CRS, EAGLE-CHG, EAGLE-SENSOR, EAGLE-INTL and EAGLE-EOL system modes, where all the ADCS hardware is considered to be turned off.

11.3.4.1.3 Scott GNC modes

1. Release mode: this mode is active during SCOTT-P&REL system mode, one of the two redundant IMUs and the ten CSSs (two per Scott side, excluding the one facing the lunar surface) are turned on.
2. Navigation mode: this mode is active during the SCOTT-COMM, SCOTT-NEM and SCOTT-NIGHT system modes. The mobility, the two cameras, the LEDs, one IMU and the CSSs are turned on, to ensure correct navigation. Note that with respect to Section 11.3.3, lights have been considered as nighttime operations are present.
3. Idle mode: active during SCOTT-EM, SCOTT-RCG and SCOTT-SAFE system mode. 1 IMU is on, and mobility is at minimum power to keep Scott stationary.
4. Off mode: this mode is active during the SCOTT-OFF, SCOTT-UPL, SCOTT-INTL and SCOTT-EOL system mode. All the GNC sensors and mobility are considered to be turned off.

11.3.4.2 Circular orbit and elliptical transfer external disturbances analysis

In a lunar orbit the main sources of external torques are the Gravity Gradient (GG) and the Solar Radiation Pressure (SRP).

GG torque arises from the gravitational field acting on an extended, nonsymmetric body. It depends on the distance between the spacecraft and the main body, and it does not originate from the non-uniformities of a planet's gravitational field, but rather from the variation in gravitational force acting on different parts of an extended body. In some cases, the GG torque can be stabilizing as it tends to align the minimum inertia axis to the local vertical [R.D. 181]. The SRP torque instead depends on the solar activity, on the surface exposed to Sun, on the surface reflectivity, spacecraft geometry and CoM position[A.D. 10].

11.3.4.2.1 Gravity gradient torque

The GG torque is evaluated considering the Equation (11.10). During circular orbit and elliptical transfer, Argonaut is modelled as a single rigid body, subject to the gravitational influence of a single, spherically symmetric central attractor. For this evaluation the considered central body is the Moon, the GG due to Earth is neglected as the maximum norm of GG torque due to Earth has been estimated to be of order $10^{-7} N \cdot m$.

$\underline{G}$ is the GG torque, $\mu = 4.90 \cdot 10^{12} \frac{m^3}{s^2}$ [R.D. 182]is the standard gravitational parameter of the Moon, $\underline{I}$ is the spacecraft inertia matrix with respect to BRF axes, provided by WP 3.5 and $\underline{R_0}$ is the position vector of the spacecraft CoM with respect to the Moon centre, evaluated considering as input the orbital dynamics provided by WP 3.6. All the vector quantities are expressed in the BRF.

$$\underline{G} = \frac{3\mu}{R_0} \hat{R}_0 \times \left(\underline{I} \cdot \hat{R}_0 \right) \tag{11.10}$$

Figure 11.29 shows the norm of the GG vector during one circular orbit and the elliptical transfer orbit, as a function of the true anomaly. The change in trend at the end of the elliptical transfer orbit is due to the change of attitude required to properly orient the thrust vector for the braking burn (Section 11.3.4.1.1).

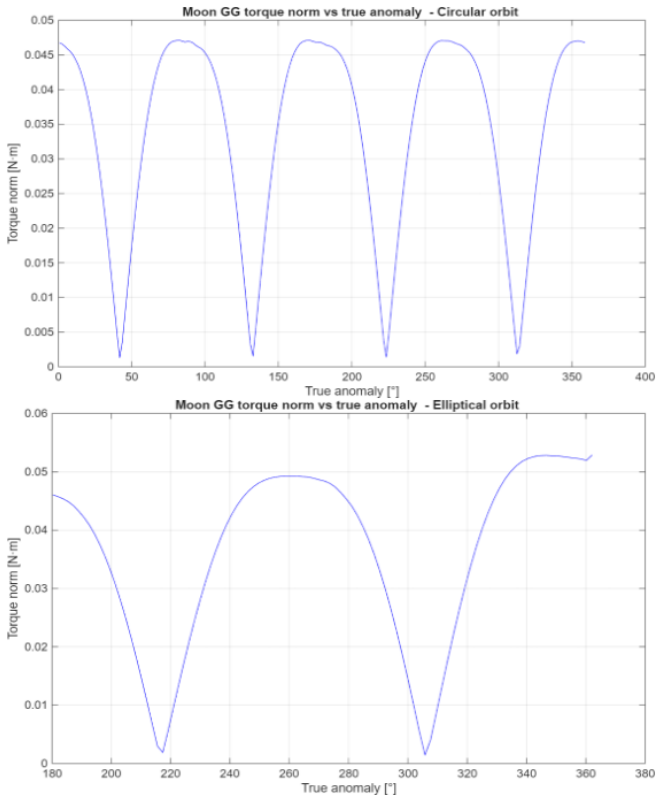

Figure 11.29: Norm of the GG torque during one circular orbit and elliptical transfer orbit

The maximum GG torque, reported in Table 11.26**,** occurs at the perilune of the elliptical transfer orbit. These values indicate that the GG due to Earth can be reasonably neglected.

11.3.4.2.2 Solar radiation pressure torque

To evaluate the torque generated by the SRP on the Argonaut lander, a simplified geometric model is adopted, approximating the structure as a regular octagonal prism. Each surface of this model, including the top, bottom, and eight lateral faces, is characterized by its area, unit normal vector, and the position of its geometric centre $\underline{r}$ relative to the CoM, assumed in the geometric centre of the prism for this calculation. The geometric features values are extracted from [A.D. 16].

The incident solar direction vector in the BRF is computed at each time step based on the Sun direction as described in Section 11.6.3.2.The solar constant S is considered equal to $1450 \frac{W}{m^2}$ [R.D. 178].

For each illuminated surface (i.e., those with a positive dot product between the surface normal and solar direction), the torque contribution is computed assuming the SRP torque model in Equation (11.11)[R.D. 183]:

$$\underline{M_{SRP}} = \frac{S}{c} A_s (1+q) \underline{r} \cos(\theta) \tag{11.11}$$

This model considers the SRP force proportional to the cosine of the angle of incidence θ (angle between the surface normal and the Sun direction), surface area A_S, and SRP $\frac{S}{c}$ (being $c = 3 \cdot 10^8 \frac{m}{s}$ the speed of the light), with a constant reflectance factor q (ranging from 0 to 1), assumed unitary to perform a conservative evaluation.

The maximum SRP torque is reported in Table 11.26, it is two orders of magnitude lower with respect to the GG torque, which is the main contribution.

Torque	Maximum value $(N \cdot m)$	Components in the BRF $(N \cdot m)$
GG	$5.29 \cdot 10^{-2}$	$(-1.18, 0.82, -5.09) \cdot 10^{-2}$
SRP	$1.31 \cdot 10^{-4}$	$(0.02, 0, 1.31) \cdot 10^{-4}$

Table 11.26: Maximum disturbance torques during circular orbit and elliptical transfer

11.3.4.3 Ramp descent analysis

The free body diagram reported in Figure 11.30 can be used to perform a preliminary analysis of the descent down the ramp. The aim is to define an acceptable region for the position of the CoM in which both the tip over of Eagle housing Scott is avoided, and the wheels roll without slipping. The problem is studied in the longitudinal plane as symmetry assumption is done in the lateral plane.

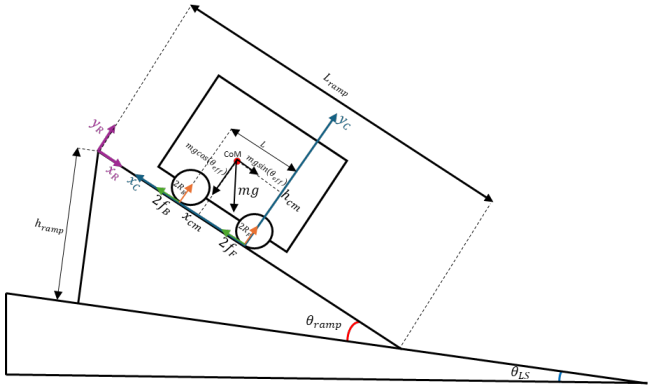

Figure 11.30: Eagle housing Scott during the descent free body diagram

- $\theta_{ramp} = 26°$ is the ramp inclination angle, provided by WP 3.5.
- $\theta_{LS} = 8°$ is the landing site slope, provided by WP 3.7.
- The reference frame centred in the contact point of the front wheel with the ramp is the constructive reference frame, x_C axis is aligned to the ramp and points towards the rear wheel, y_C is orthogonal to x_C pointing upward.
- (x_{cm}, h_{cm}) are coordinates of the CoM (red dot in Figure 11.30) in the constructive reference frame.
- x_R and y_R are the axes of the ramp reference frame, solidly to the ramp.
- $h_{ramp} = 3\ m$ is the height of the ramp with respect to the ground, equal to the LDE height [A.D. 9].
- $L = 9.62 \cdot 10^{-1} m$ is the distance between the centres of the wheels.
- $m = 675.50\ kg$ is the mass of Eagle housing Scott.
- $g = 1.62 \frac{m}{s^2}$ is the acceleration due to Moon's gravity.

To design a safe descent, the worst-case scenario is considered: θ_{LS} is the highest slope within the safe ellipse and the lander touches down on a downhill slope. The total slope to which Eagle is subjected is θ_{eff}, evaluated as in Equation (11.12).

$$\theta_{eff} = \theta_{LS} + \theta_{ramp} \tag{11.12}$$

At the CoM the weight mg is acting. Its components relative to the inclined ramp are:

- $mgcos(\theta_{eff})$, perpendicular to the ramp;
- $mgsin(\theta_{eff})$, parallel to the ramp.

The reaction forces are denoted as:

- R_B, reaction force on each back wheel;
- R_F, reaction force on each front wheel.

Due to the assumed symmetry of the system, the total vertical reaction forces acting on the front and rear wheels are $2R_B$ and $2R_F$, respectively. Similarly, friction forces are:

- f_B, reaction force on each back wheel;
- f_F, reaction force on each front wheel.

To determine the unknown forces, two equations in two unknowns are imposed: translational equilibrium along the y_R (equation (11.13)) and rotational equilibrium about the contact point of the front wheel with the ground (Equation (11.14), assuming clockwise moments as positive).

$$2R_B + 2R_F - mgcos(\theta_{eff}) = 0 \tag{11.13}$$

$$mgsin(\theta_{eff})h_{cm} - mgcos(\theta_{eff})x_{cm} + 2R_B L = 0 \tag{11.14}$$

By solving the system of equations, the reaction forces can be expressed as a function of the CoM position (Equations (11.15) and (11.16)).

$$R_B = \frac{mg}{2L}\left(x_{cm}\cos(\theta_{eff}) - h_{cm}\sin(\theta_{eff})\right) \tag{11.15}$$

$$R_F = \frac{mg}{2L}\left[(L - x_{cm})\cos(\theta_{eff}) + h_{cm}\sin(\theta_{eff})\right] \tag{11.16}$$

To ensure that the lander does not tip-over, both R_B and R_F must remain positive. This condition leads to the admissible interval for h_{cm} as a function of x_{cm} shown in relation (11.17).

$$(x_{cm} - L)\ \cot(\theta_{eff}) < h_{cm} < x_{cm}\cot(\theta_{eff}) \tag{11.17}$$

The descent is divided into two phases: an initial segment without braking to initiate motion, followed, starting from position $x_R = L_1$, by a braking phase aimed at bringing the vehicle to $v_{f,ramp} = 0\frac{m}{s}$ by the end of the ramp. In both cases a horizontal internal force F is introduced to model the constraint between front and rear wheels. During the braking, a braking torque τ_{BR} is applied to the front wheels only. This design choice is justified by the higher vertical load R_F on the front wheels with respect to R_B in the considered configuration. This implies that the friction on the front wheels can be greater before slipping occurs, making it easier to prevent slippage when applying the braking torque to the front wheels only (equations (11.27) and (11.28)). The absence of τ_{BR} in (11.15) and (11.16) is justified by assuming that the braking torque is entirely absorbed by the wheel's rotational dynamics, with no transmission to the body through the axles. Figure 11.31 shows the free body diagram employed in the analysis of the wheels dynamics.

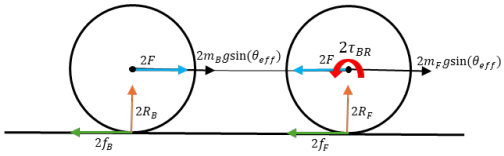

Figure 11.31: Free body diagram of the wheels

The mass distribution is represented as effective masses acting on the wheels, specifically m_B (Equation (11.18)) and m_F (Equation (11.19)) are the effective masses acting on each of the back and front wheel, respectively.

$$m_B = \frac{R_B}{\mathrm{g}\cos(\theta_{eff})} \tag{11.18}$$

$$m_F = \frac{R_F}{\mathrm{g}\cos(\theta_{eff})} \tag{11.19}$$

Assuming the wheels are part of a rigid body (i.e., the same tangential acceleration at front and rear), and considering wheel radius R_W, and moment of inertia I_W, the following system of four equations in the unknowns F, f_B, f_F and τ_{BR} can be solved:

- Equation (11.20) represents the back wheel dynamics.

$$m_B a_{req} = m_B g sin(\theta_{eff}) - f_B + F \tag{11.20}$$

- Equation (11.21) represents the front wheel dynamics.

$$m_F a_{req} = m_F g sin(\theta_{eff}) - f_F - F \tag{11.21}$$

- Equation (11.22) imposes that the rolling acceleration of the front wheel is equal to the acceleration a_{req}.

$$\frac{f_F R_w^2 - \tau_{BR} R_W}{I_w} = a_{req} \tag{11.22}$$

- Equation (11.23) imposes that the rolling acceleration of the back wheel is equal to the acceleration a_{req}.

$$\frac{f_B R_w^2}{I_w} = a_{req} \tag{11.23}$$

The required acceleration in the braking phase, a_{req} is computed from the kinematic condition of uniformly accelerated motion, to reduce velocity from $v_{no,brake}$ to $v_{f,ramp}$ in the distance $L_{ramp} - L_1$ (Equation (11.24)).

$$a_{req} = \frac{v_{f,ramp}^2 - v_{no,brake}^2(L_1)}{2(L_{ramp} - L_1)} \tag{11.24}$$

$v_{no,brake}(L_1)$ is given by Equation (11.25):

$$v_{no,brake}(L_1) = \sqrt{(2a_{no,brake})(L_{ramp} - L_1)} \tag{11.25}$$

The acceleration $a_{no,brake}$ in the initial, unbraked descent is obtained from Newton's second law Equation (11.26). Considering $\tau_{BR} = 0$ in the system of equation used for the braking phase, then $f_B = f_F = f$, and Equations (11.20), (11.21) and (11.26) constitute a system of three equations in three unknowns (f, F, and $a_{no,brake}$).

$$4f = mgsin(\theta_{eff}) - ma_{no,brake} \tag{11.26}$$

To maintain rolling without slippage, the following friction conditions must be satisfied (equations (11.27) and (11.28)):

$$f_B \leq \mu_{ramp} R_B \tag{11.27}$$

$$f_F \leq \mu_{ramp} R_F \tag{11.28}$$

By substituting the expressions for R_B and R_F into Equations (11.27) and (11.28), a second constraint on the CoM is obtained (Equation (11.29)):

$$cot(\theta_{eff})x_{cm} + \frac{2Lf_F}{\mu_{ramp} mgsin(\theta_{eff})} - Lcot(\theta_{eff}) \leq h_{cm} \leq cot(\theta_{eff})x_{cm} - \frac{2Lf_B}{\mu_{ramp} mgsin(\theta_{eff})} \tag{11.29}$$

The torque required to have a_{req} is in Equation (11.30) which must be lower than τ_{MAX} (Equation (11.31)), this can be obtained by imposing that the lower bound of Equation (11.29) has a smaller intercept than the upper bound, as both have the same slope. The dependence on the braking torque is contained in f_F.

$$\tau_{BR} = \frac{1}{2} mgsin(\theta_{eff}) R_W - a_{req}\left(\frac{mR_W}{2} + \frac{2I_W}{R_W}\right) \tag{11.30}$$

$$\tau_{MAX} = \frac{\cos(\theta_{eff}) mg\mu_{ramp} R_W}{2} - \frac{a_{req} I_W}{R_W} \tag{11.31}$$

The acceptable region for the CoM is defined by the intersection of the intervals derived from the tip-over condition (Equation (11.17)) and the pure rolling condition (Equation (11.29)). To ensure motion initiation at the start of the ramp, the static friction coefficient should enable the component of the weight parallel to the ramp to be larger than the total static friction. Considering the actual data, the maximum value of the coefficient is 0.67 , for this reason the ramp friction coefficient is not constant: the second segment of the ramp the static friction coefficient of $4.17 \cdot 10^{-1}$ is estimated by scaling the dynamic friction between titanium and CFRP [R.D. 184] by a factor of 1.5. For the remaining three ramp segments, a higher static friction coefficient of 1.10 is assumed, accounting for the application of a surface coating as described in (Section 11.5.3.3). This ensures that, given the CoM coordinates $(0.75\ m, 0.65\ m)$ provided by the WP 3.5, all the safety constraints are satisfied.

In the analysed case:

- $R_W = 40.90 \cdot 10^{-2} m$ (Section 11.5.3.1);
- I_W is evaluated considering the wheel as a uniform disk, with the mass of the wheel reported in Section 11.5.3.1;
- $L_1 = 0.01\ m$ to start the braking phase, while the velocity is still low and so the braking torque is lower.

For $x_{CM} \in [0, L]$ and $h_{CM} \in [R_W, 2.08\ m]$(the last value is the height of Eagle housing Scott, provided by WP 3.5), considering the values indicated in this paragraph, the bounds both for the no braking and the braking phase are evaluated. The acceptable regions obtained in the two cases are the green ones in Figure 11.32 and Figure 11.33, respectively. In both cases the CoM lies within this region, confirming that under the worst-case conditions, the wheels maintain pure rolling without slippage and the system remains tip-over stable. During the braking phase $\tau_{BR} = 125.32\ \mathrm{N \cdot m}$, which is acceptable as it is lower both than τ_{MAX} $(204.08\ N \cdot m)$ and of the maximum torque that can be provided by the brakes selected in W.P. 3.5 $(264.48\ N \cdot m)$. Intersecting the two regions Equation (11.32) can be obtained.

$$1.48\ x_{CM} - 0.55\ m < h_{CM} < 1.48\ x_{CM} - 0.02\ m \tag{11.32}$$

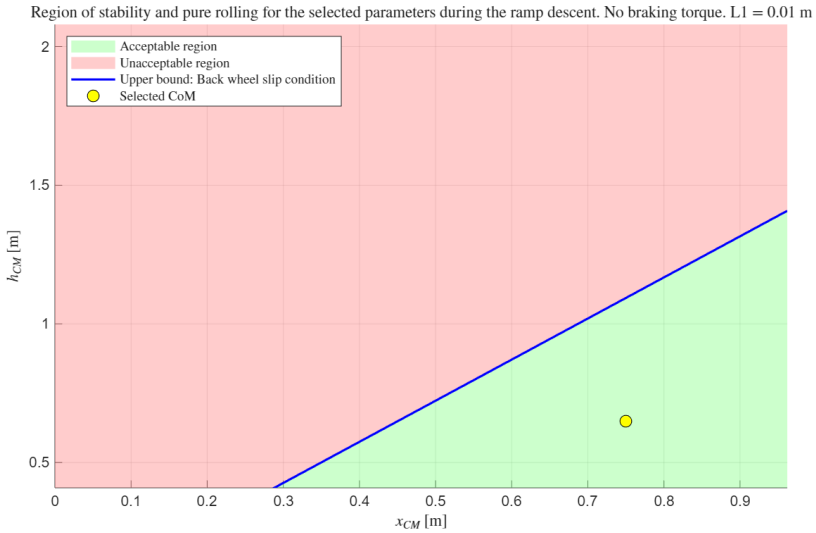

Figure 11.32: Acceptable region for the CoM during the no braking phase

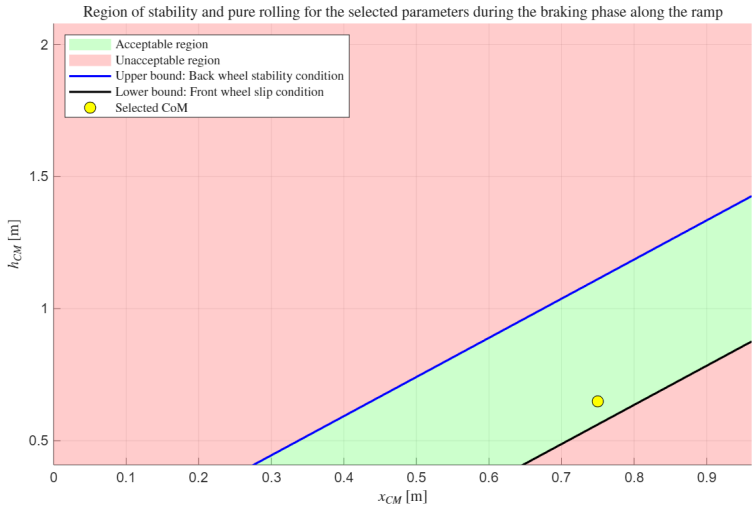

Figure 11.33: Acceptable region for the CoM during the braking phase

At this stage, it is possible to verify that Eagle does not tip-over during nominal operations (stationary and with the solar panels are deployed). Two worst-case scenarios are considered (the mass considered in the evaluations is the Eagle's one):

- Downhill case: Eagle is along a slope equal to the maximum inclination of the landing site, and the panels are deployed such that their normal lies within Eagle's longitudinal plane. In this configuration, a forward tip-over could occur. To exclude this condition, it is verified that the rear normal force R_B (Equation (11.25)) remains positive, in this case $R_B = 277.47\ N$. The centre of mass location provided by WP 3.5 is $(0.66, 0.90)\ m$ and the mass considered is that of Eagle.
- Uphill case: Eagle is along a slope equal to the maximum inclination of the landing site, and the panels are deployed such that their normal is orthogonal to Eagle's longitudinal plane. In this case, a backward tip-over may occur. Here, R_F is computed using Equation (11.33). The centre of mass position is $(0.68, 0.90)\ m$, resulting in $R_F = 80.88\ N$.

$$R_F = \frac{mg}{2L}\left[(L - x_{cm})\cos(\theta_{LS}) - h_{cm}\sin(\theta_{LS})\right] \tag{11.33}$$

11.3.4.4 Scott GNC

The block diagram provided in Figure 11.34 represents the GNC architecture adopted for Scott.

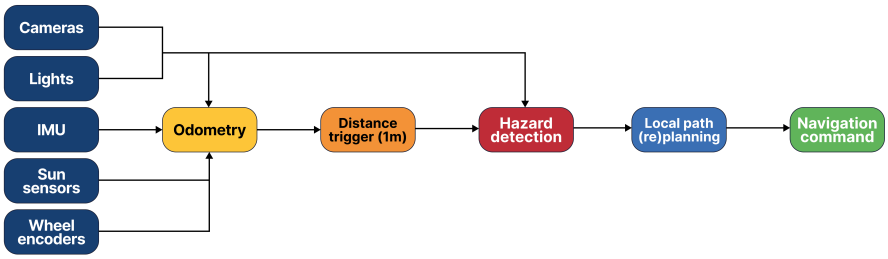

Figure 11.34: Scott GNC architecture

Scott operates on an energy budget provided by the W.P. 3.1, following a fixed 7-hour activity cycle both during daytime and nighttime. During the daytime, the rover allocates 1 hour to move away from the base station, 5 hours to remain stationary, and 1 hour to return. At night, the cycle is adjusted to 3 hours of total mobility and 4 hours of stationary operations.

As shown in Figure 11.34, sensor inputs from stereo cameras, IMU, Sun sensors, and wheel encoders are continuously integrated by the odometry module to estimate relative displacement. The lights are needed to ensure cameras visibility in case of shadows and during nighttime. Sun sensors enable both the recognition of daytime and nighttime and a better heading estimation [R.D. 185]. Every meter of motion triggers a hazard detection routine, which uses stereo disparities to assess safety [R.D. 186]. If obstacles are detected, the local path (re)planning module computes a new trajectory, which joins the original one, to avoid them. If no hazards are found, the rover proceeds along the planned straight segment. Navigation commands are issued accordingly, with a control logic based on 1-meter increments, balancing autonomy with computational simplicity, which is required considering that Scott is a resource-limited platform [R.D. 185].

Upon completion of its traversal, the rover stores the forward path and mirrors it for the return phase. Additionally, the interlink with Eagle supports relative positioning updates and helps maintain situational awareness, while absolute position updates are periodically possible as described in Section 11.4.6.

According to [R.D. 185], due to its vicinity to the terrain, a camera resolution of 1 megapixel guarantees a good pixel density at ground, similar to the one of larger rovers which have higher resolution cameras.

11.3.4.5 Hardware selection

The selection of hardware for Eagle is primarily based on the assumption that no actuators are required, as the descent has been designed to remain safe even under worst-case conditions. Therefore, only the choice of sensors is justified for this platform. In contrast, for Scott, the actuators are represented by the mobility system described in Section 11.3.4.5.2.

11.3.4.5.1 Sensors selection

This Section provides an overview of the sensors selected for Eagle and Scott, the main features of these are underlined.

The STIM377H IMU provided by Safran (Figure 11.35) is a hermetically sealed Micro Electronic Mechanical System (MEMS).

Figure 11.35: Safran STIM377H IMU [R.D. 187]

It provides outputs of angular velocity, integrated angles, linear acceleration, and integrated velocity. The unit features environmental robustness (operating range 233 K to 358 K, shock up to 500 g, MIL-STD-883J Class H), and compact packaging making it suitable for mass and volume constrained applications.

The gyroscope bias instability of 0.3 °/h, accelerometer bias instability of 0.04 mg and resolution of 1.9 µg ensure sufficient precision both for Scott's GNC and for the detection of translational accelerations and potential tip-over of Eagle during ramp descent and post-deployment operations.

Safran reports heritage in space-grade applications, including launch vehicle navigation systems and satellite attitude and orbit control systems, indicating space environment exposure. However, no evidence of passed missions using this hardware has been found, then a TRL of 5 is considered appropriate [R.D. 187].

1 IMU is on Eagle, 2 redundant IMUs are on Scott, these latter are not in function contemporary. The main features of the IMU are collected in Table 11.27.

Weight (g)	55
Power consumption (W)	1.5
Dimensions (mm)	39 x 45 x 22
Operating temperature (K)	233 to 358
TRL	5

Table 11.27: Safran STIM377H IMU specifications [R.D. 187]

The Honeywell HMR3000 (Figure 11.36) is a digital compass module considered for Eagle mainly due to its integrated fluid-based inclination sensor. This specific functionality is needed for both the static assessment of the landing site slope and for the evaluation of the braking torque required during the descent down the ramp.

Figure 11.36: Honeywell HMR3000 inclinometer [R.D. 188]

The device offers a tilt accuracy of ±0.4 ° (for inclinations below 20°) and a resolution of 0.1 degrees, with a broad tilt range of ±40°.
The HMR3000 complements the STIM377H IMU by providing a stable and independent absolute orientation reference, particularly valuable during static conditions when the power station is deployed on the lunar surface.
For its intended use in this specific lunar context, the HMR3000 is assigned an estimated TRL of 5. While its operating principle is appropriate and its inclination accuracy specifications are promising, extensive qualification and testing activities are necessary to validate its performance and durability under the Moon's conditions [R.D. 188]. HMR3000 specifications are summarized in Table 11.28.

Weight (g)	92
Nominal supply current at 6 V (mA)	35
Dimensions (mm)	38.1 x 106.7 x 22.2
Operating temperature (K)	253 to 343
TRL	5

Table 11.28: Honeywell HMR3000 inclinometer specifications [R.D. 188]

The RedwireSpace CSS (Cosine Type), shown in Figure 11.37 is a compact, passive sensor designed to measure the angle of incident solar radiation with respect to the sensor's normal axis. By providing a voltage output proportional to the cosine of the Sun's angle, it enables coarse Sun vector determination.

Figure 11.37: RedwireSpace CSS [R.D. 189]

In addition to measuring the Sun's angle for solar array coarse orientation, this sensor is useful to detect the presence or absence of sunlight, during Eagle's operations. Integrated with inertial sensors such as the STIM377H IMU and cameras, the CSS can be used for Scott's GNC. To ensure comprehensive coverage and redundancy, two CSSs will be installed on each of the faces, excluding the one facing the ground, of both in Eagle and Scott. Given its demonstrated flight heritage and maturity in lunar environment, the RedwireSpace CSS can be assigned a TRL of 9 [R.D. 189]. Specifications are provided in Table 11.29.

Weight (g)	10

Power consumption (W)	0
Dimensions (mm)	28 x 19 x 12
TRL	9

Table 11.29: RedwireSpace CSS [R.D. 189]

The NewSpace Systems NFSS-411 (Aquila-D02) FSS (Figure 11.38) is a compact, low-power, high-precision digital Sun sensor based on synthetic sapphire optics and a photodiode array architecture. Considering the features in Table 11.30, it is well suited for solar tracking applications [R.D. 190]

Figure 11.38: NewSpace Systems NFSS-411 (Aquila-D02) FSS [R.D. 190]

2 NFSS-411 sensors are installed on base of the cylinders of solar panels of Eagle to enable precise Sun vector estimation for optimal solar array orientation. These sensors operate together with CSSs, which provide low-resolution but omnidirectional Sun detection capabilities.
Given its extensive use in space missions and its qualification against harsh conditions, the NFSS-411 is assigned a TRL 8 for this application as direct lunar surface flight heritage is not confirmed.

Weight (g)	37
Power consumption (mW)	150
Dimensions (mm)	34 x 40 x 20
Operating temperature (K)	248 to 343
Accuracy (°)	±0.1° root mean square
FOV (°)	140
TRL	8

Table 11.30: NewSpace Systems NFSS-411 (Aquila-D02) FSS [R.D. 190]

The stereo vision system employed on Scott leverages heritage from the Comet Infrared and Visible Analyzer (CIVA) camera system flown on the Philae lander of ESA's Rosetta mission (Figure 11.39) [R.D. 191]. Specifications are provided in Table 11.31 In the Scott configuration, a stereo pair of cameras is mounted on a fixed baseline to enable both autonomous navigation and hazard detection during traverse.

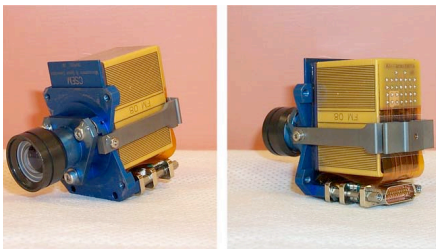

Figure 11.39: CIVA's cameras [R.D. 191]

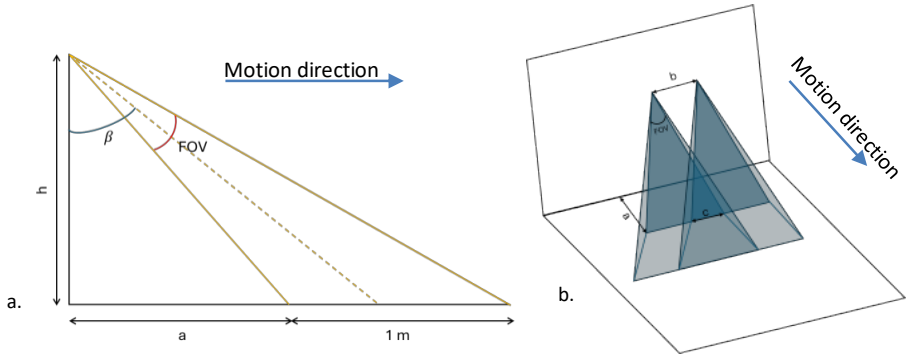

Figure 11.40: Diagram of the stereo imaging geometry in direction of the motion (a.) and in perspective (b.)

Figure 11.40 shows a diagram of the imaging geometry assuming square FOV, in the following considerations are done based on this scheme. The cameras are positioned at a height of $h = 20\,cm$ from the ground, within the section housing the lower units of the CubeRover, with a baseline $b = 4\,cm$. To ensure a swath width of 1 meter, equal to the distance crossed by Scott at each step of the path (Section 11.3.4.4), the geometric constraint in Equation (11.34) must be satisfied:

$$h\tan\left(\beta - \frac{FOV}{2}\right) + 1 = h\tan\left(\beta + \frac{FOV}{2}\right) \tag{11.34}$$

Solving this equation results in an angle of $\beta = 49.42°$. With this configuration, the FOV does not cover the region within $a = 0.071\,m$ from Scott, meaning that this portion of ground is outside the stereo vision coverage in the current step. However, since the rover moves forward in 1-meter increments, and stereo vision becomes available starting from a, this segment was already within the stereo overlap during the previous step of the path, and thus the hazard detection for it has already been completed.

At the distance a the parameter c, which indicates the intersection of the camera swaths, can be determined by inverting the Equation (11.35), which is valid assuming a flat lunar surface and considering that each triangle in Figure 11.40.b is isosceles.

$$2\left(\frac{h\tan\left(\frac{FOV}{2}\right)}{\cos\left(\beta - \frac{FOV}{2}\right)} - c\right) + c = b \tag{11.35}$$

Solving this $c = 20.48\,cm$, which is acceptable considering that the width of the CubeRover in the direction transverse to motion is 20 cm.

Given the direct flight heritage of the CIVA cameras on the Rosetta mission and their demonstrated operation on the surface of a small body in the extremely hostile environment of a cometary surface [R.D. 192], when used in a stereo configuration and integrated with modern processing units for autonomous navigation, the overall system is at TRL 8.

Single camera weight (g)	140
Single camera power consumption (W)	1.5
Single camera dimensions (mm)	70 × 52 × 3
Operating temperature (K)	≥ 170
FOV (°)	60
Detector	1024 x 1024 CCD
TRL	8

Table 11.31: CIVA's cameras specifications [R.D. 191]

Scott's GNC architecture includes the use of Broadcom/Avago HSMW-A100 white LEDs (Figure 11.41) [R.D. 193].

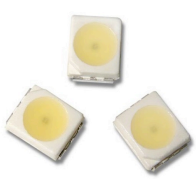

Figure 11.41: Broadcom/Avago HSMW-A100 white LEDs [R.D. 193]

An array of eight LEDs arranged in a strip beneath each camera has been implemented. Considering specifications Table 11.32, the effective illuminance on the terrain segment from 0.071 m to 1.071 m ahead of Scott can be determined. Each LED is mounted at an approximate height of 0.15 m and up to 0.08 m lateral offset from the edge of the 0.20 m swath, so the worst-case 3D distance is $r = 1.08\ m$, corresponding to an off-axis angle to the far/lateral point of $\theta \approx 9°$. Under Lambertian assumption the luminous intensity I per led is given by Equation (11.36).

$$I(\theta) = I_0 \cos(\theta) = 0.707\ cd \tag{11.36}$$

The illuminance per LED on a surface perpendicular to the beam can be evaluated as in Equation. (11.37).

$$E = \frac{I(\theta)}{r^2} = 0.60\ lux \tag{11.37}$$

With 16 LEDs well oriented, total $E \approx 16 \cdot 0.60 = 9.60\ lux$ in the worst-case condition. Considering that Scott stops to perform hazard detection, increasing the exposure time, artificial lighting is considered to ensure enough brightness. NASA's Curiosity rover uses four HSMW-A100 white LEDs on the Mars Hand Lens Imager (MAHLI) instrument to provide illumination for imaging under low-light and shadowed conditions, this application demonstrates the feasibility and durability of high-reliability LEDs in extraterrestrial environments. For this reason, their TRL is assessed as 8.

Single LED weight (mg)	70
Nominal supply current at 6 V (mA)	20
Single LED dimensions (mm)	5,2 x 1,9 x 2,8
Operating temperature (K)	233 to 373
Viewing angle (°)	120
Luminous intensity I_0 at 20 mA (cd)	0.715
TRL	8

Table 11.32: Broadcom/Avago HSMW-A100 white LEDs specifications [R.D. 193]

11.3.4.5.2 Scott mobility

Scott adopts the mobility architecture developed for Astrobotic's CubeRover platform [R.D. 54]. This configuration features a fixed-axis, four-wheel independent drive with skid steering, offering both simplicity and robustness for planetary surface operations. Each wheel is actuated independently and includes a dedicated motor, planetary gearhead, wheel mount, and encoder for precise rotation tracking. The actuators are equipped with wire harnessing and thermal strapping. The integrated wheel encoders provide real-time feedback for odometry (Figure 11.34).

For the 2U, 4U, and 6U variants, the diameter of the wheels is 20 cm [R.D. 195]. These dimensions optimize obstacle negotiation and stability. However, for larger models such as the 12U and 24U, specific wheel size information is not publicly available. It is plausible that these models use larger wheels, specifically it has been assumed that the diameter is 30 cm. To estimate the power consumption of the mobility a mean speed v_{av} of $6.50\frac{cm}{s}$ is considered based on values reported in [R.D. 185] and [R.D. 54]. The forces opposing to the motion $F_{mobility}$ (Equation (11.38)) are the rolling resistance, F_{RR}, and the gravitational force due to the landing site slope, F_{slope}. The rolling resistant coefficient c_{RR} is 0.30 [R.D. 196], while θ_{LS} is the maximum slope in the landing ellipse (i.e., 8° provided by WP 3.7).

$$F_{mobility} = F_{slope} + F_{RR} = m_{SCOTT} g sin(\theta_{LS}) + c_{RR} m_{SCOTT} g cos(\theta_{LS}) \tag{11.38}$$

Then the maximum power consumption $P_{mobility,max}$, considering a motor efficiency η of 0.70 is given in Equation (11.39).

$$P_{mobility,max} = \frac{F_{mobility} v_{av}}{\eta} = 3.35\ W \tag{11.39}$$

When Scott is stationary, it is assumed to consume 0.50 W to maintain its position.

The $11\ kg$ mass of the mobility has been considered as the 26% of the total mass, considering as reference [R.D. 185] and Mars Exploration Rover.

Considering the operational cycles described in Section 11.3.4.4, the available power resources and that the Scott path is divided into 1-meter segments, each segment including a stop for hazard detection during which mobility power consumption is at its minimum, the maximum distance achievable along a straight path is 50 meters during the daytime and 75 meters during the nighttime [R.D. 197].

Since the mobility subsystem is based on the CubeRover platform developed by Astrobotic, which has been used in lunar missions, but in a different configuration [R.D. 54], its TRL is estimated at 8.

11.4 Telemetry, Tracking & Command Subsystem

11.4.1 Introduction

The AMPERE mission's TT&C subsystem serves as a fundamental pillar supporting reliable communication between assets located at the lunar South Pole and Earth. The subsystem enables continuous monitoring of system health and

status, as well as the transmission of commands from mission control. It also plays a key role in managing and relaying data collected by the LSM, which are tasked with monitoring various environmental and operational parameters essential to the mission's objectives of energy production and surface analysis.

11.4.2 State-of-the-art analysis

Lunar communications-related literature discussed in [R.D. 260], [R.D. 261] and [R.D. 262] outlines a comprehensive spectrum strategy tailored to the unique operational needs of the Moon's environment. Early lunar missions, such as NASA's Apollo and the Soviet Luna programs, laid the groundwork for the current solutions. The Apollo program introduced the Unified S-Band system, which enabled simultaneous transmission of voice, telemetry, and video through a direct-to-Earth (DTE) architecture. Meanwhile, the Luna missions relied on frequency bands like 19.993, 183.535, 922 and 70.2 MHz for the transmission to Earth of telemetry and scientific data. Luna-17 spacecraft deployed on the Moon the first remote-controlled robotic vehicle (Lunokhod 1) that used a high gain rotatable antenna to transmit TV images to Earth, while the Telecommand and Telemetry (TM/TC) systems were equipped with lower-gain fixed antennas. Building upon these early developments, contemporary architectures for Earth-Moon direct links continue to rely on S-band and X-band frequencies now complemented by growing interest in higher-frequency bands such as the K-band to support increased data throughput. For communications between the LS and LO, a dual-band approach can be adopted: S-band for low-data-rate transmissions and Ka-band for high-data-rate services. Optical links are also being considered to support ultra-high-bandwidth applications, although their operational deployment remains limited due to technical and environmental constraints. A less mature yet increasingly relevant domain is LS-to-LS (surface-to-surface) communication. In this context, wireless technologies leveraging UHF and S-band frequencies are currently under evaluation, but these may be supplemented, or potentially replaced, by terrestrial mobile communication standards such as 3rd Generation Partnership Project (3GPP)-compliant systems, which offer flexible, scalable solutions. However, their integration into lunar operations is still in early stages and requires further validation under lunar conditions. Spectrum recommendations for these links are consolidated in [R.D. 263], which provides standardized frequency allocations for lunar communication and navigation scenarios as shown in Table 11.33. These frequency plans are essential for ensuring interoperability and interference mitigation among diverse mission assets. A detailed review in [R.D. 264] highlights how lunar-specific challenges, such as multipath propagation, signal attenuation from regolith properties, and electrostatic surface charging, impact communication reliability, particularly for LS-to-LS links. The study also surveys recent antenna solutions, including compact microstrip and sleeve dipole designs used in missions like Rashid and Chang'e-5, optimized for thermal resilience, dust mitigation and efficient surface deployment.

On the infrastructure side, both terrestrial and space-based communication assets play a pivotal role. Ground networks such as NASA's Deep Space Network (DSN) continue to serve as the backbone for Earth-Moon communications. In parallel, spaceborne relay platforms like China's Queqiao satellite have enabled persistent communication with far-side lunar assets. Looking ahead, upcoming missions will be supported by new infrastructure including NASA's Lunar Gateway and ESA's Moonlight LCNS, which are expected to significantly reduce mission complexity and the mass of the onboard communication subsystem by providing near-continuous coverage and standardized relay services. A key constraint influencing the lunar communication architecture for missions targeting the South Pole region is the limited and non-continuous Line-of-Sight (LoS) to Earth, as highlighted in [R.D. 3] and [R.D. 265]. This intermittent visibility severely restricts the reliability of DTE links, making the implementation of a relay system essential to ensure continuous communication coverage. In alignment with [A.D. 1], [AMP-C-08] and [AMP-MIS-0140], one of the primary design drivers is the integration of ESA's Moonlight system as dedicated relay node to Earth.

Link	Frequency
Earth to lunar surface	2025-2110 MHz 7190-7235 MHz 22.55-23.15 GHz
Lunar surface to Earth	2200-2290 MHz 8450-8500 MHz 25.5-27.0 GHz
Lunar orbit to lunar surface	390-405 MHz 2025-2110 MHz 23.15-23.55 GHz
Lunar surface to lunar orbit	435-450 MHz 2200-2290 MHz 27.0-27.5 GHz
Lunar surface wireless network	390-405 MHz 410-420 MHz

	435-450 Mhz 2400-2480 Mhz 5150-5835 MHz 25.25-27.5 GHz

Table 11.33: Recommended frequency bands for communications in the lunar region [R.D. 263]

11.4.3 Preliminary design considerations supporting concept selection

From WP 2.1, four mission concepts emerged. From the perspective of the telecommunication subsystem, these concepts do not significantly affect the overall architecture, except for differences related to surface element communications (MoonGrid and MoonProbe) and the inclusion of mobile elements (MoonGrid, MoonProbe and MoonRover). Consequently, a common communication architecture is proposed across all scenarios, with variations applied only where LS-to-LS communications or mobility are required. For telemetry, telecommand and scientific data transmission, the core of the system relies exclusively on Moonlight, which serves as the primary relay in both uplink and downlink. Although the use of backup DTE links and the Lunar Gateway has initially been considered a redundancy strategy, these options have ultimately been excluded. This decision is motivated by the intent to fully exploit the capabilities of Moonlight, not only to reduce system complexity, mass, and power consumption, but also to validate the end-to-end performance of the service under real mission conditions. This choice also reflects the strategic intention to validate European lunar communication and navigation technologies in an operational context, while contributing to the progressive establishment of a sustainable and service-based infrastructure to support future lunar missions. From a hardware standpoint, the communication subsystem includes a Ka-band high-gain antenna (HGA) for high-data-rate scientific data transmissions, and an S-band LGA for low-data-rate TM/TC services. Both frequency bands are aligned with Moonlight communication concepts, system requirements and service specifications presented in [R.D. 26], [R.D. 27] and [R.D. 29]. The antennas are supported by the necessary RF equipment, such as transponders and power amplifiers. For LS-to-LS communications, the use of S-band or UHF-band LGAs are a viable and standards-compliant solution. In mission scenarios requiring lunar surface positioning and navigation services, the communication subsystem includes a navigation user terminal compatible with the LCNS system [R.D. 30]. This unit is expected to be derived from existing GNSS spaceborne receivers, with limited modifications: primarily a redesigned RF front-end to operate in the S-band and software adaptations for lunar-specific navigation messages. The terminal comprises one or more S-band antennas, RF harnessing, and a receiver module capable of processing real-time positioning data.

11.4.4 Final design

Considering MoonProbe as the selected concept from the trade-off analysis, its communication architecture, in accordance with preliminary considerations outlined in the previous Sections, has been developed to ensure effective separation of data flows, robust link performance and operational continuity under varying mission conditions. Relevant literature has been reviewed, particularly [R.D. 198] which addresses modulation, coding and redundancy for a TT&C subsystem. All links are dimensioned to achieve a minimum link margin of 3 dB under worst-case conditions. Eagle's subsystem design supports both high and low-data-rate transmissions through functionally independent communication paths, in Ka-band and S-band, respectively. Scott's communication architecture also consists of two independent paths: the first is a UHF surface link shared with Eagle, dedicated to the primary exchange of data between the rover and the station and is optimized for short-range, low-power transmission using a robust and lightweight implementation. An alternative concept based on an S-band for surface communications has been also considered during the design phase. However, it has been discarded early on, as it does not offer significant advantages while incurring higher power consumption. Furthermore, the required data rates do not justify the use of a higher-bandwidth link in this context. The second path is an S-band link providing a direct communication channel between Scott and Moonlight. This channel ensures that telemetry and commanding can be maintained independently from Eagle. The TT&C subsystem is fully designed to meet Moonlight service requirements in terms of coverage, latency and performance for both uplink and downlink. An implementation loss of −2 dB is applied to all links involving Moonlight, in accordance with the system design margins specified in [R.D. 26].

11.4.4.1 Moonlight performance assessment

As part of the TT&C subsystem design process, a simulation of the Moonlight constellation's coverage capabilities has been conducted. The Moonlight architecture concept, as described in [R.D. 199], consists of four Navigation Satellites (NAVSATs) and one high-speed Communication Satellite (COMSAT) distributed across different Elliptical Lunar Frozen Orbits (ELFOs). NAVSATs have a Semi-Major Axis (SMA) of approximatively 10000 km (corresponding to an orbital period of 24 hours), while COMSAT features a semi major axis of 6000 km, resulting in a 12-hour period. To define the orbital parameters of the NAVSATs a literature review focused on LCNS constellations has been carried out, referring to [R.D. 200] and [R.D. 201]. For the COMSAT, reference configurations found in [R.D. 202] and the ELFOs design method

described in [R.D. 203] have been used to define an adequate orbit. The design of the ELFO orbit adopted for the Moonlight COMSAT has been driven by the need to ensure long-term orbital stability, polar coverage and compliance with Moonlight service availability requirements. Starting from the constraint of a 12-hour orbital period (i.e. a semi-major axis of 6143 km), the Eccentricity (ECC) has been selected within the typical ELFO range (0.6–0.7) to satisfy altitude bounds at periselene and aposelene as indicated in [R.D.5], namely a minimum altitude of 225 km and a maximum one of 9382 km. An eccentricity of 0.63 has been selected. The Inclination (INC) has been computed to satisfy the ELFO condition using Equation (11.40):

$$e^2 + \frac{5}{3}(\cos i)^2 = 1 \tag{11.40}$$

The resulting inclination, computed in the Earth orbital plane frame, has been subsequently converted in a Moon-centred inertial reference frame (i.e. Moon's J2000 frame), using the method outlined in [R.D. 6], to ensure coherence with the reference frame adopted for the NAVSATs: the resulting value is 58.26 deg. The remaining elements, Right Ascension of Ascending Node (RAAN) and mean anomaly, have been chosen to maximize coverage. The full set of orbital parameters for Moonlight satellites is listed in Table 11.34. To assess the coverage performance, a one-year simulation on GMAT has been carried out, starting on April 5, 2037, at 16:00:00.000 Universal Time Coordinated (UTC). Since Moonlight compliancy to service requirements is expected throughout the entire mission, the simulation is performed with a Keplerian propagator. The Moonlight constellation is depicted in Figure 11.42.

Parameter	COMSAT	NAVSAT 1	NAVSAT 2	NAVSAT 3	NAVSAT 4
SMA [km]	6143	9750.73	9750.73	9750.73	9750.73
ECC	0.63	0.6383	0.6383	0.6383	0.6383
INC [°]	58.26	54.33	54.33	61.96	61.96
RAAN [°]	180	277.53	277.53	59.27	59.27
AOP [°]	90	55.18	55.18	121.7	121.7
TA [°]	0	123.42	0	180	0

Table 11.34: Orbital parameters of the Moonlight constellation satellite.

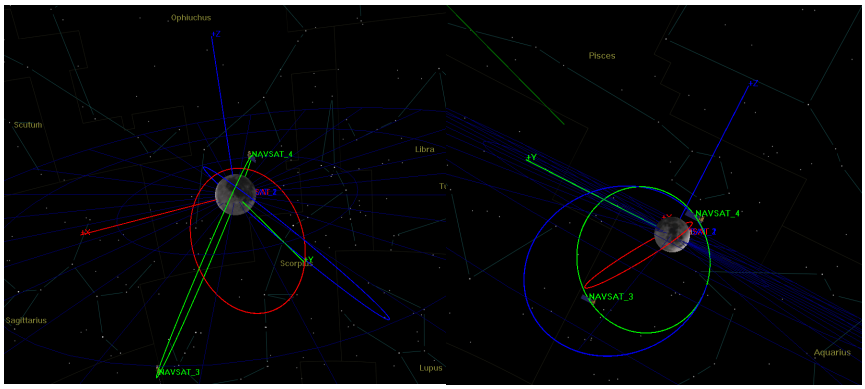

Figure 11.42: Moonlight's ELFO constellation.

The results obtained from the simulation, conducted with a minimum elevation angle of 10°, confirm that the defined constellation satisfies Moonlight requirement of ensuring a minimum service window of 18 hours. In Figure 11.43 the coverage times of the NAVSATs and COMSAT are displayed.

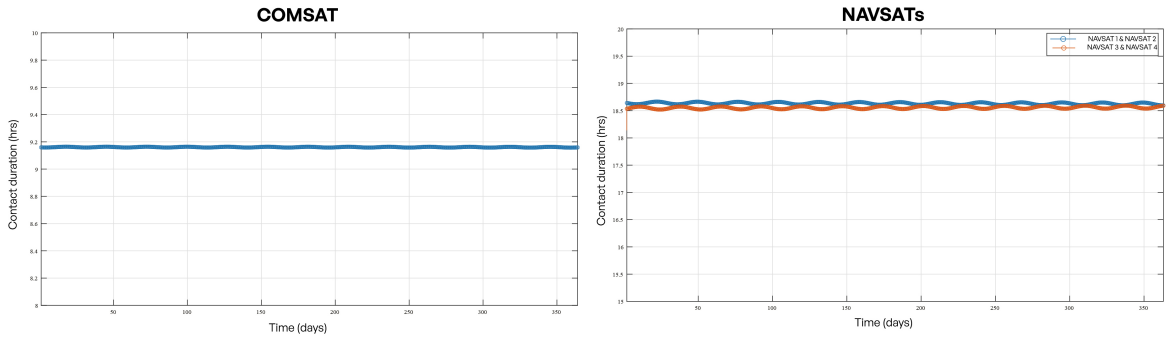

Figure 11.43: Simulated contact durations for COMSAT and NAVSATs over one year.

As stated in [R.D. 199], the Fucino ground station is currently the only confirmed site planned to support the future Moonlight service, with additional nodes expected to be integrated from ESA's DSN and the Kongsberg Satellite Services (KSAT) infrastructure. In this context, ground stations such as Punta Arenas and New Norcia are undergoing upgrades to support Ka-band communications. For this mission, it is assumed that ground reception relies on this Moonlight-compliant network, ensuring end-to-end compatibility with Moonlight data relay and control requirements, with the Mission Operation Center (MOC) interfacing with the LCNS service provider in accordance with [R.D. 27].

11.4.4.2 Data volume and OBC selection

Before proceeding with the final dimensioning of the TT&C subsystem and associated data links, it is essential to assess the data volumes to be handled by the OBCs and transmitted via the communication architecture. Scientific data volumes have been estimated based on the nominal surface operation cycle and the input provided by WP 2.3. For telemetry, different estimation methods have been applied to Eagle and Scott. For Eagle, the reference is [R.D. 3], which assumes a daily telemetry data volume of approximately 40 Mbit, derived from heritage missions such as ExoMars. Considering the European Charging Station for the Moon (ECSM) system complexity and functions, this value is deemed both appropriate and conservative. For Scott, telemetry estimation has been performed based on system characteristics such as mass, form factor, and onboard subsystems, drawing analogies from previous planetary rover missions. The resulting data volumes for each source type are summarized in Table 11.35.

Data source	Data vol. per hr [Mbit]	Data vol. per Earth day [Mbit]	Data vol. per lunar day [Mbit]
Eagle sensors	34.60	830.4	24561.40
Eagle telemetry	1.67	40	1181.71
Scott sensors	2.20	35.2	1559.80
Scott telemetry	0.10	2.5	70.90

Table 11.35: Estimated data volumes for Eagle and Scott.

Based on these values, the OBCs must reliably store, manage and prepare the data for transmission, while also supporting the processing needs of surface operations. Two systems have been selected: a Next Generation [R.D. 204] for Eagle, and the Gomspace NanoMind Z7000 [R.D. 205] for Scott. The Eagle OBC offers a memory capacity of approximately 93.5 GB, while the NanoMind Z7000 provides up to 32 GB. Both are more than adequate for the projected daily data volumes and allow for operational resilience in case of temporary communication outages. Another important task of the two OBCs is also related to data compression. In fact, lossless compression algorithms, such as POCKET+ for housekeeping and telemetry data and Fully Adaptive Prediction Error Coder (FAPEC) for scientific data, detailed in [R.D. 225] and [R.D. 226] respectively, are applied to improve transmission efficiency, thereby enhancing the performance of links for both Eagle and Scott.

11.4.4.3 Ka-band antenna sizing

To ensure a robust high-rate link between Eagle and the Moonlight constellation, a dedicated design process has been carried out for the Ka-band HGA. COTS solutions have been deemed unsuitable, either due to incompatibility with the recommended frequency bands in [R.D. 260], or due to constraints in mass and volume. Consequently, the antenna has been sized using the methodology described in [R.D. 206] which establishes an empirical correlation between antenna mass and diameter. Figure 11.44: Mass prediction of high-gain parabolic antenna shows the weight–to-diameter relationship for a parabolic reflector operating at 27 GHz, the selected transmission frequency.

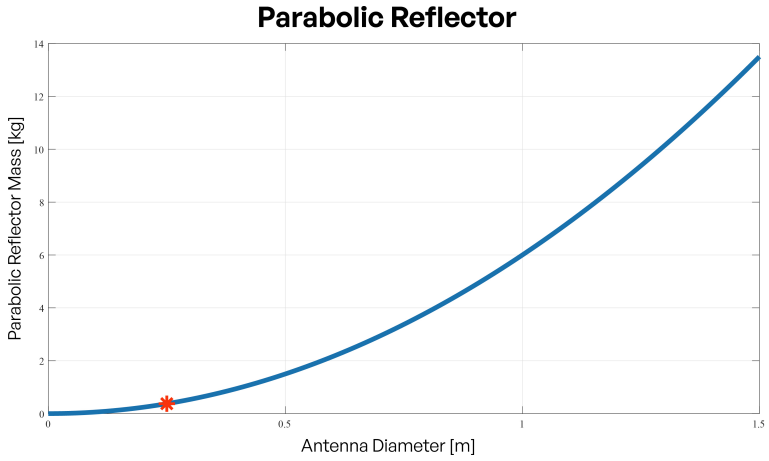

Figure 11.44: Mass prediction of high-gain parabolic antenna

The antenna diameter has been chosen in accordance with Class B and Class C terminal recommendations from [R.D. 28], which recommend maximum diameters equal to 0.25 m and 0.35 m, respectively. The final design favours the Class B configuration. While the smaller diameter implies a slightly lower gain, it results in a 50% mass reduction compared to Class C equipment. This choice is supported by the link budget analysis presented in Section 11.4.4.7, which confirms sufficient margin under worst-case assumptions. Table 11.36 reports basic antenna parameters.

Parameter	Value
Frequency [GHz]	27
Antenna gain [dBi]	34.26
Antenna diameter [m]	0.25
Antenna efficiency	0.55
Half-power beamwidth [°]	3.11

Table 11.36: Outputs from sizing of Ka-band HGA

11.4.4.4 Cruise phase

During the cruise phase, the LPS relies entirely on the LDE TT&C subsystem. To comply with the clarifications provided in [A.D. 9], this Section presents the expected data volume and corresponding data rate for this phase. The daily data volume has been conservatively assumed to be 50% of the daily data volume of Eagle during nominal operation phase, i.e. 40 Mbit, resulting in an estimate of 20 Mbit per day. Hence, combining the input LLO parameters and descent trajectory from W.P. 3.6 with the COMSAT ELFO described in Section 11.4.4.1 a simulation has been carried out to estimate the data rates during the entire duration of this phase, i.e. four days, starting on April 1, 2037, at 16:00:00.000 UTC. In Figure 11.45 the result is shown. The data rates achieved during communication with Moonlight are compared with the data rates achieved with a DTE link, resulting lower of about the 78%. However, both the peak and average data rates, 2.63 Mbps and 2.3 Mbps, respectively, are fully compliant with the LDE's capabilities, confirming that Moonlight relay service can be effectively used during this phase as well. In addition, relying on the Moonlight infrastructure improves not only communications but also orbital navigation. A more detailed description of this aspect is provided in Section 11.4.4.3. For the descent phase, given its relatively short duration, the data rate is conservatively assumed to be equal to the average rate during the cruise phase.

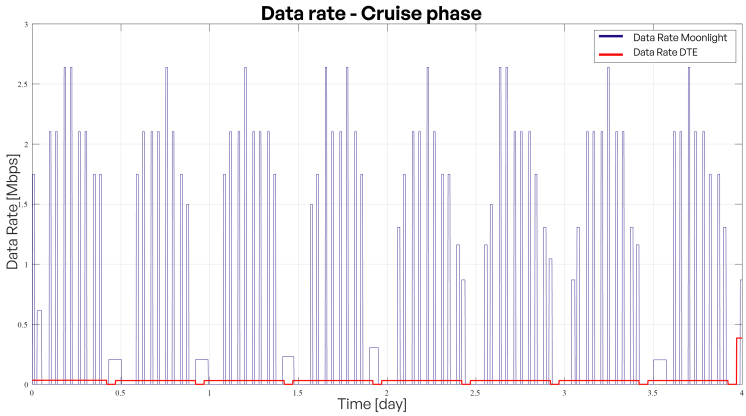

Figure 11.45: Cruise phase data rate.

11.4.4.5 TT&C modes

Starting from deployment and descent phase, and throughout the entire nominal phase, the TT&C subsystem ensures the transmission of telemetry and scientific data from both Eagle and Scott. The various communication links allow mission controllers to maintain continuous situational awareness of both assets, monitor health status, and receive updates on scientific and operational activities. In this Section the operational modes of the TT&C subsystem are defined, tailored to the different mission phases and system modes and aligned with operational requirements.

- Initial acquisition and deployment: this mode is activated to establish initial contact between the LPS and Moonlight and to initiate deployment operations. Once the interaction between Eagle and Moonlight is successfully established, a dedicated signal is transmitted to Argonaut to trigger the ramp deployment procedure. The contact is established by Eagle's S-band LGA, independently from the LDE's TT&C subsystem. Primary telemetry and housekeeping data are transmitted during this phase, followed by the deployment and commissioning sequence and the deployment of Scott, which at this stage communicates only with Eagle using the UHF-band interlink.
- Tx/Rx Moonlight relay (Eagle): this mode manages communications between Eagle and Moonlight. Scientific data are downlinked via the Ka-band high-rate channel, while for TM/TC are handled through the S-band link.
- Tx/Rx Moonlight relay (Scott): like Eagle's relay mode, this one manages Scott's communication with Moonlight. Only TM/TC are exchanged via the rover's S-band subsystem, operating at a very low-rate data rate.
- Interlink: this mode supports surface communication between surface elements and is essential for the transmission of real-time science and telemetry data from Scott to Eagle, which functions as a surface relay, as well as for the exchange of navigation or command data. This communication takes place in the UHF.
- Safe mode: it is activated to cope with anomalies or critical situations, so that only those operations essential to preserve the health of surface assets are kept active. A minimal telemetry link is maintained for both Eagle and Scott, along with basic inter-asset communication.
- Night mode: during lunar night energy usage is optimized by using Ka-band only for sending telemetry and scientific data. Eagle and Scott maintain contact with each other via UHF. In this way status updates on surface assets and scientific data collected by operational sensors during the night are still provided.

11.4.4.6 Ka-band link: Eagle

The primary high-data-rate link is established via the Ka-band channel. It supports the downlink of scientific data collected by the LSM-S and LSM-M and telemetry relayed from Scott through the surface interlink. The architecture, illustrated in Table 11.40, consists of a HGA mounted on a gimbal and two RF chains each consisting of transceiver and Solid-State Power Amplifier (SSPA). One chain is active, while the other is redundant, selectable via a switching unit in the event of a failure.

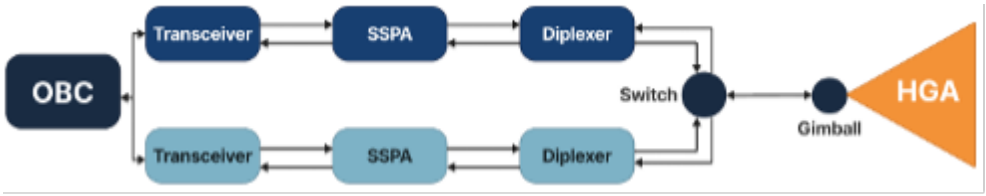

Figure 11.46: Eagle Ka-band architecture.

Thanks to the antenna gain and the RF output power, the system enables the transmission of substantial daily data volumes. To optimize energy consumption and accommodate pointing constraints associated with the HGA and its placement on Eagle, the transmissions are scheduled once per Earth Day within a 2-hour window, with an additional 30-minute operational margin. The resulting data rate is compatible with Class B user terminals as defined in [R.D. 28], which also justifies the HGA sizing process. The link budget for the Ka-band forward link (i.e. from lunar user to Moonlight) has been computed considering the maximum distance derived from GMAT simulations, along with conservative assumptions on pointing and environmental losses. The receiver antenna characteristics have been conservatively assumed from data outlined in [R.D. 202]. Output parameters of link budget analysis are shown in Table 11.37.

Parameter	Value
Distance [km]	8292
Frequency [GHz]	27
Tx data rate [kbps]	9270
Rx antenna gain [dBi]	40
Tx antenna gain [dBi]	34.46
Tx power [W]	15
G/T Rx [dB/K]	13.98
Tx EIRP [dBm]	76.02
Required BER	10^-8
Required Eb/No [dB]	5 (OQPSK + 1/2 LDPC and medium code blocks)
Free space loss [dB]	-199.45
Received isotropic power [dBm]	-113.22
Eb/N0 [dB]	10.47
Link margin [dB]	5.47

Table 11.37: Link budget analysis for Eagle's Ka-band forward communication link.

Modulation and coding conform to [R.D. 26] standards for the relevant data rate class. The selected modulation is OQPSK, preferred in Ka-band for its robustness to non-linearities and spectral efficiency. The applied coding scheme is LDPC (rate 1/2, 4K block), in line with LunaNet guidelines, detailed in [R.D. 207]. This scheme enables a significant reduction in required Eb/N_0 to achieve a Bit Error Rate (BER) of 10^{-8}, as shown in Figure 11.47. During night mode operations, Ka-band link supports also the transmission of Eagle's telemetry. Maintaining the same operational parameters, this results in a 3% decrease in link margin and in a 4.4% increase in data rate, both within the acceptable bounds of the Ka-band architecture.

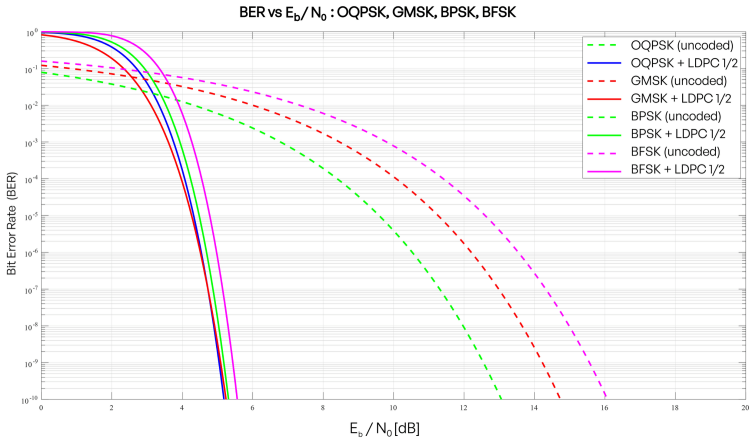

Figure 11.47: BER vs Eb/N0 for different modulation uncoded and ½ LPDC 4K block.

11.4.4.7 S-band link: Eagle

The S-band link is used to support low-data-rate telemetry transmission from Eagle. The logical structure of this subsystem is illustrated in Figure 11.48. Full redundancy of its elements, LGAs and transceivers, not only guarantees fault tolerance, but also extends coverage (achieving a quasi-omnidirectional pattern through proper antenna placement) and supports operations under emergency conditions. Although power amplifiers have been initially considered, they have been omitted, as the transceiver output power alone is sufficient to maintain a reliable link and ensure adequate link margin. In addition, the selected configuration of the transceiver, C/TT-520 spacecraft S-band multimode transponder [R.D. 208], includes also a diplexer, hence completing the transmission line.

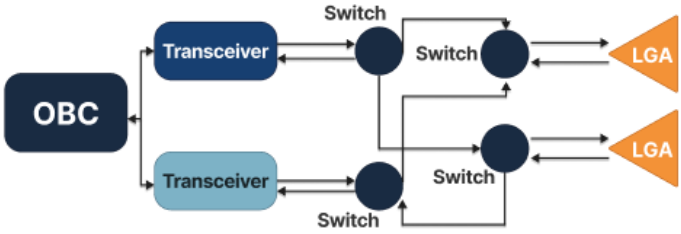

Figure 11.48: Eagle S-band architecture

Telemetry is transmitted across the full Moonlight service window, with an additional operational margin of approximately three hours. This ensures extended communication availability and an acceptable data rate consistent with Class B user terminal capabilities. The link budget analysis is based on worst-case conditions, including maximum distance and reduced antenna gain (−3 dB). The results are presented in Table 11.38.

Parameter	Value
Distance [km]	8292
Frequency [GHz]	2.2
Tx data rate [kbps]	21.82
Rx antenna gain [dBi]	23.7
Tx antenna gain [dBi]	-3
Tx power [W]	20
G/T Rx [dB/K]	-1.07
Tx EIRP [dBm]	39.91
Required BER	10^-8
Required Eb/No [dB]	6.5 (OQPSK + ½ convolutionary)
Free space loss [dB]	-177.67
Received isotropic power [dBm]	-117.43
Eb/N0 [dB]	11.38
Link margin [dB]	4.88

Table 11.38: Link budget analysis for Eagle's S-band forward communication link.

For the receiver antenna, performance parameters equivalent to those of the Lunar Pathfinder mission have been assumed, as detailed in [R.D. 209]. The modulation scheme remains OQPSK, paired with a 1/2 convolutional code, to achieve a BER of 10^{-8}. This configuration ensures compatibility with the selected hardware and adheres to LunaNet protocol standards.

11.4.4.8 S-band link: Scott

Scott's S-band link serves as communication channel with Moonlight. It is used exclusively to transmit primary telemetry and to interface directly with ground segment during surface operations, operating at very low data rates. The system, depicted in Figure 11.49, also provides a backup path for communication in the event of surface interlink unavailability or degradation. The configuration complies with [R.D. 26] requirements for very-low-data-rate terminals and consists of an omnidirectional antenna, a diplexer and a transceiver. This transmission chain is activated during each rover cycle, when Scott is separated from Eagle. It transmits a reduced telemetry dataset, estimated at 20% of Scott's daily data volume, within a one-hour communication window. This configuration balances energy efficiency and communication reliability.

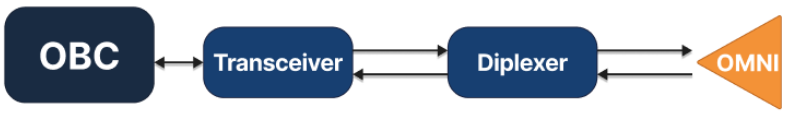

Figure 11.49: Scott S band architecture.

The S-band link budget is evaluated under the same worst-case conditions applied for Eagle's S-band channel Modulation and coding schemes are GMSK and 1/2 convolutional coding, targeting a BER of 10^{-8} and ensuring alignment with the required Eb/N_0 margins. Detailed results of the link budget analysis are provided in Table 11.39.

Parameter	Value
Distance [km]	8292
Frequency [GHz]	2.2
Tx data rate [kbps]	2.38
Rx antenna gain [dBi]	23.7
Tx antenna gain [dBi]	-3
Tx power [W]	2
G/T Rx [dB/K]	-1.07
Tx EIRP [dBm]	27.8
Required BER	10^-8
Required Eb/No [dB]	6.5 (GMSK + 1/2 LDPC and medium code blocks)
Free space loss [dB]	-178.43
Received isotropic power [dBW]	-134.38
Eb/N0 [dB]	10.05
Link margin [dB]	3.55

Table 11.39: Link budget analysis for Scott's S-band forward communication link.

11.4.4.9 Interlink

This Section describes the communication link between Scott and Eagle, which serves as Scott's primary channel for transferring both telemetry and scientific data. The architecture, shown in Figure 11.50, comprises omnidirectional antennas and half-duplex transceivers. Redundancy is implemented exclusively on Eagle. Given the relatively short operational range of Scott, the link is robust and requires minimal RF power.

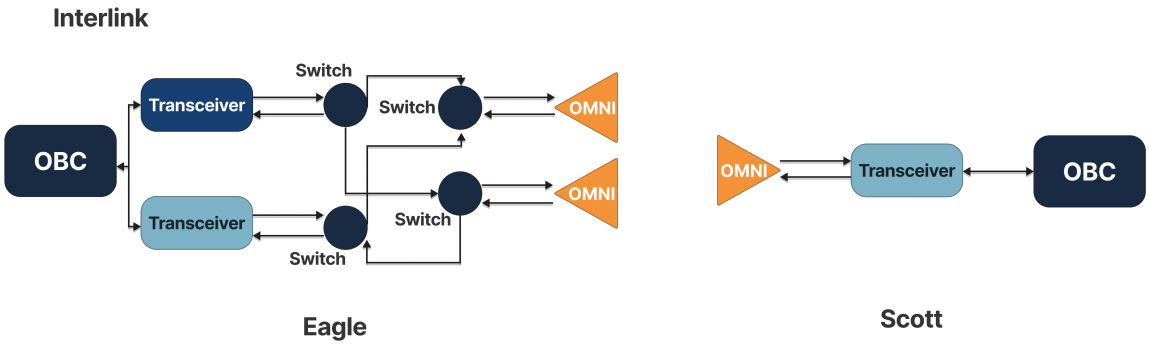

Figure 11.50: Interlink architecture.

Communication is maintained throughout Scott's activity cycle when separated from Eagle, spanning a 7-hour window. Real-time telemetry is streamed continuously to Eagle, improving power efficiency by avoiding redundant storage and delayed transmission. The system adopts a Time Division Duplexing (TDD) approach to alternate transmission and reception, which eliminates the need for full-duplex hardware. To model surface communications realistically, propagation effects of the lunar terrain have been incorporated following the findings of [R.D. 210]. Specifically, the link budget accounts for surface-induced losses, including multipath fading, reflection and diffraction, collectively estimated as an additional 11 dB attenuation. The link budget has been computed considering that all telemetry and scientific data gathered during this 7-hour period must be transmitted within the same window from maximum nighttime distance, introducing a conservative margin to ensure robust performance under operational constraints. The selected UHF transceiver, the Gomspace NanoCom AX100 [R.D. 211] offers a peak throughput of 38.9 kbps. A target BER of 10^{-5} has been considered sufficient for Scott's operational needs, without any additional error correction. Table 11.40 summarizes the results of the link budget analysis.

Parameter	Value
Distance [m]	75.00
Frequency [MHz]	440.00
Tx data rate [kbps]	34.54
Rx antenna gain [dBi]	-3.00
Tx antenna gain [dBi]	-3.00
Tx power [W]	1.00
G/T Rx [dB/K]	-24.30
Tx EIRP [dBm]	26.70
Required BER	10^-6
Required Eb/No [dB]	13 (BPSK + margin)
Free space loss [dB]	-63.01
Received isotropic power [dBm]	-81.72
Eb/N0 [dB]	62.20
Link margin [dB]	49.20

Table 11.40: Link budget analysis for UHF communication link from Scott to Eagle.

11.4.5 Hardware overview

This Section provides an overview of the selected hardware components for the TT&C subsystem. To support the high-data-rate link, considering current compatibility limitations with lunar communication recommended frequency bands, the selected components include a custom-sized high-gain antenna, the NASA wideband terminal described in[R.D. 212].and an SSPA unit, Ka-Band GaN-on-SiC MMIC Balanced HPA, detailed in [R.D. 213]. Both elements are currently at a relatively low TRL but align with the evolving standards for high-rate lunar communications. In contrast, the low-data-rate link on Eagle relies on mature, commercially available components. These include the Anywaves Compact S-band LGA [R.D. 214] and the C/TT-520 spacecraft S-band multimode transponder. The same approach applies to Scott's S-band architecture, which adopts compact, rover-compatible components: a PW 2022-111 omnidirectional antenna[R.D. 215], the EnduroSat S-band transceiver [R.D. 216] and the WiRan S-band diplexer [R.D. 217].For the interlink between Eagle and Scott, the system uses the same UHF-band transceiver on both platforms, the GomSpace NanoCom AX1000. On the antenna side, Eagle's design is derived from the model described in [R.D. 218], while Scott uses the GomSpace

ANT320 [R.D. 219], a CubeSat antenna adapted for the lunar environment. Table 11.41 and Table 11.42 list the TT&C components for Eagle and Scott, respectively, including quantity, unit mass, and current TRL.

Device	N. of elements	Mass [kg] per unit	TRL
Ka-band HGA	1	0.38	6
Wideband terminal Ka-band transceiver	2	3	6
Ka-band GaN-on-SiC MMIC Balanced HPA	2	2	6
Ka-band DPX VC222834 diplexer	2	0.04	8
Anywaves Compact S-band antenna	2	0.11	8
C/TT-520 spacecraft S-band multimode transponder	2	4	8
Omnidirectional UHF antenna	2	0.30	7
GomSpace Nanocom AX100	2	0.02	8
Next generation OBC	1	9	8

Table 11.41: TT&C hardware components for Eagle

Device	N. of elements	Mass [kg] per unit	TRL
UHF ANT430 antenna	1	0.30	7
GomSpace NanoCom AX100	1	0.02	8
PW2022-111	1	0.15	8
Endurosat S-band transceiver	1	0.20	8
WiRan diplexer	1	0.22	8
GomSpace NanoMind Z7000	1	0.80	8
LCNS terminal	1	0.21	7

Table 11.42: TT&C hardware components for Scott rover

To support a more precise characterization of the TT&C hardware and to illustrate its behaviour under different operational scenarios, the power consumption of the various modules during Tx/Rx across the different RF links is detailed in Table 11.43 In addition, Table 11.44 provides the power demand of processing and navigation units, which contribute to the overall system power budget.

Scenario	Power [W]
Tx/Rx Ka-band and Rx S-band - Eagle	108
Tx/Rx Ka band and Tx/Rx S-band -Eagle	180
Rx Ka band and Tx/Rx S-band - Eagle	118
Rx Ka-band and Rx S-band - Eagle	46
Tx/Rx UHF-band (Interlink)	5
Tx/Rx S-band and Tx/Rx UHF band -Scott	11

Table 11.43: Power consumption of TT&C modules under different link configurations.

Component	Power [W]
Next Generation OBC	38
GomSpace Nanomind Z7000	2
LCNS receiver	2.5

Table 11.44: Power consumption of processing and navigation units.

11.4.6 Lunar Radio Navigation

[R.D. 224] provides a comprehensive overview of lunar radio navigation aspects and requirements for both orbital and surface mobility. Navigation throughout the mission phases, particularly descent and surface operations, relies on a hybrid strategy that integrates traditional inertial techniques with advanced positioning services offered by LCNS. During the lunar descent phase, this hybrid architecture integrates conventional radiometric tracking with one-way navigation signals transmitted by LCNS satellites. These signals, broadcast in the S-band and based on a GNSS-like Time-Of-Arrival (TOA) concept, are designed to be processed by onboard receivers in real time. This one-way approach, extensively analysed in [R.D. 200] and specifically validated for the descent phase through variance-covariance analysis, allows the lander to meet the <100 m (3σ) accuracy requirements for precision landing at lunar south polar sites. Compared to legacy ground-based tracking, LCNS support significantly reduces operational complexity and the duration of orbit

determination phases in LLO, thanks to reduced dependency on Earth-based measurements. For surface operations, Scott is equipped with a custom LCNS-compatible receiver derived from commercial GNSS-grade space hardware, specifically the AAC Clyde Space GNSS-700 [R.D. 220] and EnduroSat GNSS patch antenna [R.D. 221].This system has been upgraded to meet the compliance requirements defined in [R.D. 27], with specific adaptations such as software reconfiguration for one-way S-band TOA processing, resilience to lunar dynamics, and support for the Moonlight navigation message format. Despite these enhancements, the unit remains compact, lightweight, and power-efficient, making it suitable for surface navigation. In addition to IMU and visual odometry used for dead reckoning and local hazard detection, the rover periodically performs absolute position updates using the LCNS one-way Positioning, Navigation and Timing (PNT) service, specifically enabled by signals from the Moonlight constellation, operating in ELFOs. Such configuration improves Geometric Dilution of Precision (GDOP) in high-latitude regions, with advantages in terms of coverage and navigation performance highlighted in [R.D. 222]. A detailed assessment of this approach is provided in [R.D. 223], which demonstrates that combining LCNS range measurements with high-resolution DEM-based altitude constraints (derived from LOLA data) enables 3σ positioning accuracy below 10 meters. This is achieved under realistic assumptions, including accurate LCNS orbit and time synchronization, a navigation-grade IMU, and an Oven-Controlled Crystal Oscillator (OCXO). Furthermore, the paper highlights that leveraging the Digital Elevation Model (DEM) for altitude constraint significantly enhances service availability, enabling position calculations with as few as three visible LCNS satellites, which is crucial for the anticipated sparser lunar constellation. This approach allows Scott to maintain surface navigation accuracy within the decametric range without relying on local infrastructure, in full alignment with the Moonlight objective of enabling scalable, infrastructure-independent lunar mobility. Furthermore, the communication link between Scott and Eagle enhances lunar navigation capabilities by providing an additional aid and serving as a reliable backup path.

11.5 Structure & Mechanisms

11.5.1 State-of-the-art analysis

After the lunar landing, the power station must be deployed from the LDE in accordance with [A.D. 1]. To address this, several deployment mechanisms have been explored. The first point to note is that, based on mission requirements, the station may be mounted on a wheeled cart, on an autonomous rover, or, if mobility is not required, directly on a fixed, non-wheeled platform.

In the case of a wheeled platform (e.g., wheeled cart or rover), deployment via a ramp represents a viable solution [R.D. 266]. The system consists of a foldable ramp composed of L-shaped plates, which are deployed from the lander through mechanical hinge mechanisms, enabling the controlled descent of the power station. This approach offers advantages in terms of structural simplicity, volumetric efficiency during launch, and overall reliability. The system has already been used in previous missions such as Chandrayaan-3 [R.D. 255]. Clearly, this solution is Table 10.69 to non-wheeled platforms.

In the case of a non-wheeled platform, alternative deployment methods can also be considered. These include the use of a robotic arm, a crane, a Davit or an Egress system, all of which can facilitate the controlled placement of the power station onto the lunar surface. Regarding the robotic arm, it would be installed on top of the LDE and must possess at least three degrees of freedom: rotation, elevation, and extension. The arm is designed to grasp the power station through dedicated attachment points, enabling it to lift and place the payload with precise, controlled motion. The deployment process can be executed autonomously, semi-autonomously, or teleoperated from Earth, depending on mission requirements. To ensure stability during operation and mitigate dynamic reactions, the vehicle must be securely anchored to the lunar surface. Examples of its use include Canadarm2, the Canadian robotic arm on the Space Station, and the one mounted on the Perseverance rover [R.D. 268], as shown in Figure 11.51.[R.D. 267].

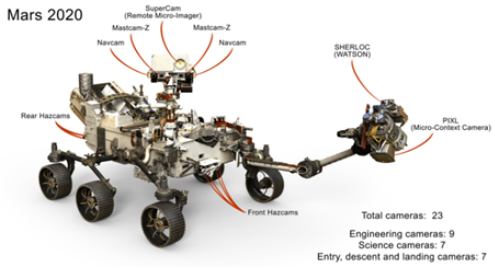

Figure 11.51: Perseverance Mars rover [R.D. 267]

Regarding the crane, an example could be the Lightweight Surface Manipulation System (LSMS), a crane-like robotic arm developed by NASA Langley Research Center to support the handling of heavy payloads on the surface of celestial

bodies such as the Moon and Mars. This technology was designed to address one of the key challenges in lunar exploration: the safe and precise deployment of large payloads up to 1000 kg in remote, dusty, and reduced-gravity environments. Unlike traditional serial robotic arms, the LSMS adopts a hybrid approach inspired by terrestrial crane engineering, using a segmented, lightweight structure with articulated joints and advanced control systems. Instead of relying on flexural forces, the LSMS transfers loads through tension and compression, resulting in a more efficient system in terms of structural mass, power consumption, and load-handling capability [R.D. 269], [R.D. 270]. A reproduction is shown in Figure 11.52 [R.D. 271].

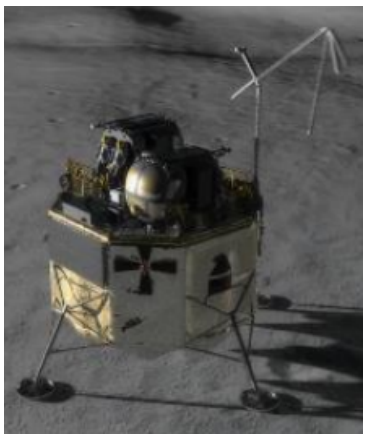

Figure 11.52: LSMS reproduction [R.D. 271]

Regarding the Davit system: it is a double Davit system, consisting of two arms hinged to the upper edge of the vehicle, equipped with synchronized winches. The arms rotate outward, extending beyond the perimeter of the lander, allowing for the vertical lowering of the payload, which is secured via ropes to a structural platform. An image of the system is shown in Figure 11.53 [R.D. 272]. A similar implementation is used in the deployment system of Blue Origin's Blue Moon lander [R.D. 273].

Figure 11.53: Davit system [R.D. 272]

The Egress system consists of a deployable inclined plane positioned on top of the LDE. It enables the controlled descent of the payload onto the lunar surface using guided rails or low-friction skids. The motion is assisted by linear actuators or passive braking mechanisms, such as eddy-current dampers, to ensure smooth and stable deployment. A comparable concept was demonstrated in the ESA Polar Explorer study [R.D. 8], which employed spring-loaded arms, a dual cable roll with an integrated eddy-current damper, and a wedge-controlled cable release system. In this design, the rover was lifted and gradually lowered using a controlled cable tensioning sequence. Key features included passive synchronization of components, automatic wedge release near the horizontal position, and complete autonomy of the deployment sequence. A schematic of the system is presented in Figure 11.54 [R.D. 8]. It is important to note that the use of these deployment technologies is not excluded for wheeled platforms.

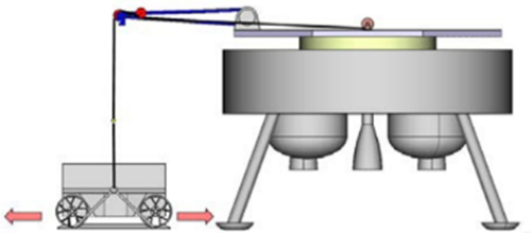

Figure 11.54: Egress system schematic [R.D. 8]

In Table 11.45 the difference between a ramp, a robotic arm, a crane, a Davit, and an Egress system are summarized in terms of mass, actuation type, release distance and other feasibility. The rationale for the latter parameter is detailed in Section 11.5.1

System	Mass	Actuation type	Release dist. (m)	Feasibility	Notes
Ramp	40–60 kg	Active	>10	Yes	Considering active hinges and a load of 600 kg
Robotic arm	≥ 3 times the load to be lifted	Active	up to 1	No	Considering a 500 kg arm, it could lift a load of at most 150 kg
Crane	≥ 2 times the load to be lifted	Active	up to 1	No	Considering a 450 kg crane, it could lift a load of at most 200 kg
Davit	20–40 kg	Passive	0.2–0.5	Yes	Considering a load of 600 kg
Egress	20–40 kg	Passive	0.2–0.5	Yes	Considering a load of 600 kg

Table 11.45: Different deployment mechanisms comparison

Regarding the locking mechanism of the station prior to release, several configurations can be considered. If a ramp-based deployment system is adopted, the station may be secured either directly to the first plate of the foldable ramp [R.D. 255] or to the LDE. In the latter case, if the station is mounted on a wheeled cart, a fixed secondary ramp must be integrated on the LDE to allow transition from the platform to the first segment of the main ramp. Conversely, if an autonomous rover is used, it can descend directly along the main ramp without the need for additional structures, and thus it can be attached to the LDE directly. Alternatively, if a crane, robotic arm, Davit or Egress system is employed, the station can be secured directly to the LDE without the use of intermediate ramps.

11.5.2 Preliminary design considerations supporting concept selection

For all the configurations, the use of a robotic arm and the crane must be excluded. Even in the MoonGrid configuration, where the stations have a reduced weight, the mass and structural complexity that the arm or the crane would require to lift the payload would be excessively high, making this option impractical given the mission constraints. For the MoonStation and MoonProbe solutions, from a structural standpoint, all considered deployment mechanisms would be theoretically feasible. However, since the stations remain fixed after deployment and lack autonomous mobility, the only truly viable option is a ramp. Other solutions would release the station too close to the lander. To mitigate risks associated with the lander's ascent phase, a ramp is required to ensure the station is positioned at a significantly greater distance. For the MoonGrid and MoonRover solutions, on the other hand, the viable deployment mechanisms are the Davit system and the Egress system. In these cases, the ramp is excluded due to constraints in terms of mass, structural footprint, and energy consumption. Therefore, the only realistic options are the Davit and the Egress system.

11.5.3 Final design

This Section discusses the preliminary design of the structures and mechanisms of Eagle, PDS and Scott for the selected concept, MoonProbe. Since it is outside the scope of AMPERE, the design of the mounting plate, serving as the mechanical interface between the LPS and the LDE, has not been performed [A.D. 9]. Instead, it has been modelled as a plate with the geometry of a regular octagon, each side measuring 1.68 m, matching that of the LDE shown in [A.D. 16].

11.5.3.1 Eagle's wheels and plate

The design of Eagle's plate and the four supporting wheels has been carried out, the chassis design is planned for the later stages of the mission. The plate is a rectangular sandwich panel, $1.78\ m\ \times\ 1.22\ m$ in size, these dimensions are

chosen because the cart is initially in a vertical position; therefore, the longitudinal dimension of the panel matches the height of the stowed ramp, while the lateral dimension corresponds to the side length of the mounting plate's octagon, minus the widths of the wheels. The centres of the wheels are assumed to be at the same level as the plate, which is 30 mm thick and is composed of CFRP face sheets and an aluminium honeycomb core. This material is selected due to its high stiffness-to-weight ratio, excellent structural performance, and proven reliability in space applications [R.D. 227]. The thickness and dimensions of the plate have been iteratively adjusted in Ansys until the minimum mass value has been achieved, while ensuring acceptable performance in terms of deformation and stress. The plate serves as the main structural support for the LPM, LSM-S and Scott throughout the mission phases. The plate weighs 45 kg and has a TRL 5, in fact, units made of the same material have been used successfully operated in lunar missions, but in a different configuration.

For efficient and accurate simulation, Finite Element Analysis(FEA) model of the panel has been performed in Ansys Mechanical Ansys Parametric Design Language (APDL) (Figure 11.55) using SHELL281 layered shell elements [R.D. 228], which support material layers with different thicknesses, making them well-suited for simulating sandwich structures. Each element incorporates a symmetric CFRP layup with multiple orthotropic plies and an isotropic core layer representing aerospace-grade aluminium honeycomb. The model accounts for both global stiffness and local deformation effects.

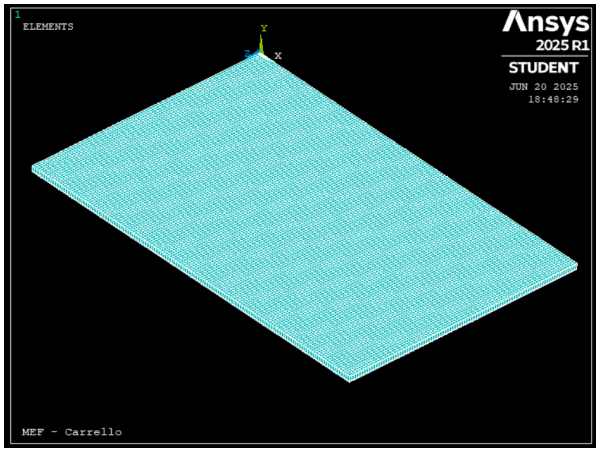

Figure 11.55: Finite Element (FE) model of Eagle's plate

To represent realistic mass distribution, the panel has been divided into four surface zones with equal dimensions of $0.89\ m \times 0.61\ m$, each assigned a specific load based on the location and weight of components. This non-uniform mass loading has been applied in both, the launch scenario, with the panel in vertical position (the boundary condition is the panel's rear short edge supported) under quasi-static loads of $6g_0$ longitudinal and $1.50g_0$ lateral [A.D. 12], and the lunar surface configuration (with the four points corresponding to the wheels attachment positions supported), under $g = 1.62\ m/s^2$ gravity, capturing localized structural effects during operations.

The simulations, shown in Figure 11.56 (where XZ is the plane of the plate, while Y is the normal direction), confirm that the panel performs well in both cases. Under launch loading, the maximum equivalent stress is $8.14\ MPa$, well below the limits of CFRP of $1500\ MPa$ [R.D. 54]. The maximum deflection reaches $0.017\ mm$, concentrated near the upper free edge. On Moon surface, stress levels are lower but exhibit sharper gradients near the wheels attachment positions, without exceeding material limits. The results in terms of deformation and stress are therefore considered acceptable.

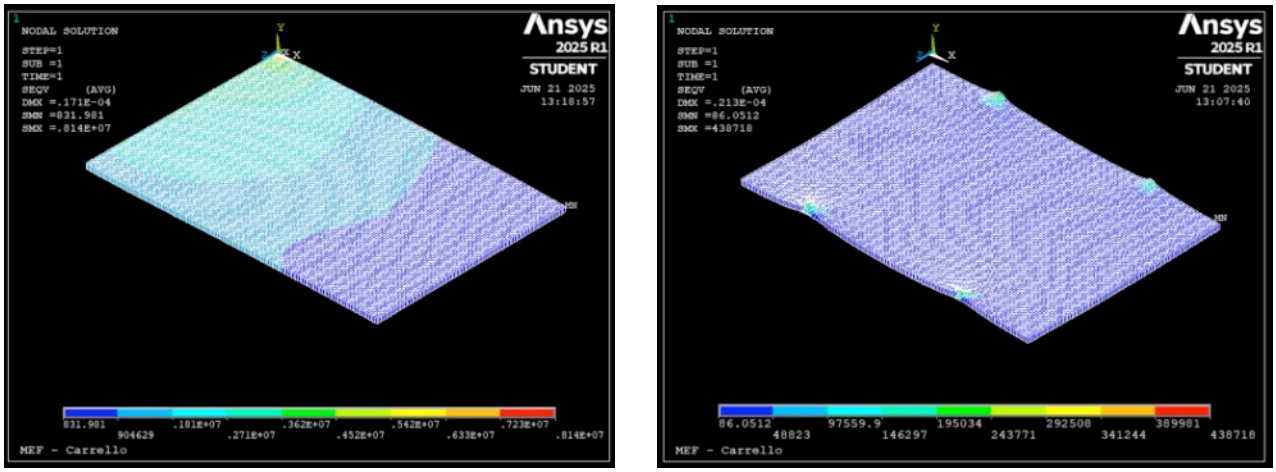

Figure 11.56: Stresses in the plate during launch (left) and surface operations (right)

A modal analysis has also been performed, using the same mass distribution model and the boundary conditions defined for the launch phase. According to the [A.D. 12], structural components mounted on the launcher must avoid natural frequencies near $50\,Hz$, as this is a critical range for potential dynamic coupling with the vehicle's vibrational environment. The analysis confirms that all natural frequencies of the platform lie well below this threshold, thereby ensuring mechanical decoupling from launcher-induced excitations. The results of this analysis are presented in Table 11.46, which shows the natural frequencies corresponding to distinct vibrational modes, the participation factor (quantifying how strongly each mode contributes to motion along Y) and the effective mass (indicating the amount of the structure's mass actively involved in that mode).

Mode	Frequency $[Hz]$	Participation factor	Effective mass $[kg]$
1	5.79	19.12	365.59
2	13.90	-1.41	1.20
3	20.30	-10.95	119.89
4	36.09	0.20	0.04
5	40.44	5.29	27.99

Table 11.46: Vibrational modes of the plate in the Y direction during launch

The wheels chosen for Eagle are those from the Apollo (LRV), shown in Figure 11.57. They feature a flexible galvanized steel mesh structure with a titanium chevron-patterned tread to enhance traction on the lunar surface. An internal rigid frame limits deformation under load. The flexible mesh design performs reliably even under extreme thermal fluctuations without cracking or degrading. The open mesh prevents heat buildup and allows abrasive regolith particles to pass through without damaging the structure [R.D. 229].

Figure 11.57: LRV wheels used for Eagle [R.D. 229]

The LRV wheels are chosen because they can support the maximum load of 306.7 N acting on the front wheels during descent down the ramp (see Section 11.3.4.3), which is the most critical load condition. Moreover, they can resist to the harsh lunar environment. The wheels' geometric and weight characteristics are summarized in Table 11.47.

Diameter	81.80 cm
Width	23 cm
Weight (without traction drive)	5.48 kg

Table 11.47: LRV wheels sizes and weight [R.D. 230]

During the descent down the ramp, it is required that a braking torque acts on each wheel. The LRV braking system can provide up to $264.48\ \mathrm{N \cdot m}$, which exceeds the torque needed during the descent down the ramp, which is $134.00\ \mathrm{N \cdot m}$, as reported in Section 11.3.4.3. The LRV brakes are drum-type and were mechanically actuated via a controller on the LRV: the more it was pulled, the greater the braking torque, up to a maximum corresponding to parking brake settings [R.D. 230]. For this reason, an actuator capable of delivering a maximum force higher than the required $100\ N$ (which is the maximum needed to move the controller) is chosen.
The actuator is the L-220 V6 by Physik Instrumente, which can work at the lunar temperature at landing and can provide a force of 125 N [R.D. 231]. It is controlled by the OBC. No precise information is given about the braking system's mass. Therefore, the mass of the braking system is calculated using a standard mass fraction of $0.021\ kg$ of brake mass per $1\ kg$ of vehicle mass [R.D. 232]. Eagle's mass (while housing Scott) with margins is $675.5\ kg$ so a mass of $14.07\ kg$ for the braking system is obtained. L-220 V6 weighs $200\ g$ and has TRL 4 as it has only been validated in laboratory environment and consumes up to $0.875\ W$, while the wheels have TRL 9 because they have been successfully operated on the lunar surface during multiple Apollo missions [R.D. 233].

11.5.3.2 Scott's structural subsystem

Scott's structural subsystem consists of the CubeRover's outer shell and mechanical elements, it is a 24U unit with a length of 6U in the direction of movement and a cross-section of 2U × 2U. It is assumed that Scott's external shell, being designed to withstand the lunar environment, provides adequate protection against the harsh radiation environment; therefore, no additional radiation shielding is foreseen. Regarding the mass of Scott's structural system, a reference value of 5.8 kg has been taken for a 12U (see Section 11.9), which has an external surface area of $3200\ cm^2$, while the one of a 24U is $5600\ cm^2$ (1.75 times the one of a 12U), so a structural mass of $11\ kg$, which is 1.9 times the mass of the 12U, has been assumed to be conservative. This system has reached TRL 8, since it has been used in lunar missions, but in a different configuration [R.D. 54].

11.5.3.3 PDS

The deployable ramp is a key subsystem enabling the safe transfer of Eagle housing Scott from the LDE to the Moon's surface. Its design ensures sufficient separation between the wheeled cart and Argonaut after the descent. The ramp consists of two parallel sections, which function as rails on which the wheels travel. The length of the ramp has been determined by assuming a $26°$ slope relative to the surface and has been designed to maximize the height occupied on the mounting plate. Each of the rails comprises five segments: the first is an overhanging part that rests on the mounting plate when the ramp is fully deployed and which is $0.29\ m$ long, the second is $1.49\ m$ long and is the one to which Eagle is attached during the flight phase and the ramp deployment. The other three segments are $1.78\ m$ long. The ramp is stowed in a compact, accordion-folded stack on the CPE (Figure 11.58).
The second segment is attached to the overhanging section and initially sits atop it, so that, together with the other three adjacent segments, the ramp reaches a height of $1.78\ m$ and does not exceed the maximum allowable height of $1.80\ m$ on the CPE, thus optimizing the space occupied. When deployed, it unfolds and extends outwards, forming an incline at its outer end and achieving a total length of $6.83\ m$ (Figure 11.58).
For each rail, the connection between the first segment and the CPE, as well as between the segments themselves, is ensured by hinges, supplemented by actuators that allow the ramp to deploy. Bars connecting the two rails are also provided to ensure stability of the ramp.

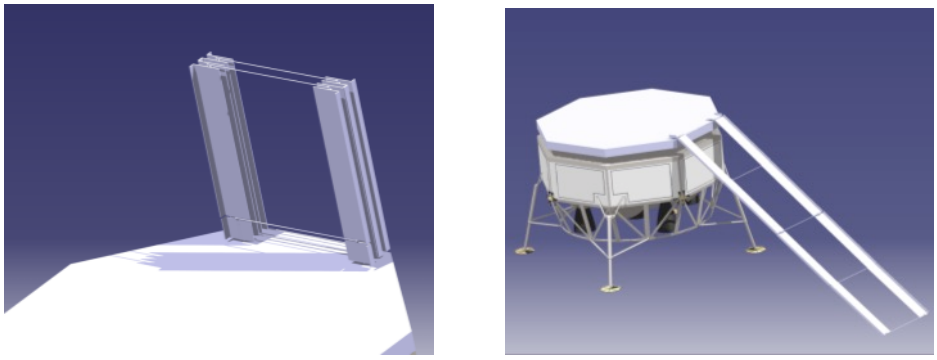

Figure 11.58: Computer Aided Design (CAD) model of the closed ramp (left) and open ramp (right)

Each of the two sections consists of CFRP box-section beams, each $40\ mm \times 40\ mm$ in size, with wall thicknesses of $6\ mm$ in the first two segments and $4\ mm$ in the others (these values are justified later in the document). Aluminum honeycomb sandwich strips, $30\ cm$ wide and $1\ cm$ thick, are bonded on top of the beams to serve as rolling tracks for the wheels. In addition, $5\ cm$ tall lateral guides are added to secure the descent process. The ramp, excluding the mechanisms that enable its deployment, has TRL 4, for the same reasons as Eagle's plate [R.D. 227].

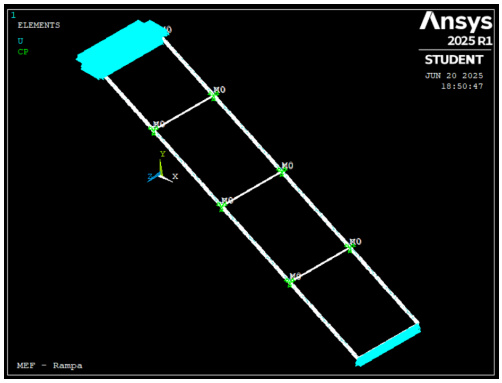

Figure 11.59: FE model of the open ramp

The open ramp during the descent of Eagle housing Scott has been modeled using Ansys Mechanical APDL (Figure 11.59). The box beams were discretized using BEAM188 elements, which allow for accurate modeling of bending and torsion in slender composite structures. The hinges between segments were simulated using COMBIN14 elements acting as rotational springs, each has been assigned a stiffness of $1.00 \cdot 10^5 \frac{N \cdot m}{rad}$ to represent the locked joints post-deployment. Table 11.48contains the properties of the materials which have been considered in the analysis.

Property		Unit	CFRP	Aluminum honeycomb
Density	ρ	kg/m^3	1500	80
In-plane Young's modulus	E_x , E_y	GPa	230	/
Out-of-plane Young's modulus	E_z	GPa	15	0.10
Shear modulus	G_{xy}	GPa	5	/
Poisson's ratio	ν_{xy}	/	0.3	0.050

Table 11.48: Material properties used for PDS analysis

To account for the deployment actuators, MASS21 elements (suitable for modeling concentrated masses) have been included at each hinge location. The first two hinges of each of the two sections of the ramp, which support Eagle during the deployment of the ramp, include two actuators of $5.2\ kg$ each, while the remaining hinges carry $0.57\ kg$ actuators (see Section 11.5.3.4.1.). The overhanging segments of the ramp (first $0.29\ m$ segments) have been fixed in all the translational degrees of freedom, simulating a rigid interface with the launch platform. The free end of the ramp was constrained vertically, representing contact with the lunar surface. Load cases were defined based on the critical deployment scenario, where the 675.5 kg wheeled cart reaches the final segment of the ramp. This position generates the maximum bending moment and deflection. The weight has been distributed across the two tracks as concentrated vertical loads applied at the beam positions beneath the wheels. A design tuning process has been performed to optimize the wall thickness of the box beams. Simulations have been run iteratively, adjusting the section parameters

until the structure achieved equivalent stresses within allowable CFRP limits, maintained controlled deflection at the ramp and a safety margin above standard thresholds. The deformations and stresses in the ramp FEM are shown in Figure 11.60.

Figure 11.60: Deformations and stresses in the ramp FE model

This process has justified the use of $6\ mm$ thickness in the initial segments, where the moment is greatest, and 4 mm in the less critical ones. A detail of the stresses in the ramp FE model is provided in Figure 11.61.

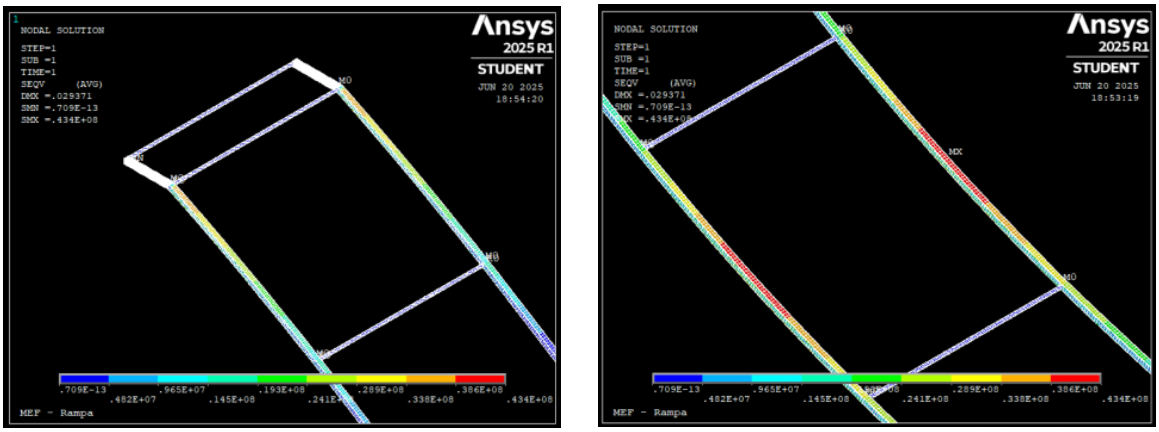

Figure 11.61: Detail of the stresses in the ramp FE

A modal analysis of the fully deployed ramp has been conducted to evaluate its dynamic behavior during the descent of Eagle. The first natural frequency has been calculated as $1.33\ Hz$, corresponding to an S-shaped bending mode. This mode is not critical for the function of the ramp under static lunar deployment loads but should be considered in future dynamic or impact analyses during descent. Table 11.49 shows the results of the modal analysis along the Y direction, which is now defined as the vertical direction.

Mode	Frequency $[Hz]$	Participation factor	Effective mass $[kg]$
1	1.33	0	0
2	3.90	0	0
3	5.43	4.28	18.29
4	5.60	0	0
5	7.73	0	0

Table 11.49: Results from the modal analysis of the ramp in the Y direction of the ramp

To ensure a high coefficient of friction equal to 1.10 in the last three segments of the ramp, so as to prevent slipping and tipping (Section 11.3.4.3), it is assumed that these are coated with a slip-resistant material in the areas in contact with the wheels. Materials of this type exhibit a coefficient of friction of 1.10 when in contact with titanium, which coats the wheels, and can withstand the environmental conditions on the Moon. These materials are widely used in terrestrial applications, but further development is required for use in space applications, for these reasons they have a TRL 3.

Considering that the length of the tape for each section of the ramp is $1.78 \times 3.00\, m$, and the width is equal to that of the wheels ($23\, cm$), the resulting mass is $2.09\, kg$ per side of the ramp, considering a surface density of $1700\, \frac{g}{cm^2}$ [R.D. 234].

11.5.3.4 Mechanisms

11.5.3.4.1 PDS's actuators

The deployment of the ramp is enabled by motorized hinges. To validate the design and assess the forces and moments required during deployment, a complete dynamic model has been developed and implemented in MATLAB. The model considers both kinematic and dynamic effects, including mass distribution, segmental inertia, lunar gravity and actuation profiles. Each rail of the ramp is divided into five rigid segments with known masses and inertia, connected by five hinges. The deployment sequence is controlled by prescribing a sinusoidal angular motion law to each hinge, simulating a smooth and coordinated actuation profile. These laws are defined as functions of time, with amplitude and offset parameters that reproduce the desired final orientation of each segment.

Each ramp segment has been assigned a defined length, mass, and moment of inertia, with additional concentrated mass applied at the hinge locations to account for the actuators. The hinge model is based on the design presented in the Chandrayaan-3 rover ramp deployment system [R.D. 235], which provides a validated approach for modeling articulated joints in space applications. The actuators are modeled as active elements that, once fully deployed, engage a mechanical locking system, effectively behaving as high-stiffness rotational springs.

The motion law is given by Equation (11.41):

$$\theta_i(t) = A_i \cdot \cos\left(\frac{2\pi t}{2T}\right) + D_i \tag{11.41}$$

where A_i is the amplitude of the movement, D_i is the offset, and T = 90s is the total deployment time of each hinge. In that way, for a hinge desired to begin at 0º, open to 180º and then retract to 0º again, A_i is set to -90º and D_i to 90º. To reduce peak power consumption during the ramp deployment phase, the hinges are activated sequentially rather than simultaneously. The deployment begins with the last three hinges, which have lower power requirements and are actuated in parallel. Once these segments are fully extended and locked, the two larger hinges, which drive the heavier sections supporting the payload, are deployed one after the other, ensuring that power demand remains within system limits and thermal loads are minimized. The dynamics of the system are solved using Newton-Euler formalism implemented as a system of linear equations. The forces and moments at each hinge are obtained by solving the equilibrium of each link. For every time step:

- Linear and angular accelerations of each segment are computed numerically.
- The resulting inertial forces and torques are applied.
- Reaction forces and moments at each hinge are computed to satisfy equilibrium.

This allows tracking angular positions, velocities, and accelerations of each joint, linear velocities and accelerations of the center of mass of each segment (Table 11.50) and reaction forces and torques at all hinges over time. The analysis shows a continuous, coordinated unfolding of the ramp, respecting the mechanical constraints. The highest reaction forces and moments occur at the first and second joints, consistent with the fact that the payload is rigidly attached to the second segment during descent.

Segment	Maximum reaction force $[N]$	Maximum reaction moment $[N \cdot m]$	Maximum linear acceleration $[m/s^2]$	Maximum angular velocity $[rad/s]$	Maximum angular acceleration $[rad/s^2]$
1	985.60	1729.70	0.00011	0.028	0.00096
2	975.27	1713.74	0.0016	0.035	0.00120
3	7.83	14.53	0.0032	0.020	0.00070
4	6.59	7.89	0.0051	0.035	0.00120
5	5.83	6.63	0.0069	0.020	0.00070

Table 11.50: Maximum reaction force and moment, angular velocity and acceleration for each segment of PDS

The maximum linear accelerations of each ramp segment remain below 0.007 m/s², which ensures structural stability and prevents dynamic amplification. Given the wide range of torques required throughout the ramp deployment sequence, two different types of actuators have been selected to drive the five motorized hinges. The first two hinges, which support the full weight of the ramp and of the wheeled cart during the deployment, are subjected to extreme

torque demand, reaching values close to 1700 Nm under lunar gravity. To meet these requirements, each hinge is actuated using two redundant Moog Model 965 rotary actuators, operating in parallel. The Moog 965 is a space-qualified actuator that integrates a brushless DC motor with an internal high-torque planetary gearbox and embedded position sensing [R.D. 236]. While the actuator provides up to 200 Nm of continuous torque, in this configuration it is coupled with an external NP 015 10:1 reduction stage by Wittenstein[R.D. 237], allowing each unit to deliver over 2000 Nm of output torque when required. This configuration provides both the torque capacity and mechanical robustness needed to initiate the ramp deployment with the payload attached. Moog965 actuator has TRL 5 since it has been used in aerial platforms and the reduction unit has a TRL 4 since it has been tested only in laboratory environment. Each actuator assembly (actuator, reduction unit and hinge) weigh approximately 7.3 kg and consumes up to 650 W at full load. The use of two actuators per segment ensures full functional redundancy, enhancing reliability in a subsystem that is critical for mission success. The structural compactness and flight heritage of the Moog 965 make it a suitable choice for such high-load joints.
The remaining hinges, which operate under significantly lower torque demands, are actuated using CubeMars AK80-8 motors [R.D. 238], the same model employed in the solar array deployment. These compact actuators are coupled with gear reduction stages by Wittenstein that have a 4:1 ratio [R.D. 239],providing sufficient torque and offering advantages in terms of weight, control precision, and system unification. The use of the same motor type across subsystems simplifies interface design and reduces the number of spare components required. The CubeMars actuators and the reduction units have TRL 4 since they have been tested in a laboratory environment. The actuators consume 230 W and actuator, hinge and reduction unit weigh around 2 kg.

11.5.3.4.2 Solar panels' deployment mechanism

The LPM includes two retractable roll-out solar panels [R.D. 3], whose deployment mechanism must fulfil three primary functions:

- Elevation above nearby equipment, particularly the antenna, to prevent mechanical interference.
- Sun-tracking capability, via rotational reorientation of the panel's normal vector.
- Allowing extension and retraction during the daytime-nighttime cycle.

The complete deployment assembly consists of:

- Two motorized hinges with mechanical locking systems.
- A SADM unit that provides a rotational degree of freedom.
- 2 roll-out solar panels initially stored in a compact cylindrical configuration as shown in Figure 11.62.

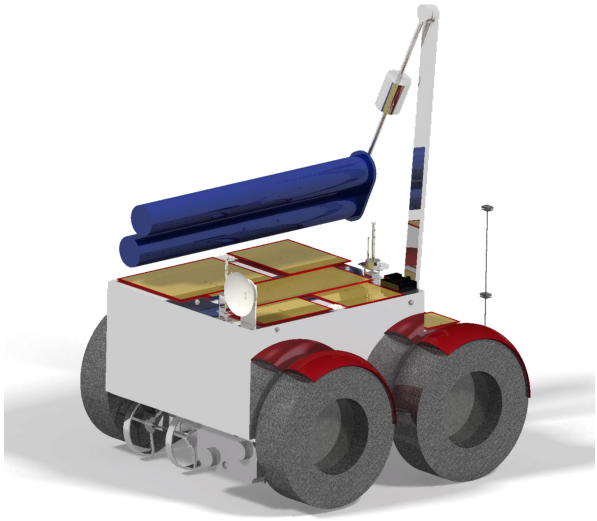

Figure 11.62: Eagle with solar panels in stowed configuration

In stowed configuration, the panels are rolled up into a $1.60\ m$ long cylinder of $11.75\ cm$ diameter, aligned with the long side of the base structure. The first hinge is mounted on a 1.70 m-high mast, indeed, considering a rod of 55 cm that connects the first hinge to the SADM, the SADM cylinder height of 20 cm, and a second rod of 55 cm connecting the SADM to the base of the solar panels (where the second hinge is located), the panel base will be at a height of 3 m when deployed, thus surpassing Argonaut, which therefore does not block solar rays when interposed between the Sun and Eagle. Since the cylinders are at a distance of 7.93 m and Argonaut is at a lower height, it will not interfere with the rotation of the panels, which are each 5.42 meters long.
The deployment proceeds in three stages:

- Elevation stage: the first hinge rotates 150°, raising the SADM to a vertical position aligned with the vertical axis. This provides almost a 3-meter elevation.
- Vertical positioning stage: the second hinge rotates 90°, positioning the rolled-up panel vertically. This completes the mechanical unfolding sequence.
- Solar array deployment and orientation: once in position, the SADM motor becomes active, enabling azimuthal rotation around the axis of the cylinders to track the Sun. The solar panel is then unrolled via an integrated motorized mechanism, forming a rectangular surface tracking the Sun direction (Figure 11.63).

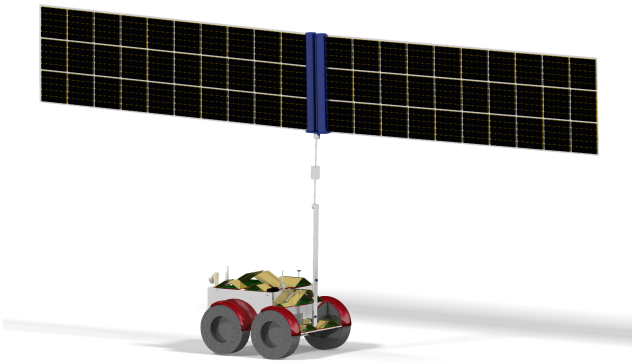

Figure 11.63: Eagle with solar panels in open configuration

All motions are motor-driven and designed for multiple cycles over the station's operational lifespan. The system is engineered with mechanical end stops and locking mechanisms at each hinge to ensure structural stability in both stowed and deployed configurations. The motors chosen for the hinges are CubeMars AK80-8 with a 4:1 reduction gearbox attached, which are the same used for the last three segments of the ramp. With a peak torque of $25\ N \cdot m$ before the reduction box, this solution provides a reliable and efficient solution for actuating the deployment mechanism. The system requires approximately $53\ N \cdot m$ of torque at the first hinge to lift the full assembly, and around $65\ N \cdot m$ at the second hinge to tilt the solar panel into its operational position. This solution strikes an effective balance between mass, power, and performance, ensuring the mechanism can operate reliably under lunar gravity while maintaining a compact and lightweight actuation system suitable for space applications. To enable controlled and precise azimuthal orientation of the solar panel after deployment, the SEPTA36 Solar Array Drive Mechanism [R.D. 240], developed by Beyond Gravity, has been selected as the system's dedicated SADM. This fully qualified and flight-proven unit offers continuous rotation in both directions, with a maximum output speed of $1°/s$ and high-resolution positioning capabilities (step size of $6.25° \cdot 10^{-3}$). The SEPTA36 can deliver more than $55\ N \cdot m$ of output torque, which exceeds the required $7\ N \cdot m$ needed for the azimuthal rotation of the solar panel, providing ample margin, ensuring long-term reliability under lunar conditions and leaving a wide enough margin to use the system also in case of irregular and inclined terrain. With a diameter of $14.4\ cm$, a length of $20.2\ cm$ and a mass of $4\ kg$, its compact design and modular interface make it highly compatible with the system architecture. The mechanism includes slip ring technology with high power transfer capacity, up to $6.3\ kW$ for the SEPTA36-1 configuration, allowing power and signal transmission across rotating interfaces without cable entanglement. This system has TRL 8 since it is flight qualified, but has never been used on a lunar surface mission. The solar array deployment system also includes beams that connect the actuators to the SADM. These are made of CFRP, and their dimensions have been determined through an iterative process in Ansys.
The mass of the rod to which the first hinge of the solar array deployment mechanism is attached has been estimated to be around 5 kg, its weight has been included together with the mounting system and it is made of aluminum.

11.5.3.4.3 Locking system

During the deployment sequence of the ramp, Eagle housing Scott remains temporarily secured to the ramp structure by four Kevlar cables type 0.95 TWA2 [R.D. 241]. Each cable weighs around $1\ g$ and is anchored near the axle of the wheels, ensuring structural stability and preventing premature motion as the ramp unfolds. While the weight distribution can vary depending on the terrain slope and the internal mass layout of Eagle, the system has been designed so that a single cable can support the entire load, ensuring a robust and fault-tolerant configuration. 4 cables have been considered to ensure stability, moreover, since the cables work in tension, the ends of the front and rear wheel cables are attached to the central part of the ramp: the front cables support Eagle until the second segment of the ramp is horizontal (during the PDS deployment), while the rear cables support Eagle when this segment begins to slope downward and before they are removed.

Each cable is equipped with two independent thermal knives, providing redundancy in the cutting mechanism in case of individual failure. The thermal knives are automatically triggered once the ramp deployment is complete, initiating the separation sequence. These devices require 150 seconds to cut through the Kevlar strands, consume $20\,W$ of electrical power each during operation and weigh around 150 grams [R.D. 242].
The cutting process is synchronized across all four attachment points to ensure a uniform release of the load. Once the cables are severed, the charging station is no longer restrained and slides down the ramp under the influence of lunar gravity, guided by the slope and the alignment of the ramp structure. This passive, energy-efficient release mechanism offers a simple, reliable, and mass-efficient solution suitable for autonomous operation in the lunar environment, with redundancy and timing control ensuring safe and precise detachment. All the Kevlar cables and thermal knives have TRL 7, since they have been used in space in similar conditions and they weigh $1.2\,kg$.

11.5.3.4.4 Antenna pointing mechanism

The Ka-band antenna needs to rotate to communicate with Moonlight; therefore, a pointing mechanism that ensures the pointing error of 0.3° as stated in [R.D. 26] and provides the necessary torques to rotate the antenna, which is a parabolic dish of 0.25 m, is needed. The antenna has been modelled as a uniform disk whose radius is 0.125 m and whose mass is 0.38 kg. The moment of inertia *I* has been calculated in Equation (11.42):

$$I = \frac{1}{2}mr^2 = 0{,}00297\ kgm^2 \tag{11.42}$$

Assuming that the system needs to rotate the antenna with an angular acceleration of 1 deg/s^2 (which is a conservative estimate), the required torque is evaluated as in Equation (11.43):

$$\tau = I\alpha = 5{,}18 \cdot 10^{-5} Nm \tag{11.43}$$

The pointing mechanism chosen is the Moog Type 33 biaxial gimbal, it provides much more than this torque and also meets the pointing error requirements: the actuator's output torque of 17 Nm and holding torque of 34 Nm, indicating ample margin, while the output step angle is 0.009°, which is 2 orders of magnitude lower than 0.3° [R.D. 243].This system has TRL 8 since it has proven orbital performance, but is not fully qualified for lunar missions, weighs 4.4 kg and consumes 10 W.

11.5.3.4.5 RDS

Scott is attached to the underside of Eagle at the four corners of its top surface using four Ejector Release Mechanisms (ERMs) developed by EBAD. The ERMs are active mechanical locking systems and non-pyrotechnic devices. For the model selection, it has been assumed that each of the ERMs supports a weight equal to one-quarter of Scott's nominal weight on the Moon. This means each ERM must support 16.52 N. For this reason, the E250 model has been chosen, as it can support a weight of up to 1112 N. Additionally, it can operate within a temperature range that matches the temperature at the Moon landing [R.D. 244]. After the mechanism is activated, the rover passively drops from a height of approximately 10 cm, with the impact absorbed by the wheels. This drop release system is considered at TRL 7 due to its mechanical simplicity and the proven reliability of similar passive release mechanisms in space applications. The four ERMs have a total mass of 0.32 kg and a combined power consumption of 26.4 W during their activation, which takes less than a second.
The wireless platform, initially attached to the underside of Eagle, must be lowered to a height of 35 cm above the lunar surface in order to make contact with Scott's upper surface for recharging. It's important to observe that the platform is suspended at this precise height, rather than resting on the surface, to facilitate accurate alignment and contact for power transfer. The wireless platform weighs 3 kg; therefore, the same system used in the Cooperative Autonomous Distributed Robotic Exploration (CADRE) project has been chosen. CADRE is developing a network of small rovers that will work together to explore the Moon [R.D. 245]. This descent system, in fact, uses a single cable to lower a rover weighing approximately 10 kg [R.D. 246], employing a controlled release mechanism via a drum powered by an electric motor. The wireless interface is lowered vertically and suspended by four cords, which branch off from the main cable to ensure stability. This cable-based deployment system is estimated at TRL 6, leveraging the heritage from the CADRE project where a similar controlled descent mechanism for a comparable payload has been developed and tested in conditions relevant to lunar operations.

11.5.3.4.6 Radiation shield and mounting system

As outlined in (Section 11.7.2.2), a radiation shield is needed to guarantee that critical components are protected from radiation and micrometeoroids impact, in particular, it was observed that a radiation shield with a thickness of 1.5 mm is sufficient to protect the components housed within it. The design of the radiation shield was carried out in such a way as to minimize its surface area, in order to reduce its mass. The mass of the radiation shield has been obtained using CATIA: by appropriately modelling the geometry of the radiation shield and selecting aluminium as the material, a mass of 16.64 kg has been obtained.

The structural mass of Eagle includes an additional 20 kg allocated to the mounting system, comprising, for instance, brackets and bolts. 20 kg are approximately 3% of Eagle's total mass (with margins) of 623.8 kg, consistent with lunar payload handling studies that identify mounting system masses in the 2-5% range [R.D. 247].

11.5.3.5 BRF definition and matrix of inertia

The BRF, centered at the CoM of Argonaut while housing the LPS and additional payload, has been defined as follows (Figure 11.64):

- The Y_{BRF} axis is antiparallel to the outward normal of the radiator surface
- The Z_{BRF} axis is parallel to Argonaut's thrust direction
- The X_{BRF} axis completes the right-handed Cartesian coordinate system

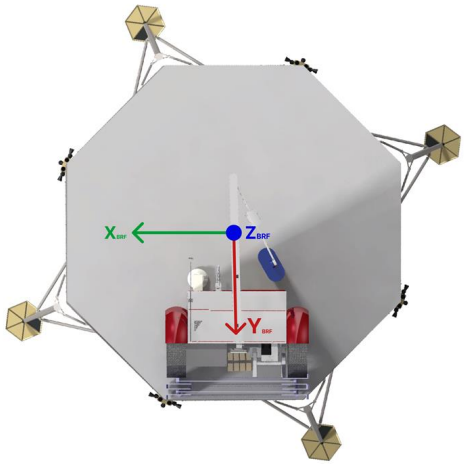

Figure 11.64: BRF axes

Starting from the assumption that Argonaut can carry 2100 kg [R.D. 248], and that 800 kg are allocated to AMPERE, it has been assumed that an additional 700 kg are present on the CPE, resulting in a mass of 600 kg for the latter. These mass values have been used for a preliminary calculation of the moments of inertia and should not be considered final. The additional mass of 700 kg has been placed on the CPE so that the CoM is at most 30 mm away from the Argonaut thrust axis (assuming that it passes through the geometric centre of the mounting deck), as required by [A.D. 12]. The values of the inertia matrix and the coordinates of the geometric centre of the CPE on the $X_{BRF}Y_{BRF}$ plane are shown in Table.

	X_{BRF}	Y_{BRF}	Z_{BRF}
X_{BRF}	28718.72	-19659.75	1196.64
Y_{BRF}	-19659.75	29677.97	1994.42
Z_{BRF}	1196.64	1994.42	47592.62

Table 11.51: Inertia moments (in kgm^2) of Argonaut with payload around the BRF axes

x	2.57
y	5.92

Table 11.52: Mounting deck's geometric centre position (in mm) of Argonaut with payload on the $X_{BRF}Y_{BRF}$ plane

The CoM values of Eagle, during the descent down the ramp and the operational phase have been obtained using the CAD model by assigning the appropriate masses to the components, the values have been reported when necessary in the other sections.

11.6 Mission Analysis

11.6.1 Introduction

This Section outlines the trajectory design process for the lunar landing phase of the mission, starting from a 100 km circular LLO. The spacecraft is assumed to be delivered into this parking orbit by an Ariane 6 launcher. As such, the design and analysis of the transfer phase to lunar orbit falls outside the scope of this study [A.D. 1]. The trajectory design under consideration begins with a manoeuvre that reduces the perilune altitude to 30 km, establishing an elliptical descent orbit. From the perilune of this orbit, a powered descent phase is initiated to perform a soft landing at the designated site on the lunar surface. The objective of the mission analysis is to define the required manoeuvres, ΔV and timing to ensure accurate targeting of the landing site while meeting the mission's constraints.

11.6.2 State-of-the-art analysis

The design of lunar descent trajectories has evolved from analytical approximations used in early missions to high-fidelity numerical optimization approaches in modern programs. The key objective remains the same: compute a feasible, fuel-efficient trajectory that brings the lander from its initial orbit (typically an LLO) to a soft landing at a predefined site, satisfying constraints. The standard architecture of a descent trajectory is typically divided into the following phases [A.D. 9]:

- Deorbit burn: a retrograde manoeuvre lowers the perilune to 30 km (a typical value), near the target site to initiate descent.
- Braking phase: the maximum thrust of the main engines is used to reduce the velocity.
- Pitch-up phase: the thrust vector is reoriented to an almost vertical direction.
- Powered descent and diverts: performed in the last few hundreds of meters to reach a desired state above the landing site.
- Vertical descent and landing: starting from the Vertical Gate (VGA) at a given constant vertical speed to ensure a soft.
- Divert manoeuvring (optional): up to two divert manoeuvres may be included in the descent trajectory, the first at a Low Gate (LGA) altitude of 500 m, the second at a Hazard Detection and Avoidance (HDA) altitude of 150 m. Their combination may introduce a horizontal deviation at VGA entry up to ± 120 m.

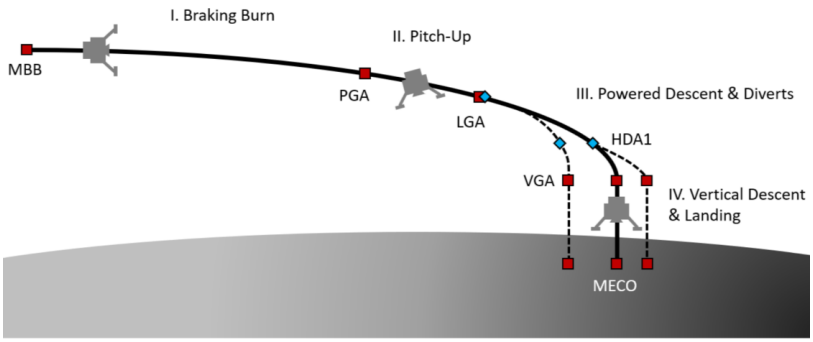

Figure 11.65: Powered descent phases [A.D. 9]

The last five phases constitute the powered descent shown in Figure 11.65. The literature highlights that the most common way to perform the design of the powered descent trajectories on Moon, is formulating a classical optimal control problem: the goal is to determine the time history of the control inputs (typically engine thrust) that minimizes (or maximizes) a given cost function (for instance fuel consumption), while satisfying the system dynamics and a set of constraints on states, controls, and boundary conditions.
To solve this problem numerically, four main approaches are commonly used [R.D. 33]:

- Indirect methods: these methods are based on Pontryagin's maximum principle, which provides the necessary conditions for optimality. The original problem is reformulated into a system of coupled differential equations, including the equations of motion (for the state variables) and the so-called costate equations (derived from the Hamiltonian). The resulting Boundary Value Problem (BVP) can yield highly accurate solutions but is often sensitive to initial guesses and difficult to solve for complex or highly constrained systems.
- Direct methods: in these approaches, the optimality conditions are not derived explicitly. Instead, the state and control trajectories are discretized over the time horizon, transforming the continuous-time optimal control problem into a NonLinear Programming (NLP) that can be solved using standard numerical optimization techniques. Common direct methods include direct shooting, direct collocation, fractional programming, dynamic programming, quadratic programming, convex optimization formulations.

- Evolutionary Algorithms (EAs): EAs use mechanisms inspired by biological evolution, such as reproduction, mutation, recombination, and selection. Candidate solutions to the optimization problem play the role of individuals in a population, and their quality is evaluated through a fitness function. The evolution process then begins, leveraging large populations to explore the solution space and gradually move towards a global optimum according to specific rules. There are various types of EAs, and Genetic Algorithms (GAs) are among the most widely used.
- Hybrid methods: these methods aim to combine the strengths of both direct and indirect approaches. Typically, a direct method is first used to generate a good initial guess, which is then refined using an indirect method to achieve accurate convergence. Several hybrid techniques have been applied to trajectory optimization problems, including impulsive solution guessing, multiple shooting, response surface methodology, and dynamic programming based on the Hamilton–Jacobi–Bellman equation.

11.6.3 Final design

11.6.3.1 Proposed solution

The idea is to divide the trajectory analysis into two main phases: an initial orbital phase, consisting of revolutions in LLO and the transfer ellipse, and a final powered descent phase. The physical assumptions underlying this design are as follows:

- the only acting forces are the gravitational interactions between the spacecraft and the Moon and thrust;
- the Moon is assumed to have a spherical symmetric mass distribution; hence gravity is radial;
- the Moon's geometry is approximated as spherical; however, during the powered descent, due to the low altitude, a further simplification is adopted by treating the lunar surface as flat;
- the thrust is applied only within the orbital plane, so there are no out-of-plane force components, and the orbital plane remains unchanged over time.

As mentioned in Section 11.6.1, the mission analysis begins in a circular LLO at an altitude of 100 km. The spacecraft is required to remain in this orbit for a number of days, denoted with n_{days}, ranging from 4 to 14 [R.D. 8]. After this period, the perilune must be lowered to 30 km. The proposed approach is to perform this manoeuvre using a Hohmann transfer-like ellipse. The first step is to select the orbital parameters of the LLO. Assuming that the inclination is equal to ninety degrees, i.e., $i = 90°$ (polar orbit), the choice of the RAAN is closely linked to the desired epoch for touchdown on the lunar surface. Specifically, the goal is to choose the RAAN of the orbit so that, considering the Moon's rotation around its own axis, the landing site lies exactly in the orbital plane at the time of perilune passage. By doing so, it can be assumed that the landing site will remain in the orbital plane during the powered descent phase: this phase lasts approximately 10 minutes, during which the effect of the Moon's rotation can be neglected, given that the lunar rotation period is about 27 days. To sum up:

- INC, $i = 90°$;
- RAAN, Ω depends on the desired touchdown epoch;
- ECC, $e = 0$;
- SMA, $a = 1837.40\ km$;
- AOP, $\omega = 0°$ (by convection);
- TA at the initial time $t_0, \nu(t_0)$ depends on the outcome of the powered descent phase analysis, which will be carried out later in this document.

The trajectory of the landing site observed from an inertial reference frame is the one in red in Figure 11.66. Specifically, the inertial reference frame is the Moon-Centred Inertial primed (MCI') frame, whose origin coincides with the Moon's centre, its positive $Z_{MCI'}$-axis is aligned with the Moon's rotation axis, pointing in the direction of lunar rotation at the J2000 epoch, while the $X_{MCI'}$ $Y_{MCI'}$-plane of this frame coincides with the lunar equatorial plane. Specifically, the $X_{MCI'}$ and $Y_{MCI'}$ axes being fixed directions defined according to GMAT's body-inertial option. It can be observed that, at any generic time t, the right ascension of the landing site is $\alpha_{LS}(t)$ (green in Figure 11.66).

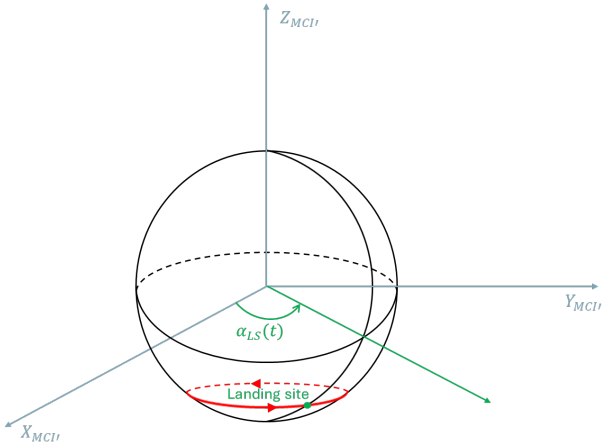

Figure 11.66: Landing site in MCI' frame

Given the Moon's angular velocity (ω_{moon}), the landing site's right ascension can be calculated using Moon's rotational period of 27 days, 7 hours, 43 minutes, and 11.60 seconds, the time of perilune t_p, shown in Equation (11.44), that is the moment when the spacecraft reaches perilune, and the number of days (n_{days}). This is because, at time t_p, the right ascension of the landing site needs to be equal to the orbit's RAAN (Equation (11.45)). This alignment ensures that the landing site lies within the plane of the polar orbit:

$$t_p = t_0 + n_{days} + \Delta t_{orbit} + \Delta t_{tran} \tag{11.44}$$

$$RAAN = \alpha_{LS}(t_p) = \alpha_{LS}(t_0) + \omega_{moon}(t_p - t_0) \tag{11.45}$$

Where:

- $\Delta t_{orbit} = 632.47\ s$ is the time required to complete the last orbit after n_{days} have elapsed, in order to reach the correct position for performing the Hohmann transfer manoeuvre. It can be calculated simply by evaluating the fractional part of $\frac{n_{days}}{\tau_{orbit}}$, where it has been considered $n_{days} = 4 \cdot 86400\ s$, and evaluating τ_{orbit} as in Equation (11.46), where $\mu_{moon} = 4.90 \cdot 10^{12}\ \frac{m^3}{s^2}$:

$$\tau_{orbit} = \frac{2\pi\ a^{\frac{3}{2}}}{\sqrt{\mu_{moon}}} = 7065.97\ s \tag{11.46}$$

- $\Delta t_{tran} = 3432.52\ s$ is the time needed to travel half of the Hohmann transfer ellipse, evaluated in Equation (11.47).

$$\Delta t_{tran} = \frac{\pi\ a_{tran}^{\frac{3}{2}}}{\sqrt{\mu_{moon}}} \tag{11.47}$$

  a_{tran} is given by Equation (11.48), considering $R_{moon} = 1737.4\ km$.

$$a_{tran} = \frac{(R_{moon} + 100\ km) + (R_{moon} + 30\ km)}{2} \tag{11.48}$$

- $\alpha_{LS}(t_0)$ is the right ascension of the landing site at time t_0, which can be obtained from GMAT based on the known value of t_0.

The RAAN value of the orbit will be defined after completing the powered descent analysis, as the epoch of perilune can be obtained by subtracting the powered descent duration from the selected touchdown date. The analysis of the subsequent phase can proceed without any issue, as the in-plane geometry remains unaffected by the RAAN value. The powered descent must be designed first also to determine the required downrange distance for landing; this allows the computation of the true anomaly $\nu(t_0)$ and the argument of periapsis of the elliptical transfer orbit (ω_{tran}). This strategy is possible because, under the assumption of spherical Moon, the descent from perilune onward remains unchanged regardless of the ω_{tran} value. The idea is to obtain an initial estimate by applying the following simplifications [R.D. 251]:

- The Moon is assumed to be flat, so the local and vertical horizons remain constant over time from the perspective of an inertial reference frame.
- The lunar gravitational acceleration is assumed to be constant and equal to 1.62 $\frac{m}{s^2}$.

- The control vector $\underline{u}$, whose time law is to be determined to achieve a soft landing at the desired location while satisfying all the constraints described in [A.D. 9], consists of the thrust magnitude T and the pitch angular velocity ω_y (Equation (11.49)).

$$\underline{u}(t) = \Big(T(t), \omega_y(t) \Big) \quad (11.49)$$

A clarifying scheme is shown in Figure 11.67.

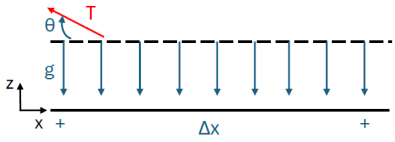

Figure 11.67: Flat Moon scheme

Δx represents the total horizontal distance required for landing, which will be used as an approximate value for the downrange necessary to land in a more realistic scenario involving a spherical Moon. In other words, the case in Figure 11.68 is being approximated using the previously simplified case.

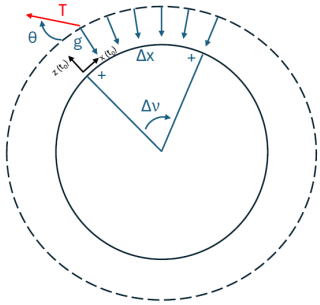

Figure 11.68: Circular Moon scheme

Consequently, once Δx is known, it is possible to compute the ω_{tran} by using Δv, obtained as in Equation (11.50).

$$\Delta v = \frac{\Delta x}{R_{moon}} \quad (11.50)$$

After performing the landing design using a trial-and-error approach on the elements of the control vector and running numerous simulations until all the constraints described in [A.D. 9] were satisfied, a consistent powered-descent solution has been obtained.
In Table 11.53 the initial conditions are summarized, all the initial conditions were known except for θ_0, which emerged only after repeated simulations.

$t_0[s]$	$x_0[m]$	$z_0[m]$	$V_{x_0}\left[\frac{m}{s}\right]$	$V_{z_0}\left[\frac{m}{s}\right]$	$\theta_0[\circ]$	$m[kg]$
0	0	30000	1681.5	0	27.72	6965.62

Table 11.53: Initial time and initial state vector

Table 11.54 shows the control vector components during each phase.

Phase name	$T[N]$	$\omega_y\left[\frac{\circ}{s}\right]$
Braking phase	18000	0
Pitch-up phase	15995	5
Powered descent and diverts	6022	0
Vertical descent and landing	$\in [\,5773.10, 5816.90\,]$	0

Table 11.54: Control vector

Table 11.55 shows the instant of time t_f representing the end of the phase and the corresponding components of the state vector.

Phase name	$t_f[s]$	$x_f[m]$	$z_f[m]$	$V_{x_f}\left[\frac{m}{s}\right]$	$V_{z_f}\left[\frac{m}{s}\right]$	$\theta_f[\circ]$	$m_f[kg]$
Braking phase	549.90	512886.90	675.58	25.22	-23.28	27.72	3908.08
Pitch-up phase	562.36	512996.21	490.60	0	1.64	90	3846.53
Powered descent and diverts	705.84	512996.21	30	0	2	90	3579.63
Vertical descent and landing	720.90	512996.21	0	0	2	90	3552.67

Table 11.55: Time and state vector

Figure 11.69 and Figure 11.70 show the evolution in time of the control vector and of the state vector components, respectively.

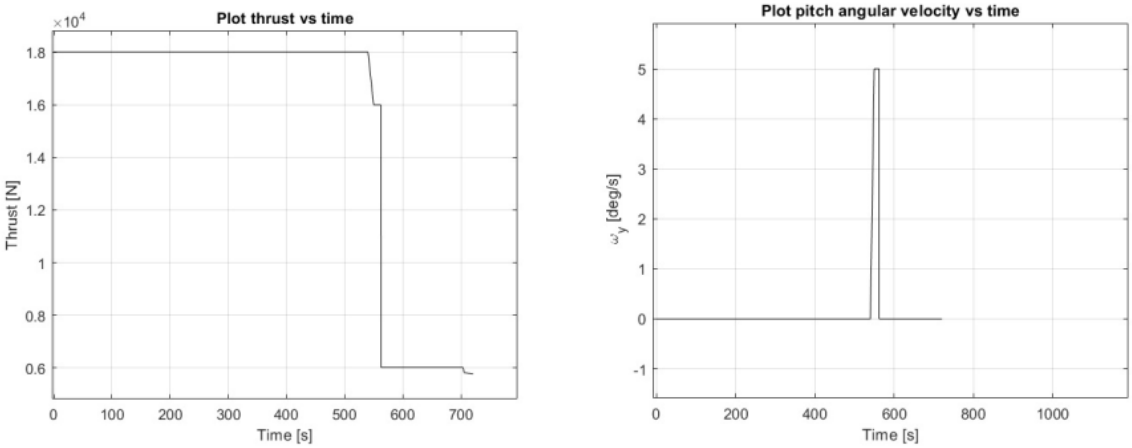

Figure 11.69: Plots of the control vector components over time

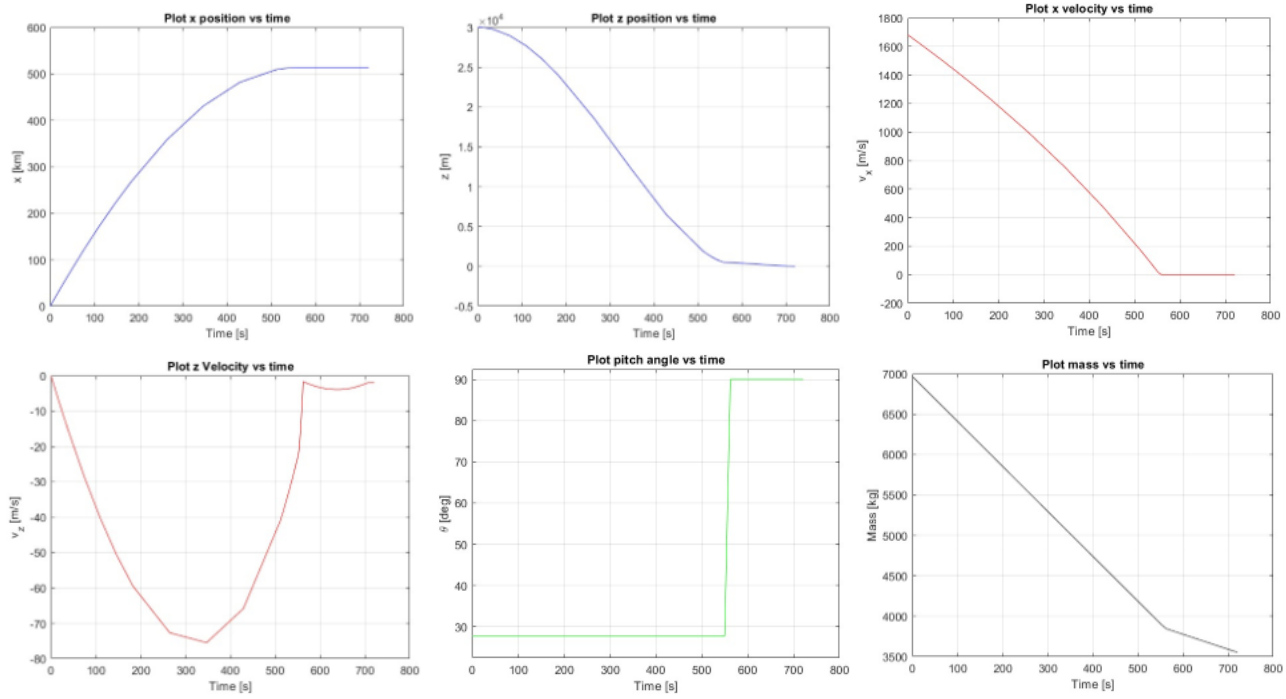

Figure 11.70: Plots of state vector components over time

It is then possible to compute the time evolution of the norm of the total acceleration vector, shown in Figure 11.71.

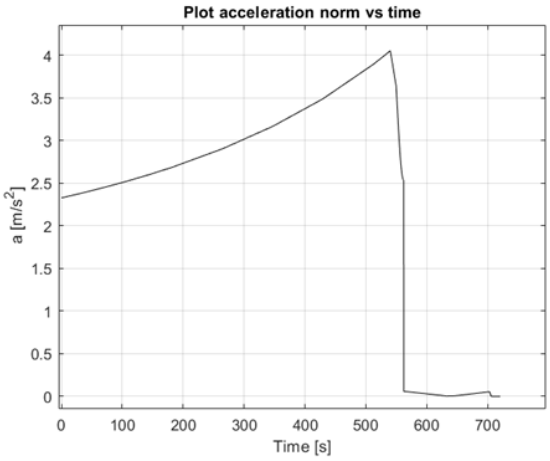

Figure 11.71: Plot of the acceleration norm over time

It can be observed that the maximum acceleration during the powered descent is $4.05\ m/s^2$, which does not pose any structural issues, as can be verified in Section 11.5.
The system of differential Equations (11.51) has been used to compute the evolution of the state vector:

$$\underline{\dot{x}} = \underline{f}\left(t, \underline{x}(t), \underline{u}(t)\right) = \begin{cases} \dot{x}(t) = V_x(t) \\ \dot{z}(t) = V_z(t) \\ \dot{V}_x(t) = -\dfrac{T(t)}{m}\cos\left(\theta(t)\right) \\ \dot{V}_z(t) = \dfrac{T(t)}{m}\sin\left(\theta(t)\right) - g \\ \dot{\theta}(t) = \omega_y(t) \\ \dot{m}(t) = -\dfrac{T(t)}{c} \end{cases} \qquad (11.51)$$

Having the time required to perform the powered descent ($t_{PD} = 720.90\ s$, provided in Table 11.55) and considering the touchdown date as 05 April 2037 16:00:00.000, it is possible to determine the initial epoch t_0, thus the $\Omega(t_0)$= 302.69°.
Once the mass at touchdown, m_{TD}, is obtained, an estimate of the manoeuvre cost in terms of ΔV has been made (Equation (11.52)).

$$\Delta V_{TOT} = I_{sp} g_0 \ln\left(\frac{m_0}{m_{TD}}\right) = 2195.57 \frac{m}{s} \qquad (11.52)$$

Where the specific impulse provided in [A.D. 9] is $I_{sp} = 330\ s$, $g_0 = 9.81 \frac{m}{s}$ is the gravity acceleration of the Earth , the mass at t_0 is $m_0 = 7000\ kg$ [A.D. 9], and $m_{TD} = 3552.67\ kg$ (Table 11.55). Subtracting the Hohmann manoeuvre ΔV_{HOM} used to lower the perilune from 100 km to 30 km (in Equation (11.53)) to the total ΔV_{TOT}, the result ΔV_{PD}, which represents the cost of the powered descent has been obtained in Equation (11.54).

$$\Delta V_{HOM} = V_{tran} - V_{circ} = \sqrt{\mu_{moon}\left(\frac{2}{R_{moon} + 100\ km} - \frac{1}{a_{tran}}\right)} - \sqrt{\frac{\mu_{moon}}{R_{moon} + 100\ km}} = -15.94 \frac{m}{s} \qquad (11.53)$$

$$\Delta V_{PD} = \Delta V_{TOT} - |\Delta V_{HOM}| = 2179.63 \frac{m}{s} \qquad (11.54)$$

A first estimate of the order of magnitude of the powered descent could be obtained as in Equation (11.55).

$$\frac{1}{2} m V^2 + mgh = \frac{1}{2} m {V_{TD}}^2 \Longrightarrow V_{TD} = \sqrt{V^2 + 2gh} = 1710.24\ \frac{m}{s} \qquad (11.55)$$

With: $m = 6965.62$ kg; $g = 1.625 \frac{m}{s^2}$; $h = 30000\ m$; $V = 1681.5 \frac{m}{s}$.
Once the touchdown velocity V_{TD}, is obtained, that is the velocity the vehicle would have at touchdown if the Moon were flat and the body were allowed to fall freely under gravity, we can get a first estimate of the ΔV required to brake

the vehicle to zero velocity at touchdown, by imposing $\Delta V = V_{TD}$. Observing the obtained result, it can be noted that the actual ΔV (obtained in Equation (11.54)) is higher than this initial ideal estimate. The reason is that the selected control law is not optimized to minimize fuel consumption; rather, it is simply designed to satisfy the trajectory constraints. By implementing an optimized control, for example using optimal control theory, it is possible to reduce the ΔV to about 1.9 km/s [R.D. 252]. At this point, once Δx is known, ω_{tran} can be derived.

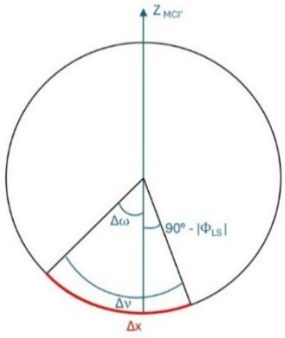

Figure 11.72: Representation of Δv, $\Delta \omega$ and Δx

From Equation (11.50), $\Delta v = 16.32°$ is obtained. As shown in Figure 11.72, $\Delta \omega$ can be derived (Equation (11.56)), where $\phi_{LS} = -89.4°$ is the latitude of the landing site.

$$\Delta \omega = \Delta v - (90° - |\phi_{LS}|) = 15.72° \quad (11.56)$$

At this point, ω_{tran} and the true anomaly at t_0 can be evaluated as in Equations (11.57) and (11.58), respectively.

$$\omega_{tran} = 270° - \Delta \omega = 254.28° \quad (11.57)$$
$$v(t_0) = 90° - \Delta \omega = 74.28° \quad (11.58)$$

Therefore, the revolutions in the initial circular orbit will begin and end at the point where the Hohmann manoeuvre is performed, as shown in Figure 11.73.

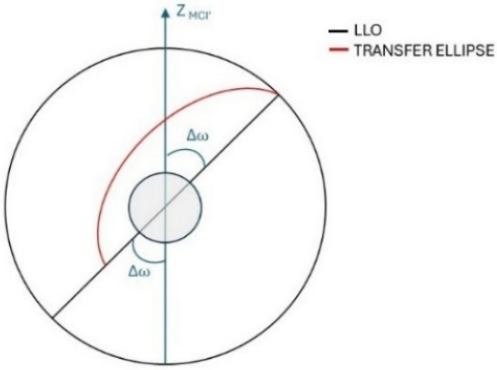

Figure 11.73: Representation of Hohmann transfer

The figures shown below are obtained by GMAT and MATLAB and depict, respectively, the orbital phase (Figure 11.74) and the powered descent (Figure 11.75 and Figure 11.76).

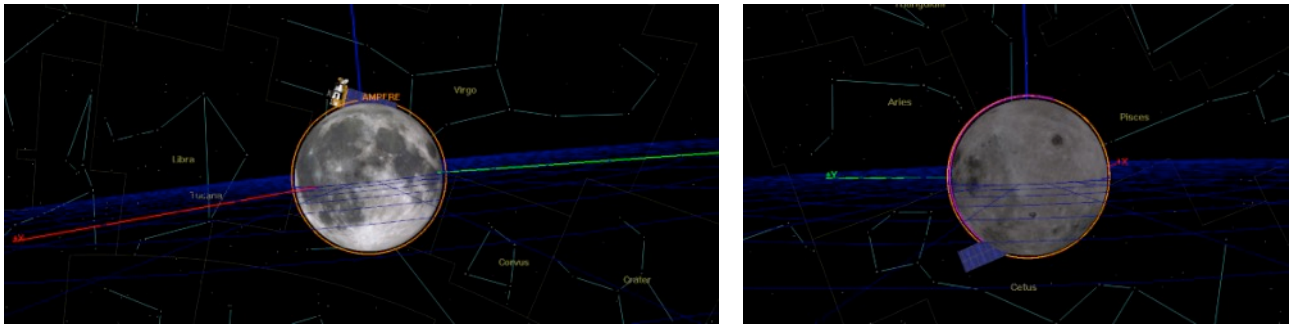

Figure 11.74: Representation in GMAT using MCI' of LLO (in orange) on the left and of LLO (in orange) and elliptical transfer orbit (in fuchsia) on the right

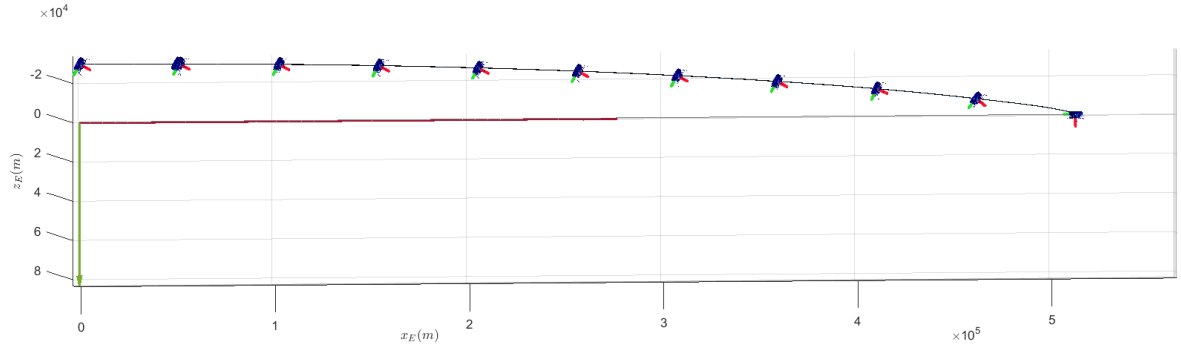

Figure 11.75: Representation of the entire power descent under flat Moon hypothesis

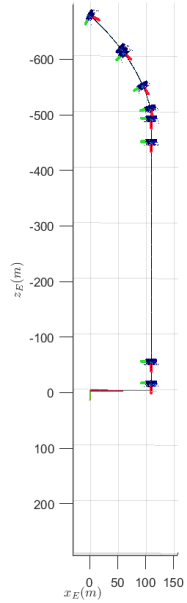

Figure 11.76: Representation of the last phases of the power descent under flat Moon hypothesis

If anomalies at perilune prevent the initiation of the powered descent, the spacecraft is programmed to complete the entire elliptical orbit and return to perilune after a time interval equal to $2 \cdot \Delta t_{tran} = 2 \cdot 3432.52\ s$. This strategy avoids additional ΔV expenditure.

11.6.3.2 Sun incidence angles

During the circular orbit and transfer ellipse phases, which have a significant duration, defining the Sun incidence angles relative to the spacecraft is important for WP 3.2 and WP 3.3. This problem can be easily solved by using the spacecraft's relative position to the Moon, $\underline{r}_{spacecraft-moon}$, and the Sun's relative position to the Moon, $\underline{r}_{sun-moon}$. The latter vector was obtained using the NASA NAIF/SPICE toolkit kernels, and the results are expressed in the Moon-Fixed Frame (MFF), defined in [R.D. 253]. At this point, the Sun's position vector relative to the spacecraft, $\underline{r}_{sun-spacecraft}$, can be derived by the vector operation in (11.59). The mentioned vectors are represented in Figure 11.77.

$$[\underline{r}_{sun-spacecraft}\ (t)\ ]_{MFF} = [\underline{r}_{sun-moon}(t)]_{MFF} - [\underline{r}_{spacecraft-moon}(t)]_{MFF} \quad (11.59)$$

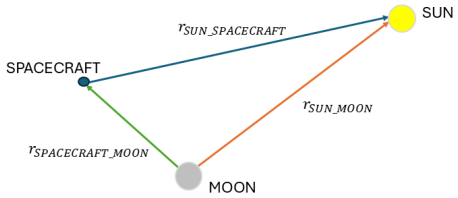

Figure 11.77: Position vectors representation

The components of this vector are expressed in the MFF, but the objective is to rotate them into the BRF in order to analyse how the Sun's rays impact the spacecraft. To achieve this, a series of reference frame transformations is required: $MFF \longrightarrow MCI' \longrightarrow PERIFOCAL \longrightarrow ORF \longrightarrow BRF$.
To perform the rotation from $MCI' \longrightarrow MFF$, a type-3 rotation must be applied by an angle equal to the right ascension of the Moon's prime meridian, α_{PM}, as reported in Equation (11.60).

$$M_{MCI'\rightarrow MFF}(t) = M_3\big(\alpha_{PM}(t)\big) \quad (11.60)$$

Where being λ_{LS} is landing site's longitude of the landing site, $\alpha_{PM}(t)$ can be expressed as in Equation (11.61), with $\alpha_{PM}(t_0)$ given by Equation (11.62).

$$\alpha_{PM}(t) = \alpha_{PM}(t_0) + \omega_{moon}(t - t_0) \quad (11.61)$$

$$\alpha_{PM}(t_0) = \alpha_{LS}(t_0) - \lambda_{LS} \quad (11.62)$$

So $M_{MFF\rightarrow MCI'}$ can be retrieved as in Equation (11.63).

$$M_{MFF\rightarrow MCI'}(t) = M_3\big(\alpha_{PM}(t)\big)^T \quad (11.63)$$

Next, it is necessary to transform from $MCI' \longrightarrow PERIFOCAL$ frame, which is done through the typical 3-1-3 sequence of rotations (Equation (11.64)).

$$M_{MCI'\rightarrow PERIFOCAL} = M_3(\omega)M_1(i)M_3(\Omega) \quad (11.64)$$

When performing this transformation, it should be kept in mind that for the circular orbit, the argument of periapsis $\omega = 0°$ (by convention), whereas for the transfer ellipse, $\omega_{tran} = 254.28°$.
To perform the transformation from the $PERIFOCAL \longrightarrow ORF$ the Equation (11.65) and Equation (11.66) must be applied in the case of circular orbit and transfer ellipse, respectively.

$$M_{PERIFOCAL\rightarrow ORF} = M_2(\nu + 90°)M_1(270°) \quad (11.65)$$

$$M_{PERIFOCAL\rightarrow ORF} = M_2(\nu - 270°)M_1(270°) \quad (11.66)$$

Finally, to perform the transformation $ORF \longrightarrow BRF$, the rotation shown in Equation (11.67) must be applied.

$$M_{ORF\rightarrow BRF} = M_2(270°) \quad (11.67)$$

To be more precise, at $t = t_p$, the angle to be used for the type-2 rotation is $270° - 27.72°$, since the spacecraft will have performed a pitch angle change to initiate the powered descent with the correct attitude. In the end, Equation (11.68) is obtained to pass from MFF to BRF.

$$M_{MFF\rightarrow BRF}(t) = M_{MFF\rightarrow MCI'}(t)M_{MCI'\rightarrow PERIFOCAL}M_{PERIFOCAL\rightarrow ORF}M_{ORF\rightarrow BRF} \quad (11.68)$$

Afterwards, it is possible to calculate $\underline{r}_{sun-spacecraft}$ components in the BRF, as shown in Equation (11.69).

$$\begin{bmatrix} x_{sun-spacecraft}(t) \\ y_{sun-spacecraft}(t) \\ z_{sun-spacecraft}(t) \end{bmatrix}_{BRF} = M_{MMF \rightarrow BRF}(t) \begin{bmatrix} x_{sun-spacecraft}(t) \\ y_{sun-spacecraft}(t) \\ z_{sun-spacecraft}(t) \end{bmatrix}_{MFF} \quad (11.69)$$

Once the components of the Sun position vector relative to the spacecraft are available in the BRF, the two angles that uniquely define the Sun's direction (Figure 11.78) are evaluated in Equations (11.70) and (11.71).

$$\chi(t) = atan2\left(\frac{y_{sun-spacecraft}(t)}{x_{sun-spacecraft}(t)}\right) \quad (11.70)$$

$$\eta(t) = \text{asin}\left(\frac{z_{sun-spacecraft}(t)}{|r_{sun-spacecraft}(t)|}\right) \quad (11.71)$$

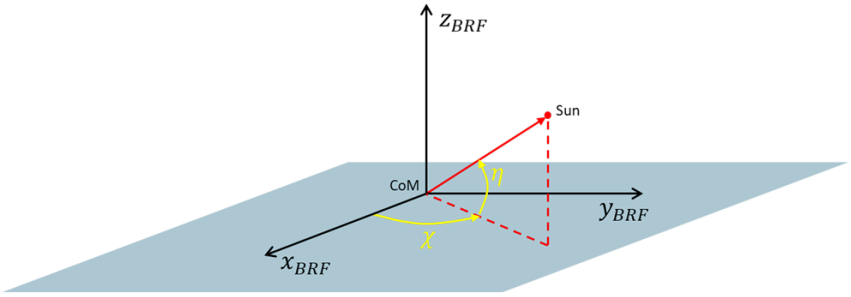

Figure 11.78: Representation of the Sun direction in BRF

The analysis of the angles is performed only between t_0 and t_p, thus excluding the powered descent phase, Figure 11.79 and Figure 11.80 show χ and η evolution in this time span, respectively.

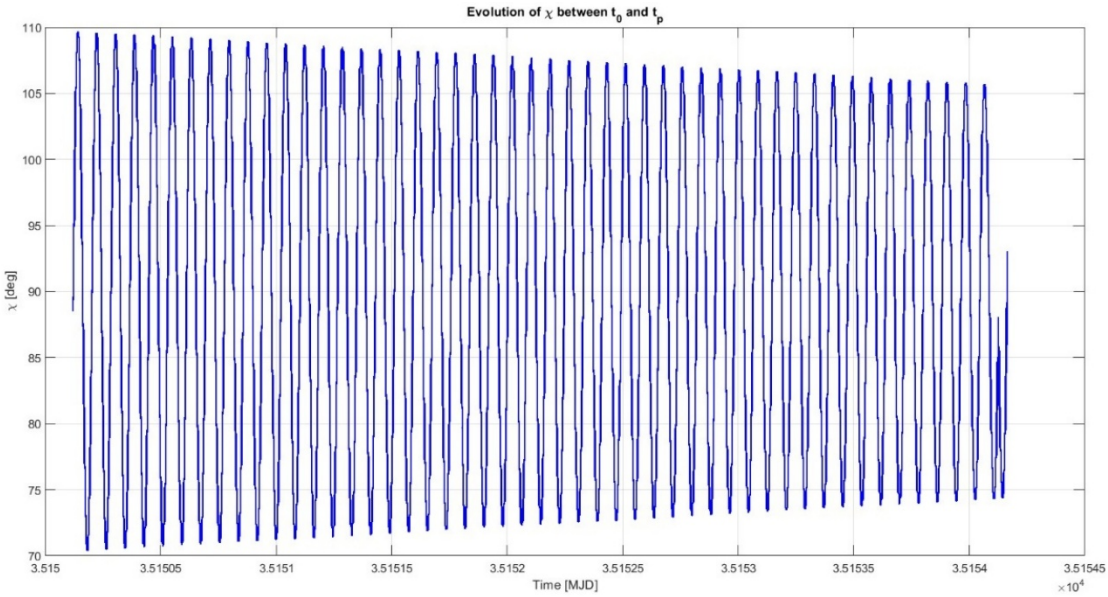

Figure 11.79: Plot of χ evolution between t_0 and t_p

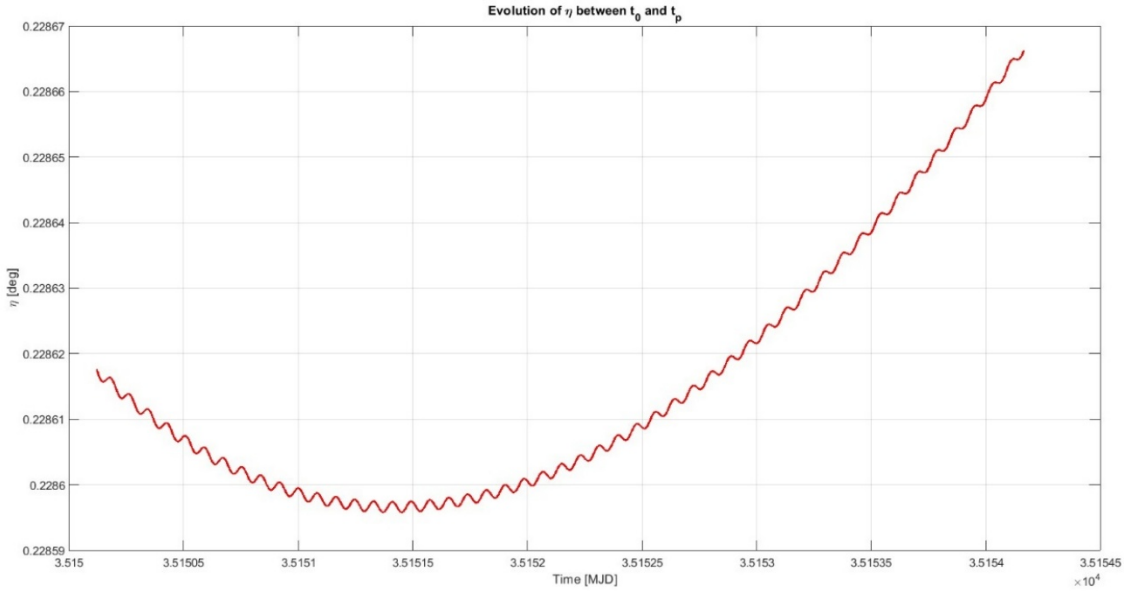

Figure 11.80: Plot of η evolution between t_0 and t_p

11.7 Environmental analysis

11.7.1 State-of-the-art analysis

The lunar environment has been investigated to ensure safe landing conditions and to consider all critical aspects for payload survival and operativity. In particular, the elements considered are surface temperatures, radiation, dust and regolith, internal heat fluxes, meteoroids and moonquakes, Earth visibility, morphology, and illumination conditions.
The interest in the lunar South Pole has increased significantly in recent years: for this reason, most of these aspects which need in-situ analyses have been estimated with orbital missions such as LRO and with prediction models for Chang'e program.
Surface temperatures have been analysed by Diviner Lunar Radiometer Experiment onboard the LRO. Diviner is providing the most comprehensive view of how regolith on airless bodies stores and exchanges thermal energy with the space environment. Approximately a quarter trillion calibrated radiance measurements of the Moon, acquired over 5.5 years by Diviner, have been compiled into a 0.5° resolution global dataset with a 0.25 h local time resolution [R.D. 274]. The key aspect to consider while analysing Moon surface temperatures is the latitude, as expected due to the low inclination of rotation axis of the satellite. For this reason, no further estimations have been made regarding the different potential landing sites and for the entire mission a range of 50 K to 200 K for surface temperature is set, for all South Pole regions outside the PSRs, with an average temperature of 115 K [R.D. 274]. Maximum and minimum global surface temperature maps are shown in Figure 11.81.

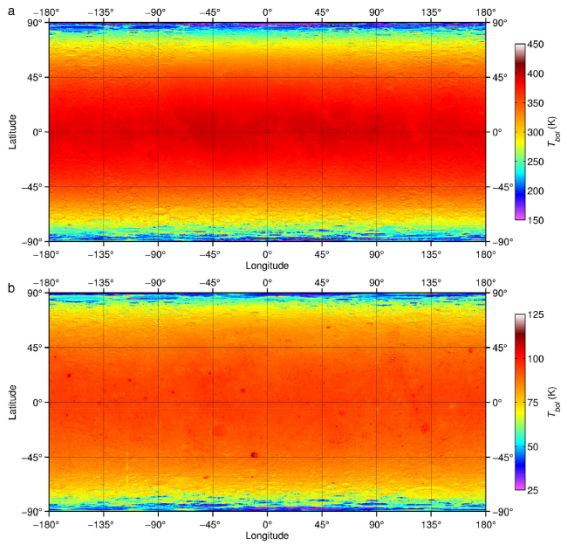

Figure 11.81: Maximum (a) and minimum (b) global temperatures [R.D. 274]

Radiation effects are the most challenging to be evaluated without in-situ analyses: the main data were given by Apollo missions and, more recently, by Chandrayaan-1's mission and LRO. The radiation that hits the Moon is very diverse. It includes huge fluxes of $\sim 1 \frac{keV}{u}$ solar wind ions, a few high-energy (>1 GeV) GCR particles, and high-energy Solar Cosmic Rays (SCR) particles intermittently emitted from the Sun [R.D. 39]. The most concerning aspect is that the heavy nuclei in the galactic cosmic rays and the many secondary particles, especially neutrons, that the GCR generate in the lunar soil, require the use of shielding to protect humans and sensitive electronic equipment on the Moon [R.D. 39]. Radiation Dose Monitoring (RADOM) instrument (operated during the Indian Chandrayaan Mission) and the Cosmic Ray Telescope (CRaTER) instrument of the NASA LRO mission's result are reported in [R.D. 275].
RADOM measured average doses of $0.227 \frac{mGy}{d}$ in a 100 km lunar orbit and $0.257 \frac{mGy}{d}$ at 200 km, while the CRaTER measured an exposure of about $0.22 - 0.27 \frac{mGy}{d}$ in a nominal orbit of 50 km of altitude. The main consequence on those rays is the interaction with the lunar soil: when immersed in space plasma or exposed to sunlight, dust particles start to collect or emit electrons and ions, thus charging the dust particles. In [R.D. 276] it is shown that the low temperatures and low solar altitudes typical of the lunar South Pole result in low conductivity of the soil, enabling high surface potential charging and significant quantities of electrostatically levitated dust. At low solar altitude angles, the surface potential value is around 0.1 V, enough to generate an electrostatic force sufficient to counteract the gravitational force, particularly for nanoparticles. In this scenario, the lunar dust spatial density is approximately $10^{8.9}\ m^{-3} - \ 10^{11.5}\ m^{-3}$within 30 meters, with higher densities ($10^{10.9}\ m^{-3} - \ 10^{11.5} m^{-3}$) near the surface.
Dust also impact on TCS performance, as well discussed in [R.D. 3]and [R.D. 12]: increasing of absorptivity and emissivity are expected when radiators are covered by dust; on the other hand, louvers are not able to protect radiators due to very small size of the lunar dust (60 to 80 µm in average [R.D. 39]), especially during phases where a high accumulation of dust is expected.
Lunar regolith consists of glassy, mineral and agglutinated fragments. Typical density values are around 1.3 g/cm³ and 1.9 g/cm³ (it increases with depth). Lunar regolith has a very good load-bearing capacity, it's easily excavatable and it's an exceptional thermal insulator. At the same time, regolith tends to adhere to every surface, due to high electrostatic charges and irregular and sharp surface of the particles.
No analyses have been conducted on internal heat fluxes in South Pole: during Apollo 15 and 17 missions in-situ analyses reported a value around $3 \times 10^{-6} \frac{W}{cm^2}$ [R.D. 39]. In the same document, 0.16 perforations by meteoroids per m^2 per day were estimated, with an impact velocity of 13 to 18 km/s. A median value of $0.3976 \times 10^{-16} \frac{g\ cm^2}{s}$ of meteoroid mass flux (rate of mass of meteoroid material impacting a given surface area of the Moon per unit time) is calculated, while the median value of energy flux (i.e. total energy released by meteoroids) is $100.11 \times 10^{-16} \frac{kJ}{cm^2 s}$ [R.D.132]. These impacts are on the main responsible of moonquakes: some stronger (but rarer) shallow lunar earthquakes may occur due to tectonic processes and meteorite impacts, which vary widely in terms of energy. Other sources of seismicity include the monthly deep-focus moonquakes caused by Earth-Moon tidal stresses and thermal degradation of young lunar surface features [R.D. 39]. A recent PSHA (Probabilistic Seismic Hazard Analysis) was performed for developing a hazard map near the lunar South Pole. In this PSHA result, a seismic event of a PGA (Peak Ground Acceleration) of 1.625 m/s² is estimated, with a period of return of 475 years (i.e., probability of exceedance of 10% in 50 years), on Nobil Rim, close to Shackleton region [R.D. 278]. For mobile structures, those risks are less relevant than planted facilities, and so there is less relevance concerning AMPERE mission.
As seen in Section 10.4.4.6, the illumination conditions and morphology are the main drivers for this mission. 5 potential landing sites were identified in [R.D. 94], [R.D. 95] and [R.D. 96], named S1, S2, D, CR1 and CR2 in Section 10.1. Comparing the documents, it is possible to define the extension of these areas: the Shackleton regions cover an area around 17 km^2, while D span 27 km^2, CR1 11 km^2 and CR2 5 km^2. In [R.D. 95] a short debrief on Earth visibility is made, which is important to ensure a backup communication link directly with earth (see Section 11.4): the Earth visibility values for each location on Moon were calculated by comparing the elevation of the local horizon to the elevation of the Earth at a given time by simulating the trajectories of Earth over local horizon. The Earth visibility values range between 0 (never visible) and 1 (always visible) and indicate the percentage of time steps where any fraction of the Earth disc was visible at each pixel. For Shackleton regions (i.e. S1 and S2) 29% of Earth visibility was calculated, while for D, CR1 and CR2 are 44%, 30% and 31%, respectively. In [R.D. 94] and [R.D. 96] a 400 x 400 km Digital Terrain Model (DTM) of the lunar poles from LOLA ranging measurements is provided; it has been used to simulate illumination conditions at surface level for 50 x 50 km regions, centered on the poles. Illumination has been derived in one-hour increments from January 1, 2017 to January 1, 2037 to cover the lunar precessional cycle of 18.6 years. Illumination at the poles depends not only on local topography and the slight seasons caused by the 1.54° tilt, but also on the height above ground and on the lunar precessional cycle. For this reason, simulations at 0,2 and 10 m above the ground, for different landing sites (SR1, SR2, D, CR1 and CR2), have been conducted ([R.D. 94], [R.D. 95], [R.D. 96]): the second case

is the one of more interest for AMPERE to fit architecture dimensions and constraints. The results are presented in Table 11.56.

	SR1	SR2	D	CR1	CR2
Average maximum illumination (%)	89.8	73.9	80.0	88.0	78.0

Table 11.56: Average maximum illumination of the landing sites

Average maximum illumination measures how much of the Sun was visible on average, ranging from 0 (never visible) to 1 (fully visible all the time). A value like 0.5 could mean partial visibility throughout or full visibility for half the time. It reflects light intensity, not exact duration [R.D. 94]. In [R.D. 95] are also reported the maximum hours in shadow for each landing site: the same definition for average illumination can be given for average darkness. Consequently, the maximum time in shadow is defined as the longest uninterrupted darkness duration within average darkness intervals (i.e. the opposite of the average maximum illumination). This is a crucial aspect for AMPERE mission, as it represents a worst-case scenario for a correct design of the EGSD. Simulation at 2 m above the ground showed that maximum time in shadow is reduced by 70% with respect to the same values on the ground [R.D. 94]: S1 and S2 are characterized by 66 hours of longest time in shadow, while D, C1 and C2 by 151, 165 and 112 hours, respectively.
In [R.D. 95] a morphology description of the different landing sites is reported. As required in the [A.D. 1] and [A.D. 9], the LDE legs provide landing stability on lunar slopes up to 15° and ensure sufficient ground clearance to avoid contact with rocks up to 0.5 m in height. Different data about slopes are available in [R.D. 94], [R.D. 95], showing different results with respect to [R.D. 96]: because of that, an average value of the slopes is presented in Table 11.57, excluding high peak values due to PSRs regions, which are reported in the document.

	SR1	SR2	D	CR1	CR2
Average slope (°)	11.1	6.0	14.0	11.5	10.6

Table 11.57: Average slopes of the landing sites

Figure 11.82 and Figure 11.83 better represent morphology of the interested areas. Different ranges of slopes are described in Figure 11.82: the maximum slope values are relatively high (about 45°), but these steep values are confined only to small crater walls that can be avoided while planning rover traverses [R.D. 96].

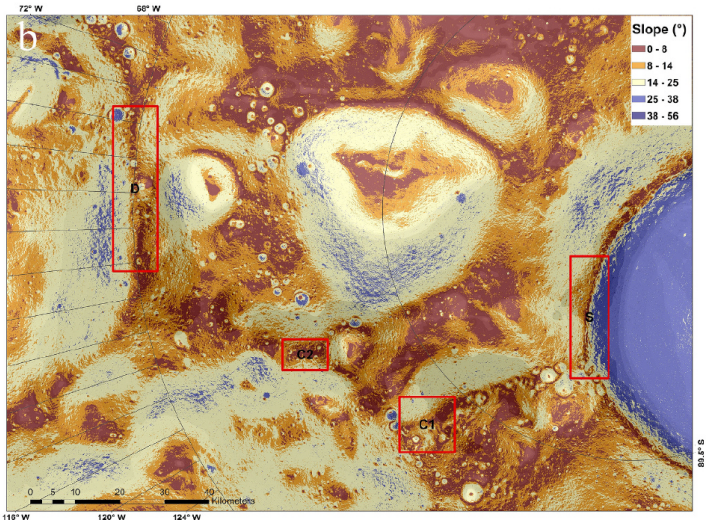

Figure 11.82: Slope map of the landing sites [R.D. 95]

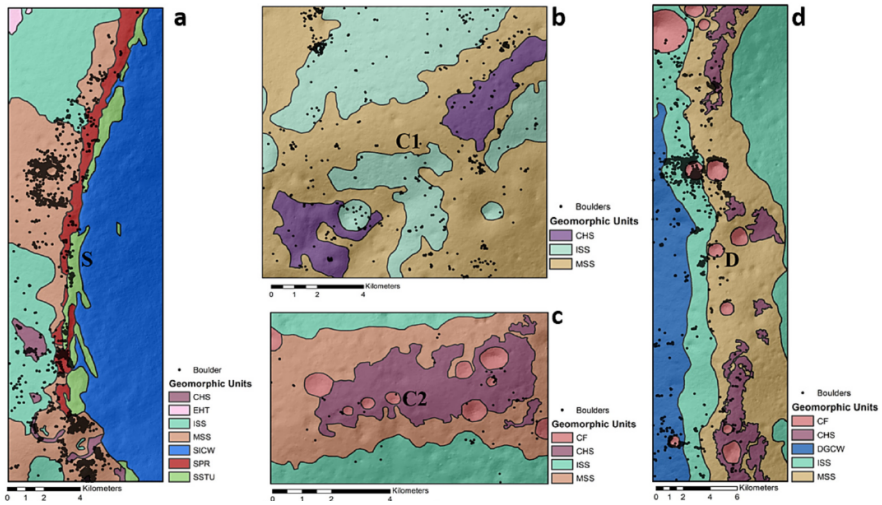

Figure 11.83: Site-specific geomorphology map of landing sites [R.D. 95]

In Figure 11.83 geomorphology map of the landing site is shown: the areas are divided in geomorphic units, which are better described in [R.D. 95]and [R.D. 279].

According to these analyses, the Shackleton region is suitable for landing, but only in a small portion of the area; the Shackleton Perched Rim (SPR) zones are very close to a PSR and high boulder density reduces positive landing probability, making rover exploration challenging. The same analysis can be made for D, where zones with 20° and 25° slopes are predominant with respect to the others. CR1 and CR2 are characterized by flatter areas, with less boulder density. At the end, the sites CR1 and CR2 are categorized as 'excellent' for landing and traverse planning. The trafficability map is shown in Figure 11.84. Site S (S1 and S2) is highly challenging for landing and rover operations due to steep slopes and rough terrain, with a safe zone limited to a narrow patch of area on the Shackleton rim, while site D has a much wider areal distribution of trafficable zone. Site CR2 is the best option for landing and rovering as indicated by the widespread distribution of green areas across the site. Site CR1 also offers good conditions. Therefore, sites CR1 and CR2 are classified as 'excellent' [R.D. 95].

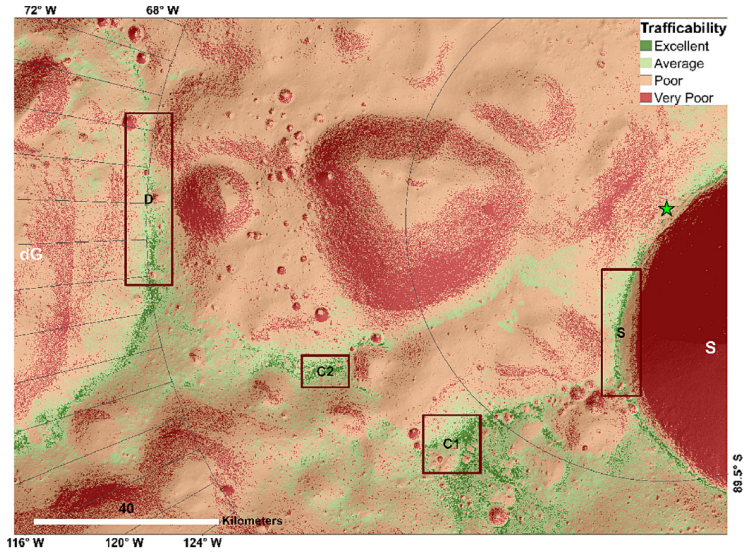

Figure 11.84: Trafficability map [R.D. 95]

11.7.2 Final design

Environmental analyses focused on the following key aspects: illumination condition, surface temperatures at the landing site, slope evaluation, radiation on lunar surface, micrometeoroids and dust impact on Eagle and Scott. The outcomes of these analyses were used as inputs for the other design WPs to properly size their subsystems.

11.7.2.1 Illumination and temperature analysis

Understanding the daytime-nighttime alternation at the landing site has been essential to maximize energy production and to estimate the duration of available charging windows necessary for the survival of Eagle and Scott. At the same

time, estimating the expected temperature range at the landing site has allowed for preliminary assessments of suitable components and the potential need for active heating in low-temperature conditions. To evaluate illumination at the landing site, a MATLAB code has been developed considering as input data the relative position between Moon and Sun. Given the known position of the landing site, the relative position of the Sun with respect to CR1 is calculated over the course of one year, using a sampling interval of 15 minutes, and in ephemeris time. The vector is evaluated in Moon Centered Moon Fixed (MCMF) reference frame: a rotation matrix has been calculated to evaluate the coordinates of it in a local reference frame cantered in the landing site. Therefore, elevation angles are calculated to estimate the illumination condition; when these angles are greater than zero, the Sun is above the horizon and so visible on the landing site. These values are increased by the maximum terrain slope angle (later detailed in the document) when over the horizon, since the landing site is a morphological singularity that enhances solar exposure, while CSPICE estimation is based on a perfectly spherical surface. When the Sun is below the horizon, elevation is forced to 0.
The simulation has revealed an alternation between light and dark periods, showed as an extended time window spent in shadow. Simulations have been carried out from 2021 to 2037: the first year corresponds to the one for which the time evolution of the visible solar disk at C1 is described in [R.D. 96] while the second is the final year for which robust illumination data are available in the open literature. This recurring pattern has been observed for each simulated year, indicating a limitation of the numerical approach rather than a realistic representation of the Sun's apparent motion.
As a first step, the start and end of the darkness time window in simulation in 2021 have been identified and analysed through graphical comparison with respect to results showed in Figure 11.85. This allowed a refinement of the darkness period: the longest continuous darkness interval has been found to be approximately 5 days, followed by a 7-day light period. On average, the data suggested a recurring sequence of 2 days of darkness followed by 7 days of light.
This pattern has been incorporated into the simulation code by discretizing the long dark window into two 12-day cycles (7 days of light followed by 5 of darkness), separated by a 9-day cycle (2 days of darkness and 7 of light), repeated at least nine times. Outside this window, a maximum of 15 consecutive days of light has been observed, followed by 2 days of darkness.

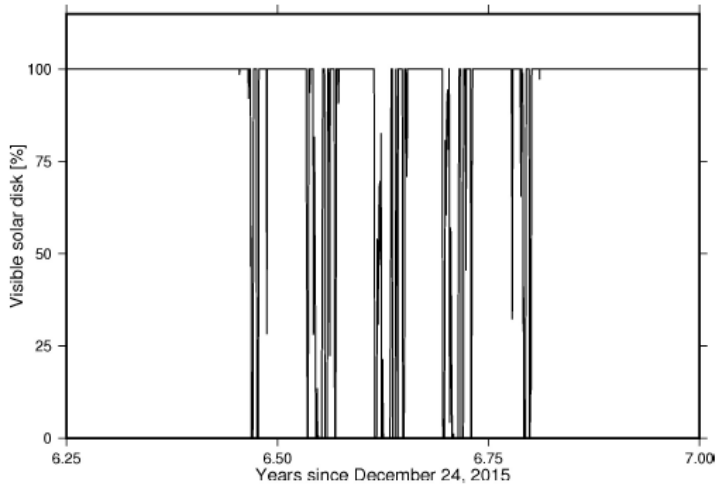

Figure 11.85: Time evolution of the visible solar disk at CR1 in 2021 [R.D. 96]

Additionally, a mathematical model has been developed to estimate the variation in illumination with altitude. This model considers the maximum solar flux as a function of the incidence angle, and an exponential increase in illumination with altitude, based on data from [R.D. 94] and [R.D. 96] (i.e., 88% of the maximum average illumination at 2 meters and 92% at 10 meters). Temperatures on lunar soil are calculated by considering two main effects: incident solar radiation on the lunar surface and heat conduction through the regolith due to its thermic resistance: the lunar surface is comprised of two layers of lunar regolith of varying physical properties as determined during the Apollo 15 and 17 missions. The top 2 cm consists of a loose regolith commonly known as "fluff." The fluff layer is characterized by a lower thermal conductivity ranging between $0.9 \cdot 10^{-5} \frac{W}{cm\,K}$ at 0 K and $3 \cdot 10^{-5} \frac{W}{cm\,K}$ at 400 K with an average density of $1.3 \frac{g}{cm^3}$. Beneath this fluff layer lies regolith of a much higher compaction level and density equal to approximately $1.8 - 2.0 \frac{g}{cm^3}$ and a thermal conductivity of 0.93x10^{-4} at 0 K to $1.94 \cdot 10^{-4} \frac{W}{cm\,K}$ at 400K [R.D. 178].
These data are considered as input to simulate the thermal conduction process in a one-meter soil layer discretized to represent both the fluff layer and the regolith, each with their respective densities and thermal conductivities. An average specific heat is used to estimate thermal diffusivity. Thus, the surface temperature is calculated as a function of incoming flux (i.e. geothermal and solar contributes) and of temperature of the adjacent node, which is updated

every 15 minutes through central finite difference method. The initial temperature profile is set to 50 K to represent the worst-case conditions (see Section 11.7.1).
Surface temperature is calculated integrating Equation (11.72), with a Runge-Kutta method, presented in the same document, in which the starting condition is fixed at 200 K, in compliance with data presented in Section 11.7.1.

$$\frac{dT}{dt} = \frac{1}{MC}[(S\,A\cos\beta_s + \alpha_s G_i A) - (A\varepsilon\sigma T^4 + (1-\alpha_s)\,S\,A\cos\beta_s)] \quad (11.72)$$

S is the maximum solar radiation power, equal to 1450 $\frac{W}{m^2}$. A is the potential area of interest, estimated as 2.25 m^2, β_s is the incidence angle, meaning the complementary angle of elevation with respect to the normal at the surface, α_s is the surface absorptivity, equal to 0.87, G_i is the internal heating power, equal to $0.031\frac{W}{m^2}$, while $\varepsilon = 0.97$ and σ are respectively the surface emissivity and the Stefan-Boltzmann constant[R.D. 178].
The difference between the temperature evaluated including conduction effects and temperature calculated using Equation (11.72) is computed; the results have suggested that conduction has a greater impact during dark phases. As a first approach, the two effects are linearly combined; during the mission a minimum temperature of 97.70 K and a maximum temperature of 286.80 K is estimated. Figure 11.86 and Figure 11.87 show, respectively, the trend of temperature and illumination percentage throughout the year. The second plot shows the behaviour of illumination percentage with respect to the maximum level registered in the analyses, reached on the 365th day: the minimum value, 0.37%, is reached on the 200th day. A low temperature value at day 0 depends on numerical calculations and can be estimated as equal to temperature at the next instant, around 225 K. Temperature at the expected landing date is 285K. Before the light/dark alternation, a period of 109 Earth days of continuous illumination is observed, while afterward it, 69 days of constant light are computed.

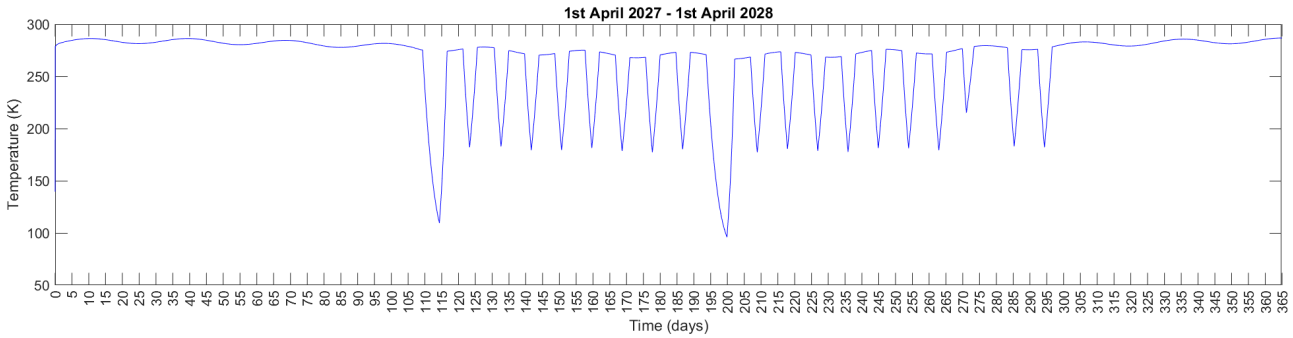

Figure 11.86: Temperature trend in days

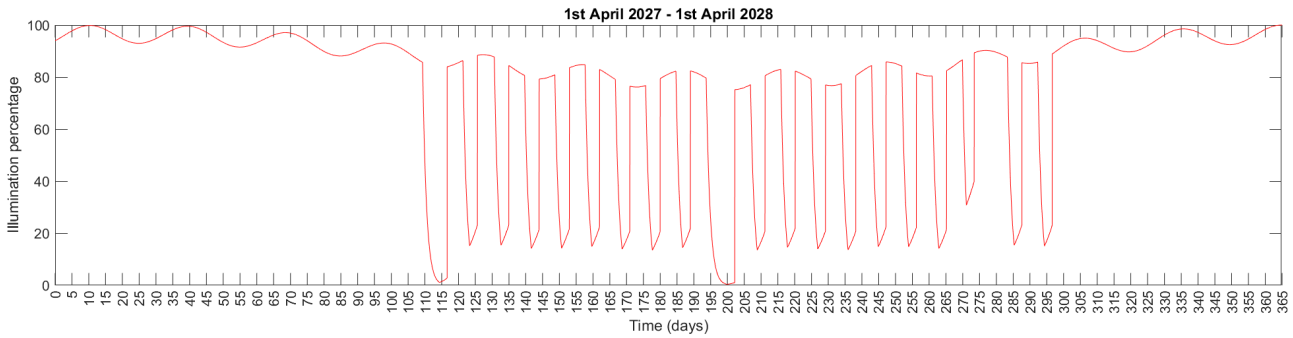

Figure 11.87: Illumination percentage trend in days

11.7.2.2 Radiation and micrometeoroids

A shield to protect critical components from radiation and micrometeoroid effects is designed to guarantee mission success (see Section 11.5).As the protection system is already foreseen for Scott by the manufacturer, the sizing of the shield has been conducted only for Eagle. The shield can protect Eagle by both micrometeoroids impact and radiations from deep space as it is made of aluminium; this material has good resistance to penetrations despite its lightness (density around 2700 $\frac{kg}{m^3}$), and excellent solar radiation reflection properties, which are the main radiation effects on lunar surface: the exposure to GCR is inevitable but generally contributes a low dose rate compared to the sporadic, unpredictable, but sometimes very intense SPEs in which solar energetic particles are accelerated close to the Sun by

solar flares and coronal mass ejections. Exposure to large SPEs in a situation with insufficient shielding may cause severe acute effects [R.D. 280]. By SPENVIS simulation, a graph of absorbed doses with respect to aluminium thickness is provided: the analysis is conducted using the SHIELDOSE-2 and the target material (i.e., the ones which absorb the radiation) is set as silicium, which most electronic components are made of. A total dose greater than $10^4 rads$ delivered to silicon-based devices could affect their performance or cause damage, based on open literature: for this reason, this order of magnitude is set as minimum condition for absorbable radiation.
Creating equations for hypervelocity particles impacting monolithic structures are given in Equation (11.70) [R.D. 281]:

$$t = 5.24\, d^{\frac{19}{18}}\, H^{-0.25} \left(\frac{\rho_p}{\rho_t}\right)^{0.5} \left(\frac{V_n}{C}\right)^{\frac{2}{3}} \tag{11.73}$$

Where t stands for the penetration thickness, while H and C are parameters of the protection material: the first is the Brinell hardness, while the second one is sound of speed in the material, values reported in [R.D. 281]. The density of the meteoroids is set $at\ 500 \frac{kg}{m^3}$ by SPENVIS Meteoroids and debris model, for particles with a mass > $10^{-2} g$. By SPENVIS simulation, a critical diameter of 1 cm at $5 \frac{km}{s}$ is defined, while for real impact velocity (around $18 \frac{km}{s}$ as described in Section 11.7.1) the critical diameter is smaller. To be totally safe, a diameter of 5 cm at $18 \frac{km}{s}$ is set in the equation. The result reports a shield thickness of 1.5 mm which is sufficient to let the main components absorb a maximum level of radiation of $\approx$ 5000 rad (Figure 11.88), respecting the safety margins for absorbed doses. Also, a 20% margin for the shield has been considered in the mass budget, thus being able to guarantee more robust protection.

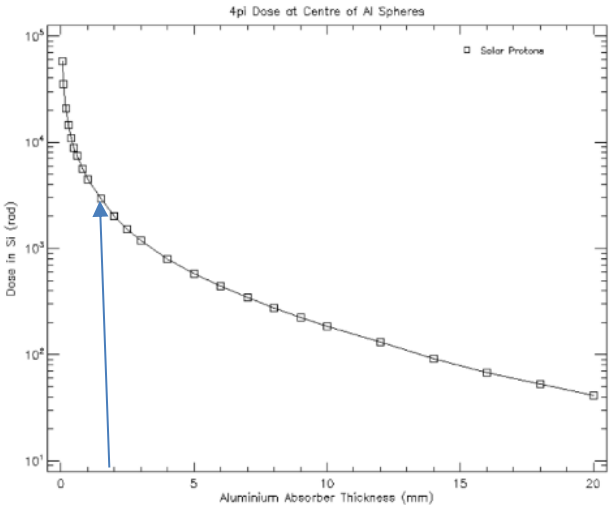

Figure 11.88: Dose in rad absorbed by silicium in function of aluminium shield thickness

11.7.2.3 Dust

Lunar regolith is a very challenging environmental element to deal with: lunar dust can stick to mechanical and electronic devices, due to both physical and electrical properties, better described in Section 11.7.1. Thus, an active system which can remove dust attached to Eagle and Scott is considered necessary to guarantee the success of the mission. The EDS consists of a series of parallel electrodes connected to a voltage source that generates a travelling wave, acting as a contactless conveyor. The working principle relies on generating a strong, non-uniform, and time-varying electric field, generated with a 4-phase square-wave which is applied to each electrode to exert electric forces that can mobilize particles [R.D. 282]. The non-uniformity of the electric field defines areas at different field intensity, generating an electrostatic force gradient which promotes dust removal. A coating dielectric layer is required for EDS, preventing direct contact between dust particles (which may be charged or induce charges) and the electrodes themselves and favouring a correct distribution of the waves on the surface. The coating that covers the EDS electrodes is typically a 0.1mm borosilicate glass from SCHOTT, but can be other coating materials as well, such as Kapton [R.D. 282]. The MLI and SMLI for both Eagle and Scott are dielectrics, so it is not demanding to add any other dielectric layer to coat the EDS.
For preliminary sizing, no further investigation about the position of electrodes on Eagle has been conducted, focusing on the force that the system can provide with respect to SMLI surface and frequency of activation to ensure dust removal. Power consumption per unit of area of $4 \frac{W}{m^2}$ is estimated by application of this system in past missions, such

as Materials International Space Station Experiment (MISSE). Thus, the estimated power consumption during activation was 49.5 W for Eagle and 1.61 W for Scott (12.36 m^2 for Eagle and 0.402 m^2 for Scott, see Section 11.2).
Four main forces are responsible for dust adhesion on surfaces, as well described in [R.D. 283] and resumed in the following table:

Forces	Formulas	Physical Meaning
Van der Waals	$F_{vdW} = 4\pi R\gamma$	Attractive adhesive force generated by short-range interactions between atoms/molecules on the surface of the particle and the plane
Image	$F_{imm} = -\frac{\alpha Q^2}{16\pi\varepsilon_0 R^2}$	Attractive force between a charged particle and a conductive surface, which induces a charge distribution that attracts the particle
Patch (triboelectric effect)	$F_{patch} = -\frac{\sigma^2 A_c}{2\varepsilon_0}$	Localized force caused by a patch of the charged particle after contact/rubbing
Field	$F_{field} = QE$	Force exerted on a charged particle immersed in an electric field

Table 11.58: Adhesion phenomena formula resume.

In these equations, R stands for the mean radius of dust, estimated as 25 μm based on open literature, while γ is the specific surface energy relative to the two materials: it is the energy needed to separate the two surfaces, estimated as the square product of γ of each surface. The particle may come into contact with aluminium radiator and SMLI. Since γ of the SMLI is very low, only γ of aluminum has been considered conservative in calculations. α is a correction factor which depends on the polarization of the dielectric particle (i.e. non-conductive). A mean k-factor (dielectric constant of the material) depending on the composition of the lunar dust has been identified: regolith can be considered as composed of silicium, aluminium oxide, dry basalt rock and other minerals which lead to a correction factor = 1.45. Q is the particle charge, estimated with Equation (11.74) [R.D. 283]:

$$Q = C\Phi_s = 4\pi\Phi_s\varepsilon_0 R \tag{11.74}$$

Φ_s is the surface potential, equal to 0.1 V [R.D. 276] and ε_0 is the dielectric constant in vacuum. σ stands for the charge surface density with respect to A_c, which is the contact area between particle and surface: A small fraction, like 20 percent, of the charged surface area, might be in close proximity to the conducting surface [R.D. 283]. E is the electric field, approximated with an exponential model (Equation (11.75)), in which λ is the characteristic length of the potential gradient above the surface.

$$E = \frac{\Phi_s}{\lambda} e^{-\frac{z}{\lambda}} \tag{11.75}$$

The sum of the terms in Table 11.58 is the adhesion force for a single particle; to verify if an active system to remove dust is necessary, this force is compared to gravity force, considered as the only natural term that can be opposed to adhesion phenomena. The adhesion force results in 5 orders of magnitude major for Eagle and 4 orders of magnitude for Scott, thus making the design of EDS indispensable for both. To evaluate the total force on Eagle and Scott, the spatial density of the particle in function of the respective areas is calculated: a honeycomb disposition is assumed to prevent particles overlapping and to avoid particles occupying surface, in a more realistic way. The total number of the particles is calculated as the product between the spatial density and the area of the analysed surface, corrected with a 0.11 factor, a threshold value set as only 11 percent dust coverage results in a doubling of the solar absorptance, thus affecting TCS properties [R.D. 284]. Finally, the total force is calculated as the product between the number of particles and the adhesion force for a single particle: for Eagle it is equal to $1.03 \cdot 10^5 N$, while for Scott it is equal to 108 N.
The electric field that the EDS generates at each activation is estimated at $2\frac{kVpp}{mm}$ [R.D. 285]. Thus, the force generated is defined with Equation (11.76):

$$F_{EDS} = E_{EDS}^2 \varepsilon_0 A_{surf} \tag{11.76}$$

Since it can be considered as a force for a single activation of an estimated duration of one second, the ratio between the total adhesion force and F_{EDS} is equal to the duration of EDS activation in seconds.
The gap in time between two consecutive activations depends on adhesion probability. Van der Waals force is considered as the main adhesion factor, as can be seen from the calculations: the distance between a particle and a

surface in which this phenomenon occurs (d_{vdW}) is in the order of $10^{-9}m$. A homogeneous distribution of dust [R.D. 276] in a radius δ of 10^{-4}m of distance from the surface is considered: the ratio between d_{vdW} and δ is adhesion probability. The Van der Waals adhesion time is estimated in 10 seconds, multiplied for adhesion probability: consequently, the time between two consecutive EDS activation for Eagle is equal to $1.0 \cdot 10^5 s$ meaning one activation of 4 minutes (by previous calculations) per day. The same analyses are conducted for Scott, corresponding to an 8-second-long activation of EDS every day.

11.7.2.4 Morphology and slopes

To define the landing safe ellipse and the slope of the ground, a correlation between two maps (Figure 11.82 zoomed in CR1 and Figure 11.83) converted in grayscale is individuated and shown in Figure 11.89.The first image describes better the slope angles in the landing site and presents a discretization grid defined as a function of longitude and latitude angles: this made it possible to confirm the coordinates of the chosen landing site to set the landing ellipse. The second makes a clear distinction between different regions, classifying them as discussed in Section 11.7.1, and describing the presence of boulders, which are undesired obstacles for landing. By overlapping the two images, it can be concluded that the comparison between them is robust and, consequently, the Cratered Highlands Surface (CHS) regions are characterized by a slope angle of 8 degrees. As a result, the safe ellipse is defined within one of these areas, described on the map on the right shown in Figure 11.89. Morphology and slope assessments also played a fundamental role, providing input to the WPs 3.3 and 3.6 to ensure stability during deployment and to avoid excessive inclination or risk of overturning during descent and deployment.

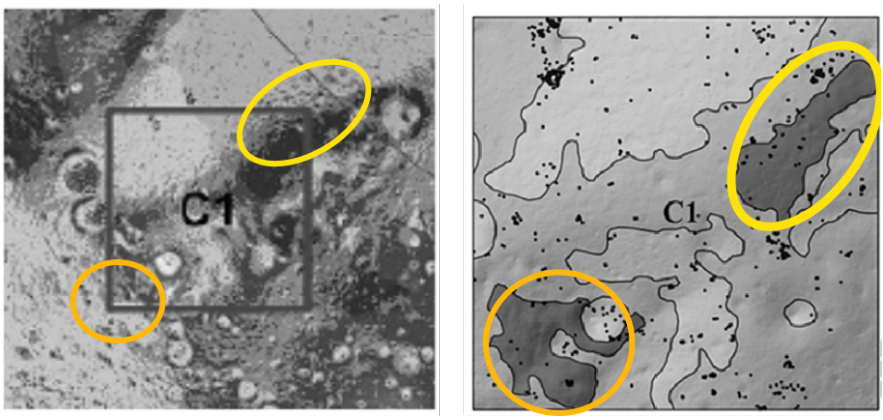

Figure 11.89: A zoomed version of Figure 11.82 (on the left) and Figure 11.83 (on the right), both in greyscale. The yellow and orange markers highlight similar areas

Several safe ellipses were defined to find the optimum choice; in figure 6, the white one corresponds to the chosen one, i.e. cantered on the landing site. GEL3-USR-050 in [R.D. 8] specify that The LDE shall be capable of landing within an ellipse cantered on the target landing site, with a 50m semi-minor axis and 250m semi-major axis. These dimensions are therefore fixed for AMPERE's landing site ellipses, to minimize variations in environmental conditions within the area. Small angular deviations lead to similar illumination and temperature conditions and thus ensure consistent overall system performance at any point inside the ellipse. Also, the risk of unexpected obstacles or significant slope changes is reduced. [A.D. 9] specifies additional guidelines for defining a safe landing ellipse. The one selected for AMPERE is located away from craters, boulders, and PSRs, features a maximum slope of 8 degrees, and offers at least 100 Earth days of favourable illumination following landing. A detailed analysis of the map shown in Figure 11.90 confirms that the terrain inside it can otherwise be considered flat. Therefore, the landing ellipse meets all the criteria specified in [A.D. 9], and there are no natural obstacles that could hinder post-landing operations, such as solar panel deployment or opening.

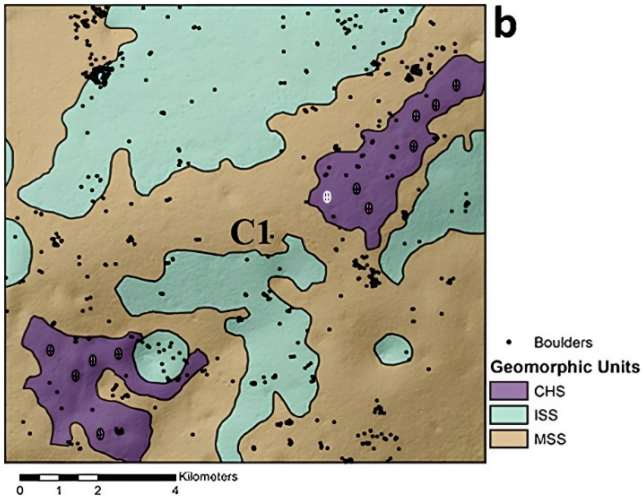

Figure 11.90: Definition of safe landing ellipses.

11.8 TRL Assessment

The maturity of each subsystem's technology of EAGLE, SCOTT and PDS has been assessed through a TRL analysis based on ECSS guidelines [R.D. 91], with the results consolidated in Table 11.59 and Table 11.60.

ID	Component	Component TRL	Subsystem TRL
STR&MEC	Wheel	9	3
	Cart's plate	5	
	Braking actuator	4	
	Solar Array Drive Electronics	7	
	Pointing mechanism	8	
	Solar Array Deployment	3	
	Solar Array Drive Mechanism	8	
	Radiation shield	5	
TT&C	Ka-band antenna	6	6
	Ka-band transceiver	6	
	Ka-Band amplifier	6	
	Ka-band diplexer	6	
	S-band antenna	8	
	S-band transponder	8	
	OBC	8	
	UHF antenna	7	
	UHF transceiver	8	
TCS	Generator for EDS	8	5
	EDS	8	
	MLI Teflon	9	
	MLI mylar + VDA	9	
	Heaters	8	
	Loop Heat Pipe	7	
	Radiator	5	
	Temperature sensor	8	
	MLI smart	5	
EGSD	Solar panel	6	4
	RFCS	4	

	Battery	8	
	PCDU	4	
	Wireless interface	7	
	Dock interface	6	
	Connector	6	
ADCS	IMU	5	5
	Inclinometer	5	
	CSS	9	
	FSS	8	
RDS	Drop-release system	7	6
	Winch + Worm gear + Motor + Dyneema cables	6	
LSM_S	RADFET	7	7
	Magnetometer	8	
	Boom	8	
	RTD	7	
	Radiation monitor	8	
PDS	Ramp	5	3
	Hinges	5	
	Thermal knives	7	
	Kevlar cables	7	
	Ramp actuator moog965	5	
	Ramp actuator CubeMars	4	
	Reduction unit	4	
	Reduction unit moog965	4	
	Slip resistant material	3	
	Battery	8	

Table 11.59: EAGLE and PDS components TRL assessment

ID	Component	Component TRL	Subsystem TRL
TT&C	UHF antenna	7	7
	UHF transceiver	8	
	S-band antenna	8	
	S-band transceiver	8	
	S-band diplexer	8	
	OBC	8	
	LCNS unit	7	
STE&MEC	Astrobotic Cuberover system	9	9
EPS	Battery	8	7
	Wireless interface	7	
	PCDU	7	
GNC	IMU	5	7
	CSS	9	
	Camera	8	
	Astrobotic Cuberover system	9	
	LED	8	
LSM_M	IES	7	7
	INMS	7	

	SRDS	7	
	Langmuir Probe	8	
	Boom	8	
TCS	MLI teflon	9	5
	Generator for EDS	8	
	EDS	8	
	Heaters	8	
	MLI smart	5	
	MLI mylar + VDA	9	
	Temperature sensor	8	
	Loop Heat Pipe	6	
	Radiator	5	

Table 11.60: Scott components TRL assessment

The TRL of each subsystem has been assigned according to the lowest TRL among its individual components. From this analysis, it is evident that the most critical subsystems are Structure & Mechanisms, EGSD and the PDS of Eagle. To ensure their development within the AMPERE Phase C schedule, it is essential to conduct the associated testing campaign during AMPERE Phase D. However, there are currently no stringent minimum TRL requirements, as the mission is scheduled for launch in 2037

11.9 Evolution of the mass budget over time and final mass budget

After selecting the final concept, MoonProbe, the masses of the various subsystems have been better reallocated. As a result, the mass budget has been adjusted to be more representative of the different infrastructures included in this concept. In particular, in accordance with what is defined in Section 10.5 a global mass budget has been established for the LPS, which includes the nominal masses of PDS, Eagle and Scott, expressed as percentages of the nominal mass of the LPS. To this, a system margin equal to 20% of the LPS nominal mass and 5% for harness is added, as shown in Table 11.61.

LPS mass budget		
Systems	Percentage	Mass (kg)
PDS nominal mass	9.4 %	60.0
Eagle nominal mass	86.1 %	551.0
Scott nominal mass	4.5 %	29.0
LPS nominal mass	/	640.0
Harness	5.0 %	32.0
System margin	20.0 %	128.0
Total mass	/	800.0

Table 11.61: LPS preliminary mass budget

The nominal masses of PDS, Scott and Eagle have been allocated by taking into account additional missions compared to the previous approach used in Section 10.3. Specifically, once a certain class of rover has been selected [R.D. 195][R.D. 286][R.D. 287] and the ramp size estimated accordingly [R.D. 256][R.D. 267], Eagle's overall dimensions and mass have been derived as a consequence. Starting from Eagle's nominal mass, the mass percentages of the various subsystems, expressed as fractions of this nominal mass, have been assigned in the same way as in Section 10.3, based on the same previous Concurrent Design Facility (CDF) studies and missions [R.D. 3][R.D. 106][R.D. 256]. These mass percentages are presented in Table 11.62. Similarly, starting from Scott's nominal mass, the subsystem mass percentages, expressed relative to its nominal mass, have been derived based on analogous values from comparable rover designs [R.D. 288], [R.D. 289] and are shown in Table 11.63.

Eagle mass budget		
Subsystems	Percentage	Mass (kg)
EGSD	54.3 %	299.0
RDS	2.0 %	11.0
STR&MEC	26.0 %	143.0
TCS	10.0 %	55.0
Eagle sensors	0.5 %	3.0
TT&C	7.0 %	39.0
ADCS	0.2 %	1.0
Eagle nominal mass	/	551.0

Table 11.62: Eagle preliminary mass budget

Scott mass budget		
Subsystems	Percentage	Mass [kg]
EPS	17.0 %	4.9
GNC	27.0 %	7.8
STR&MEC	20.0 %	5.8
Scott sensors	14.0 %	4.0
TCS	8.5 %	2.5
Scott payload & accommodation	3.5 %	1.0
TT&C	10.0 %	3.0
Nominal mass	/	29.0

Table 11.63: Scott preliminary mass budget

At this point, it is important to clearly state what is included in the various subsystems of Eagle, Scott and PDS. As previously mentioned, following the selection of MoonProbe as the mission concept, the allocation of components within the subsystems has changed compared to the configuration described in Section 10.3 due to the introduction of a clearer distinction between the different modules comprising the LPS.
As for Eagle, the EGSD subsystem includes all components necessary for power generation, storage and distribution, as well as the charging interfaces. The RDS includes the mechanism for rover deployment and the mechanism for lowering the rover charging interface. The STR&MEC subsystem comprises the wheeled cart, all pointing, rotation, and deployment mechanisms, the radiation shield and the locking systems for the various components. The TCS includes all components required to ensure the survival of the station during both daytime and nighttime, as well as a system for dust removal (EDS). The Eagle sensors subsystem contains the fixed-position sensors used to carry out scientific measurements (LSM-S). The TT&C subsystem comprises all antennas and communication devices for interfacing with MoonLink and Scott, as well as the OBC dedicated to data handling. Finally, the ADCS contains instruments for determining the orientation of the station over time. Regarding Scott, the EPS includes the charging interface, the battery, which serves as the rover's sole energy source and the PCDU. The GNC subsystem includes both the mobility system and the instrumentation used to determine orientation over time and to assess the rover's position and movement. The STR&MEC subsystem comprises all the rover's structural and mechanical elements. The Scott sensors subsystem includes the instruments used to perform environmental analyses not from a fixed point, but within an area near Eagle (LSM-M). The TCS includes the components necessary to ensure the rover's survival during both daytime and nighttime, plus the EDS. The Scott payload & accommodation subsystem provides space that remains available for the integration of additional sensors, to be added by the customer or user. One of the 24 U available on the rover is allocated to this subsystem, which is constrained to a maximum mass of 1 kg and a peak power consumption of 1 W. Further details are provided in Section 10.7. The TT&C subsystem contains the OBC and the communication equipment needed to connect with both MoonLink and Eagle. As for PDS, it includes the ramp, the hinges used for its deployment, a battery and the mechanism that secures Eagle in place. Since PDS no longer comprises individual subsystems, no further breakdown is provided. A separate mass budget for this system has been considered unnecessary, as it is directly included in the overall LPS mass budget.
The preliminary mass budgets shown in Tables 10.10, 10.11 and 10.12 have been used during the design phase by the respective design WPs as reference budgets. This means that these budgets haven't been binding for subsystem sizing, but served instead as guidelines to help ensure that no major issues would arise in the final mass consolidation.
Throughout the various iterations, the mass percentages allocated to each subsystem evolved. In particular, four main iterations have been necessary before reaching the final design, in which not only the mass requirements but also the power requirements have been fully satisfied. Table 11.64, Table 11.65 and Table 11.66, illustrate the evolution of the mass distribution for LPS, Eagle and Scott; respectively. It should be noted that in the tables above, "I" stands for "Iteration". In these figures, the version marked as I-0 represents the preliminary mass budgets, as presented in Table 11.61, Table 11.62 and Table 11.63. The version labeled I-4 corresponds to the outcome of the final iteration and thus reflects the definitive design. In accordance with [R.D. 107],the following mass margin philosophy has been applied to the design of Eagle, Scott, and PDS at the equipment level, based on design maturity of the components:

- 5% for COTS items (i.e., standard components with no modifications);
- 10% for COTS items requiring minor modifications (e.g., minor mechanical adjustments, etc.);
- 20% for items that are newly designed, developed, or require major modifications or redesign.

Additionally, the harness mass is assumed to be 5% of the nominal dry mass. The total mass at launch includes a 20% system-level mass margin applied to the nominal dry mass.

LPS systems	I-0 mass [kg]	I-1 mass (kg)	I-2 mass (kg)	I-3 mass (kg)	I-4 mass (kg)
PDS nominal mass	60.0	47.0	61.0	45.7	77.1
Eagle nominal mass	551.0	556.5	784.9	560.4	499.0
Scott nominal mass	29.0	32.3	26.4	27.7	41.4
Total mass	800.0	795.0	1090.4	791.4	771.9

Table 11.64: LPS mass budget evolution over time

Eagle subsystems	I-0 mass (kg)	I-1 mass (kg)	I-2 mass (kg)	I-3 mass (kg)	I-4 mass (kg)
EGSD	299.0	380.4	385.5	307.8	280.7

RDS	11.0	5.1	5.1	2.3	2.3
STR&MEC	143.0	115.1	297.5	173.8	148.0
TCS	55.0	17.8	56.9	40.0	34.6
Eagle sensors	3.0	1.7	1.8	1.8	1.8
TT&C	39.0	36.2	37.7	34.4	31.3
ADCS	1.0	0.2	0.3	0.3	0.3

Table 11.65: Eagle mass budget evolution over time

Scott subsystems	I-0 mass (kg)	I-1 mass (kg)	I-2 mass (kg)	I-3 mass (kg)	I-4 mass (kg)
EPS	4.9	5.6	5.6	5.6	5.6
GNC	7.8	6.6	6.7	7.9	14.7
STR&MEC	5.8	5.8	5.8	5.8	11.6
Scott sensors	4.0	4.0	4.0	4.1	4.1
TCS	2.5	2.0	2.0	2.1	2.2
Payload & accommodation	1.0	1.1	1.1	1.1	1.1
TT&C	3.0	7.3	1.3	1.2	2.1

Table 11.66: Scott mass budget evolution over time

At this stage, it is important to provide a rationale for the changes in mass across the various iterations. Therefore, the modifications introduced from iteration I, representing the first actual design, through iteration II, and so on up to iteration IV, the final design, will be explained in detail.

From iteration I to iteration II, a detailed analysis of illumination as a function of the Sun's incidence angle and the thermal transient behaviour prior nighttime phase have been performed. Additionally, multiple safe ellipses have been evaluated. The descent and landing trajectory has been assessed, the Sun incidence angles with respect to BRF axes throughout the orbital phase have been preliminarily defined. Regarding the PDS, the number of support plates has been increased from 4 to 5 in order to reduce the ramp's inclination angle and to meet ADCS constraints related to potential tipping. Regarding Eagle, the S-band amplifiers have been removed, being no longer necessary due to changes in the transceivers. The antenna has been replaced with a smaller and lighter S-band patch antenna. An IMU has been replaced with an inclinometer to support braking torque determination and tip over detection, while Sun sensors have been made redundant to ensure fault tolerance. A radiator has been added to dissipate excess heat, and a preliminary estimate of the EDS has been introduced. A preliminary radiation shield has been included to protect all components. The solar panel size has been reduced to save space, while the number of RFCS units has increased to meet nighttime power demand: the power production changed from 9 kW to 7 kW during daytime, while the system's nighttime output increased from 360 W to 420 W to meet higher demand. A docking interface for the user has also been selected. Some sensors have been modified and made redundant. Regarding Scott, the LCNS receiving module has been replaced due to excessive weight, the amplifier removed and a lighter, smaller S-band patch antenna has been adopted; CSS units have been added.

From iteration II to iteration III, the propellant consumption during the powered descent phase has been reassessed and disturbance torques caused by the gravity gradient throughout the orbital phase have been calculated. The thermal transients before daytime have been analysed, making necessary the implementation of the Runge-Kutta method to improve temperature prediction. Illumination has been recalculated as a function of altitude, and the safe ellipse has been redefined. Regarding Eagle, the antenna has been replaced with a UHF antenna for surface communication, and UHF transceiver dimensions have been updated. An SMLI has been added, which allowed for a reduction in heater power consumption. The operation time of the EDS has been reduced to 2 hours every 2 days. The thickness of the radiation shield has been revised so that it could also serve as protection against micrometeoroids. A new deployment mechanism for the solar panel has been implemented. Due to space constraints, both panels' size and the number of RFCs units have been reduced: the daytime power decreased from 7 kW to 5 kW, and the system's nighttime output reduced from 420 W to 310 W. The battery capacity has also been reduced from 5100 Wh to 3910 Wh. The rover locking and release systems has been improved and some sensors modified. Regarding Scott, the UHF antenna and S-band transceiver have been replaced for surface communication. LEDs have been added and the camera system have been modified. Performance in terms of distance travelled has been estimated and linear paths assumed, unless interrupted

by detected obstacles The TCS has been redesigned to include MLI, radiator, heaters and the EDS. Preliminary charging/discharging cycles for the battery have also been defined.
From iteration III to iteration IV, the actual Sun incidence angles throughout the full orbital period have been defined, and the disturbance torque models updated accordingly, to account for the effects of SRP. Regarding the PDS, the last three plates of the ramp have been coated with a slip resistant material that increased the friction coefficient with Eagle's wheels, helping to prevent slippage and tipping. Furthermore, the motorized hinges have been redundantly implemented to enhance deployment reliability; in addition, also the locking system has been changed and a battery added for the deployment and closure of the ramp. Regarding Eagle, the radiation shield has been redefined to protect only the electronic components, which reduced overall mass. A braking system has been added to the wheeled cart. The final solar panel deployment mechanism has been improved by replacing a single vertical panel with two horizontally deployed ones to enhance structural balance and reduce instability. Based on the dissipated power during daytime and nighttime and the effective surface area of the station, heaters and radiator sizes have been reassessed, as well as the operating time of the EDS has been reduced. Final input data on the centre of mass have been implemented in the ramp descent codes, together with the use of brakes and the ramp coating to modify friction, verifying the absence of tipping or sliding issues. Final charge/discharge profiles have been defined for both the batteries and RFCS, confirming that power demands is met in all operational modes. Regarding Scott, the communication cycle has been finalized and the S-band antenna has been replaced with an omnidirectional one. The GNC and Structures & Mechanisms subsystems have been redesigned as the rover configuration has changed from 12U to 24U, to address component allocation challenges within the internal volume. Based on daytime and nighttime heat dissipation, heater and radiator sizes have been re-evaluated. The operating time of EDS has been further reduced. The power consumption of the mobility system has decreased by adopting a lower operational speed and the final assessment of the distance to be covered has been completed. Moreover, final charge and discharge cycles of the rover battery have been defined for both daytime and nighttime operations.
The final mass budget, resulting from all above iterations, already shown in Table 11.64, Table 11.65 and Table 11.66, is graphically presented in Figure 11.91. Specifically, the figure shows the mass percentages of the various subsystems, harness, and margins for Eagle, Scott, and PDS, with respect to their respective total masses (including margins), which are 623.8 kg, 51.8 kg, and 96.4 kg, respectively. In particular, the margin segment includes both equipment-level margins and the system-level margin.

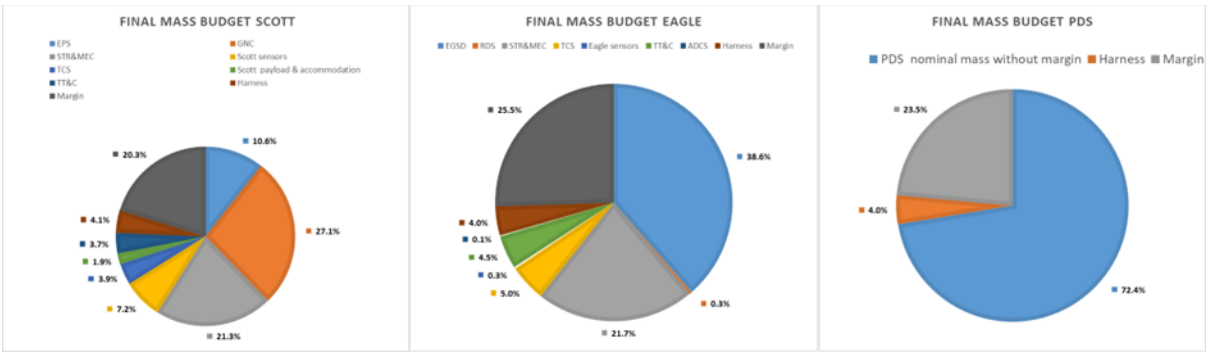

Figure 11.91: Final mass budget of Eagle, Scott, and PDS

In conclusion, it is important to highlight that the final total mass of the LPS, including all margins, amounts to 771.9 kg. This value represents the minimum mass required to carry out the mission and remains within the 800 kg limit imposed by the [A.D. 1]. The available residual mass could potentially be used to introduce redundancy for critical components, increase the thickness of protective elements (e.g., radiation shielding), or enhance the robustness of mechanical constraints.

11.10 Evolution of the power budget over time and final power budget

To preliminarily assess Eagle's ability to meet the power requirements of its subsystems, ensure nighttime survival, enable rover recharging and potentially support external loads, a preliminary power budget has been developed. This analysis has been carried out after the sizing of the photovoltaic panels, RFCS and energy storage systems, with the goal of verifying consistency and adequacy with respect to the overall energy demands of the mission. In this phase, different preliminary critical modes have been introduced for both Eagle and Scott, to identify the worst-case power demand scenarios and assess their feasibility within the preliminary power budget.
For Eagle, the following preliminary modes have been defined: Eagle Deployment (ED), Charging (C), Day Users Supply (DUS), Night Operations (NO), Night Rover Supply (NRS). During the ED mode, Eagle is initialized, prepared for

subsequent operations, and descends from the ramp. In the C mode, the solar panels supply power to the subsystems, recharge the battery and power the RFCs. In the DUS mode, the energy generated by the solar panel is used to power the subsystems and a potential external load, while the battery is used to recharge the rover. During the NO mode, the RFCs operate at full capacity to ensure the functioning of the subsystems in the absence of solar power. Finally, in the NRS mode, the RFCs provide minimal power to the subsystems, while the battery is used to recharge the rover.
Scott is also associated with different critical modes: Scott Deployment (SD), Day Charging (DC), Day Motion (DM), Night Charging (NC), Night Motion (NM). During SD, the rover is activated and released from Eagle. In the DC mode, the rover is recharged and communicates with Eagle. The DM mode represents the active movement phase, with sensors operating to conduct environmental measurements. In the NC mode, the rover continues to recharge and maintains communication with Eagle during the night. Finally, in the NM mode, the rover is once again in motion, with sensors active during nighttime.
The preliminary modes are listed in Figure 11.92 and Figure 11.93, which represent the preliminary power budgets for Eagle and Scott, respectively. In these tables, for each mode and each power-consuming subsystem, three values are reported:

- P_{max} presents the sum of the power consumption of active or standby components within the specific mode and subsystem, including subsystem margins.
- Duty is the ratio between the subsystem's active time during the specific mode and a defined reference time.
- P_{av}, calculated as the product between P_{max} and Duty, represents the average power consumed by each subsystem in that mode.

Summing the P_{av} of all subsystems within a mode yields the total average power consumption without system margin ($P_{av,tot}$ without system margin). By adding the system margin to this value, the final $P_{av,tot}$ is obtained, which is the value shown in the preliminary power budget used to compare the energy expenditure across different modes, as illustrated in Figure 11.94, for both Eagle and Scott.
To clarify the data presented in Figure 11.92 and Figure 11.93, it is important to note that the P_{max} values used at this stage are based on estimated power consumption for the various subsystems, derived from comparable past missions [R.D. 3] and preliminary results obtained during the final phase of the trade-off analysis. As for the Duty values, only in these budgets, identical values were assigned to all subsystems operating within the same mode. The chosen reference time periods are 12 Earth days for Eagle, representing the daytime/nighttime alternation, and 1 Earth Day for Scott, representing the rover's charge/discharge cycle.

CRITICAL MODES		EAGLE DEPLOYMENT (ED)			CHARGING (C)			DAY USERS SUPPLY (DUS)			NIGHT OPERATIONS (NO)			NIGHT ROVER SUPPLY (NRS)		
	SUBSYSTEMS	P_max (W)	Duty	P_av (W)	P_max (W)	Duty	P_av (W)	P_max (W)	Duty	P_av (W)	P_max (W)	Duty	P_av (W)	P_max (W)	Duty	P_av (W)
EAGLE	EGSD	100.00	7.00%	7.00	100.00	19.00%	19.00	100.00	19.00%	19.00	100.00	27.50%	27.50	100.00	27.50%	27.50
	STR&MEC	250.00		17.50	40.00		7.60	40.00		7.60	20.00		5.50	20.00		5.50
	TCS	0		0	0		0	0		0	200.00		55.00	200.00		55.00
	EAGLE SENSORS	0		0	5.00		0.95	5.00		0.95	5.00		1.38	5.00		1.38
	TT&C	150.00		10.50	150.00		28.50	150.00		28.50	130.00		35.75	130.00		35.75
	ADCS	2.00		0.14	0		0	0		0	0		0	0		0
P_av_tot without system margin (W)				35.14			56.05			56.05			125.13			125.13
SYSTEM MARGIN	20.00%			7.03			11.21			11.21			25.03			25.03
P_av_tot (W)				42.17			67.26			67.26			150.15			150.15

Figure 11.92: Eagle preliminary power budget

CRITICAL MODES		SCOTT DEPLOYMENT (SD)			DAY CHARGING (DC)			DAY MOTION (DM)			NIGHT CHARGING (NC)			NIGHT MOTION (NM)		
	SUBSYSTEMS	P_max (W)	Duty	P_av (W)	P_max (W)	Duty	P_av (W)	P_max (W)	Duty	P_av (W)	P_max (W)	Duty	P_av (W)	P_max (W)	Duty	P_av (W)
SCOTT	RDS	20.00	10.00%	2.00	0	15.00%	0	0	45.00%	0	0	15.00%	0	0	45.00%	0
	EAGLE SENSORS	0		0	5.00		0.75	10.00		4.50	5.00		0.75	10.00		4.50
	TT&C	5.00		0.50	5.00		0.75	15.00		6.75	5.00		0.75	15.00		6.75
	GNC	0		0	0		0	40.00		18.00	0		0	45.00		20.25
P_av_tot without system margin (W)				2.50			1.50			29.25			1.50			31.50
SYSTEM MARGIN	20.00%			0.50			0.30			5.85			0.30			6.30
P_av_tot (W)				3.00			1.80			35.10			1.80			37.80

Figure 11.93: Scott preliminary mass budget

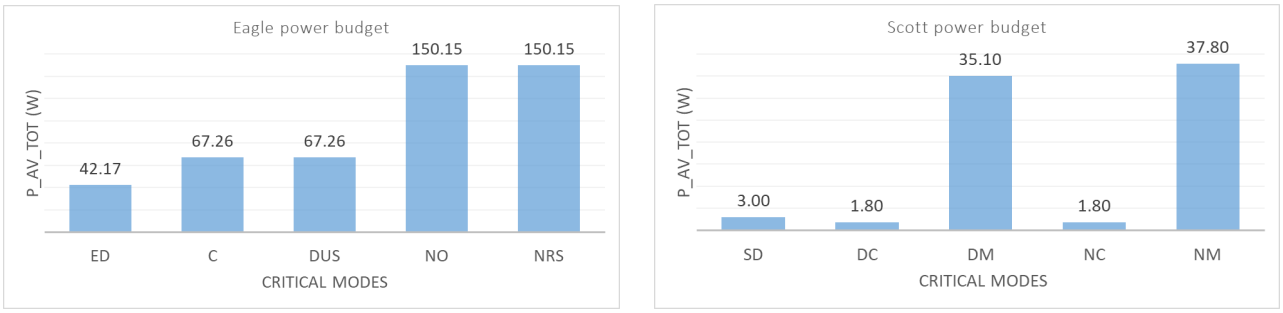

Figure 11.94: $P_{av,tot}$ evaluated over the preliminary critical modes for Eagle and Scott

A preliminary power budget was also developed for the PDS. The only critical mode identified is the PDS Deployment (PD), during which the ramp is extended. In this phase, the total average power consumption is estimated at $P_{av,tot} = 0.50\ W$. As with the mass budget, this power budget has not been a strict constraint for subsystem design but served as an initial guideline to better estimate the energy production and storage requirements. Once all system modes for Eagle and Scott have been defined, as shown in Section 10.6, and additional system modes have been introduced for the PDS, the power budget has been refined to include all possible modes for the various components of the LPS. Following the definition of the mission phase timelines, as described in Section 10.6, maximum durations have been assigned to each mode and new reference times have been established for Eagle, Scott and PDS. Additionally, the duty cycles of the various subsystems have been adjusted per mode, where necessary. For each iteration, power budgets have been calculated as already described, by considering the corresponding P_{max} and Duty values of each subsystem in every mode, and it has been verified whether the power required during both daytime and nighttime was compatible with the power generated and stored. In the first two iterations, it became evident that survival during nighttime was not ensured, which led to significant design changes, as already discussed in Section 11.9. Furthermore, the operational cycles of several subsystems have been revised to reduce overall power consumption and avoid critical power shortages, especially during the nighttime.
Despite power budgets for all iterations are not present here, the final power budgets of the last iteration are shown. In accordance with [R.D. 107], at equipment level and for conventional electronic units, the following design maturity power margins have been applied:

- 5% for COTS items;
- 10% for COTS items requiring minor modifications;
- 20% for items that are newly designed, developed, or require major modifications or redesign.

The total power budget of the LPS includes a system level power margin of 20 % of the nominal power requirements. Figure 11.95, Figure 11.96 and Figure 11.97 display the total average power consumption $P_{av,tot}$ across the system modes for Eagle, Scott and PDS, respectively, while Figure 11.98, Figure 11.99 and Figure 11.100, show the average power consumption for each subsystem and mode. To obtain the results shown in the previously mentioned figures and diagrams, several considerations have been made. For Eagle, a reference timeline of 12 Earth days has been adopted, corresponding to the alternation between daytime and nighttime conditions on the lunar surface.
During each operational mode, certain subsystems are active, others are in standby and some remain off:

- During the EAGLE-CRS mode, RDS remains in standby, and within TT&C, only the OBC is active. For this mode, which lasts approximately 4 Earth days, all power requirements are provided by Argonaut.
- During EAGLE-COMM mode, EGSD is active, with consumption only driven by the PCDU. TCS temperature sensors and all Eagle sensors are active, while the RDS remains in standby. The TT&C operates both the S and Ka bands for functionality checks, while the ADCS activates the IMU and inclinometer. In STR&MEC, the antenna pointing mechanism is active. This mode lasts approximately 12 Earth hours.
- During the EAGLE-DESN mode, the PCDU remains active and the RDS is in standby, while the TT&C activates the S-band and OBC. The ADCS also operates, with both the IMU and inclinometer active. In STR&MEC, the wheel braking system is engaged. The mode lasts approximately 2 Earth minutes.
- During the EAGLE-RDEP mode, which lasts about 2 Earth hours, the PCDU remains active, the EDS is briefly activated by the TCS, thermal sensors remain operational and the RDS performs the rover release; TT&C and ADCS are both active.
- During the EAGLE-SECCOMM mode, all subsystems are activated for a full functionality check. In ADCS, the IMU and FSSs are on, while the inclinometer is in standby.
- During the EAGLE-PGEN mode, the solar panels are responsible for recharging both the batteries and fuel cells, and for supplying the remaining power to Eagle. STR&MEC is active, mainly for the deployment and retraction

of the solar panels and solar tracking via the SADA mechanism. Within TT&C, only the OBC and the S-band are active for 18 hours per Earth Day. ADCS operates at full capacity. This mode lasts 7 Earth days.

- During the EAGLE-NIGHT mode, the PCDU and OBC are active, while the TCS powers the heaters. The ADCS is configured in a reduced-consumption mode: CSSs are on, IMU is off, and both FSSs and the inclinometer are in standby. This mode lasts 5 Earth days.
- During the EAGLE-CHG mode, only the power consumption related to Scott recharging from Eagle is considered. This mode overlaps with EGLE-PGEN and EGLE-NIGHT, therefore all other subsystems are excluded. The total duration is 2 Earth hours × 33 charge cycles, as expected over the reference timeline.
- During the EAGLE-SENSOR mode, which also overlaps with EAGLE-PGEN and EAGLE-NIGHT, all Eagle sensors are active, the EDS operates within the TCS, and the power demand from the SMLI is included. STR&MEC is used for antenna pointing, and the Ka band in TT&C is active for 2 hours per Earth Day. This mode is considered active throughout the full reference period.
- During the EAGLE-INTL mode, which also overlaps with EAGLE-PGEN and EAGLE-NIGHT, only the UHF band of TT&C is active, during intervals compatible with SCOTT-NEM or SCOTT-EM activity.
- During the EAGLE-SAFE mode, all subsystems are either in standby or powered off. The ADCS is configured identically to the EAGLE-NIGHT mode.
- Finally, during the EAGLE-EOL mode, all systems are deactivated, and no power consumption occurs.

For Scott, a reference timeline of 9 Earth hours has been considered, corresponding to a full charge-discharge cycle of the rover during both daytime and nighttime. During each operational mode, certain subsystems are active, others are in standby and some remain off:

- During the SCOTT-OFF mode, all subsystems are deactivated and no power consumption occurs.
- During the SCOTT-P&REL mode, only the PCDU within the EPS is active; within TT&C, the OBC, UHF band, and LCNS receiver are operational, while the GNC operates with one IMU and the CSSs active. This mode lasts 2 Earth hours.
- During the SCOTT-COMM mode, all subsystems are activated to perform a full functionality check, with a total duration of 2 Earth hours.
- During the SCOTT-NEM mode, all Scott sensors are active, the PCDU is operational, and additional power consumption is considered for the Scott Payload & Accommodation subsystem. Within the TCS, both the EDS and the smart MLI are active. The TT&C operates the OBC and the LCNS, while the GNC is fully active, including the mobility system that works for 2 Earth hours.
- During the SCOTT-NIGHT mode, only one of the Scott sensors remains active, while all other subsystem configurations match those of the NEM mode. The duration is 3 Earth hours.
- During the SCOTT-EMD mode, the same subsystems are active as in the NEM mode, but the GNC is configured for minimal power consumption since the rover is stationary; LEDs and cameras are turned off. The mode lasts 5 Earth hours.
- During the SCOTT-EMN mode, the configuration is identical to the NIGHT mode, with the GNC operating at reduced power and both LEDs and cameras off. The duration is 4 Earth hours.
- During the SCOTT-RCH mode, the TT&C remains in standby, while the GNC is active solely to stabilize the rover during the recharge process. This mode lasts 2 Earth hours.
- During the SCOTT-UPL mode, which overlaps with EMD and EMN, only the S-band of the TT&C is active for 1 Earth hour.
- During the SCOTT-INT mode, which overlaps with NEM, NIGHT, EMD, and EMN, only the UHF band of the TT&C is active for 7 Earth hours.
- During the SCOTT-SAFE mode, all subsystems are either in standby or powered off; the GNC configuration matches that of the RCH mode.
- Finally, during the SCOTT- EOL mode, all systems are shut down and no power consumption occurs.

For PDS, a reference duration of approximately 4 Earth days has been adopted, which corresponds to the timeframe in which Argonaut remains in lunar orbit prior to landing. During the PDS-STBY mode, power consumption is considered null, since the mechanical systems do not consume power even in standby. During the PDS-DEP mode, the hinges and the release mechanism of Eagle are activated, and the duration of the mode is approximately 2 Earth hours.

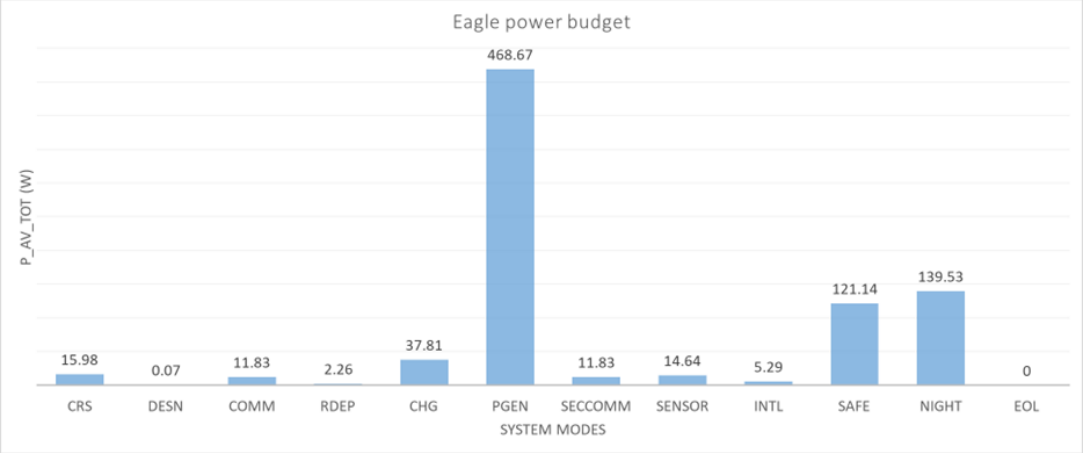

Figure 11.95: $P_{av,tot}$ evaluated over all the system modes for Eagle

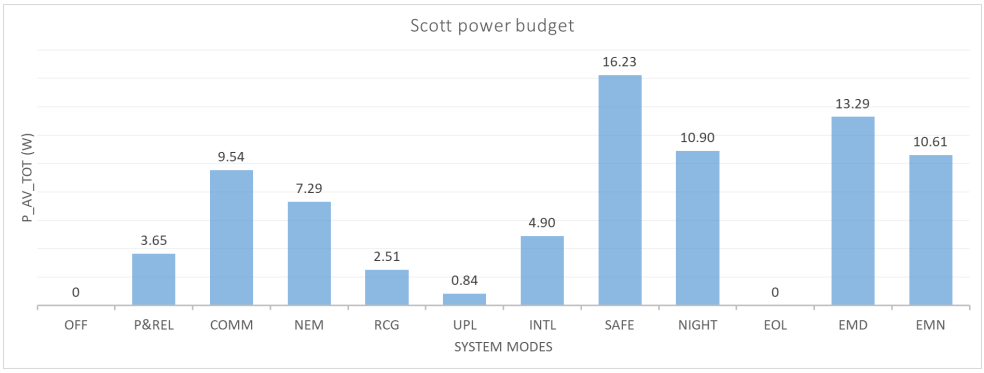

Figure 11.96: $P_{av,tot}$ evaluated over all the system modes for Scott

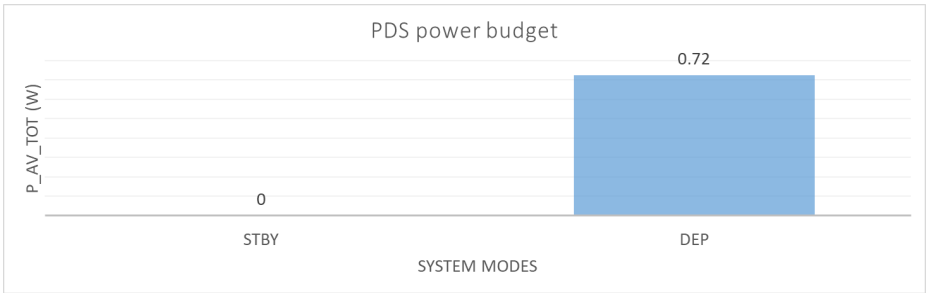

Figure 11.97: $P_{av,tot}$ evaluated over all the system modes for PDS

System modes		CRS	DESN	COMM	RDEP	CHG	PGEN	SECCOMM	SENSOR	INTL	SAFE	NIGHT	EOL
Eagle	Subsystems	P_av (W)	P_av (W)	P_av (W)	P_av (W)	P_av (W)	P_av (W)	P_av (W)	P_av (W)	P_av (W)	P_av (W)	P_av (W)	P_av (W)
	EGSD	0	0.01	2.08	0.35	31.51	301.59	2.08	0	0	50.00	20.83	0
	STR&MEC	0	0.01	0.56	0	0	27.71	0.56	0.92	0	0	0	0
	TCS	0	0	0.01	0.30	0	0	0.01	0.15	0	0	78.75	0
	Eagle sensors	0	0	0.05	0.01	0	0	0.05	1.13	0	0.36	0	0
	RDS	0.02	0.01	0.01	0.01	0	0	0	0	0	0	0	0
	TT&C	13.30	0.02	7.07	1.22	0	60.02	7.07	10.00	4.41	48.85	16.63	0
	ADCS	0	0.01	0.07	0.01	0	1.23	0.08	0	0	1.74	0.07	0
P_av_tot without system margin (W)		13.32	0.06	9.86	1.89	31.51	390.56	9.85	12.20	4.41	100.95	116.28	0
SYSTEM MARGIN	20.00%	2.66	0.01	1.97	0.38	6.30	78.11	1.97	2.44	0.88	20.19	23.26	0
P_av_tot (W)		15.98	0.07	11.83	2.26	37.81	468.67	11.83	14.64	5.29	121.14	139.53	0

Figure 11.98: Eagle final power budget

System modes		OFF	P&REL	COMM	NEM	RCG	UPL	INTL	SAFE	NIGHT	EOL	EMD	EMN
Scott	Subsystems	P_av (W)	P_av (W)	P_av (W)	P_av (W)	P_av (W)	P_av (W)	P_av (W)	P_av (W)	P_av (W)	P_av (W)	P_av (W)	P_av (W)
	Scott sensors	0	0	2.21	2.21	0	0	0	2.99	0.65	0	5.53	0.86
	EPS	0	0.37	0.37	0.37	0	0	0	1.65	0.55	0	0.92	0.73
	Scott payload & accommodation	0	0	0.22	0.22	0	0	0	0	0.33	0	0.56	0.44
	TCS	0	0	0.01	0.01	0	0	0	0	2.67	0	0.01	3.56
	TT&C	0	2.32	3.02	1.16	1.62	0.70	4.08	7.31	1.73	0	2.89	2.31
	GNC	0	0.35	2.12	2.10	0.47	0	0	1.58	3.16	0	1.17	0.93
P_av_tot without system margin (W)		0	3.04	7.96	6.07	2.09	0.70	4.08	13.52	9.09	0	11.07	8.84
System margin	20.00%	0	0.61	1.59	1.21	0.42	0.14	0.82	2.70	1.82	0	2.21	1.77
P_av_tot (W)		0	3.65	9.54	7.29	2.51	0.84	4.90	16.23	10.90	0	13.29	10.61

Figure 11.99: Scott final power budget

System modes		STBY	DEP
PDS		P_av (W)	P_av (W)
		0	0.60
P_av_tot without system margin (W)		0	0.60
SYSTEM MARGIN	20.00%	0	0.12
P_av_tot (W)		0	0.72

Figure 11.100: Scott final power budget

Once the power budget has been finalized, it has been necessary to verify that the system operated correctly under all expected conditions. This included ensuring that the solar panels could sustain the maximum peak load, that both the batteries and the RFCS would recharge in time before their next duty cycle, that sufficient energy could be provided to external users, and that the rover's charging cycles would not introduce constraints or issues. To carry out this verification, worst-case scenarios were considered, assuming full overlap of all potentially concurrent operational modes. The analysis is presented in Section 11.1 and demonstrates that the system can survive the cold lunar nighttime, operating at full capacity during daytime, also supplying substantial amounts of energy to external users.

12 Task 4 End-of-Mission planning and impact assessment

Figure 12.1 shows the phases E and F of the AMPERE mission schedule (see Figure 10.21) with a specific focus on the disposal phase, developed in compliance with the [A.D. 1] and [A.D. 2].

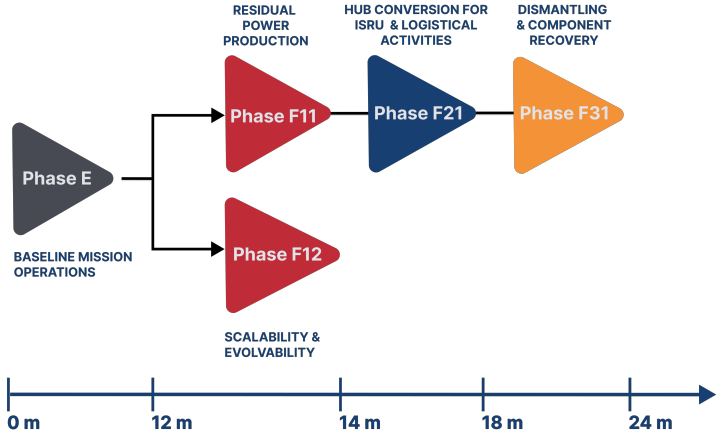

Figure 12.1: AMPERE mission phase E/F

- Phase E:
  It considers the nominal mission operations, during which both Eagle and Scott are functioning, and it is designed to last for 12 months. During this phase, the system is able to supply power both to Scott and to potential external users. Comprehensive information regarding power generation and supply is detailed in Section 11.1. Table 12.1 systematically reassesses the average power requirements of potential users (initially evaluated in Section 9.1.2) considering that LPM can provide up to 3 kW for them.

Power consuming unit	Active power range (kW)	Survival power range (kW)
ISRU: Demonstration	3 to 7	0.5 to 1
Unpressurized electric rover	1 to 3	0.2 to 0.5
Small rover	<1	<0.2
Large rover	1 to 7	0.5 to 1
Small robotic lander	<1	<0.2
Medium robotic lander	1 to 3	0.2 to 0.5
Large robotic lander	3 to 7	0.5-1
Communication system	0.3 to 1 per transmitter	Not applicable
Lunar nighttime operation and heating systems	1 to 2	Not applicable

Table 12.1: Average power ranges required for potential external users.

Following Phase E the mission timeline splits into two branches: one unfolds into three sequential phases: F11, F21 and F31, adopting an approach aimed at maximizing the exploitation of available resources at every level, starting from power, followed by structural elements and ultimately addressing material utilization. The other branch leads to a more general solution, referred to as phase F12, which involves the actual scalability and evolution of the system, enabling its possible integration into future missions. For instance, AMPERE could provide support for the production and supply of a lunar base, since its operational location is a prospective site for such a base (see Section 10.1). The choice of following one branch with respect to another is made near the end of Phase E. At this time, if a future lunar mission expresses interest in integrating and scaling the AMPERE power generation and storage components as a starting point to enhance its power production and supply, a signal will be transmitted to the OBC that triggers the Phase F21. Otherwise, Phase F11 will be pursued.

- Phase F11 “Residual power production”:
  Following one year of baseline mission operations, the system continues to produce a reduced amount of power for 2 additional months. The duration of this phase is dictated by the illumination condition analyses done in Section 11.7, which lead to a continuous daytime period lasting approximately 70 days, following Phase E. Therefore, all operations during this phase are assumed to occur in daytime conditions, with lunar nights

being neglected. Based on the analyses detailed in Section 11.1, a worst-case scenario has been considered to determine the system's power autonomy: solar panels' efficiency is reduced by 50% with the respect to phase E, due to materials degradation and lunar dust accumulation over time. In this scenario, the maximum power output from the solar panels is assumed to be halved compared to the baseline mission, resulting in 2.5 kW. Due to this generated power reduction, the Scott module ceases its operative life and is stowed beneath the Eagle module. While not intended for reactivation within this mission framework, its integrity, maintained by the Eagle module, allows for its potential implementation in future missions. Therefore, only 268 W of the total power generated is used for system survival (for more details see Section 11.1), leaving the remainder available for the potential external users shown in Table 12.1. A few days before the conclusion of this phase, the solar panels are fully shut down and stowed. The computation of these days is done considering that from this point both the batteries and the fuel cells are completely charged. A portion of this stored energy continuously powers the telemetry system, which is composed of the OBC, the PCDU and the S-Band. It actively monitors and transmits real-time battery status updates to external users and issues a low-charge alert when the battery charge level drops below a predefined threshold of 20%. Based on the analyses detailed in Section 11.1, the system survival time, considering only telemetry, is computed considering that the total system capacity (Fuel Cells + Batteries) is equal to 28704 Wh, while the telemetry power consumption is equal to 208.68 W. Since only the 80% of the power can be used, the total survival time is shown in Equation (12.1):

$$Total\ continuous\ hours = \frac{28704 \cdot 0.8\ Wh}{208.68\ W} = 110\ h \tag{12.1}$$

that in Earth days is given by Equation (12.2):

$$T_{Earth_{days}} = 4\ d\ , 13\ h \tag{12.2}$$

Assuming an external user which requires 3 kW continuously, the total available time is represented in Equation (12.3):

$$Total\ continuous\ hours = \frac{28704 \cdot 0.8\ Wh}{3208.68\ W} = 7\ h \tag{12.3}$$

As expected, the survival time dramatically drops when power is provided to an external user. Upon reaching the critical threshold, the telemetry system initiates the shutdown sequence for the Eagle module, marking the end to this phase.

- Phase F21 "Hub conversion for ISRU & logistical activities":
  This phase represents a critical transformation of AMPERE's utility, shifting it from active power generation to a passive, supportive role as a hub for ISRU and general logistical activities. This phase is projected to last for up to 4 months. At this stage, the solar panels are permanently stowed, and the LPM fully ceases its power production. From this point onward, the primary utility of the Eagle module stems from its resistance to the harsh lunar environment and its inherent transportability. Regarding its robustness to the lunar environment, it can be served as a secure, shielded warehouse, perfect for safeguarding sensitive equipment, critical instruments, life support consumables and radiation-vulnerable components from the intense lunar environment. Furthermore, Eagle design allows for repositioning to various locations on the lunar surface, providing a fundamental, relocatable protected environment. However, with the thermal control subsystem no longer active in this phase, components within the Eagle and Scott modules will begin to degrade, as their nominal operating temperature range can no longer be maintained.
- Phase F31 "Dismantling & component recover":
  This phase represents the final stage in the AMPERE's lifecycle. After 18 months it has been assumed that Eagle module's structural integrity, which previously provided shielding against radiation, is no longer maintained due to the accumulated effects of the lunar environment. Consequently, the system undergoes a controlled dismantling process, extracting and recovering any instruments or subsystems that remain functional. These salvaged elements can then be integrated into new lunar architectures, such as future habitats or scientific outposts [R.D. 40], [R.D. 41], [R.D. 42], [R.D. 52] or be repurposed for subsequent missions. This approach maximizes resource utilization and significantly reduces the need for entirely new manufacturing on Earth, aligning with the second mission objective of integrating this mission into future endeavours (see Section 9.2). However, only a few components can be recovered due to natural degradation, initially observed during phase F22 and further aggravated in this phase by intense radiation. These elements are the electrodynamic dust shield, the generator for the electrodynamic dust shield and the temperature sensors. Their inherent ease of extraction is another critical factor, significantly aiding the dismantling process.

- Phase F12 “Scalability & Evolvability”:
  The AMPERE system design is adaptable and future-proof, engineered with an architecture that supports dynamic growth and technological refreshment. This means that scalability can be achieved either by replacing the existing solar panels with larger ones, by adding modular battery stacks, or more generally, by systematically replicating the entire LPM unit to meet increased power demands[R.D. 41]. At the same time, its design facilitates evolvability, allowing for the integration of emerging and more efficient technologies, such as advanced solar panels, next-generation fuel cells, or higher-density battery chemistries, to enhance performance or adapt to evolving mission requirements. These include, more generally, power distribution to lunar habitats and full-scale ISRU [R.D. 41], and more specifically, providing power for the construction of the first lunar railway system, a concept which falls into NASA's Project Flexible Levitation On A Track (FLOAT) [R.D. 53]. This capability directly supports and fulfils AMPERE’s secondary objectives. However, implementing these expansions and technological upgrades requires external intervention, whether through human-led activities or autonomous robotic operations.

13 Conclusions

This document represents the outcome of the study carried out by the AMPERE team, aiming not only to develop the preliminary design of a lunar power station, but also to demonstrate the feasibility of recharging an external user, supporting its operations, through a dedicated wireless interface. The mission aligns with ESA's long-term goals for sustainable and scalable lunar exploration beyond 2035, making optimal use of European resources to pave the way for future lunar infrastructure. For this reason, working within the strict volume and mass constraints imposed by the Argonaut LDE, the study first has focused on identifying the core needs of the European scientific community, particularly in the context of long duration lunar surface activities; from this, AMPERE team has defined clear mission objectives and has developed four mission concepts, leading to a structured trade-off analysis.

As a result, the study has led to the preliminary design of two lunar modules, Eagle and Scott, engineered to survive the extreme environmental conditions. The most demanding challenge has been the development of the EGSD subsystem, being LPM the mission's core. Despite these complexities, the final sizing of the solar arrays and energy storage systems has led to promising results, confirming the South Pole as the optimal landing site selection for this mission purposes. Indeed, the energy generated is not only sufficient to power AMPERE's internal subsystems but also demonstrates the feasibility of supplying power to Scott, which acts as a demonstrative user.

Other critical subsystems, such as TT&C and TCS, have been carefully addressed but delivered encouraging results. In particular, the integration of a European communication infrastructure like Moonlight has showcased the mission’s potential to operate autonomously within a European framework, reducing reliance on third-party assets and minimizing operational complexities. Additionally, thermal performance assessments have confirmed the system’s robustness against the harsh lunar environment, reinforcing the mission’s long-term viability and setting a promising precedent for future European surface operations.

Throughout the design evolution, the study has been consistently guided by the principles of COSPAR’s Planetary Protection Policy. AMPERE qualifies as Category II mission, with careful consideration given to future integration and compliance with Task 4 activities: the mission indeed is designed to be scalable, modular and minimally invasive to the lunar environment, facilitating long-term reuse of core technologies.

With these premises, AMPERE naturally opens the door to future expansions and integrations, aiming not only to support a broad range of users throughout its operational lifetime, but also to become pioneer for lunar infrastructure such as energy hubs and human habitats. In this vision, AMPERE represents a concrete step towards establishing a lasting human footprint beyond Earth.

14 Attachments

14.1 Standard Specifications

The AMPERE mission aims to develop a demonstrative power station and one of its four primary objectives (AMP-PMO-04) is to foster standard specifications for power generation and distribution for any future potential user. For this reason, it has been planned from the outset to issue a technical datasheet serving as a reference framework for all the future beneficiaries intending to exploit this power source. Therefore, this document provides key technical specifications, relative to Eagle module, about the available power resources, energy storage capacity and the electrical interface requirements needed to safely and efficiently recharge from it. During lunar daytime operations (which is the worst-case scenario), the LPM is supplied by solar panels capable of producing up to 3 kW of available power for external user recharge; some of the energy harvested during daylight is stored in a Li-Ion battery pack with a total capacity of 4884 Wh, of which only the 80% (approximately 3907 Wh) is usable, to ensure safe discharge limits and battery longevity. These technical data are summarized in Table 14.1.

Available power produced by solar panels	3 KW (daytime)
Energy stored in Li-Ion battery	4884 Wh

Table 14.1: Power and energy supply specifications

Two types of recharging interfaces are provided: a wireless interface to ease operations for mobile assets; its recharging capability is demonstrated through Scott's operations, and a fixed dock interface for compatible energy storage systems. The wireless interface is available for mobile systems equipped with an onboard charger and receiver coil which allows energy to be transferred directly from the LPM's battery to the user system without the need for physical connection. Users intending to recharge must be equipped with compatible receiver electronics and onboard power management devices, capable of accepting the specified voltage range and power level. The fixed dock interface draws power directly from the solar panels and is designed for systems compatible with LESSH-placed astronaut-rated 28 V batteries. Charging is managed via a BCM. This interface is optimized for fast and reliable charging but requires the presence of internal battery storage within the asset being charged. These technical data are summarized in Table 14.2 and Table 14.3.

On board charger and receiver coil	
Maximum energy transfer rate	125 Wh
Voltage in output	12-36 V DC

Table 14.2: Wireless recharging interface specifications

LESSH BCM	
Charging power	215 W
Current (output)	0 A- 9.4 A
Voltage	24 V- 33.6 V
Charging time	4 hours from 20% to 100%

Table 14.3: Dock recharging interface specifications